

On the aqueous phase chemistry of atmospheric-pressure plasma jets for biomedical applications

I n a u g u r a l d i s s e r t a t i o n

zur

Erlangung des akademischen Grades eines

Doktors der Naturwissenschaften (Dr. rer. nat.)

der

Mathematisch-Naturwissenschaftlichen Fakultät

der

Universität Greifswald

vorgelegt von

Giuliana Bruno

geboren am 04.05.1991

in Salerno, Italien

Greifswald, 09.04.2021

Dekan: Prof. Dr. Gerald Kerth

1. Gutachter: Prof. Dr. Michael Lalk

2. Gutachter: Prof. Dr. Jan Benedikt

Tag der Promotion: 09.04.2021

Contents

1. Introduction	1
1.1. Major findings in plasma medicine	1
1.2. Relevance of the plasma-liquid chemistry	4
1.3. Scope and structure of the work	6
1.4. Experimental strategy: amino acids as tracers of reactive species.....	7
2. Plasma-generated Reactive Species in Liquid: Origin and Reaction Pathways	10
2.1. Oxygen-centered reactive species (A1).....	10
2.2. Nitrogen-centered reactive species (A2 and A3).....	12
2.3. Outcome – Plasma-induced pattern of modifications as a model.....	14
3. Applications of the Cysteine Model in Analyzing the Plasma-liquid Chemistry	16
3.1. Biochemical comparison of plasma sources (A1 and A2).....	16
3.2. Variability induced by changing treatment conditions (A4).....	18
3.3. Plasma-stimulated chemistry of aerosols in the effluent (A5).....	19
4. Summary & Outlook	21
5. References	24
6. Original Publications	37
Article A1.....	39
Article A2.....	51
Article A3.....	79
Article A4.....	105
Article A5.....	117
7. Eigenständigkeitserklärung	147
8. Curriculum Vitae	148
9. List of Publications & Conference Contributions	150
10. Acknowledgments	153

Abbreviations

CAP	cold atmospheric-pressure plasma
RSH	cysteine
RSNO	S-nitrosocysteine
RSO ₂ H	cysteine sulfinic acid
RSO ₃ H	cysteine sulfonic acid
RSOH.....	cysteine sulfenic acid
RSSR	cystine
RSSO ₃ H	cysteine S-sulfonate
CRDS	cavity ring-down spectroscopy
DBD	dielectric barrier discharge
EPR.....	electron paramagnetic resonance
FTIR.....	Fourier-transform infrared spectroscopy
HPLC	high-pressure liquid chromatography
HR	high resolution
IC	ion chromatography
MRM	multiple reaction monitoring
MS	mass spectrometry
MS ²	tandem mass spectrometry
OES	optical emission spectroscopy
RF	radio-frequency
RNS	reactive nitrogen species
ROS	reactive oxygen species
RSS	reactive sulfur species
slm.....	standard liter per minute
TALIF	two-photon absorption laser-induced fluorescence
TOF	time of flight analyzer
Tyr-NO	nitrosotyrosine
Tyr-NO ₂	nitrotyrosine
UV	ultraviolet
VUV	vacuum ultraviolet

1. Introduction

Plasma medicine is an emerging field based on the use of cold atmospheric-pressure plasmas (CAPs) as therapeutic agents in biomedical applications.¹⁻⁴ Plasmas were introduced in 1970 as a medical technology for surgical coagulation⁵⁻⁷ and surface modification.⁸⁻¹¹

In the past two decades, the field has evolved, and CAPs found applications in biological decontamination,¹²⁻¹⁴ dentistry,¹⁵⁻¹⁷ skin-related diseases,¹⁸⁻²⁰ and in vivo promotion of wound healing²¹⁻²⁶ and cancer regression.²⁷⁻²⁹ Plasmas are in the fourth state of matter and can be formed by energy transfer to a gas (e.g., air, helium, or argon), which occur commonly by applying an electric field in the case of CAPs. The partial gas ionization yields radiation, electrons, magnetic fields, and ionized and neutral species (e.g., radicals and excited species).³⁰

CAPs are characterized by having components with different temperatures: electrons have low densities and temperatures between 10^4 – 10^5 K, while neutral atoms have high densities and room temperatures. The resulting net plasma temperature is low (around 300 K), allowing CAPs to be used for in vivo medical applications.³¹ To date, various plasma sources are proposed for biomedical applications.^{4, 32} The biological effects can variate with the source design and treatment modality. Tuning various parameters induces a differential production and delivery on the target of plasma components.³³⁻³⁴ Among these, small reactive species have been identified as key players of plasma effectiveness, by inducing the modulation of cellular redox signaling pathways.³⁵⁻³⁹ Plasma-generated redox-reactive species can be oxygen-centered, such as hydroxyl radicals, hydrogen peroxide, ozone, singlet oxygen, and atomic oxygen, or nitrogen-centered, such as nitric oxide radicals and peroxyxynitrite.^{2, 39}

However, the formation pathways of these reactive species and their mechanisms of action on the biological target remain to be studied. Before reaching the target, most highly reactive gaseous species are likely to decay or react with the surrounding molecules, also due to their short half-life (nanoseconds to milliseconds). Considering that the biological effects induced by CAPs occur in long time scales (seconds to days), further reactions might be stimulated in liquid compartments surrounding cells and tissues. The chemistry generated in liquid could mediate the plasma effects by modifying and amplifying the cocktails of reactive species effectively reaching the target. The elucidation of the chemistry induced in liquid by CAPs is the major topic discussed in this thesis. The mechanisms of transport and modification of gaseous species and de novo formation of species in liquid are elucidated. The presented results aim to control and eventually optimize the formation of individual reactive species in liquid compartments and, consequentially, on the biological target. These elements are necessary to improve the safety and efficacy of plasma treatments, to finalize the concept of plasma dose, and to standardize protocols for clinical applications.^{37, 40}

1.1. Major findings in plasma medicine

Cold plasma sources with different concept designs have been proposed for medical applications (Figure 1.1). In Germany, two CE-certified plasma sources are PlasmaDerm (Cinogy GmbH, Germany) and kINPen MED (neoplas tools GmbH, Germany). Both have been

used in clinical trials to promote wound healing. Recently, another dielectric barrier discharge (DBD)-based plasma source named Plasma care (terraplasma medical GmbH, Germany) received certification as a medical device. Plasma care and PlasmaDerm are DBDs, while kINPen MED is a DBD-type plasma jet.⁴¹⁻⁴⁶

The basic differences between these designs are the modality of plasma generation and the delivery of plasma components on the target. In the case of plasma jets, a carrier or “working” gas (helium or argon) passes through two electrodes, powered by high voltage, and produces a visible plasma effluent ejected by the source. In contrast, ambient air is the gas ionized in DBDs. In this case, the source contains one electrode, while the target represents the counter electrode (volume discharge); alternatively, the plasma is generated on the surface of a specifically designed electrode arrangement (surface discharge) (Figure 1.1).

The generated gaseous chemistry and the interaction with the target vary in the two cases. The tuning of multiple parameters (e.g., gas composition and flow rate), especially in plasma jets, controls the generated plasma components and correlates with the resulting biological effects.^{32, 47-48} Due to their versatility, plasma jets were studied in the present work.

An introductory overview of the major findings regarding the variability of the gaseous chemistry and biological effects of CAPs is provided in the subsequent section.

Modulation of the gas-phase chemistry

Among the various plasma sources proposed as medical tools, the gas-phase chemistry of the argon-driven kINPen 09 (neoplas tools GmbH, a kINPen MED predecessor) and the helium-driven COST-jet (COST Reference Microplasma Jet) has been well characterized. The primary techniques used have been spectroscopy-based methods (e.g., TALIF, FTIR, and OES), on beam mass spectrometry, and computational fluid dynamics.^{46, 49-54} In argon-only kINPen 09 plasmas, the formation of argon-excited states initiates reactions with ambient air molecules (e.g., H₂O, N₂, or O₂), generating secondary species, such as short-lived atomic oxygen ([•]O), singlet oxygen (¹O₂), and low amounts of nitrogen oxide radicals ([•]NO).

The increase of distance from the jet leads to the conversion of these species into long-lived species, such as ozone (O₃).⁵⁵⁻⁵⁷ A similar behavior has been observed in the helium-driven COST-jet, primarily with admixtures of O₂ in the carrier gas.⁵⁸⁻⁵⁹ The gaseous chemistry of kINPen 09 has been investigated by changing conditions related to the gas composition, e.g., in presence of gas admixtures (maximum 1% O₂ and/or N₂) or water molecules (< 320 ppm).

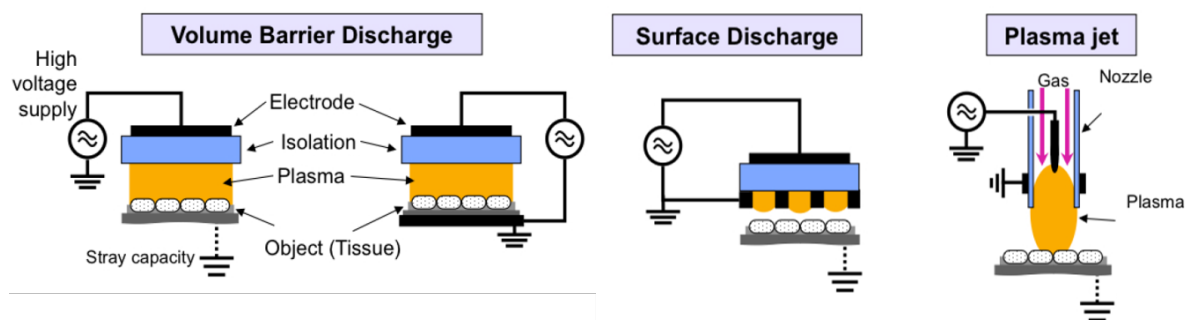


Figure 1.1. Different designs of cold atmospheric-pressure plasma sources currently proposed for biomedical applications. Reprinted with permission from ⁴⁸. © 2013 Elsevier B.V.

A dominant oxygen chemistry in short (mostly $\cdot\text{O}$ and $^1\text{O}_2$) and long distances (mostly O_3) has been measured by admixing O_2 in the working gas.^{55-56, 60} In presence of water molecules, water-derived species, such as hydroxyl radicals ($\cdot\text{OH}$), hydrogen peroxide (H_2O_2), and superoxide anion radicals ($\cdot\text{O}_2^-$) have been also detected in the plasma effluent. However, amounts of water molecules above 320 ppm generate high densities of water-derived species, with an absolute decrease of other gaseous species. The high densities of $\cdot\text{OH}$ formed in the effluent by water dissociation recombine to form high levels of H_2O_2 .^{49, 61-62} A differential species production has been detected using a shielding gas device, which allows the modulation and control of ambient air composition surrounding the plasma. The application of a shielding gas around the principal driven gas contributes to guide the stream to the target and control the ongoing chemistry, minimizing uncontrolled reactions with ambient air.^{60, 63}

An increased nitrogen chemistry has been observed in the presence of a N_2 shielding gas, and N_2/O_2 in working gas, yielding nitric dioxide radicals ($\cdot\text{NO}_2$). A further improvement of the nitrogen chemistry has been achieved in presence of small amounts of water molecules in the working gas. In this case, a switch from O_x -based to N_x -based chemistry has been measured, resulting in the production of gaseous $\cdot\text{NO}$ and nitric acid (HNO_3).⁵¹ Finally, a variable cocktail of gaseous reactive species can be produced by tuning the plasma jet parameters.

Biological effects of cold plasmas

Downstream biological effects of CAPs have been investigated using different models (e.g., cell cultures, animal models), as well as in patients. The generated effects had a biphasic character, ranging from regulatory to lethal, depending on the applied parameters and consequentially, the produced pattern of reactive species reaching the target.⁶⁴

Using KINPen 09, various experiments have been performed by modulating the treatment duration, the working gas composition (e.g., gases and the presence of water molecules), and the shielding gas.⁶⁵⁻⁶⁷ Highly oxidative conditions (e.g., long treatment times and oxygen in working gas) led to inflammation, apoptosis, an endogenous increase of reactive species, and lipid peroxidation. In contrast, softer stimulations (e.g., short treatment times) increased cell proliferation, promoting tissue regeneration, blood coagulation, and platelet activation.³⁶

Oxidative conditions are currently used in applications for cancer regression in vitro and in animal models,^{27, 68-71} as well as for antimicrobial effects.¹²⁻¹⁴ In these cases, CAPs provide high amounts of oxidative reactive species, which can directly induce necrosis on the target or stimulate redox-sensitive proteins to release kinases that mediate different types of apoptosis (e.g., ferroptosis, necroptosis, and autophagy).³⁶ Work conducted in mice models has confirmed that oxidative conditions of plasmas (e.g., high $\cdot\text{O}$ production) induce a high immunogenic death of tumor cells due to an intra-tumoral infiltration of CD8^+ cytotoxic T-cells.⁷² Regarding clinical applications, CAPs have been applied to end-stage head and neck cancer patients. The intense bacterial load presented in these cases was reduced, along with tumor regression and acceleration of wound healing.⁷³⁻⁷⁵ Besides, repetitive treatments in situ reduced lesions provoked by carcinomas or precancerous lesions (e.g., oral lichen planus and actinic keratosis) in patients.⁷⁶⁻⁷⁷ The plasma technology has also been proposed as an adjuvant to treatments based on the use of chemotherapeutic agents and radiation against cancer.⁷⁸⁻⁸⁰

Highly oxidative conditions are also applied in dentistry for biological decontamination.¹⁵⁻¹⁷ In contrast, a softer stimulation via plasma exogenous reactive species (e.g., short treatment times) has been shown to modulate the activity of transcription factors, for example inducing the translocation of Nrf2 and p53 into the nuclei. This resulted in the activation of cellular reprogramming and stimulated inflammatory, angiogenetic, and growth factors. Also the re-epithelization and integrin and cytoskeleton rearrangements in animal models were promoted.^{18, 21-23, 81-83} These mechanisms could be responsible for plasma effectiveness in accelerating the wound healing process, as shown in vivo.^{18, 24-25} The antimicrobial effects of cold plasmas have also been proposed as responsible for promoting wound healing.^{41, 84-85}

However, studies performed on patients with diabetic foot ulcers and general chronic wounds have confirmed that the efficacy of plasmas is mostly due to the reduction of wound closure times and the induction of granulation.²⁵⁻²⁶ Although physiological effects have been observed, key molecular reaction mechanisms of small reactive species are still under study.

The modification of biological structures (e.g., nucleic acids, proteins, and lipids) of the cell and the extracellular matrix has been proposed as the primary effect of CAPs.³⁹ The ability of plasmas in inducing oxidative additions on biomolecules was proven in vitro and ex vivo.⁸⁶⁻⁹⁰

Such modifications could trigger the modulation of cellular redox signaling pathways, leading to the observed systemic effects in vivo in long time scales.³⁶ For example, structural changes of lipids induced by argon plasmas were considered essential in reducing patients' rashes and pruritus.⁹¹⁻⁹² Modifications occurring on proteins induce a loss or gain of functions and impair the redox and phosphorylation signaling.^{36, 93} Among all, the functionalization of the sulfur moiety of the amino acid cysteine was identified as the most sensitive structure towards plasma-derived reactive species, for example inducing glyceraldehyde-3-phosphate dehydrogenase and RNase A inactivation of bacteria upon plasma-driven oxidation.^{86-87, 94-96}

Finally, the amount and type of plasma-generated species reaching the target are essential to define the biological response of the target. Relevant results have been obtained in controlling the gas-phase chemistry. However, the molecular mechanisms connecting the action of short-lived gaseous species and the long time scales of the biological effects are still unclear.

1.2. Relevance of the plasma-liquid chemistry

The interaction of ionized driven gases with ambient air, molecular admixtures, and plasma radiation (e.g., thermal, visible, and ultraviolet) amplify the production of gaseous species in plasmas.^{46, 55-56, 60, 97-99} Aquaporins have been suggested to transport these species into the cellular cytosol (especially for H₂O₂).¹⁰⁰⁻¹⁰¹ However, only stable species with a relatively long half-life (e.g., H₂O₂, O₃, nitrite [NO₂⁻], and hypochlorite [OCl⁻]) are likely to reach the biological target. The migration radiuses of some relevant species (e.g., [•]O, ¹O₂, [•]NO_x, and [•]OH) are in the microsecond range, and their half-life goes from nanoseconds to milliseconds.¹⁰²

These short-lived species are likely to be destroyed or to react with other molecules before reaching cellular structures. The liquid compartments surrounding cells and tissues might mediate the travel of short-lived species, as presented in Figure 1.2. Here various reaction pathways could be stimulated, including the diffusion, transformation, and de novo formation

of reactive species. The chemistry delivered by CAPs on the target has the potential to be amplified and modulated in the liquid environment in immediate contact with the biological target. Finally, the pattern of reactive species generated in liquid could be responsible for the observed effects of CAPs. For these reasons, the present work focused on studying the liquid chemistry induced by cold plasmas. Plasma-liquid chemistry is a dynamic matrix, difficult to analyze and characterize comprehensively. In cold plasmas ignited by jets, the application of an electric field generates partial ionization of the driven gas (e.g., Ar or He), yielding primary species such as excimers and metastable in the gas phase. Chemical compounds in or surrounding the effluent (e.g., O₂, N₂, and H₂O) interact with these excited states to form secondary species. Gaseous primary and secondary species finally interact with the biological target, directly or through reactions occurring in aqueous compartments. The resulting plasma-liquid chemistry is defined as tertiary chemistry and depends on the plasma treatment conditions. In studying the dynamics of plasma-liquid chemistry, crucial reactions occurring at the plasma-liquid interface must be considered. This gas-liquid interface acts as a transition zone of a few nanometers between gas and liquid.¹⁰³⁻¹⁰⁵ Here density changes occur and complex chemical dynamics regulate phase equilibria and transport processes.^{37, 103}

Molecular simulations show that this zone is not atomically flat, but rather presents corrugations and rapid exchanges (e.g., dissolution and desolvation processes) with gaseous components and water molecules in the target.^{37, 103-104} It is the first contact area of gaseous reactive species with the liquid, and many reactions can occur: the species can be repulsed or diffused on the base of their hydrophobicity and solubility (Henry's law) or can react with water molecules and solutes to generate new species.³⁷ Molecular dynamic simulations have shown that densities of species with high Henry's constants (e.g., [•]O, H₂O₂, and HNO_x) decrease at the interface (being consumed or diffused), while those with low Henry's constants (e.g., O₃) remain constant above the interface (not being solubilized). The high density of species at the interface results in competitive reactions and a local lowering of the pH.¹⁰⁵ Here radiation amplifies the production of reactive species, inducing water photolysis (vacuum ultraviolet [VUV] radiation, < 195 nm)¹⁰⁶ or excitation of biomolecules with the possible formation of organic radicals (ultraviolet radiation, 200 – 400 nm).¹⁰⁷⁻¹⁰⁹

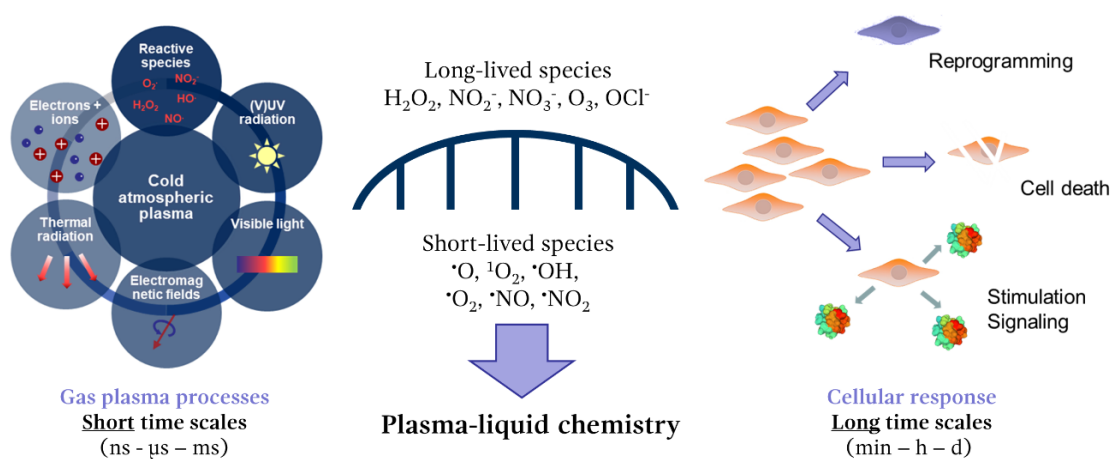


Figure 1.2. Relevance of the aqueous liquid environment in mediating the effects of cold atmospheric-pressure plasmas on biological targets (image by courtesy of Kristian Wende).

Figure 1.3 provides a simplified overview of the potential chemical processes occurring in plasma-treated liquids. In the past, research groups have focused on investigating the plasma-liquid chemistry. Generally, many of the data have been collected via dynamic simulations.^{105, 110-111} Alternatively, the long-lived species (e.g., H_2O_2 , NO_2^- , and NO_3^-) have been analyzed using probes for colorimetric detection.¹¹²⁻¹¹³ The formation of short-lived species, such as radicals, has also been investigated via electron paramagnetic resonance (EPR) spectroscopy, primarily for kINPen 09¹¹⁴⁻¹¹⁶ and COST-jet¹¹⁷ plasmas. Using this method, the high variability of plasma-generated species formed in liquid promotes aspecific reactions with the EPR probe, at times overestimating the targeted species, and neglecting the action of unexpected species.

Deeper investigations are required to characterize the plasma-liquid chemistry comprehensively, with focus on both major and minor induced reaction pathways. In this way, a rapid comparison of chemistries induced by various plasma sources and treatment conditions could be achieved, facilitating the use of CAPs in biomedical applications.

1.3. Scope and structure of the work

The principal aim of plasma medicine is to underline the molecular mechanisms leading to the observed biological effectiveness. Besides, it is required to improve the ability to control the amount and type of plasma components delivered on biological targets. Different conditions can be tuned (e.g., plasma source, plasma jet parameters, treatment modality), and this leads to a variation of the resulting cocktails of plasma components. To date, many plasma sources and treatment conditions are proposed to improve the targeted use of plasmas in biomedical applications (e.g., cancer regression versus wound healing promotion). However, the tunable pattern of reactive species must be characterized, controlled, and possibly optimized to ensure the safe and efficient usage of cold plasmas in clinical practice.

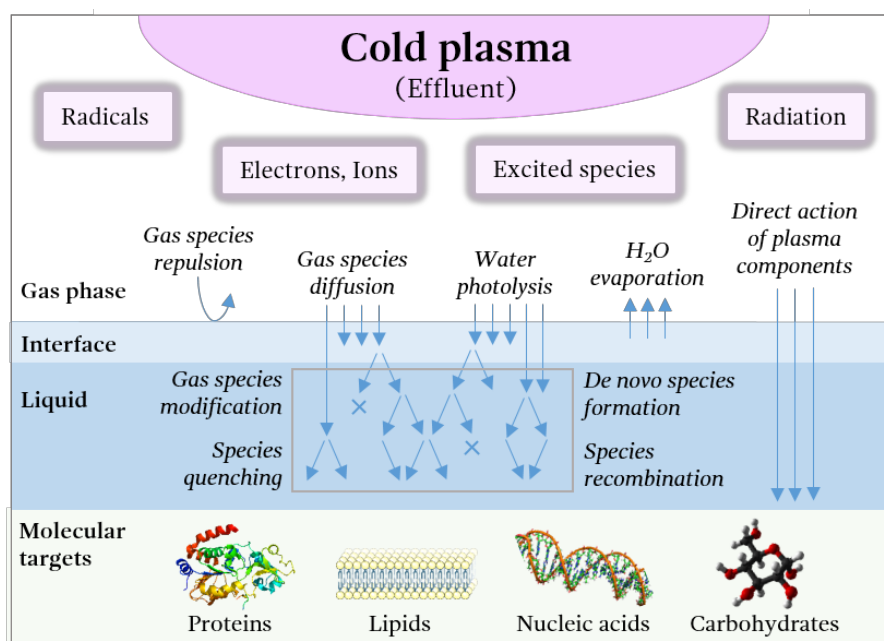


Figure 1.3. Reactions at the gas-liquid interface and in the bulk of liquids treated by cold plasma jets (e.g. COST-jet, kINPen MED). In these treatments, the plasma effluent is not in direct contact with the liquid.

As introduced in Section 1.3, the chemistry stimulated in liquid by plasmas could modulate and amplify the gaseous chemistry, mediating the plasma effects induced on the biological target. Although various studies have been performed, the action mechanisms occurring in the liquid are not fully clarified. Novel tools are needed to achieve the comprehensive characterization of the plasma-liquid chemistry in various conditions. The present thesis offers the tools and results to address this problem, in particular, focusing on the following aims:

- a) Disentangle the reaction pathways of individual gaseous species at the interface and in the bulk of the liquid (e.g., diffusion, modification, decay, recombination, triggered reactions).
- b) Investigate the de novo formation of reactive species in aqueous liquid targets.
- c) Control and characterize comprehensively predominant chemical pathways resulting from tuning treatment conditions (e.g., type of plasma jet, gas composition, treatment duration).

To achieve these aims, this work proposes to use the biochemical reactivity of small biomolecules towards reactive species and the pattern of all the possibly generated structural changes (e.g., oxidative additions or losses) to identify reaction pathways occurring in liquid. Section 1.4 presents additional details on the experimental strategy and the applied methods. The overall results of the thesis are presented in form of five peer-reviewed publications (Articles A1 through A5), which are briefly introduced in the following chapters.

Chapter 2 presents relevant results for points a) and b). Here the amino acids cysteine and tyrosine are applied as molecular beacons in solutions. The origin and reaction mechanisms of plasma components at the interface and in the bulk of the liquid are clarified, and attention is given to the oxygen-driven (Section 2.1, Article A1) and nitrogen-driven chemistry (Section 2.2, Articles A2 and A3). As result, individual reactive species generated specific structural modifications of cysteine and tyrosine. For this reason, the pattern of amino acid modifications is proposed as a model in Section 2.3 to control, tune, and characterize comprehensively the plasma-liquid chemistry generated by modulating treatment conditions.

Chapter 3 implements and discusses the potential of the cysteine model in various applications, providing key results for the resolution of point c). In particular, the cysteine product pattern was applied to characterize and to compare the oxidation potential and the pattern of reactive species produced by different plasma sources (kINPen 09 and COST-jet) (Section 3.1, Articles A1 and A2), treatment conditions (gas composition and treatment duration) (Section 3.2, Article A4), and presence of aerosol droplets dispersed in the effluent (Section 3.3, Article A5). A summary of the presented results is given in Chapter 4, together with an outlook on how to tune plasmas for biological applications, considering the potential of CAPs in modifying cellular biological structures such as cysteine and tyrosine.

1.4. Experimental strategy: amino acids as tracers of reactive species

By treating with CAPs aqueous solutions of small biomolecules, peculiar structural changes (e.g., oxidative additions or losses) may be generated by reactive species deposited or formed in liquid. Mass spectrometry was used as a method to characterize the possible modifications induced on biomolecules by plasma treatments. This technique allows the identification of the

entire pattern of modifications, which has a descriptive potential of the overall reaction pathways stimulated in liquid by tuning treatment conditions. For these reasons, sensitive biomolecules towards different reactive species were chosen in this work: the amino acids cysteine and tyrosine. Previous studies confirmed that these are major structures target of plasma-derived reactive species.^{86-87, 94-96} In the cellular environment, the amino acid cysteine is modified by various reactive species (e.g., $\cdot\text{O}$, $^1\text{O}_2$, $\cdot\text{OH}$, H_2O_2 , O_3 , peroxyxynitrite [ONOO^\cdot], and dinitrogen trioxide [N_2O_3]), and the generated chemo-types are essential for the protein structure, functioning, localization, and reactivity. The sulfur atom of cysteine can modulate its oxidation state from -2 to +6, generating a rich pattern of cysteine derivatives in the cell. These structures are particularly relevant in regulating the physiological redox homeostasis of the cell, as well as in reacting to conditions of oxidative stress.¹¹⁸⁻¹²¹ The reactivity in the liquid of the thiol moiety towards specific reactive species (e.g., H_2O_2 , $\cdot\text{O}_2^-$ and O_3) strictly depends on the pH, which regulates the presence of thiolate.¹²²⁻¹²⁵

Considering the potential of cysteine in being differentially modified by various reactive species, this amino acid was used as a probe in most of the articles (A1, A2, A4, and A5) presented in the thesis. To support and enrich the results obtained in Article A2 regarding the nitrogen-centered reactive species produced by CAPs in liquid, tyrosine was used as a tracer in Article A3. This amino acid has a key role in forming the hydrophobic cores of proteins, regulating their structure and function. Besides, the post-translational modifications physiologically induced on tyrosine, such as oxidation and phosphorylation, regulate multiple signaling pathways. In particular, the addition of oxidative functional groups on the aromatic moiety is a primary event occurring in the NO-mediated signaling pathways, making tyrosine an essential amino acid in regulating the cellular homeostasis of reactive nitrogen species (e.g., $\cdot\text{NO}$, $\cdot\text{NO}_2$, ONOO^\cdot) and in responding to conditions of nitrosative stress.¹²⁶⁻¹²⁹

The methods applied in this thesis included 1) tuning parameters for treatments with cold plasmas, 2) characterizing the structural changes of the tracers by mass spectrometry, and 3) interpreting the chemistry stimulated in liquids under controlled conditions (Figure 1.4). Below, an overview of methodic details is provided:

- 1) Plasma jets were chosen as sources to modulate the treatment parameters and therefore, the produced reactive species. The argon-driven kINPen 09 (Figure 1.4) was used (Articles A1 through A4) due to the well-characterized gaseous chemistry, together with the helium-driven COST-jet as a reference source (Articles A1 and A2). An argon-driven radio-frequency (RF) jet equipped with a nebulizer device was used to evaluate the influence of aerosol droplets in the generated chemistry (Article A5). Other parameters mainly modulated were the duration of the treatments (from 15 to 600 seconds), the distance of the jet nozzle to the liquid surface (from 2 to 12 millimeters), and the presence or absence in the working gas of molecular admixtures (1% of N_2 and/or O_2) or water molecules (< 320 ppm H_2O). In some treatments with kINPen 09, the shielding device (Figure 1.4) was installed to control the composition of the gas surrounding the plasma.
- 2) The complete pattern of plasma-induced structural changes in amino acids cysteine and tyrosine was identified via direct infusion high-resolution mass spectrometry (HR-MS), using a time-of-flight (TOF) analyzer (Articles A1 to A5). The fragmentation spectra were

acquired using tandem mass spectrometry (MS²). Cysteine, tyrosine, and the oxidation products cystine, cysteine sulfonic acid, cysteine sulfinic acid, cysteine S-sulfonate, and nitrotyrosine were quantified via high-pressure liquid chromatography (HPLC) coupled to mass spectrometry (MS) (Articles A3 and A5). Given the polarity of the analyzed compounds, hydrophilic liquid chromatography (HILIC) was used. A triple quadrupole was tuned in the Multiple Reaction Monitoring (MRM) mode, for the accurate quantification of the structures. The anion sulfite and sulfate were quantified using ion chromatography (IC).

3) Additional strategies were included to characterize the plasma-liquid chemistry. The long-lived species H₂O₂, NO₂⁻ and NO₃⁻, were quantified via colorimetric assays and ion chromatography (Articles A2 and A4). Isotopically labeled oxygen or nitrogen from gas (¹⁸O₂ and ¹⁵N₂) or oxygen from water (H₂¹⁸O) were used to treat cysteine or tyrosine solutions and to trace the origin of reactive oxygen and nitrogen species (Articles A1 and A3). In Article A3, tyrosine solutions were treated with cold plasmas in the presence of scavengers for [•]NO and ONOO⁻ (cPTIO and ergothioneine, respectively) or incubated with commercially available oxidants (ONOO⁻, [•]NO, H₂O₂, NO₂⁻ and NO₃⁻). The concentrations of cysteine or tyrosine were modulated (from 0.3 to 100 millimolar) to investigate the chemistry resulting in an environment with reduced water amounts (Articles A3 and A4).

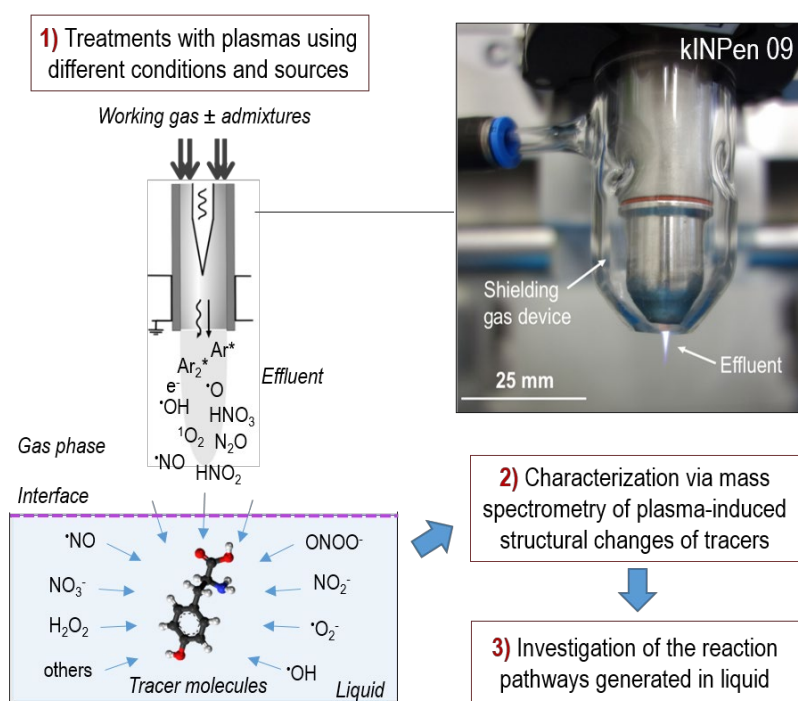


Figure 1.4. Overview of the experimental strategy applied in this thesis. The kINPen 09 plasma jet is shown, also equipped with a shielding gas device (right). *Modified and adapted from Article A3.*

2. Plasma-generated Reactive Species in Liquid: Origin and Reaction Pathways

This chapter describes major findings regarding the origin, the mechanisms of action, and the conditions to improve the formation of relevant reactive oxygen and nitrogen species in liquid. The action of plasma-induced gaseous species at the interface and in the bulk of the liquid is clarified. In parallel, the formation of tertiary species and the contribution of the liquid in the generated chemistry are described, also applying different treatment conditions.

Section 2.1 summarizes the results obtained in Article A1, which clarifies the origin and reaction pathways in the liquid of individual reactive oxygen species. In this case, cysteine was used as a tracer, and isotopically labeled oxygen was used in gaseous or water molecules to trace the oxygen incorporation into the cysteine chemo-types via mass spectrometry.

In Section 2.2, the formation and reactivity of specific nitrogen-centered species are analyzed, as a summary of the Articles A2 and A3. In this case, both cysteine and tyrosine were used as molecular beacons. In Article A3, isotopically labeled water and gases (oxygen and nitrogen) were applied to identify the origin of the species. Besides, scavengers in solution were used to identify the presence and action of individual nitrogen reactive species. Finally, major findings are resumed in Section 2.3. Here the pattern of modifications induced by cold plasmas on the amino acids cysteine and tyrosine is presented as a tool able to characterize both the reactivity of individual reactive species and the overall reaction pathways generated in liquid in specific plasma treatment conditions.

2.1. Oxygen-centered species (A1)

In plasma jets such as kINPen 09 and COST-jet, the reaction of primary reactive species (e.g., Ar or He excimers and metastable) with ambient or admixed O₂ yield secondary reactive oxygen species (ROS) such as atomic oxygen ($\cdot\text{O}$), singlet oxygen ($^1\text{O}_2$), and ozone (O₃).^{52, 54, 115, 130-131} In presence of water molecules in the effluent, hydroxyl radicals ($\cdot\text{OH}$), hydrogen peroxide (H₂O₂), and superoxide anion radicals ($\cdot\text{O}_2^-$) are formed in the gas phase.^{117, 132}

When operating in Ar-only (standard conditions for medical applications), a dominant oxygen-driven chemistry is generated in the effluent of kINPen MED.¹³³ Gaseous ROS could have a relevant role in the plasma effectiveness for various biomedical applications. However, their mechanisms of action, possibly mediated by liquids surrounding biological structures, are still unclear. The fate of gaseous ROS in a liquid target was investigated in Article A1, and the major findings are resumed in this section. Treatments of cysteine solutions with kINPen 09 and COST-jet plasmas generated a pattern of oxygen-driven modifications on the thiol moiety of cysteine. Relevant structures identified via direct infusion HR-MS were cysteine (RSH, Structure 1), cystine (RSSR), cysteine sulfinic acid (RSO₂H), cysteine sulfonic acid (RSO₃H, Structure 2), and cysteine S-sulfonate (RSSO₃H, Structure 3) (Figure 2.1). To underline the origin of the ROS, the incorporation of isotopically labeled oxygen in the working gas ($^{18}\text{O}_2$) or in the liquid target (H₂¹⁸O) was traced using mass spectrometry.

As a first result, both gaseous or water oxygen atoms were introduced in the cysteine structures (Table 1 and 2, Article A1). Two opposite cases were the cysteine sulfonic acid (RSO_3H), formed by 70% of oxygen atoms per molecule from the gas, and the cysteine S-sulfonate (RSSO_3H), which incorporated 90% oxygen atoms per molecule from the water, independently from the used working gas and plasma source (Figure 4 and 5, Article A1). This result shows that the liquid phase is involved in the plasma-induced chemistry, and tertiary species can be produced de novo. Water-derived species can be formed by water dissociation induced by vacuum UV (VUV) radiation ($< 195 \text{ nm}$, emitted from Ar_2^*), yielding $\cdot\text{OH}$ and $\cdot\text{H}$.^{37, 114, 116} Besides, the reaction of $\cdot\text{O}$ with water molecules yield water homolysis, with the production of $\cdot\text{OH}$.¹³⁴⁻¹³⁶ The rapid recombination of $\cdot\text{OH}$ forms H_2O_2 ($k = 4 \times 10^9 \text{ M}^{-1} \text{ s}^{-1}$)¹³⁷. At the used pH (pH 6.2 after treatment), the reactivity of the long-lived species O_3 and H_2O_2 towards cysteine was limited, due to the low availability of cysteine thiolate.^{122-125, 138} The pH-independent reaction of the short-lived species $\cdot\text{OH}$, $\cdot\text{O}$, and $^1\text{O}_2$ with cysteine was rather considered, yielding cysteine sulfenic acid (RSOH) in case of $\cdot\text{OH}$ ^{125, 139} and $\cdot\text{O}$ ¹⁴⁰⁻¹⁴¹, and cysteine sulfinic acid (RSO_2H) by reaction with $^1\text{O}_2$.¹⁴²⁻¹⁴³ The higher amounts of both RSO_3H and RSSO_3H were produced in conditions with O_2 in the working gas, corresponding to the conditions with highest densities of gaseous ROS.⁵⁵⁻⁵⁶ In the case of RSO_3H , its production depended from the oxidation of RSOH by gaseous $\cdot\text{O}$ and $^1\text{O}_2$ (Figure 4, Article A1).

Considering the incorporation of up to three ^{18}O gaseous atoms per RSO_3H molecule, these ROS reacted directly with cysteine molecules, without being modified or quenched by water molecules in the target. The reaction, however, could occur only at the interface, due to the short half-life of $\cdot\text{O}$ and $^1\text{O}_2$ (Figure 2.1).^{115, 144-145} Regarding RSSO_3H , its formation was connected to the increase of gaseous ROS, although aqueous $\cdot\text{OH}$ was needed to generate this cysteine derivative. The water homolysis induced by $\cdot\text{O}$ was considered as the leading process for the formation of $\cdot\text{OH}$ in conditions with oxygen in the working gas. However, the higher $\cdot\text{OH}$ and H_2O_2 generation in the liquid was previously detected in conditions with Ar-only, due to the higher emission of VUV radiation.^{116, 146}

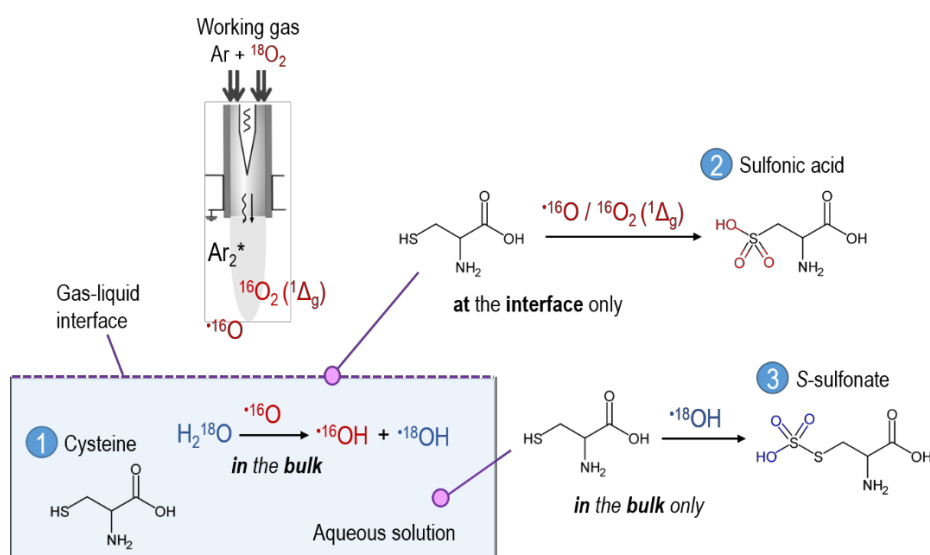


Figure 2.1. Structures of cysteine (1), sulfonic acid (2), and S-sulfonate (3). Reaction pathways in liquid of gaseous and water-derived oxygen species induced by kINPen 09 plasmas. Adapted from Article A1.

It was concluded that the water dissociation induced by Ar_2^* and VUV radiation at the interface of the liquid could lead to a local overproduction of $\cdot\text{OH}$, which rapidly recombines in H_2O_2 . In this case, the fast decay of RSSO_3H , which is a labile structure, was promoted, due to competitive reactions. In contrast, the reaction of $\cdot\text{O}$ with water molecules in the first layers below the interface,¹⁴⁴ stimulated the water homolysis also in the bulk of the liquid, where RSSO_3H could be formed and stabilized. Figure 2.1 presents the suggested reaction pathways.

The reaction of $\cdot^{16}\text{O}$ with H_2^{18}O would generate a 1:1 amount of $\cdot^{16}\text{OH}$ and $\cdot^{18}\text{OH}$. An exchange of O-H single bonds between H_2^{18}O and $\cdot^{16}\text{OH}$ could occur in the bulk of the liquid, where H_2^{18}O is in a much higher density of $\cdot^{16}\text{O}$.¹⁴⁷ This mechanism would favor a final higher amount of $\cdot^{18}\text{OH}$ in the bulk, which is responsible for RSSO_3H formation.¹⁴⁸ These results show that the reactivity of gaseous species is not limited at the interface but propagates in the bulk of the liquid, according to Yusupov et al.¹⁴⁹ Finally, it was proven that water-derived species can be formed de novo in the bulk of the liquid, and not only in the gas phase from water molecules introduced in the working gas or evaporated from the target.^{105, 117}

2.2. Nitrogen-centered species (A2 and A3)

Most of the cold plasma sources used in biomedical applications generate a gaseous O_x -based chemistry (e.g., kINPen MED, PlasmaDerm).^{133, 150} The enrichment of the pattern of reactive nitrogen species (RNS) is of interest to improve the bactericidal effects of CAPs,¹⁵¹⁻¹⁵² as well as to induce cell stimulation (e.g., promoting wound healing).^{36, 153-159} An increased production of RNS can be fostered in kINPen 09 by introducing N_2 and O_2 in the working gas, or in presence of a N_2 shielding gas in the effluent. In these conditions, nitric dioxide radicals ($\cdot\text{NO}_2$) are mostly produced.^{51, 60} A complete switch from O_x -based to N_x -based gaseous chemistry can be tuned by enriching the working gas of kINPen 09 plasmas with water molecules (< 320 ppm). In this case, higher amounts of nitric oxide radicals ($\cdot\text{NO}$) and nitric acid (HNO_3) are generated.⁵¹ As for gaseous ROS, potential reaction pathways of gaseous RNS occurring in a liquid target were barely investigated, especially for plasmas not in contact with the liquid target. This section presents an overview of the results obtained in Article A2 and Article A3. Here the mechanisms of action, diffusion, transformation, and optimization of gaseous RNS in liquid were discussed. Besides, the de novo formation of RNS in the aqueous target was analyzed. In Article A2, solutions with or without cysteine were treated with kINPen 09 and COST-jet plasmas. The cysteine derivatives were characterized using direct infusion HR-MS. Some RNS were also measured: $\cdot\text{NO}$ via EPR spectroscopy; NO_2^- and NO_3^- using IC. Overall, the oxidized products RSO_2H , RSO_3H , and RSSR were mostly produced, with a low yield of *S*-nitrosocysteine (RSNO) (Figure 3 and 4, Article A2). Overall, the highest amounts of RSNO, $\cdot\text{NO}$, NO_2^- , and NO_3^- were measured in liquid after treatment with kINPen 09 plasmas using an $\text{Ar} + \text{N}_2/\text{O}_2$ (1%) working gas, and an N_2 shielding gas (Figure 4, 5, and 7 Article A2). An enhanced N_x -based chemistry was induced in the liquid target, potentially originating from the high densities of $\cdot\text{NO}_2$ previously measured in the gas phase.⁵¹ Interestingly, the amounts of NO_2^- drastically increased in solutions with cysteine than without cysteine. This anion could be produced as a by-product of the reaction of cysteine with dinitrogen dioxide (N_2O_3) or peroxyxynitrite (ONOO^-)¹¹⁸, yielding RSNO ($k = 6.6 \times 10^6 \text{ M}^{-1} \text{ s}^{-1}$

and $5\text{--}6 \times 10^3 \text{ M}^{-1} \text{ s}^{-1}$, respectively).^{160–161} Due to the low solubility of N_2O_3 ($H^{\text{cp}} = 5.9 \times 10^{-3} \text{ Pa}^{-1}$)¹³⁸, its plasma-induced generation in liquid was not likely to occur. The formation of ONOO^- by the reaction of gaseous $\cdot\text{NO}_2$ with $\cdot\text{OH}$ formed in liquid was rather considered.¹⁶² ONOOH was detected in previous works only at low pH (pH 3.3), mostly by the reaction of H_2O_2 with HNO_2 in treatments with plasmas in contact with liquid.^{105, 163}

Considering the lability of RSNO, tyrosine was chosen as an alternative probe to further investigate the formation and reactivity of RNS in the liquids at neutral pH (7.4). Major findings using tyrosine are discussed in Article A3. Overall, a rich pattern of N-containing derivatives of tyrosine was identified using direct infusion HR-MS after treatment with kINPen 09 plasmas (Table 1, Article A3). Over tyrosine (Tyr, Structure 1), relevant discussed structures were nitrosotyrosine (Tyr-NO, Structure 2), and nitrotyrosine (Tyr- NO_2 , Structure 3) (Figure 2.2). The addition of up to four functional groups (of the same type or mixed, e.g., OH, NO_2 , and NO groups) on the benzene moiety of tyrosine was also detected. According to the higher production of RSNO, N-containing derivatives of tyrosine were highly produced in conditions with Ar + N_2/O_2 (1%) as working gas and a N_2 shielding gas (Figure 4, Article A3).

These derivatives included Tyr- NO_2 (Figure 3, Article A3), which was also quantified using a HILIC-MRM method. Additionally, except for Tyr- NO_2 , similar amounts of N-containing derivatives were generated also in conditions with Ar + O_2 (1%) as working gas. These results highlighted that the shielding gas contributes actively to the formation of reactive species in the effluent of plasmas, affecting the resulting liquid chemistry. In this case, N_2 present in the shielding gas was the only source of N atoms for the generation of RNS.⁵¹ Nitrating agents formed by CAPs were gaseous $\cdot\text{NO}_2$ and possibly aqueous ONOO^- , as previously discussed. $\cdot\text{NO}_2$ can form Tyr- NO_2 by reaction with tyrosyl radicals ($k = 3.0 \times 10^9 \text{ M}^{-1} \text{ s}^{-1}$).^{128–129} ONOOH reacts with Tyr only via the previous dissociation in $\cdot\text{NO}_2$ and $\cdot\text{OH}$, or formation of a transition intermediate during the isomerization process in NO_3^- (Figure 1, Article A3).^{164–165} Using isotopically labeled gas ($^{15}\text{N}_2$ or $^{18}\text{O}_2$) or water (H_2^{18}O), the direct reaction of gaseous $\cdot\text{NO}_2$ with Tyr to form Tyr- NO_2 was confirmed.

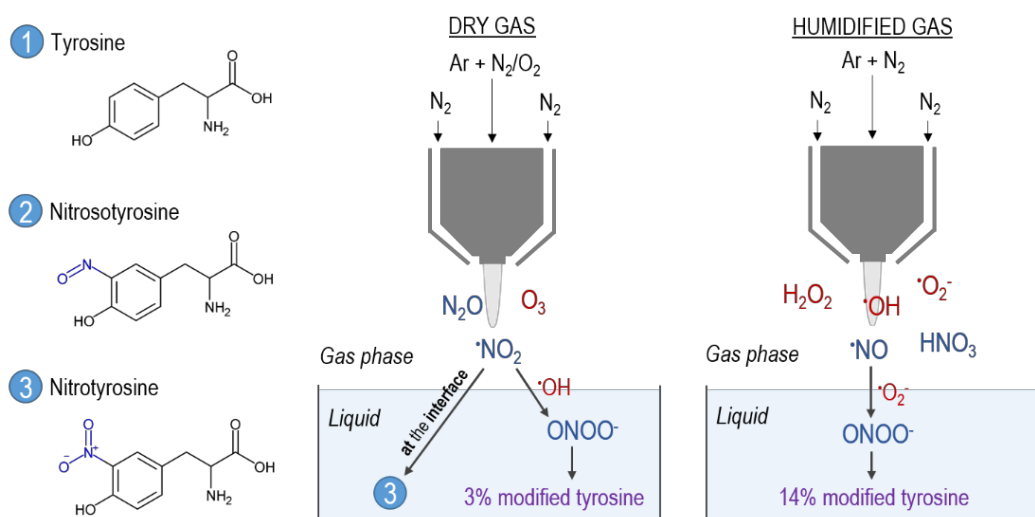


Figure 2.2. Structures of tyrosine (1), nitrosotyrosine (2), and nitrotyrosine (3). Mechanisms of action in the liquid of gaseous and water-derived reactive nitrogen species, in conditions without (left) and with (right) water molecules (320 ppm) in the working gas of kINPen 09 plasmas. *Modified and adapted from Article A3.*

Indeed, Tyr-NO₂ incorporated 100% N atoms and 80% O atoms per molecule from the working gas (Figure 9, Article A3). This reaction could occur at the interface, due to the low [•]NO₂ solubility ($H^{cp} = 3.4 \times 10^{-2} \text{ Pa}^{-1}$).¹⁶⁶ By treating Tyr solutions in presence of a scavenger for ONOO⁻ (ergothioneine), the production in the liquid of ONOO⁻ was confirmed, possibly by the reaction of gaseous [•]NO₂ with aqueous [•]OH (Figure 2.2).¹⁶⁷⁻¹⁶⁹ Previous studies shown that a switch between O_x to N_x-based chemistry, can be achieved in presence of water molecules (< 320 ppm) in the working gas of kINPen 09 plasmas, yielding gaseous [•]NO, HNO₃, and water-derived species (e.g., [•]O₂⁻, H₂O₂, and [•]OH).^{49, 51, 117} To verify the effects of these species in liquid, tyrosine solutions were treated with working gases containing H₂O. As result, the quantities of Tyr-NO₂ increased 10-fold, especially in treatment without O₂ (Figure 3, Article A3). In presence of ergothioneine or a scavenger for [•]NO (CPTIO), all the detected N-containing derivatives were reduced (Figure 10, Article A3), confirming the action of ONOO⁻ in these conditions, originating from the reaction of gaseous [•]NO with water-derived [•]O₂⁻ in the effluent (Figure 2.2). Finally, an enhanced production in liquid at physiological pH of RNS, in particular ONOO⁻, rather than an O_x-based chemistry, was obtained by introducing water molecules in the working gas of kINPen 09 plasmas.

2.3. Outcome – Plasma-induced pattern of modifications as a model

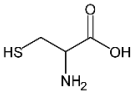
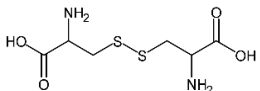
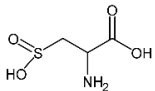
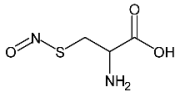
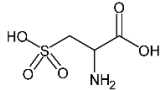
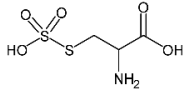
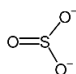
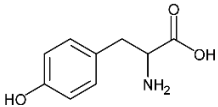
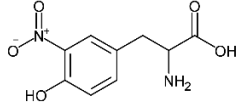
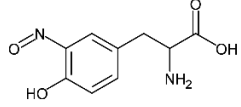
The action and transformation processes of plasma-induced gaseous ROS and RNS have been clarified. The small biomolecules cysteine and tyrosine were used as a molecular beacon to disentangle major reaction pathways in liquid. The densities of gaseous species such as [•]O, O₃, ¹O₂, [•]NO, HNO₃, and [•]NO₂ could be optimized by differently tuning the composition of the applied working gas. Gaseous species produced in presence of O₂ or O₂/N₂ admixtures reacted at the gas-liquid interface directly with the used molecular tracer. In particular, [•]O and ¹O₂ yielded cysteine sulfonic acid, while [•]NO₂ was responsible for nitrotyrosine formation.

In contrast, less soluble species (O₃) were repulsed at the gas-liquid interface. The reaction of gaseous species with water molecules generated also new reactive species in liquid. [•]O induced water homolysis, with consequential production of water-derived [•]OH in the bulk of the liquid. Also, Ar₂^{*} and VUV radiation stimulated water dissociation at the interface, yielding [•]H and [•]OH. [•]OH was responsible for the formation of cysteine S-sulfonate, while the direct impact of VUV radiation on cysteine generated the sulfite, via C-S bond breakage. Due to the high local amounts of [•]OH produced at the interface, [•]OH recombined rapidly in H₂O₂, a more stable and soluble species. At the used pH, the reactivity of H₂O₂ towards cysteine was limited, mostly yielding cystine. Finally, the reaction of some gaseous RNS (e.g., [•]NO, HNO₃) with water-derived species present in the effluent ([•]O₂⁻ and [•]OH) generated high amounts of ONOO⁻ in liquid. ONOO⁻ was responsible for the formation of S-nitrosocysteine, nitrotyrosine, nitrosotyrosine, and other N-containing tyrosine derivatives.

Finally, every discussed reactive species induced peculiar structural changes in the used tracer (Table 2.1). The pattern of cysteine or tyrosine modifications varied qualitatively and quantitatively in relation to the applied conditions for the plasma treatment. This result reflected a variable generation and action in the liquid of the plasma components. For these reasons, the pattern of modifications induced by CAPs in tyrosine or cysteine is proposed as a

tool to investigate rapidly the overall effects of plasmas in liquids, for example using different sources or treatment modalities. The pattern of plasma-induced products of cysteine was previously proposed as a model.¹²⁴ The present thesis presented additional results clarifying the formation mechanisms of the cysteine derivatives, and the individual reactive species involved. Due to these findings, Chapter 3 applies the cysteine product pattern as a model to investigate predominant chemical pathways and bioactive components stimulated in liquid under different plasma treatment conditions (e.g., treatment time, gas composition, and plasma source). This tool could be used to standardize the plasma treatments by controlling the cocktail of plasma components delivered on the target and possibly by optimizing it in relation to specific biomedical applications.

Table 2.1. Principal plasma-induced cysteine and tyrosine derivatives. The formula, structure, and plasma components involved in the formation of each derivative are shown. *Modified and adapted from Article A5.*

Name	Formula	Plasma components	Structure
Cysteine (RSH)	C ₃ H ₇ NO ₂ S	none	
Cystine (RSSR)	C ₆ H ₁₂ N ₂ O ₄ S ₂	•OH, H ₂ O ₂	
Cysteine sulfinic acid (RSO ₂ H)	C ₃ H ₇ NO ₄ S	•OH, •O, ¹ O ₂	
S-nitrosocysteine (RSNO)	C ₃ H ₅ N ₂ O ₃ S	ONOO•	
Cysteine sulfonic acid (RSO ₃ H)	C ₃ H ₇ NO ₅ S	•O, ¹ O ₂	
Cysteine S-sulfonate (RSSO ₃ H)	C ₃ H ₇ NO ₅ S ₂	•OH	
Sulfite (SO ₃ ²⁻)	SO ₃	VUV, •OH, •O, ¹ O ₂	
Tyrosine (Tyr)	C ₉ H ₁₁ NO ₃	none	
Nitrotyrosine (Tyr-NO ₂)	C ₉ H ₁₀ N ₂ O ₅	•NO ₂ , ONOO•	
Nitrosotyrosine (Tyr-NO)	C ₉ H ₁₀ N ₂ O ₄	•NO, ONOO•	

3. Applications of the Cysteine Model in Analyzing the Plasma-liquid Chemistry

The oxidation product pattern of cysteine was proposed as a tool to describe the formation in the liquid of individual species and to characterize comprehensively the major pathways stimulated in liquid by cold plasmas. This chapter discusses the potential of the cysteine model in investigating the liquid chemistry generated by tuning various conditions.

Section 3.1 (Articles A1 and A2) applies the cysteine model to describe and compare the overall induced chemistry of two plasma sources, the kINPen 09 and the COST-jet. Variability in the production and delivery of reactive species on the target, indeed, could be obtained by using sources with different concept designs. Section 3.2 (Article A4) applies the model to give a detailed overview and comparison of the chemical variability induced by diverse working gas compositions and treatment durations. This section aims to provide the knowledge to select and finely tune the optimal conditions for a given application, based on the pattern of species produced in liquid. Here kINPen 09 was used as a plasma source.

Finally, Section 3.3 (Article A5) illustrates an application of the cysteine model in understanding the chemistry stimulated in aerosol droplets dispersed in the effluent. This conformation is of interest in plasma medicine for diverse reasons, such as for the delivery on the biological target of topical drugs or plasma-derived reactive species, as well as for lowering temperatures on the target. The strategy adopted in this case included the treatment of cysteine solutions, as well as their introduction as nebulizer solutions. In this work, an RF-jet equipped with a nebulizer device was used.

3.1. Biochemical comparison of plasma sources (A1 and A2)

This section presents the potential of the cysteine model in comparing the chemistry induced in liquids by two plasma sources, with a focus on reactive oxygen (Articles A1) and nitrogen (Article A2) species. The chosen plasma sources were the argon-driven kINPen 09 and the helium-driven COST-jet due to the availability of data on the gas chemistry generated in various conditions.^{55-56, 59, 170} The principal differences regarding the two plasma jets are the concept design and the driven noble gas.¹²⁴

Considering the results described in Section 2.1, the liquid chemistry induced by kINPen plasmas in presence of O₂ was dominated by gaseous oxygen species ([•]O and ¹O₂), reacting directly with cysteine at the interface or in the bulk of the liquid to form [•]OH. Overall, a similar reaction pathway was induced by COST-jet plasmas in presence of O₂, and both gaseous ROS and water-derived ROS contributed to the formation of cysteine derivatives (Figure 3.1).

Standard parameters were used for the treatments performed with each source, therefore the distance of the jet to the liquid was 4 mm for COST-jet and 9 mm for kINPen plasmas. Previous studies have shown that a similar amount of gaseous [•]O is produced at 4 mm distances (around 10¹⁴ cm⁻³) for both jets. However, the increase of distance from the target induces the rapid decay of [•]O, in favor of the formation of ¹O₂ and, at higher distances, O₃.^{52, 54, 171}

Considering these data about the distances, $\cdot\text{O}$ could be the species mostly involved in COST-jet plasmas, while its densities were lower in treatments with kINPen plasmas using 9 mm distance. However, a similar pattern of oxidized cysteine derivatives was achieved. In longer distances (9 mm), the densities of $^1\text{O}_2$ were relevant for both sources (around 10^{14} cm^{-3}),^{115, 131} and could be the most relevant species involved in the chemistry induced by kINPen plasmas. Regarding the RNS chemistry, Article A2 provides a comparison of the two plasma sources. In this analysis, significant attention was given to the production of S-nitrosocysteine and the reactive nitrogen species responsible for its formation. The highest amounts of RSNO and $\cdot\text{NO}$ were measured (using MS and EPR, respectively) in kINPen 09 plasmas using an Ar + N₂/O₂ (1%) working gas, and a N₂ shielding gas (Figure 4 and 5, Article A2). Similar amounts of RSNO and $\cdot\text{NO}$ were measured in treatments with COST-jet operating in ambient air and with a He + O₂ (0.5%) working gas (Figure 4 and 5, Article A2). Interestingly, the pathways of formation of RNS were different between the used plasma jets. The N₂ present in the ambient air participated actively in the production of bioactive RNS by COST-jet plasmas, being the only source of N atoms. In contrast, the presence of N₂ in the working gas and in shielding gas was both for kINPen plasmas to produce and stabilize the RNS.^{51, 60} In particular, in the presence of H₂O in the effluent, the N₂ shielding gas had a key role to produce an enhanced RNS chemistry in Ar-only conditions with kINPen plasmas (Section 2.2). It could be concluded that a differential gas and liquid chemistry can be induced by changing plasmas sources.

Finally, the plasma-induced pattern of cysteine products was a valid tool to investigate and compare the characteristic pattern of RNS and ROS produced in liquid by the kINPen 09 and COST-jet plasmas, and potentially of other sources proposed for biomedical applications.

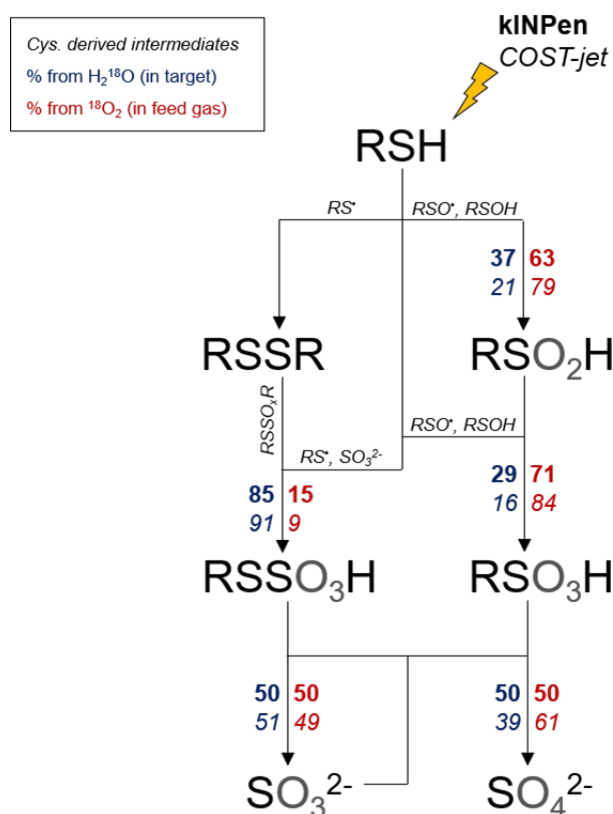


Figure 3.1. Comparison of the contribution of gaseous and water-derived species in the liquid chemistry induced by kINPen 09 and COST-jet plasmas. Reprinted from Article A1.

3.2. Variability induced by changing treatment conditions (A4)

Current certified conditions for treating wound healing with kINPen MED consist of 5 slm of argon-only working gas for 0.5–1.0 min per cm².²⁵ The mechanisms of action of reactive species delivered on the target in these conditions are under study. Especially in clinical medical applications, the standardization of the treatments is essential to achieve a desired and reproducible production of plasma components. The variation of treatment conditions (e.g., gas composition, distance from the target, treatment duration) corresponds to a modified pattern of reactive species delivered on the target. In parallel, the type of treated target could influence the produced chemistry, therefore modulating the final plasma effects. The modulation of treatment conditions is also of interest in some biomedical and industrial applications of CAPs (e.g., to optimize the antimicrobial properties), which aim to optimize the plasma chemistry and maximize the desired effects.

To tackle these points, the oxidation potential of plasma treatments using different working gases, treatment durations, and liquid saturations were analyzed and compared in Article A4. This section resumes major findings discussed in Article A4. Here kINPen 09 was used as a plasma source, given the possibility to tune various parameters and study the effects on the liquid chemistry. The overall cysteine oxidation was quantified using the Ellman's reagent, and the cysteine derivatives were identified using direct infusion HR-MS.

Overall, short treatment duration (60 to 180 seconds) and working gases without molecular oxygen (Ar-only and Ar + N₂ [1%]) resulted in mild oxidative conditions, yielding the partial functionalization of cysteine, predominantly in labile derivatives (e.g., cysteine sulfinic acid, cystine, cysteine *S*-sulfonate, and cysteine disulfoxide) (Figure 5, Article A4).

In contrast, long treatment durations (300 to 600 seconds) and working gases with molecular oxygen (Ar + O₂/N₂ [1%] and Ar + O₂ [1%]) generated strong oxidative conditions, yielding complete oxidation of cysteine, and the predominant formation of stable derivatives (e.g., cysteine sulfonic acid, hydroxy-sulfonic acid, and deamino-sulfonic acid) (Figure 5, Article A4). By increasing the oxidation potential of the treatments, labile compounds were oxidized in highly oxidized derivatives, as represented in Figure 3.2 using RSO₃H and RSO₂H as examples of stable and labile structures, respectively. These results could be explained by the time-dependent accumulation of reactive species with increasing the treatment duration, as well as by the formation of highly oxidizing gaseous species (e.g., •NO₂, •O, ¹O₂) in presence of molecular admixtures (N₂ and O₂) in the working gas. This was confirmed by the formation of cysteine sulfonic acid and its derivatives. To study the involvement of the target in the plasma-induced liquid chemistry, high concentrated cysteine solutions were also treated. In these solutions, the availability of water molecules mediating the effects of gaseous species was reduced. While 2 mM cysteine solutions were completely oxidized after 600 seconds treatments with Ar + O₂, only 14% of 100 mM cysteine solutions were oxidized. These results indicated that water molecules mediate a consistent part of the oxidation of biomolecules treated by plasmas, independently from the applied conditions. Major oxidation of 100 mM cysteine solutions occurred in treatment with molecular admixtures than with Ar-only working gases, also in short treatment durations.

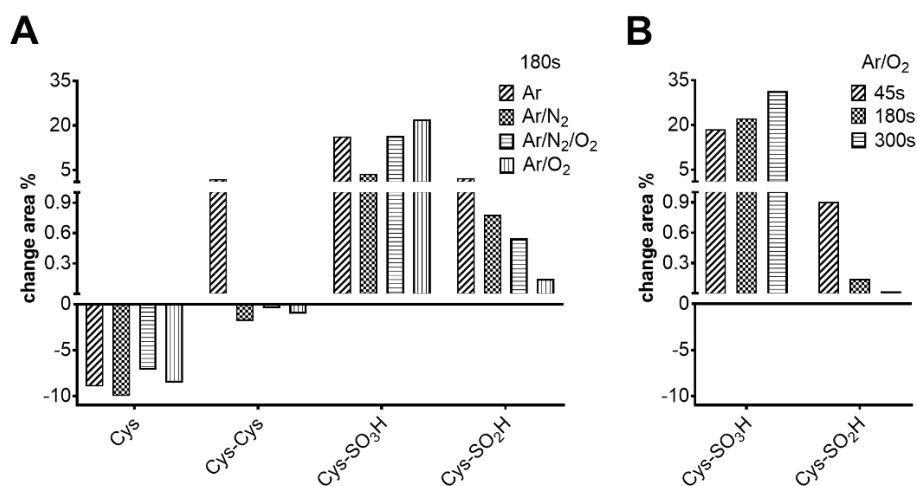


Figure 3.2. Relative amounts of relevant cysteine (Cys) derivatives produced by modulating the working gas composition (A) of kINPen 09 plasmas and the treatment duration (B). Cystine (Cys-Cys), cysteine sulfonic acid (Cys-SO₂H), cysteine sulfonic acid (Cys-SO₃H). Reprinted from Article A4.

Therefore, it was confirmed that in working gases with admixtures, the short-lived ROS and RNS ($\cdot\text{NO}_2$, $\cdot\text{O}$, $^1\text{O}_2$) were able to directly modify the tracer at the interface. The effectiveness of Ar-only treatments depended strongly on the availability of water molecules (in the target or the working gas). In these conditions, the absence of molecular admixtures in the working gas rather favored higher densities of Ar_2^* in the gas phase, and consequentially of the emitted VUV radiation.¹⁷² As previously discussed (Section 2.1, Article A1), both Ar_2^* and VUV radiation can induce water dissociation in the liquid, with the generation of $\cdot\text{OH}$, H_2O_2 , $\cdot\text{O}_2^-$, and $\cdot\text{H}$. The production of these species and the stimulation of tertiary chemistry were the predominant reaction pathways leading to the tracer modification in treatment with Ar-only.

This hypothesis was confirmed by the fact that the most produced cysteine derivatives in these conditions were those dependent on water-derived species (e.g. RSSR, RSSO_3H), as well as from the direct impact of VUV radiation (e.g., SO_3^{2-}). Finally, these results can be used to tune the plasma treatment conditions for specific biological applications. In treatments with Ar-only, the dominant effects are given by the direct impact of Ar_2^* and VUV radiation on the biomolecules, or on the water molecules in the target. The presence of liquid amplifies the production of ROS ($\cdot\text{OH}$, H_2O_2) in the target in these conditions. Using plasmas with molecular admixtures, highly produced gaseous reactive species ($\cdot\text{NO}_2$, $\cdot\text{O}$, $^1\text{O}_2$) react directly with the target biomolecules, or with water molecules to form tertiary species ($\cdot\text{OH}$, $\text{ONOO}\cdot$).

3.3. Plasma-stimulated chemistry of aerosols in the effluent (A5)

Recently, dispersed aerosol droplets in the plasma effluent have been proposed to lower the temperature of plasmas or as a vehicle for the topical delivery of pharmaceutical drugs and reactive species.^{37, 173} This section describes the major results obtained in Article A5, where the chemistry induced in aerosol droplets dispersed in the effluent was characterized using the cysteine model. With this purpose, an RF-jet equipped with a nebulizer device was used as a plasma source. In this case, relevant cysteine derivatives were quantified via HILIC-MRM (cysteine, cystine, cysteine-S-sulfonate, cysteine sulfonic acid, and cysteine sulfinic acid) and

IC (sulfite and sulfate). Cysteine solutions were treated both as liquid targets and independently as nebulizer solutions, meaning that the cysteine was contained in the collected aerosol droplets in the second case. The modulation of the jet distance from the target resulted in an essential parameter for the functionalities of the aerosol droplets. Generally, the presence of aerosol droplets reduced the impact of radiation and gaseous oxygen species on the liquid target, mostly in longer distances (12 mm), possibly due to the interaction of ROS and VUV radiation with water molecules. In shorter distances (2 mm), instead, a slight increase of the transport in the liquid of gaseous species was measured (e.g., for $^1\text{O}_2$), inducing a higher production of sulfonic acid in the target liquid (Figures 10 and 11, Article A5).

The conversion in species of aerosol droplets along the effluent path was analyzed by introducing cysteine in the nebulizer. After the collection of the droplets, the cysteine derivatives were quantified (Figure 13, Article A5). As a result, by increasing the time (60 seconds) and distance from the target (12 mm), cysteine derivatives marker of $\cdot\text{OH}$ and H_2O_2 production increased as well (e.g., *S*-sulfonate, and cystine). It was confirmed that $\cdot\text{O}$ and VUV radiation produced by the plasmas acted directly on the target in absence of aerosol droplets, while were quenched in presence of aerosols in the effluent (Figure 3.3). The reaction in the effluent of $\cdot\text{O}$ and VUV radiation with water molecules could have led to water dissociation, justifying the formation of $\cdot\text{OH}$ and H_2O_2 .^{62, 116-117, 172} The production of $\cdot\text{OH}$ in the droplets was maximized increasing the treatment time and distance, accordingly to an increase of cysteine derivatives commonly formed by water-derived species such as $\cdot\text{OH}$ and H_2O_2 (Figure 13, Article A5). Aerosol droplets have the potential to be used in short distances and treatment times as a carrier of reactive species or scavengers of radiation. In contrast, in long distances and treatment times, aerosol droplets were partially converted into water-derived species; in consequence, these settings could be used to deliver $\cdot\text{OH}$ and H_2O_2 on the target. An overview of the discussed results is presented in Figure 3.3

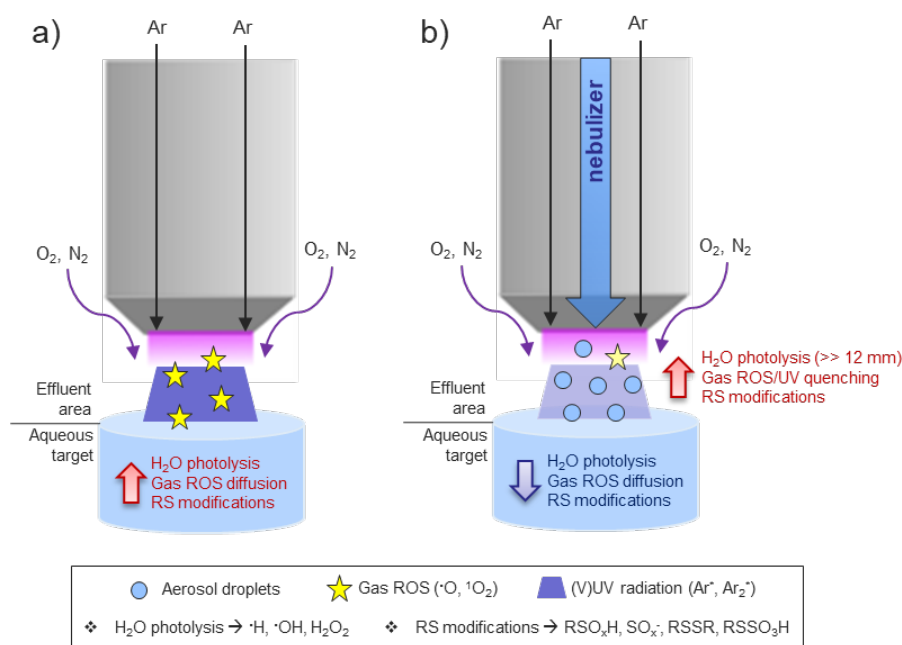


Figure 3.3. Overview of effects induced in the gas and liquid phase in the absence (a) and presence (b) of aerosol droplets dispersed in the effluent of an argon-driven RF-jet. Reprinted from Article A5.

4. Summary & Outlook

Cold atmospheric-pressure plasmas (CAPs) are emerging tools proposed in various biomedical applications, e.g., for biological decontamination, and to promote wound healing and cancer regression. The plasma technology consists of the partial ionization of a gas (e.g., ambient air, helium, argon) with formation and delivery on the biological target of various components, such as electrons, radiation, and reactive species (e.g. ions, radicals, excited species).

The plasma-generated reactive oxygen and nitrogen species have been considered as key effectors in the biological effectiveness of CAPs, and various studies have been performed to control their production in the gas phase of plasma jets. In this thesis, the modification and transformation of gaseous reactive species in the liquid have been discussed and clarified, with a focus also on the *de novo* production of reactive species in liquid. Indeed, liquid compartments surrounding the target molecular structures in the cell could mediate and amplify the reactive species production and the overall biological effects of CAPs.

The experimental strategy applied in this thesis consisted of using the reactivity of small biomolecules, such as of the amino acids cysteine and tyrosine, towards reactive species. For this reason, aqueous solutions containing cysteine or tyrosine have been treated using plasma jets as sources. Possible structural modifications, indicators of the presence of defined reactive species, were characterized via mass spectrometry. In Chapter 2, the reaction pathways in the liquid of gaseous oxygen-centered (Article A1) and nitrogen-centered reactive species (Article A2 and A3) have been investigated using the kINPen 09 plasma jet. Through the use of isotopically labeled gases ($^{15}\text{N}_2$ or $^{18}\text{O}_2$) or water molecules (H_2^{18}O), the origin of reactive species modifying the cysteine and tyrosine structures was traced with mass spectrometry. Considering that both gaseous and water-derived atoms were incorporated in the tracers' derivatives, it could be concluded that reactive species formed in both gas and liquid phase contribute to the molecular effects of plasmas on biological structures. In particular, the direct reaction at the interface of gaseous species atomic oxygen and singlet oxygen yielded cysteine sulfonic acid, while nitric dioxide radicals were responsible for nitrotyrosine formation. The action of gaseous atomic oxygen, however, was not confined at the interface, but it could act in the bulk of the liquid by promoting water homolysis and hydroxyl radicals generation. Hydroxyl radicals yielded cysteine *S*-sulfonate. At the gas-liquid interface, argon excimers and vacuum ultraviolet radiation contributed to the formation of water-derived species (hydroxyl radicals and hydrogen peroxide) and sulfite, originating from the C-S bond breakage of the cysteine structures. It was shown through the use of specific scavengers, that the *de novo* production in liquid of peroxyxynitrite, yielding nitrotyrosine, nitrosotyrosine and other N-containing tyrosine derivatives, was promoted in presence of water molecules in the effluent and N_2 in the working gas or as a shielding gas. Finally, the action in the liquid of each reactive species generated characteristic tyrosine or cysteine derivatives. Therefore, in Chapter 3 the pattern of cysteine modifications was used to investigate and compare the major reaction pathways stimulated in liquid by plasmas, using different plasma parameters (e.g., working gas composition, treatment duration) and plasma sources (e.g., kINPen 09, COST-jet, RF-jet).

Firstly, the pattern of reactive species produced by kINPen 09 and COST-jet plasmas have been compared (Article A1 and A2). A similar pattern of cysteine derivatives was produced by the two plasma sources. In presence of O₂ in the working gas, atomic and singlet oxygen were predominantly produced in the gas phase of both plasma jets.

However, using standard distances for the two sources, it was shown that COST-jet plasmas can deliver on the target predominantly atomic oxygen, while kINPen plasmas deliver mostly singlet oxygen. Regarding the reactive nitrogen species, kINPen plasmas required the presence of N₂ and O₂ in the working gas and a N₂ surrounding atmosphere. COST-jet plasmas operating in ambient air produced similar amounts of S-nitrosocysteine and nitric oxide radicals in liquid in presence of low amounts of O₂ in the working gas. These results suggested firstly that plasma sources have different pathways of formation of reactive species, and secondary that the gases in both working gas and atmosphere surrounding the effluent are involved in the production of species in the gas and in the liquid phase. A distinction of the oxidation potential generated by varying the working gas and the treatment time was also investigated using kINPen 09 (Article A4). Overall, long treatments (300 to 600 seconds) induced species accumulations in liquid, yielding highly oxidized structures such as cysteine sulfonic acid. Strong oxidizing conditions were also those containing O₂ in the working gas, which acted predominantly via formation and action in the liquid of gaseous oxygen species, such as singlet oxygen and atomic oxygen. In contrast, conditions without molecular admixtures yielded a weak cysteine oxidation, and the formation of reversible modifications on cysteine such as cystine, cysteine S-sulfonate, and cystine S-oxides. In conditions with argon-only, predominantly identified pathways were those driven by argon excimers and vacuum ultraviolet radiation, which led to water dissociation and major production of hydroxyl radicals and hydrogen peroxide in liquid.

Finally, the impact on the liquid chemistry in conditions with water molecules in the working gas was investigated (Article A5). Here aerosols droplets were introduced in the effluent by using an RF-jet equipped with a nebulizer device. Water-derived species such as hydroxyl radicals were generated in the gas phase by the action of vacuum UV radiation and atomic oxygen, yielding the highest amounts of cystine and cysteine S-sulfonate in long distances. In parallel, the impact of plasma components produced in the gas phase was minimized on the liquid target. The diagnostics of the plasma-induced liquid chemistry using small biomolecules can be used as a tool to comprehensively characterize the pattern of reactive species generated in liquid using different plasma sources and treatment conditions. Finally, the findings presented in this thesis contribute to improving the control and optimization of plasma-generated species effectively reaching the target. These elements are necessary to achieve the standardization of the protocols and the plasma dose in biomedical and clinical applications.

Outlook – Tuning Plasmas for Biological Applications

The potential of cold atmospheric-pressure plasmas in modifying biological structures was shown in aqueous models of amino acids, but also in protein solutions^{86-87, 94-96} and the proteomes of wound exudates (Article A3). The structural changes of biomolecules driven by reactive species could be the principal molecular mechanism of action of plasmas.

Considering the variable pattern of modifications induced by cold plasmas in amino acids, different treatment conditions can be tuned to achieve variable cellular effects. Overall, plasma conditions producing reversible modifications can be used to induce positive oxidative stress in the cell environment, promoting cell proliferation, reprogramming, reorganization, and wound healing acceleration. It has been already shown that short plasma treatments without O₂ in the working gas promote the acceleration of wound healing in patients.²⁵⁻²⁶ In the same conditions, the high impact of vacuum ultraviolet radiation generated aqueous hydroxyl radicals and hydrogen peroxide, leading to cysteine-derived disulfide S-oxides (cysteine disulfide, disulfone, S-sulfonate) formation in cysteine solutions. These labile structures could be formed also in the cell, and potentially act as antioxidants, by modifying reversibly protein thiols, and forming mixed disulfides and sulfenic acids. These mechanisms, which occur under oxidative stress conditions in the cell, have the purpose to restore the physiological redox signaling, as well as to induce a positive cell stimulation.¹⁷⁴⁻¹⁷⁵

The presence of N₂ in the ambient air or in the working gas promoted a mild action of reactive nitrogen species such as gaseous nitric dioxide radicals, and aqueous nitric oxide radicals and peroxyxynitrite. These generated S-nitrosocysteine in solution. The formation of this derivative in the cell would act as NO-donor for NO-dependent enzymes. These enzymes are cellular antioxidants, being highly produced during defense and inflammation processes, for example against pathogens attack and cancer progression.¹⁷⁶⁻¹⁷⁸ In these conditions, a moderate nitration and nitrosylation of tyrosine, which was measured in treated tyrosine solutions, would represent an antioxidant system in conditions of nitrosative stress.¹⁷⁹ In particular, tyrosine nitration occurring on the metalloproteinase-13 could lead to its release by endothelial cells, with an increase of cell migration and angiogenesis. Finally, these events could be involved in the plasma-mediated promotion of wound healing.¹²⁶

In contrast, long treatment time and presence of oxygen in the working gas could generate irreversible protein modifications, leading to the loss of protein function, protein ubiquitinylation, and activation of pathways for cell death or apoptosis.¹⁸⁰⁻¹⁸¹ Indeed, treatments with oxygen in the working gas induced immunogenic cell death of cancerous cells in murine models.⁷² Additionally, lethal effects were induced by treatment in presence of humidity in the plasma effluent in skin cells.^{49, 65} Using the same conditions for the treatment of cysteine and tyrosine solutions, high densities of gaseous atomic and singlet oxygen, and aqueous peroxyxynitrite, yielded irreversible modifications, such as cysteine sulfonic acid and tyrosine nitration. In conditions of high oxidative stress in the cell, these irreversible modifications would lead to protein ubiquitinylation.^{118, 129, 182} Therefore, strong oxidizing plasma conditions could be tuned to achieve the lethal effects of plasmas, for example for the biological decontamination and cancer regression. Further investigations must be performed on this topic, considering that the reactivity of single amino acids in solutions is different than in the cell environment. The pH, as well as the hydrophobicity of neighbor amino acids and the protein structure, are relevant parameters regulating the oxidative modifications occurring on thiol and benzene moieties in the cell.¹¹⁸

5. References

1. Fridman, G.; Shereshevsky, A.; Peddinghaus, M.; Gutsol, A.; Vasilets, V.; Brooks, A.; Balasubramanian, M.; Friedman, G.; Fridman, A. In *Bio-medical applications of non-thermal atmospheric pressure plasma*, 2006; pp 5-8.
2. von Woedtke, T.; Schmidt, A.; Bekeschus, S.; Wende, K.; Weltmann, K. D., Plasma Medicine: A Field of Applied Redox Biology. In vivo (Athens, Greece) 33 (4), (2019), 1011-1026.
3. von Woedtke, T.; Metelmann, H. R.; Weltmann, K. D., Clinical Plasma Medicine: State and Perspectives of in vivo Application of Cold Atmospheric Plasma. Contrib Plasm Phys 54 (2), (2014), 104-117.
4. Weltmann, K. D.; Polak, M.; Masur, K.; von Woedtke, T.; Winter, J.; Reuter, S., Plasma Processes and Plasma Sources in Medicine. Contrib Plasm Phys 52 %6 (7), (2012), 644-654 %&.
5. Raiser, J.; Zenker, M., Argon plasma coagulation for open surgical and endoscopic applications: state of the art. J Phys D Appl Phys 39 (16), (2006), 3520-3523.
6. Stalder, K. R.; McMillen, D. F.; Woloszko, J., Electrosurgical plasmas. J Phys D Appl Phys 38 (11), (2005), 1728-1738.
7. Malick, K. J., Clinical applications of argon plasma coagulation in endoscopy. Gastroenterol Nurs 29 (5), (2006), 386-91; quiz 392-3.
8. Ohl, A.; Schroder, K., Plasma-induced chemical micropatterning for cell culturing applications: a brief review. Surf Coat Tech 116, (1999), 820-830.
9. Chu, P. K.; Chen, J. Y.; Wang, L. P.; Huang, N., Plasma-surface modification of biomaterials. Mat Sci Eng R 36 (5-6), (2002), 143-206.
10. Barradas, A. M.; Lachmann, K.; Hlawacek, G.; Frielink, C.; Truckenmoller, R.; Boerman, O. C.; van Gastel, R.; Garritsen, H.; Thomas, M.; Moroni, L.; van Blitterswijk, C.; de Boer, J., Surface modifications by gas plasma control osteogenic differentiation of MC3T3-E1 cells. Acta Biomater 8 (8), (2012), 2969-77.
11. Trimukhe, A. M.; Pandiyaraj, K. N.; Tripathi, A.; Melo, J. S.; Deshmukh, R. R., Plasma Surface Modification of Biomaterials for Biomedical Applications. In *Advances in Biomaterials for Biomedical Applications*, 2017; pp 95-166.
12. Brandenburg, R.; Ehlbeck, J.; Stieber, M.; von Woedtke, T.; Zeymer, J.; Schluter, O.; Weltmann, K. D., Antimicrobial treatment of heat sensitive materials by means of atmospheric pressure rf-driven plasma jet. Contrib Plasm Phys 47 (1-2), (2007), 72-79.
13. Moreau, M.; Orange, N.; Feuilleley, M. G., Non-thermal plasma technologies: new tools for bio-decontamination. Biotechnol Adv 26 (6), (2008), 610-7.
14. Matthes, R.; Hubner, N. O.; Bender, C.; Koban, I.; Horn, S.; Bekeschus, S.; Weltmann, K. D.; Kocher, T.; Kramer, A.; Assadian, O., Efficacy of different carrier gases for barrier discharge plasma generation compared to chlorhexidine on the survival of *Pseudomonas aeruginosa* embedded in biofilm in vitro. Skin pharmacology and physiology 27 (3), (2014), 148-57.
15. Jablonowski, L.; Koban, I.; Berg, M. H.; Kindel, E.; Duske, K.; Schroder, K.; Weltmann, K. D.; Kocher, T., Elimination of *E. Faecalis* by a New Non-Thermal Atmospheric Pressure

- Plasma Handheld Device for Endodontic Treatment. A Preliminary Investigation. *Plasma Processes and Polymers* 10 (6), (2013), 499-505.
16. Duske, K.; Jablonowski, L.; Koban, I.; Matthes, R.; Holtfreter, B.; Sckell, A.; Nebe, J. B.; von Woedtke, T.; Weltmann, K. D.; Kocher, T., Cold atmospheric plasma in combination with mechanical treatment improves osteoblast growth on biofilm covered titanium discs. *Biomaterials* 52, (2015), 327-34.
 17. Duske, K.; Koban, I.; Kindel, E.; Schroder, K.; Nebe, B.; Holtfreter, B.; Jablonowski, L.; Weltmann, K. D.; Kocher, T., Atmospheric plasma enhances wettability and cell spreading on dental implant metals. *J Clin Periodontol* 39 (4), (2012), 400-7.
 18. Schmidt, A.; Bekeschus, S.; Wende, K.; Vollmar, B.; von Woedtke, T., A cold plasma jet accelerates wound healing in a murine model of full-thickness skin wounds. *Exp Dermatol* 26 (2), (2017), 156-162.
 19. Bernhardt, T.; Semmler, M. L.; Schäfer, M.; Bekeschus, S.; Emmert, S.; Boeckmann, L., Plasma Medicine: Applications of Cold Atmospheric Pressure Plasma in Dermatology. *Oxidative Medicine and Cellular Longevity* 2019, (2019), 3873928.
 20. Liu, D. W.; Zhang, Y. H.; Xu, M. Y.; Chen, H. X.; Lu, X. P.; Ostrikov, K., Cold atmospheric pressure plasmas in dermatology: Sources, reactive agents, and therapeutic effects. *Plasma Processes and Polymers*, (2020), 25.
 21. Shome, D.; von Woedtke, T.; Riedel, K.; Masur, K., The HIPPO Transducer YAP and Its Targets CTGF and Cyr61 Drive a Paracrine Signalling in Cold Atmospheric Plasma-Mediated Wound Healing. *Oxid Med Cell Longev* 2020, (2020), 4910280.
 22. Schmidt, A.; von Woedtke, T.; Vollmar, B.; Hasse, S.; Bekeschus, S., Nrf2 signaling and inflammation are key events in physical plasma-spurred wound healing. *Theranostics* 9 (4), (2019), 1066-1084.
 23. Hartwig, S.; Doll, C.; Voss, J. O.; Hertel, M.; Preissner, S.; Raguse, J. D., Treatment of Wound Healing Disorders of Radial Forearm Free Flap Donor Sites Using Cold Atmospheric Plasma: A Proof of Concept. *J Oral Maxillofac Surg* 75 (2), (2017), 429-435.
 24. Assadian, O.; Ousey, K. J.; Daeschlein, G.; Kramer, A.; Parker, C.; Tanner, J.; Leaper, D. J., Effects and safety of atmospheric low-temperature plasma on bacterial reduction in chronic wounds and wound size reduction: A systematic review and meta-analysis. *Int Wound J* 16 (1), (2019), 103-111.
 25. Stratmann, B.; Costea, T. C.; Nolte, C.; Hiller, J.; Schmidt, J.; Reindel, J.; Masur, K.; Motz, W.; Timm, J.; Kerner, W.; Tschöpe, D., Effect of Cold Atmospheric Plasma Therapy vs Standard Therapy Placebo on Wound Healing in Patients With Diabetic Foot Ulcers: A Randomized Clinical Trial. *JAMA Netw Open* 3 (7), (2020), e2010411.
 26. Moelleken, M.; Jockenhofer, F.; Wiegand, C.; Buer, J.; Benson, S.; Dissemond, J., Pilot study on the influence of cold atmospheric plasma on bacterial contamination and healing tendency of chronic wounds. *J Dtsch Dermatol Ges*, (2020).
 27. Liedtke, K. R.; Bekeschus, S.; Kaeding, A.; Hackbarth, C.; Kuehn, J. P.; Heidecke, C. D.; von Bernstorff, W.; von Woedtke, T.; Partecke, L. I., Non-thermal plasma-treated solution demonstrates antitumor activity against pancreatic cancer cells in vitro and in vivo. *Sci Rep* 7 (1), (2017), 8319.
 28. Liedtke, K. R.; Freund, E.; Hackbarth, C.; Heidecke, C.-D.; Partecke, L.-I.; Bekeschus, S., A myeloid and lymphoid infiltrate in murine pancreatic tumors exposed to plasma-treated medium. *Clinical Plasma Medicine* 11, (2018), 10-17.

29. Pasqual-Melo, G.; Gandhirajan, R. K.; Stoffels, I.; Bekeschus, S., Targeting malignant melanoma with physical plasmas. *Clinical Plasma Medicine* 10, (2018), 1-8.
30. Bruggeman, P.; Brandenburg, R., Atmospheric pressure discharge filaments and microplasmas: physics, chemistry and diagnostics. *J Phys D Appl Phys* 46 (46), (2013), 464001.
31. Rezaei, F.; Vanraes, P.; Nikiforov, A.; Morent, R.; De Geyter, N., Applications of Plasma-Liquid Systems: A Review. *Materials (Basel)* 12 (17), (2019).
32. Weltmann, K. D.; Kindel, E.; von Woedtke, T.; Hahnel, M.; Stieber, M.; Brandenburg, R., Atmospheric-pressure plasma sources: Prospective tools for plasma medicine. *Pure Appl Chem* 82 (6), (2010), 1223-1237.
33. Khlyustova, A.; Labay, C.; Machala, Z.; Ginebra, M. P.; Canal, C., Important parameters in plasma jets for the production of RONS in liquids for plasma medicine: A brief review. *Frontiers of Chemical Science and Engineering* 13 (2), (2019), 238-252.
34. Weltmann, K. D.; Kindel, E.; Brandenburg, R.; Meyer, C.; Bussiahn, R.; Wilke, C.; von Woedtke, T., Atmospheric Pressure Plasma Jet for Medical Therapy: Plasma Parameters and Risk Estimation. *Contrib Plasm Phys* 49 (9), (2009), 631-640.
35. Graves, D. B., The emerging role of reactive oxygen and nitrogen species in redox biology and some implications for plasma applications to medicine and biology. *Journal of Physics D: Applied Physics* 45 (26), (2012), 263001.
36. Privat-Maldonado, A.; Schmidt, A.; Lin, A.; Weltmann, K. D.; Wende, K.; Bogaerts, A.; Bekeschus, S., ROS from Physical Plasmas: Redox Chemistry for Biomedical Therapy. *Oxid Med Cell Longev* 2019, (2019), 9062098.
37. Bruggeman, P. J.; Kushner, M. J.; Locke, B. R.; Gardeniers, J. G. E.; Graham, W. G.; Graves, D. B.; Hofman-Caris, R. C. H. M.; Maric, D.; Reid, J. P.; Ceriani, E.; Rivas, D. F.; Foster, J. E.; Garrick, S. C.; Gorbanev, Y.; Hamaguchi, S.; Iza, F.; Jablonowski, H.; Klimova, E.; Kolb, J.; Krcma, F.; Lukes, P.; Machala, Z.; Marinov, I.; Mariotti, D.; Thagard, S. M.; Minakata, D.; Neyts, E. C.; Pawlat, J.; Petrovic, Z. L.; Pflieger, R.; Reuter, S.; Schram, D. C.; Schroter, S.; Shiraiwa, M.; Tarabova, B.; Tsai, P. A.; Verlet, J. R. R.; von Woedtke, T.; Wilson, K. R.; Yasui, K.; Zvereva, G., Plasma-liquid interactions: a review and roadmap. *Plasma Sources Science & Technology* 25 (5), (2016), 053002.
38. Jablonowski, H.; von Woedtke, T., Research on plasma medicine-relevant plasma-liquid interaction: What happened in the past five years? *Clinical Plasma Medicine* 3 (2), (2015), 42-52.
39. Wende, K.; von Woedtke, T.; Weltmann, K. D.; Bekeschus, S., Chemistry and biochemistry of cold physical plasma derived reactive species in liquids. *Biol Chem* 400 (1), (2018), 19-38.
40. Fridman, A. A.; Lin, A.; Miller, V.; Bekeschus, S.; Wende, K.; Weltmann, K.-D., The Plasma Treatment Unit: An Attempt to Standardize Cold Plasma Treatment for Defined Biological Effects. *Plasma Medicine* 8 (2), (2018), 195-201.
41. Isbary, G.; Morfill, G.; Schmidt, H. U.; Georgi, M.; Ramrath, K.; Heinlin, J.; Karrer, S.; Landthaler, M.; Shimizu, T.; Steffes, B.; Bunk, W.; Monetti, R.; Zimmermann, J. L.; Pompl, R.; Stolz, W., A first prospective randomized controlled trial to decrease bacterial load using cold atmospheric argon plasma on chronic wounds in patients. *Brit J Dermatol* 163 (1), (2010), 78-82.
42. Isbary, G.; Heinlin, J.; Shimizu, T.; Zimmermann, J. L.; Morfill, G.; Schmidt, H. U.; Monetti, R.; Steffes, B.; Bunk, W.; Li, Y.; Klaempfl, T.; Karrer, S.; Landthaler, M.; Stolz,

- W., Successful and safe use of 2 min cold atmospheric argon plasma in chronic wounds: results of a randomized controlled trial. *Brit J Dermatol* 167 (2), (2012), 404-410.
43. Metelmann, H.-R.; Vu, T. T.; Do, H. T.; Le, T. N. B.; Hoang, T. H. A.; Phi, T. T. T.; Luong, T. M. L.; Doan, V. T.; Nguyen, T. T. H.; Nguyen, T. H. M.; Nguyen, T. L.; Le, D. Q.; Le, T. K. X.; von Woedtke, T.; Bussiahn, R.; Weltmann, K.-D.; Khalili, R.; Podmelle, F., Scar formation of laser skin lesions after cold atmospheric pressure plasma (CAP) treatment: A clinical long term observation. *Clinical Plasma Medicine* 1 (1), (2013), 30-35.
44. Brehmer, F.; Haenssle, H. A.; Daeschlein, G.; Ahmed, R.; Pfeiffer, S.; Gorlitz, A.; Simon, D.; Schon, M. P.; Wandke, D.; Emmert, S., Alleviation of chronic venous leg ulcers with a hand-held dielectric barrier discharge plasma generator (PlasmaDerm((R)) VU-2010): results of a monocentric, two-armed, open, prospective, randomized and controlled trial (NCT01415622). *J Eur Acad Dermatol Venereol* 29 (1), (2015), 148-55.
45. Klebes, M.; Ulrich, C.; Kluschke, F.; Patzelt, A.; Vandersee, S.; Richter, H.; Bob, A.; von Hutten, J.; Krediet, J. T.; Kramer, A.; Lademann, J.; Lange-Asschenfeld, B., Combined antibacterial effects of tissue-tolerable plasma and a modern conventional liquid antiseptic on chronic wound treatment. *J Biophotonics* 8 (5), (2015), 382-91.
46. Reuter, S.; von Woedtke, T.; Weltmann, K. D., The kINPen-a review on physics and chemistry of the atmospheric pressure plasma jet and its applications. *J Phys D Appl Phys* 51 (23), (2018).
47. Lu, X.; Laroussi, M.; Puech, V., On atmospheric-pressure non-equilibrium plasma jets and plasma bullets. *Plasma Sources Science & Technology* 21 (3), (2012).
48. von Woedtke, T.; Reuter, S.; Masur, K.; Weltmann, K. D., Plasmas for medicine. *Physics Reports* 530 (4), (2013), 291-320.
49. Reuter, S.; Winter, J.; Iseni, S.; Schmidt-Bleker, A.; Dunnbier, M.; Masur, K.; Wende, K.; Weltmann, K. D., The Influence of Feed Gas Humidity Versus Ambient Humidity on Atmospheric Pressure Plasma Jet-Effluent Chemistry and Skin Cell Viability. *IEEE T Plasma Sci* 43 (9), (2015), 3185-3192.
50. Schmidt-Bleker, A.; Winter, J.; Iseni, S.; Dunnbier, M.; Weltmann, K. D.; Reuter, S., Reactive species output of a plasma jet with a shielding gas device-combination of FTIR absorption spectroscopy and gas phase modelling. *J Phys D Appl Phys* 47 (14), (2014), 145201.
51. Schmidt-Bleker, A.; Bansemer, R.; Reuter, S.; Weltmann, K.-D., How to produce an NO_x-instead of Ox-based chemistry with a cold atmospheric plasma jet. *Plasma Processes and Polymers* 13 (11), (2016), 1120-1127.
52. Golda, J.; Held, J.; Redeker, B.; Konkowski, M.; Beijer, P.; Sobota, A.; Kroesen, G.; Braithwaite, N. S. J.; Reuter, S.; Turner, M. M.; Gans, T.; O'Connell, D.; Schulz-von der Gathen, V., Concepts and characteristics of the 'COST Reference Microplasma Jet'. *Journal of Physics D: Applied Physics* 49 (8), (2016), 084003.
53. Ellerweg, D.; von Keudell, A.; Benedikt, J., Unexpected O and O₃production in the effluent of He/O₂microplasma jets emanating into ambient air. *Plasma Sources Sci T* 21 (3), (2012), 034019.
54. Ellerweg, D.; Benedikt, J.; von Keudell, A.; Knake, N.; Schulz-von der Gathen, V., Characterization of the effluent of a He/O₂microscale atmospheric pressure plasma jet by quantitative molecular beam mass spectrometry. *New Journal of Physics* 12 (1), (2010), 013021.
55. Reuter, S.; Winter, J.; Schmidt-Bleker, A.; Schroeder, D.; Lange, H.; Knake, N.; Schulz-von der Gathen, V.; Weltmann, K. D., Atomic oxygen in a cold argon plasma jet: TALIF

- spectroscopy in ambient air with modelling and measurements of ambient species diffusion. *Plasma Sources Science & Technology* 21 (2), (2012), 024005 %&.
56. Reuter, S.; Winter, J.; Iseni, S.; Peters, S.; Schmidt-Bleker, A.; Dunnbier, M.; Schafer, J.; Foest, R.; Weltmann, K. D., Detection of ozone in a MHz argon plasma bullet jet. *Plasma Sources Science & Technology* 21 (3), (2012), 034015.
 57. Iseni, S.; Zhang, S.; van Gessel, A. F. H.; Hofmann, S.; van Ham, B. T. J.; Reuter, S.; Weltmann, K. D.; Bruggeman, P. J., Nitric oxide density distributions in the effluent of an RF argon APPJ: effect of gas flow rate and substrate. *New Journal of Physics* 16 (12), (2014), 123011.
 58. Murakami, T.; Niemi, K.; Gans, T.; O'Connell, D.; Graham, W. G., Chemical kinetics and reactive species in atmospheric pressure helium–oxygen plasmas with humid-air impurities. *Plasma Sources Sci T* 22 (1), (2012).
 59. Waskoenig, J.; Niemi, K.; Knake, N.; Graham, L. M.; Reuter, S.; Schulz-von der Gathen, V.; Gans, T., Atomic oxygen formation in a radio-frequency driven micro-atmospheric pressure plasma jet. *Plasma Sources Science & Technology* 19 (4), (2010), 045018.
 60. Schmidt-Bleker, A.; Winter, J.; Bosel, A.; Reuter, S.; Weltmann, K. D., On the plasma chemistry of a cold atmospheric argon plasma jet with shielding gas device. *Plasma Sources Science & Technology* 25 (1), (2016), 015005.
 61. Winter, J.; Tresp, H.; Hammer, M. U.; Iseni, S.; Kupsch, S.; Schmidt-Bleker, A.; Wende, K.; Dunnbier, M.; Masur, K.; Weltmann, K. D.; Reuter, S., Tracking plasma generated H₂O₂ from gas into liquid phase and revealing its dominant impact on human skin cells. *J Phys D Appl Phys* 47 (28), (2014).
 62. Klose, S. J.; Manfred, K. M.; Norman, H. C.; Ritchie, G. A. D.; van Helden, J. H., The spatial distribution of HO₂ in an atmospheric pressure plasma jet investigated by cavity ring-down spectroscopy. *Plasma Sources Sci T* 29 (8), (2020).
 63. Reuter, S.; Winter, J.; Schmidt-Bleker, A.; Tresp, H.; Hammer, M. U.; Weltmann, K. D., Controlling the Ambient Air Affected Reactive Species Composition in the Effluent of an Argon Plasma Jet. *IEEE T Plasma Sci* 40 (11), (2012), 2788-2794.
 64. Boehm, D.; Bourke, P., Safety implications of plasma-induced effects in living cells - a review of in vitro and in vivo findings. *Biol Chem* 400 (1), (2018), 3-17.
 65. Winter, J.; Wende, K.; Masur, K.; Iseni, S.; Dunnbier, M.; Hammer, M. U.; Tresp, H.; Weltmann, K. D.; Reuter, S., Feed gas humidity: a vital parameter affecting a cold atmospheric-pressure plasma jet and plasma-treated human skin cells. *J Phys D Appl Phys* 46 (29), (2013).
 66. Schmidt, A.; Bekeschus, S.; Jablonowski, H.; Barton, A.; Weltmann, K. D.; Wende, K., Role of Ambient Gas Composition on Cold Physical Plasma-Elicited Cell Signaling in Keratinocytes. *Biophys J* 112 (11), (2017), 2397-2407.
 67. Kapaldo, J.; Han, X.; Ptasinska, S., Shielding-gas-controlled atmospheric pressure plasma jets: Optical emission, reactive oxygen species, and the effect on cancer cells. *Plasma Processes and Polymers* 16 (5), (2019).
 68. Bekeschus, S.; Moritz, J.; Helfrich, I.; Boeckmann, L.; Weltmann, K.-D.; Emmert, S.; Metelmann, H.-R.; Stoffels, I.; von Woedtke, T., Ex Vivo Exposure of Human Melanoma Tissue to Cold Physical Plasma Elicits Apoptosis and Modulates Inflammation. *Applied Sciences* 10 (6), (2020), 1971.

69. Bauer, G.; Sersenová, D.; Graves, D. B.; Machala, Z., Cold Atmospheric Plasma and Plasma-Activated Medium Trigger RONS-Based Tumor Cell Apoptosis. *Scientific Reports* 9 (1), (2019), 14210.
70. Semmler, M. L.; Bekeschus, S.; Schafer, M.; Bernhardt, T.; Fischer, T.; Witzke, K.; Seebauer, C.; Rebl, H.; Grambow, E.; Vollmar, B.; Nebe, J. B.; Metelmann, H. R.; Woedtke, T. V.; Emmert, S.; Boeckmann, L., Molecular Mechanisms of the Efficacy of Cold Atmospheric Pressure Plasma (CAP) in Cancer Treatment. *Cancers (Basel)* 12 (2), (2020).
71. Bekeschus, S.; Lippert, M.; Diepold, K.; Chiosis, G.; Seufferlein, T.; Azoitei, N., Physical plasma-triggered ROS induces tumor cell death upon cleavage of HSP90 chaperone. *Sci Rep* 9 (1), (2019), 4112.
72. Bekeschus, S.; Clemen, R.; Niessner, F.; Sagwal, S. K.; Freund, E.; Schmidt, A., Medical Gas Plasma Jet Technology Targets Murine Melanoma in an Immunogenic Fashion. *Adv Sci (Weinh)* 7 (10), (2020), 1903438.
73. Schuster, M.; Seebauer, C.; Rutkowski, R.; Hauschild, A.; Podmelle, F.; Metelmann, C.; Metelmann, B.; von Woedtke, T.; Hasse, S.; Weltmann, K. D.; Metelmann, H. R., Visible tumor surface response to physical plasma and apoptotic cell kill in head and neck cancer. *J Craniomaxillofac Surg* 44 (9), (2016), 1445-52.
74. Metelmann, H.-R.; NedreLOW, D. S.; Seebauer, C.; Schuster, M.; von Woedtke, T.; Weltmann, K.-D.; Kindler, S.; Metelmann, P. H.; Finkelstein, S. E.; Von Hoff, D. D.; Podmelle, F., Head and neck cancer treatment and physical plasma. *Clinical Plasma Medicine* 3 (1), (2015), 17-23.
75. Metelmann, H.-R.; Seebauer, C.; Miller, V.; Fridman, A.; Bauer, G.; Graves, D. B.; Pouvesle, J.-M.; Rutkowski, R.; Schuster, M.; Bekeschus, S.; Wende, K.; Masur, K.; Hasse, S.; Gerling, T.; Hori, M.; Tanaka, H.; Ha Choi, E.; Weltmann, K.-D.; Metelmann, P. H.; Von Hoff, D. D.; Woedtke, T. v., Clinical experience with cold plasma in the treatment of locally advanced head and neck cancer. *Clinical Plasma Medicine* 9, (2018), 6-13.
76. Wirtz, M.; Stoffels, I.; Dissemond, J.; Schadendorf, D.; Roesch, A., Actinic keratoses treated with cold atmospheric plasma. *J Eur Acad Dermatol Venereol* 32 (1), (2018), e37-e39.
77. Seebauer, C.; Hasse, S.; Segebarth, M.; Bekeschus, S.; von Woedtke, T.; Weltmann, K.-D.; Schuster, M.; Rutkowski, R.; Metelmann, H.-R., Cold Atmospheric Plasma for the treatment of Oral Lichen Planus as intraoral precancerous lesion. *Clinical Plasma Medicine* 9, (2018), 44-45.
78. Pasqual-Melo, G.; Sagwal, S. K.; Freund, E.; Gandhirajan, R. K.; Frey, B.; von Woedtke, T.; Gaipf, U.; Bekeschus, S., Combination of Gas Plasma and Radiotherapy Has Immunostimulatory Potential and Additive Toxicity in Murine Melanoma Cells in Vitro. *Int J Mol Sci* 21 (4), (2020).
79. Sagwal, S. K.; Pasqual-Melo, G.; Bodnar, Y.; Gandhirajan, R. K.; Bekeschus, S., Combination of chemotherapy and physical plasma elicits melanoma cell death via upregulation of SLC22A16. *Cell Death Dis* 9 (12), (2018), 1179.
80. Gandhirajan, R. K.; Rodder, K.; Bodnar, Y.; Pasqual-Melo, G.; Emmert, S.; Griguer, C. E.; Weltmann, K. D.; Bekeschus, S., Cytochrome C oxidase Inhibition and Cold Plasma-derived Oxidants Synergize in Melanoma Cell Death Induction. *Sci Rep* 8 (1), (2018), 12734.

81. Schmidt, A.; Bekeschus, S.; Jarick, K.; Hasse, S.; von Woedtke, T.; Wende, K., Cold Physical Plasma Modulates p53 and Mitogen-Activated Protein Kinase Signaling in Keratinocytes. *Oxid Med Cell Longev* 2019, (2019), 7017363.
82. Barton, A.; Wende, K.; Bundscherer, L.; Hasse, S.; Schmidt, A.; Bekeschus, S.; Weltmann, K.-D.; Lindequist, U.; Masur, K., Nonthermal Plasma Increases Expression of Wound Healing Related Genes in a Keratinocyte Cell Line. *Plasma Medicine* 3 (1-2), (2013), 125-136.
83. Schmidt, A.; Bekeschus, S., Redox for Repair: Cold Physical Plasmas and Nrf2 Signaling Promoting Wound Healing. *Antioxidants (Basel)* 7 (10), (2018).
84. Bernhardt, T.; Semmler, M. L.; Schafer, M.; Bekeschus, S.; Emmert, S.; Boeckmann, L., Plasma Medicine: Applications of Cold Atmospheric Pressure Plasma in Dermatology. *Oxid Med Cell Longev* 2019, (2019), 3873928.
85. Bekeschus, S.; Schmidt, A.; Weltmann, K.-D.; von Woedtke, T., The plasma jet kINPen – A powerful tool for wound healing. *Clinical Plasma Medicine* 4 (1), (2016), 19-28.
86. Lackmann, J. W.; Baldus, S.; Steinborn, E.; Edengeiser, E.; Kogelheide, F.; Langklotz, S.; Schneider, S.; Leichert, L. I. O.; Benedikt, J.; Awakowicz, P.; Bandow, J. E., A dielectric barrier discharge terminally inactivates RNase A by oxidizing sulfur-containing amino acids and breaking structural disulfide bonds. *J Phys D Appl Phys* 48 (49), (2015).
87. Lackmann, J.-W.; Edengeiser, E.; Schneider, S.; Benedikt, J.; Havenith, M.; Bandow, J. E., Effects of the Effluent of a Microscale Atmospheric Pressure Plasma-jet Operated with He/O₂ Gas on Bovine Serum Albumin. *Plasma Medicine* 3 (1-2), (2013), 115-124.
88. Lackmann, J. W.; Bandow, J. E., Inactivation of microbes and macromolecules by atmospheric-pressure plasma jets. *Appl Microbiol Biotechnol* 98 (14), (2014), 6205-13.
89. Striesow, J.; Lackmann, J. W.; Ni, Z.; Wenske, S.; Weltmann, K. D.; Fedorova, M.; von Woedtke, T.; Wende, K., Oxidative modification of skin lipids by cold atmospheric plasma (CAP): A standardizable approach using RP-LC/MS(2) and DI-ESI/MS(2). *Chem Phys Lipids* 226, (2020), 104786.
90. Wenske, S.; Lackmann, J.-W.; Bekeschus, S.; Weltmann, K.-D.; Von Woedtke, T.; Wende, K., Non-enzymatic post-translational modifications in peptides by cold plasma-derived reactive oxygen and nitrogen species. *Biointerphases*, (2020).
91. Marschewski, M.; Hirschberg, J.; Omairi, T.; Hofft, O.; Viol, W.; Emmert, S.; Maus-Friedrichs, W., Electron spectroscopic analysis of the human lipid skin barrier: cold atmospheric plasma-induced changes in lipid composition. *Exp Dermatol* 21 (12), (2012), 921-5.
92. Isbary, G.; Morfill, G.; Zimmermann, J.; Shimizu, T.; Stolz, W., Cold atmospheric plasma: a successful treatment of lesions in Hailey-Hailey disease. *Arch Dermatol* 147 (4), (2011), 388-90.
93. Clemen, R.; Bekeschus, S., Oxidatively Modified Proteins: Cause and Control of Diseases. *Applied Sciences* 10 (18), (2020).
94. Zhou, R.; Zhou, R.; Zhuang, J.; Zong, Z.; Zhang, X.; Liu, D.; Bazaka, K.; Ostrikov, K., Interaction of Atmospheric-Pressure Air Microplasmas with Amino Acids as Fundamental Processes in Aqueous Solution. *PLoS One* 11 (5), (2016), e0155584.
95. Takai, E.; Kitamura, T.; Kuwabara, J.; Ikawa, S.; Yoshizawa, S.; Shiraki, K.; Kawasaki, H.; Arakawa, R.; Kitano, K., Chemical modification of amino acids by atmospheric-pressure cold plasma in aqueous solution. *J Phys D Appl Phys* 47 (28), (2014), 285403.

96. Lackmann, J. W.; Schneider, S.; Edengeiser, E.; Jarzina, F.; Brinckmann, S.; Steinborn, E.; Havenith, M.; Benedikt, J.; Bandow, J. E., Photons and particles emitted from cold atmospheric-pressure plasma inactivate bacteria and biomolecules independently and synergistically. *Journal of the Royal Society, Interface / the Royal Society* 10 (89), (2013), 20130591.
97. Schneider, S.; Dunnbier, M.; Hubner, S.; Reuter, S.; Benedikt, J., Atomic nitrogen: a parameter study of a micro-scale atmospheric pressure plasma jet by means of molecular beam mass spectrometry. *J Phys D Appl Phys* 47 (50), (2014), 505203.
98. Iseni, S.; Reuter, S.; Weltmann, K. D., NO₂ dynamics of an Ar/Air plasma jet investigated by in situ quantum cascade laser spectroscopy at atmospheric pressure. *J Phys D Appl Phys* 47 (7), (2014), 075203.
99. Iseni, S.; Bruggeman, P. J.; Weltmann, K.-D.; Reuter, S., Nitrogen metastable (N₂(A³Σ⁺)) in a cold argon atmospheric pressure plasma jet: Shielding and gas composition. *Appl Phys Lett* 108 (18), (2016), 184101.
100. Yan, D. Y.; Xiao, H. J.; Zhu, W.; Nourmohammadi, N.; Zhang, L. G.; Bian, K.; Keidar, M., The role of aquaporins in the anti-glioblastoma capacity of the cold plasma-stimulated medium. *J Phys D Appl Phys* 50 (5), (2017), 055401.
101. Bienert, G. P.; Chaumont, F., Aquaporin-facilitated transmembrane diffusion of hydrogen peroxide. *Biochim Biophys Acta* 1840 (5), (2014), 1596-604.
102. Winterbourn, C. C., Reconciling the chemistry and biology of reactive oxygen species. *Nat Chem Biol* 4 (5), (2008), 278-86.
103. Carey, V. P.; Wemhoff, A. P., Relationships among liquid-vapor interfacial region properties: Predictions of a thermodynamic model. *International Journal of Thermophysics* 25 (3), (2004), 753-786.
104. Garrett, B. C.; Schenter, G. K.; Morita, A., Molecular simulations of the transport of molecules across the liquid/vapor interface of water. *Chem Rev* 106 (4), (2006), 1355-74.
105. Verlackt, C. C. W.; Van Boxem, W.; Bogaerts, A., Transport and accumulation of plasma generated species in aqueous solution. *Phys Chem Chem Phys* 20 (10), (2018), 6845-6859.
106. Zoschke, K.; Bornick, H.; Worch, E., Vacuum-UV radiation at 185 nm in water treatment—a review. *Water Res* 52, (2014), 131-45.
107. Mikkelsen, R. B.; Wardman, P., Biological chemistry of reactive oxygen and nitrogen and radiation-induced signal transduction mechanisms. *Oncogene* 22 (37), (2003), 5734-54.
108. Pattison, D. I.; Davies, M. J., Actions of ultraviolet light on cellular structures. *EXS* (96), (2006), 131-57.
109. Pattison, D. I.; Rahmanto, A. S.; Davies, M. J., Photo-oxidation of proteins. *Photochem Photobiol Sci* 11 (1), (2012), 38-53.
110. Van Boxem, W.; Van der Paal, J.; Deben, C.; Verlackt, C. C. W.; Smits, E.; Bogaerts, A., Gaining Insight In The Selectivity And Plasma-Liquid Chemistry For Plasma Treatment Of Cancer. *Clinical Plasma Medicine* 9, (2018), 30.
111. Gorbanev, Y.; Verlackt, C. C. W.; Tinck, S.; Tuenter, E.; Foubert, K.; Cos, P.; Bogaerts, A., Combining experimental and modelling approaches to study the sources of reactive species induced in water by the COST RF plasma jet. *Phys Chem Chem Phys* 20 (4), (2018), 2797-2808.

112. Boehm, D.; Curtin, J.; Cullen, P. J.; Bourke, P., Hydrogen peroxide and beyond - the potential of high-voltage plasma-activated liquids against cancerous cells. *Anticancer Agents Med Chem*, (2017).
113. Girard, P. M.; Arbabian, A.; Fleury, M.; Bauville, G.; Puech, V.; Dutreix, M.; Sousa, J. S., Synergistic Effect of H₂O₂ and NO₂ in Cell Death Induced by Cold Atmospheric He Plasma. *Sci Rep* 6, (2016), 29098.
114. Jablonowski, H.; Bussiahn, R.; Hammer, M. U.; Weltmann, K.-D.; von Woedtke, T.; Reuter, S., Impact of plasma jet vacuum ultraviolet radiation on reactive oxygen species generation in bio-relevant liquids. *Physics of Plasmas* 22 (12), (2015), 122008.
115. Jablonowski, H.; Santos Sousa, J.; Weltmann, K. D.; Wende, K.; Reuter, S., Quantification of the ozone and singlet delta oxygen produced in gas and liquid phases by a non-thermal atmospheric plasma with relevance for medical treatment. *Sci Rep* 8 (1), (2018), 12195.
116. Jablonowski, H.; Schmidt-Bleker, A.; Weltmann, K. D.; von Woedtke, T.; Wende, K., Non-touching plasma-liquid interaction - where is aqueous nitric oxide generated? *Phys Chem Chem Phys* 20 (39), (2018), 25387-25398.
117. Gorbanev, Y.; O'Connell, D.; Chechik, V., Non-Thermal Plasma in Contact with Water: The Origin of Species. *Chemistry* 22 (10), (2016), 3496-3505.
118. Paulsen, C. E.; Carroll, K. S., Cysteine-mediated redox signaling: chemistry, biology, and tools for discovery. *Chem Rev* 113 (7), (2013), 4633-79.
119. Conte, M. L.; Carroll, K. S., The chemistry of thiol oxidation and detection. In *Oxidative stress and redox regulation*, Springer: 2013; pp 1-42.
120. Reddie, K. G.; Carroll, K. S., Expanding the functional diversity of proteins through cysteine oxidation. *Curr Opin Chem Biol* 12 (6), (2008), 746-54.
121. Gupta, V.; Carroll, K. S., Sulfenic acid chemistry, detection and cellular lifetime. *Biochim Biophys Acta* 1840 (2), (2014), 847-75.
122. Sharma, V. K.; Graham, N. J. D., Oxidation of Amino Acids, Peptides and Proteins by Ozone: A Review. *Ozone-Sci Eng* 32 (2), (2010), 81-90.
123. Gilbert, E.; Hodenberg, S. v., Ozonation Of Sulfur-Containing Aliphatic Compounds In Aqueous Solutions. II. Cysteine, Cystine and Thioglycolic Acid. *Ozone: Science & Engineering* 19 (2), (1997), 145-156.
124. Lackmann, J. W.; Wende, K.; Verlackt, C.; Golda, J.; Volzke, J.; Kogelheide, F.; Held, J.; Bekeschus, S.; Bogaerts, A.; Schulz-von der Gathen, V.; Stapelmann, K., Chemical fingerprints of cold physical plasmas - an experimental and computational study using cysteine as tracer compound. *Sci Rep* 8 (1), (2018), 7736.
125. Trujillo, M.; Alvarez, B.; Radi, R., One- and two-electron oxidation of thiols: mechanisms, kinetics and biological fates. *Free Radic Res* 50 (2), (2016), 150-71.
126. Lizarbe, T. R.; Garcia-Rama, C.; Tarin, C.; Saura, M.; Calvo, E.; Lopez, J. A.; Lopez-Otin, C.; Folgueras, A. R.; Lamas, S.; Zaragoza, C., Nitric oxide elicits functional MMP-13 protein-tyrosine nitration during wound repair. *Faseb J* 22 (9), (2008), 3207-15.
127. Yakovlev, V. A.; Bayden, A. S.; Graves, P. R.; Kellogg, G. E.; Mikkelsen, R. B., Nitration of the tumor suppressor protein p53 at tyrosine 327 promotes p53 oligomerization and activation. *Biochemistry* 49 (25), (2010), 5331-9.
128. Carballal, S.; Bartesaghi, S.; Radi, R., Kinetic and mechanistic considerations to assess the biological fate of peroxyxynitrite. *Biochim Biophys Acta* 1840 (2), (2014), 768-80.

129. Ferrer-Sueta, G.; Campolo, N.; Trujillo, M.; Bartesaghi, S.; Carballal, S.; Romero, N.; Alvarez, B.; Radi, R., Biochemistry of Peroxynitrite and Protein Tyrosine Nitration. *Chem Rev* *118* (3), (2018), 1338-1408.
130. Schmidt-Bleker, A.; Norberg, S. A.; Winter, J.; Johnsen, E.; Reuter, S.; Weltmann, K. D.; Kushner, M. J., Propagation mechanisms of guided streamers in plasma jets: the influence of electronegativity of the surrounding gas. *Plasma Sources Science & Technology* *24* (3), (2015), 035022.
131. Sousa, J. S.; Niemi, K.; Cox, L. J.; Algwari, Q. T.; Gans, T.; O'Connell, D., Cold atmospheric pressure plasma jets as sources of singlet delta oxygen for biomedical applications. *J Appl Phys* *109* (12), (2011), 123302.
132. Klose, S.-J.; Gianella, M.; Reuter, S.; Press, S. A.; Aguila, A. L.; Manfred, K.; Schmidt-Bleker, A.; Ritchie, G. A. D.; van Helden, J.-P. H., On the Chemical Kinetics of HO₂ in a Cold Atmospheric Plasma Jet. In *Light, Energy and the Environment 2018 (E2, FTS, HISE, SOLAR, SSL)*, 2018.
133. Pavlovich, M. J.; Chang, H. W.; Sakiyama, Y.; Clark, D. S.; Graves, D. B., Ozone correlates with antibacterial effects from indirect air dielectric barrier discharge treatment of water. *J Phys D Appl Phys* *46* (14), (2013), 145202.
134. Cuerda-Correa, E. M.; Alexandre-Franco, M. F.; Fernández-González, C., Advanced Oxidation Processes for the Removal of Antibiotics from Water. An Overview. *Water* *12* (1), (2019).
135. Peyton, G. R.; Glaze, W. H., Destruction of pollutants in water with ozone in combination with ultraviolet radiation. 3. Photolysis of aqueous ozone. *Environ Sci Technol* *22* (7), (1988), 761-7.
136. Benedikt, J.; Mokhtar Hefny, M.; Shaw, A.; Buckley, B. R.; Iza, F.; Schakermann, S.; Bandow, J. E., The fate of plasma-generated oxygen atoms in aqueous solutions: non-equilibrium atmospheric pressure plasmas as an efficient source of atomic O(aq). *Phys Chem Chem Phys* *20* (17), (2018), 12037-12042.
137. Robl, S.; Worner, M.; Maier, D.; Braun, A. M., Formation of hydrogen peroxide by VUV-photolysis of water and aqueous solutions with methanol. *Photochem Photobiol Sci* *11* (6), (2012), 1041-50.
138. Sander, R., Compilation of Henry's law constants (version 4.0) for water as solvent. *Atmos Chem Phys* *15* (8), (2015), 4399-4981.
139. Enescu, M.; Cardey, B., Mechanism of cysteine oxidation by a hydroxyl radical: a theoretical study. *Chemphyschem* *7* (4), (2006), 912-9.
140. Omlid, S. M.; Zhang, M.; Isor, A.; McCulla, R. D., Thiol Reactivity toward Atomic Oxygen Generated during the Photodeoxygenation of Dibenzothiophene S-Oxide. *J Org Chem* *82* (24), (2017), 13333-13341.
141. Zhang, M.; Ravilious, G. E.; Hicks, L. M.; Jez, J. M.; McCulla, R. D., Redox switching of adenosine-5'-phosphosulfate kinase with photoactivatable atomic oxygen precursors. *J Am Chem Soc* *134* (41), (2012), 16979-82.
142. Devasagayam, T. P. A.; Sundquist, A. R.; Di Mascio, P.; Kaiser, S.; Sies, H., Activity of thiols as singlet molecular oxygen quenchers. *Journal of Photochemistry and Photobiology B: Biology* *9* (1), (1991), 105-116.
143. Rougee, M.; Bensasson, R. V.; Land, E. J.; Pariente, R., Deactivation of singlet molecular oxygen by thiols and related compounds, possible protectors against skin photosensitivity. *Photochem Photobiol* *47* (4), (1988), 485-9.

144. Omlid, S. M.; Dergunov, S. A.; Isor, A.; Sulkowski, K. L.; Petroff, J. T.; Pinkhassik, E.; McCulla, R. D., Evidence for diffusing atomic oxygen uncovered by separating reactants with a semi-permeable nanocapsule barrier. *Chem Commun* 55 (12), (2019), 1706-1709.
145. Khan, A. U.; Wilson, T., Reactive Oxygen Species as Cellular Messengers. *Chemistry & Biology* 2 (7), (1995), 437-445.
146. Lackmann, J. W.; Bruno, G.; Jablonowski, H.; Kogelheide, F.; Offerhaus, B.; Held, J.; Schulz-von der Gathen, V.; Stapelmann, K.; von Woedtke, T.; Wende, K., Nitrosylation vs. oxidation - How to modulate cold physical plasmas for biological applications. *PLoS One* 14 (5), (2019), e0216606.
147. Quiller, R. G.; Baker, T. A.; Deng, X.; Colling, M. E.; Min, B. K.; Friend, C. M., Transient hydroxyl formation from water on oxygen-covered Au(111). *J Chem Phys* 129 (6), (2008), 064702.
148. Jiang, P.; Chi, X.; Zhu, Q.; Cheng, M.; Gao, H., Strong and selective isotope effect in the vacuum ultraviolet photodissociation branching ratios of carbon monoxide. *Nat Commun* 10 (1), (2019), 3175.
149. Yusupov, M.; Neyts, E. C.; Simon, P.; Berdiyrov, G.; Snoeckx, R.; van Duin, A. C. T.; Bogaerts, A., Reactive molecular dynamics simulations of oxygen species in a liquid water layer of interest for plasma medicine. *J Phys D Appl Phys* 47 (2), (2014), 025205.
150. Dobrynin, D.; Fridman, G.; Friedman, G.; Fridman, A., Physical and biological mechanisms of direct plasma interaction with living tissue. *New Journal of Physics* 11 (11), (2009), 115020.
151. Zhou, R.; Zhou, R.; Prasad, K.; Fang, Z.; Speight, R.; Bazaka, K.; Ostrikov, K., Cold atmospheric plasma activated water as a prospective disinfectant: the crucial role of peroxyxynitrite. *Green Chemistry* 20 (23), (2018), 5276-5284.
152. Naïtali, M.; Herry, J.-M.; Hnatiuc, E.; Kamgang, G.; Brisset, J.-L., Kinetics and Bacterial Inactivation Induced by Peroxyxynitrite in Electric Discharges in Air. *Plasma Chemistry and Plasma Processing* 32 (4), (2012), 675-692.
153. Ulrich, C.; Kluschke, F.; Patzelt, A.; Vandersee, S.; Czaika, V. A.; Richter, H.; Bob, A.; von Hutten, J.; Painsi, C.; Hugel, R.; Kramer, A.; Assadian, O.; Lademann, J.; Lange-Asschenfeldt, B., Clinical use of cold atmospheric pressure argon plasma in chronic leg ulcers: A pilot study. *Journal of Wound Care* 24 (5), (2015), 196-203.
154. Emmert, S.; Brehmer, F.; Haenßle, H.; Helmke, A.; Mertens, N.; Ahmed, R.; Simon, D.; Wandke, D.; Maus-Friedrichs, W.; Daeschlein, G.; Schoen, M. P.; Vioel, W., Atmospheric pressure plasma in dermatology: Ulcus treatment and much more. *Clinical Plasma Medicine* 1 (1), (2013), 24-29.
155. van Gils, C. A. J.; Hofmann, S.; Boekema, B. K. H. L.; Brandenburg, R.; Bruggeman, P. J., Mechanisms of bacterial inactivation in the liquid phase induced by a remote RF cold atmospheric pressure plasma jet. *Journal of Physics D: Applied Physics* 46 (17), (2013), 175203.
156. Bekeschus, S.; Freund, E.; Spadola, C.; Privat-Maldonado, A.; Hackbarth, C.; Bogaerts, A.; Schmidt, A.; Wende, K.; Weltmann, K. D.; von Woedtke, T.; Heidecke, C. D.; Partecke, L. I.; Kading, A., Risk Assessment of kINPen Plasma Treatment of Four Human Pancreatic Cancer Cell Lines with Respect to Metastasis. *Cancers (Basel)* 11 (9), (2019).
157. Bekeschus, S.; von Woedtke, T.; Weltmann, K.-D.; Metelmann, H.-R., Plasma, Cancer, Immunity. *Clinical Plasma Medicine* 9, (2018), 13-14.

158. Bekeschus, S.; Favia, P.; Robert, E.; von Woedtke, T., White paper on plasma for medicine and hygiene: Future in plasma health sciences. *Plasma Processes and Polymers* 16 (1), (2019), 1800033.
159. Shekhter, A. B.; Pekshev, A. V.; Vagapov, A. B.; Butenko, A. V.; Fayzullin, A. L.; Rudenko, T. G.; Sharapov, N. A.; Serejnikova, N. B.; Vasilets, V. N., Dose-dependent effect of plasma-chemical NO-containing gas flow on wound healing. An experimental study. *Clinical Plasma Medicine* 19-20, (2020).
160. Zeida, A.; Gonzalez Lebrero, M. C.; Radi, R.; Trujillo, M.; Estrin, D. A., Mechanism of cysteine oxidation by peroxyxynitrite: An integrated experimental and theoretical study. *Arch Biochem Biophys* 539 (1), (2013), 81-6.
161. Kharitonov, V. G.; Sundquist, A. R.; Sharma, V. S., Kinetics of nitrosation of thiols by nitric oxide in the presence of oxygen. *J Biol Chem* 270 (47), (1995), 28158-64.
162. Olson, L. P.; Bartberger, M. D.; Houk, K. N., Peroxynitrate and peroxyxynitrite: a complete basis set investigation of similarities and differences between these NO_x species. *J Am Chem Soc* 125 (13), (2003), 3999-4006.
163. Lukes, P.; Dolezalova, E.; Sisrova, I.; Clupek, M., Aqueous-phase chemistry and bactericidal effects from an air discharge plasma in contact with water: evidence for the formation of peroxyxynitrite through a pseudo-second-order post-discharge reaction of H₂O₂ and HNO₂. *Plasma Sources Sci T* 23 (1), (2014), 015019.
164. Koppenol, W. H.; Moreno, J. J.; Pryor, W. A.; Ischiropoulos, H.; Beckman, J. S., Peroxyxynitrite, a cloaked oxidant formed by nitric oxide and superoxide. *Chem Res Toxicol* 5 (6), (1992), 834-42.
165. Ramezani, M. S.; Padmaja, S.; Koppenol, W. H., Nitration and hydroxylation of phenolic compounds by peroxyxynitrite. *Chem Res Toxicol* 9 (1), (1996), 232-40.
166. Sander, R., *Compilation of Henry's Law Constants for Inorganic and Organic Species of Potential Importance in Environmental Chemistry*. Max-Planck Institute of Chemistry, Air Chemistry Department Mainz, Germany: 1999.
167. Shilov, V. P.; Fedoseev, A. M., Role of peroxyxynitrite in oxidation of f-element ions in HNO₃ solutions. *Radiochemistry* 55 (4), (2013), 366-368.
168. Lobachev, V. L.; Rudakov, E. S., The chemistry of peroxyxynitrite. Reaction mechanisms and kinetics. *Usp Khim* 75 (5), (2006), 422-444.
169. Koppenol, W. H., The Reduction Potential of the Couple O₃ O₃⁻ - Consequences for Mechanisms of Ozone Toxicity. *Febs Letters* 140 (2), (1982), 169-172.
170. Murakami, T.; Niemi, K.; Gans, T.; Connell, D. O.; Graham, W. G., Afterglow chemistry of atmospheric-pressure helium-oxygen plasmas with humid air impurity. *Plasma Sources Science & Technology* 23 (2), (2014).
171. Schmidt-Bleker, A.; Reuter, S.; Weltmann, K. D., Quantitative schlieren diagnostics for the determination of ambient species density, gas temperature and calorimetric power of cold atmospheric plasma jets. *J Phys D Appl Phys* 48 (17), (2015), 175202.
172. Bruggeman, P.; Schram, D. C., On OH production in water containing atmospheric pressure plasmas. *Plasma Sources Science & Technology* 19 (4), (2010).
173. Stancampiano, A.; Galligani, T.; Gherardi, M.; Machala, Z.; Maguire, P.; Colombo, V.; Pouvesle, J. M.; Robert, E., Plasma and Aerosols: Challenges, Opportunities and Perspectives. *Appl Sci-Basel* 9 (18), (2019).
174. Giles, G. I.; Tasker, K. M.; Jacob, C., Oxidation of biological thiols by highly reactive disulfide-S-oxides. *Gen Physiol Biophys* 21 (1), (2002), 65-72.

175. Giles, G. I.; Nasim, M. J.; Ali, W.; Jacob, C., The Reactive Sulfur Species Concept: 15 Years On. *Antioxidants (Basel)* **6** (2), (2017), 38.
176. Sun, J.; Steenbergen, C.; Murphy, E., S-nitrosylation: NO-related redox signaling to protect against oxidative stress. *Antioxid Redox Signal* **8** (9-10), (2006), 1693-705.
177. Stamler, J. S.; Lamas, S.; Fang, F. C., Nitrosylation. the prototypic redox-based signaling mechanism. *Cell* **106** (6), (2001), 675-83.
178. Floyd, R. A.; Kotake, Y.; Towner, R. A.; Guo, W.-X.; Nakae, D.; Konishi, Y., Nitric Oxide and Cancer Development. *Journal of Toxicologic Pathology* **20** (2), (2007), 77-92.
179. Ischiropoulos, H., Biological selectivity and functional aspects of protein tyrosine nitration. *Biochem Biophys Res Commun* **305** (3), (2003), 776-83.
180. Giles, G. I.; Tasker, K. M.; Collins, C.; Giles, N. M.; O'Rourke, E.; Jacob, C., Reactive sulphur species: an in vitro investigation of the oxidation properties of disulphide S-oxides. *Biochem J* **364** (Pt 2), (2002), 579-85.
181. Kumar, A.; Dejanovic, B.; Hetsch, F.; Semtner, M.; Fusca, D.; Arjune, S.; Santamaria-Araujo, J. A.; Winkelmann, A.; Ayton, S.; Bush, A. I.; Kloppenburg, P.; Meier, J. C.; Schwarz, G.; Belaidi, A. A., S-sulfocysteine/NMDA receptor-dependent signaling underlies neurodegeneration in molybdenum cofactor deficiency. *J Clin Invest* **127** (12), (2017), 4365-4378.
182. Rubbo, H.; Radi, R., Protein and lipid nitration: role in redox signaling and injury. *Biochim Biophys Acta* **1780** (11), (2008), 1318-24.

6. Original publications

The present work is based on peer-reviewed articles published or submitted in international scientific journal. These are listed below together with the authors' contribution.

Article A1

K. Wende, G. Bruno, M. Lalk, K.-D. Weltmann, T. von Woedtke, S. Bekeschus, J.-W. Lackmann. "On a heavy path – determining cold plasma-derived short-lived species chemistry using isotopic labelling". *RSC Advances*, vol. 10, no. 20, pp. 11598-11607, 2020.

The experiment was designed by KW, JWL and GB. The measurements, data evaluation and visualization were performed by GB. The manuscript was written by GB, JWL and KW, and edited by all co-authors.

Article A2

J.-W. Lackmann & G. Bruno, H. Jablonowski, F. Kogelheide, B. Offerhaus, J. Held, V. S.-von der Gathen, K. Stapelmann, T. von Woedtke, K. Wende. "Nitrosylation vs. oxidation - How to modulate cold physical plasmas for biological applications". *PLoS One*, vol. 14, no. 5, p. e0216606, 2019.

The experiment was designed by JWL. The mass spectrometry analysis, ion chromatography and colorimetric assays were performed by GB. The EPR measurements were performed by HJ. The raman spectroscopy experiments were performed by JWL. The manuscript was written by GB and JWL, and edited by all co-authors.

Article A3

G. Bruno, S. Wenske, J.-L. Lackmann, M. Lalk, T. von Woedtke, K. Wende. "On the liquid chemistry of the reactive nitrogen species peroxynitrite and nitrogen dioxide generated by physical plasmas". *Biomolecules*, under revision, 2020.

The experiment was designed by GB and KW. The experiments and data evaluation were performed by GB, with the help of SW for the proteomics data elaboration. The manuscript was written by GB and edited by KW and JWL.

Article A4

G. Bruno, T. Heusler, J.-W. Lackmann, T. von Woedtke, K.-D. Weltmann, and K. Wende. "Cold physical plasma-induced oxidation of cysteine yields reactive sulfur species (RSS)". *Clinical Plasma Medicine*, vol. 14, p. 100083, 2019.

The experiment was designed by GB and KW. The experiments and data evaluation were performed by GB. The manuscript was written by GB and edited by KW.

Article A5

I. Sremački & G. Bruno, H. Jablonowski, C. Leys, A. Nikiforov, K. Wende. "Influence of aerosol injection on the liquid chemistry induced by an RF argon plasma jet". *Plasma Sources Science and Technology*, under revision, 2020.

The experiment was designed by KW, GB, IS. The experiments and data evaluation were performed by GB and IS. The manuscript was written by GB and IS, and edited by KW and AN.

Approved:

Date

Giuliana Bruno

Date

Prof. Dr. Michael Lalk

Article A1

On a heavy path – determining cold plasma-derived short-lived species chemistry using isotopic labelling

K. Wende, G. Bruno, M. Lalk, K.-D. Weltmann, T. von Woedtke, S. Bekeschus, J.-W. Lackmann. *RSC Advances*, vol. 10, no. 20, pp. 11598-11607, 2020.

© The Royal Society of Chemistry 2020

PAPER



Cite this: DOI: 10.1039/c9ra08745a

On a heavy path – determining cold plasma-derived short-lived species chemistry using isotopic labelling†

Kristian Wende,^{id}*^a Giuliana Bruno,^a Michael Lalk,^b Klaus-Dieter Weltmann,^c Thomas von Woedtke,^{id}^{cd} Sander Bekeschus^a and Jan-Wilm Lackmann^a

Cold atmospheric plasmas (CAPs) are promising medical tools and are currently applied in dermatology and epithelial cancers. While understanding of the biomedical effects is already substantial, knowledge on the contribution of individual ROS and RNS and the mode of activation of biochemical pathways is insufficient. Especially the formation and transport of short-lived reactive species in liquids remain elusive, a situation shared with other approaches involving redox processes such as photodynamic therapy. Here, the contribution of plasma-generated reactive oxygen species (ROS) in plasma liquid chemistry was determined by labeling these *via* admixing heavy oxygen $^{18}\text{O}_2$ to the feed gas or by using heavy water H_2^{18}O as a solvent for the bait molecule. The inclusion of heavy or light oxygen atoms by the labeled ROS into the different cysteine products was determined by mass spectrometry. While products like cysteine sulfonic acid incorporated nearly exclusively gas phase-derived oxygen species (atomic oxygen and/or singlet oxygen), a significant contribution of liquid phase-derived species (OH radicals) was observed for cysteine-S-sulfonate. The role, origin, and reaction mechanisms of short-lived species, namely hydroxyl radicals, singlet oxygen, and atomic oxygen, are discussed. Interactions of these species both with the target cysteine molecule as well as the interphase and the liquid bulk are taken into consideration to shed light onto several reaction pathways resulting in observed isotopic oxygen incorporation. These studies give valuable insight into underlying plasma–liquid interaction processes and are a first step to understand these interaction processes between the gas and liquid phase on a molecular level.

Received 24th October 2019
Accepted 25th February 2020

DOI: 10.1039/c9ra08745a

rsc.li/rsc-advances

Introduction

Cold atmospheric pressure plasmas (CAPs) have recently transitioned from laboratories to clinics, offering a safe and effective application directly to the patient's body.^{1–3} Major applications of medical plasmas are wounds, skin-derived diseases and, as off-label use, palliation in cancer patients.^{4–12} CAPs offer a well-documented efficacy in inactivating bacteria¹³ that may contribute to the stimulation of wound healing processes.^{14,15} Plasma treatment influences cell or tissue physiology at various levels, including metabolism, signaling, and

cell fate, leading to immunomodulation, angiogenesis, tissue proliferation, or migration.^{16–19} High intensity treatment results in the shutdown of cellular processes and cell death by apoptosis or necrosis-like processes.^{20,21} These effects, especially in combination with immune cell modulation, are currently investigated for cancer treatment.^{22–25}

Medical plasmas are multicomponent systems containing electrons, ions, electric fields, and a multiplicity of reactive oxygen and nitrogen species (ROS/RNS). Depending on plasma source, feed gas composition, and distance to the target, ROS/RNS generation varies.^{26–30} A major role of these plasma-derived ROS/RNS is assumed,^{31,32} but incongruity regarding the mode of action exists. It was argued that cell membrane-associated proteins pick up and translate the induced signals³³ or that species can cross the cell membrane using specific pore proteins³⁴ and trigger intracellular responses *via* cytosolic sensor proteins³⁵ or the mitochondria.³⁶ With regard to the lifetime of most reactive species described for CAPs, it must be acquiesced that only a small fraction can indeed diffuse into a cell or the cell's vicinity, leaving the question of the ultimate mechanism still open.^{37,38} With the controllability of plasma treatments in biomedical applications becoming increasingly

^aZIK Plasmatis, Leibniz Institute for Plasma Science and Technology (INP Greifswald), Felix-Hausdorff-Str. 2, Greifswald 17489, Germany. E-mail: jan-wilm.lackmann@inp-greifswald.de; kristian.wende@inp-greifswald.de

^bCellular Biochemistry & Metabolomics, University of Greifswald, Felix-Hausdorff-Str. 4, Greifswald 17487, Germany

^cLeibniz Institute for Plasma Science and Technology (INP Greifswald), Felix-Hausdorff-Str. 2, Greifswald 17489, Germany

^dInstitute for Hygiene and Environmental Medicine, Greifswald University Medical Center, Walther-Rathenau-Str. 48, Greifswald 17489, Germany

† Electronic supplementary information (ESI) available. See DOI: 10.1039/c9ra08745a

relevant to improve safety and efficacy,³⁹ knowledge of the relevant players in plasma–target interaction, their respective trajectories and – most importantly – their (bio) chemistry is mandatory. It can be concluded that another route of interplay between the plasma-derived species and the biological system is the covalent modification of biomolecules and the subsequent change of their activity or biological value. It has been shown that plasma-derived ROS/RNS are capable of oxidizing amino acids,⁴⁰ proteins,^{41–45} or lipids.^{46,47} Thiol groups are one of the major targets for plasma-generated species.^{48–50} Hence, CAP impact can yield to (non-enzymatic) post-translational modifications (PTMs), with some of which transport significant influence in cellular signaling.^{51–54} However, so far no specific member of the various ROS or RNS could be attributed to be the major driver of these reactions. One of the reasons is the limited knowledge that is present on plasma-derived liquid chemistry. Hydrogen peroxide is a frequently reported product of the plasma liquid interaction, yet its reactivity is too low to oxidize biomolecules significantly ($E_{\text{O}} = 1.35 \text{ V}$, $\text{H}_2\text{O}_2 + 2\text{H}^+ + 2\text{e}^- \rightleftharpoons 2\text{H}_2\text{O}$).^{55,56} The presence of other species, such as hydroxyl radicals, superoxide anion radicals, or nitric oxide can be shown in liquids by electron paramagnetic resonance,⁵⁷ assumed from gas phase distributions,^{27,58,59} or from the detection of modified organic or inorganic targets by the plasma treatment.^{51,60} Given their high reactivity, the contribution of short lived ROS and RNS to the modification of biomolecules is assumingly significant.

It is a major challenge in plasma chemistry that has so far not been fully met: to determine the short lived species reactivity and to distinguish between species stemming from primary reactions in the gas phase and species created in secondary or tertiary reactions at or in the target – a liquid, a gel, or a tissue.²⁶ Gorbanev *et al.*,⁶¹ and Benedikt *et al.*⁶² presented first indications by showing the activity of gas phase-derived species in aqueous model systems.

In this work, the stable oxygen isotope ^{18}O was used in the gas ($^{18}\text{O}_2$) and liquid phase (H_2^{18}O) to shed light onto the behavior and reactivity of reactive oxygen species (ROS) following CAP treatment. Predominantly, the argon-driven atmospheric-pressure plasma jet kINPen with shielding gas⁶³ was utilized to treat cysteine as a chemical probe while selected experiments included the use of the helium-driven COST microplasma jet as a reference source.⁶⁴ The chemical impact on cysteine was assessed using high-resolution mass spectrometry with a special focus on isotope distribution patterns. These results allow insight into the trajectories of plasma-generated ROS hitting a liquid surface and their reaction with organic tracer molecules, indicating that both gas phase-derived species and liquid phase-derived species have a biochemical potential.

Experimental

Short-lived species generation (plasma sources)

The argon-driven atmospheric-pressure plasma jet kINPen 09 (neoplas)⁶³ was used together with a curtain gas device⁶⁵ to provide defined atmospheric conditions for the experiments.

The kinpen was powered by 1.1 W at a frequency of 1 MHz. Gas flux was kept constant for all conditions at 3 standard liter per minutes (slm) of pure, dry argon (5.0, Air Liquide) with the curtain gas set to 5 slm of nitrogen (5.0, Air Liquide). Besides pure argon, 1% oxygen (purity 4.8, Air Liquide, Ar/O₂) was used for the experiments as these conditions offered promising oxidative thiol modification potential.³³ The COST-jet⁶⁴ was powered by constant 300 mW at a frequency of 13.56 MHz. Total gas flux was kept constant at 1 slm of pure dry helium (5.0, Air Liquide) with 1% oxygen admixture (purity .8, Air Liquide, He/O₂). For the experiments with the kINPen, either light oxygen or heavy isotope oxygen (purity 99%, $^{18}\text{O}_2$, Sigma-Aldrich) was used. Due to costs, only light oxygen was used for the control experiments with the COST-jet. All connections were flushed with nitrogen prior to switching from one oxygen variant to the other.

Sample preparation and treatment

Cysteine (L-cysteine, Sigma-Aldrich) was dissolved in double-distilled water (MilliQ) or water with isotopically labelled oxygen (H_2^{18}O , 97% purity, Eurisotop) to a final concentration of 300 μM . Simultaneous treatments with ^{18}O labeled water and ^{18}O labeled gas were not performed. Treatments of the cysteine solutions were performed with the different gas compositions in 24-well plates using 750 μl of solution per sample and a distance between jet nozzle and liquid surface of 9 mm. All treatments were performed for 60 s and resulting samples were stored on ice and directly measured.

High-resolution mass spectrometry

Analysis. Mass spectrometry was carried out on a TripleTOF 5600 system (Sciex). Samples were diluted 1: 1 with alkaline buffer (0.3% ammonium hydroxide in methanol) and directly infused using an electronically controlled syringe pump. Each sample was acquired for 1 min using identical system settings for all samples (capillary temperature 150 °C, curtain gas: 35 psi N₂, ion source gas 1 : 20 psi N₂, ion source gas 2: 25 psi N₂, ion spray voltage: –4 kV). To identify the structures of all observed masses, each peak of interest was isolated, fragmented, and resulting fragment masses acquired (MS/MS, collision energy –24 eV, declustering potential –10 kV) and annotated. To allow a relative quantification of observed signals, an internal standard (IS) was mixed into the sample directly in front of the mass spectrometer emitter using a mixing tee connector. Here, the amino acid valine (L-valine, Sigma-Aldrich) was used due to its mass difference to other expected signals and little interference with the rest of the spectrum. All measurements were performed in triplicates.

Data analysis and branching calculation. After acquisition, samples were processed using the Analyst software (Analyst TF 1.7, Sciex). First, background noise was determined and 300 counts subtracted from the full spectrum (15 times background) to increase signal-to-noise quality. Afterwards, molecule structures were identified using the acquired MS/MS data and the “Formula Finder” as well as “Mass Calculator” functions of the PeakView software (PeakView 1.2.0.3, Sciex). The

areas of all isotope peaks were calculated and normalized on the internal standard area to allow quantitative comparison between measuring runs or each identified structure, the theoretical isotope pattern was calculated. Intensities for all observed peaks were adjusted to remove naturally occurring ^{13}C isotope intensities to prevent interference with isotope signals stemming from integrated ^{18}O . Further isotope traces identified for each compound in treatments with pure argon in unlabeled water were considered as controls for impurities. Therefore, the values of isotopic masses identified in treatments with argon-only were subtracted from each corresponding isotopic mass identified in experiments with labeled oxygen. The error estimation was done by considering biological triplicates for each condition and technical duplicates for each sample, for six measurements total. Other several potential systematic errors were considered in the presented analyses. First, both isotopic labeled gas and water were not of 100% purity. Therefore, an additional error of 1% had been taken into account for all quantifications using $^{18}\text{O}_2$ as well as 3% using H_2^{18}O . Furthermore, evaporation had to be considered when working with isotopically labeled water. After treatment of 60 s, 20 μl of the 750 μl were evaporated. Evaporated heavy water might be dissociated in the discharge, thereby becoming a primary species while erroneously considered as a tertiary species. Therefore, an additional systematic error of 4% has to be considered. In total, expected systematic error were 1% for treatments with $^{18}\text{O}_2$ and 7% for treatments with H_2^{18}O . However, errors regarding $^{18}\text{O}_2$ are underestimated due to imperfection of the shield gas device (see Results and discussion). The corresponding values were incorporated into all acquired standard deviations. To allow a quick overview about differences in data sets, principal component analysis (PCA) was performed with the normalized spectra using Perseus.⁶⁶

Results and discussion

Cysteine as model compound

Cysteine and derivatives have been suggested as model systems to estimate the liquid phase chemistry of plasma sources, to compare the impact of discharge parameter variations such as working gas composition, and to facilitate the standardization of treatment procedure of plasma discharges for biomedical applications.^{48,50} The products resulting from the reaction between the CAP-derived species and cysteine were analyzed by mass spectrometry (Fig. 1). As reported previously, covalent changes to the cysteine (structure 1) by the plasma-derived species were observed, with cystine (RSSR, structure 2), cysteine sulfinic acid (RSO_2H , structure 3), cysteine sulfonic acid (RSO_3H , structure 4), and cysteine-S-sulfonate (RSSO_3H , structure 5) and the sulfite (SO_3^{2-}) and sulfate (SO_4^{2-}) ions as dominant products. These compounds were chosen for their relevance in the transformation pathway of cysteine under certain redox conditions. The presence of RSO_3H or SO_4^{2-} indicates a strongly oxidizing environment (oxygen in the feed gas, long treatments), whereas the presence of RSSR, RSO_2H , or RSSO_3H reveals weakly oxidizing conditions (short treatments, nitrogen shielded feed gas).⁵³ Here, this model was used to

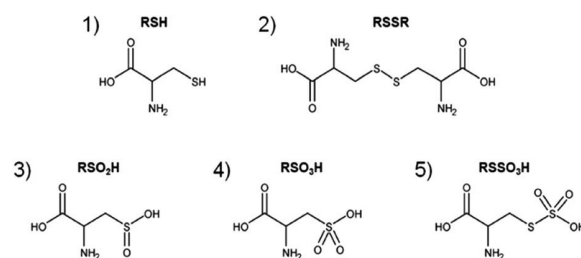


Fig. 1 Major products after direct CAP treatment of cysteine solutions. Cysteine (1, $m = 121.0197u$, RSH), cystine (2, $m = 240.0238u$, RSSR), cysteine sulfinic acid (3, $m = 153.0096u$, RSO_2H) and cysteine sulfonic acid (4, $m = 169.0045u$, RSO_3H) as well as cysteine-S-sulfonate (5, $m = 200.9766u$, RSSO_3H).

investigate transport processes at the interface between the gas phase (the effluent) and the target (cysteine solutions). To monitor such reactions, the chosen cysteine model with its multiple oxidation states of the thiol moiety seemed to be superior to the phenol model.

Gas phase and liquid phase-derived species contribute to plasma liquid chemistry

To trace the reactive species, the ^{18}O oxygen isotope ($u = 17.9992$), either located in the feed gas ($^{18}\text{O}_2$) or in the solvent (H_2^{18}O), was used during different plasma treatments. In comparison, the normal oxygen isotope ^{16}O has a mass of $u = 15.9949$, generating a mass shift of $2.0043 m/z$ for each included ^{18}O atom that could easily be followed by mass spectrometry (examples in Fig. 2). Hence, a differentiation between gas phase and liquid phase-derived reactive species could be made. Indeed, the transfer of gas phase ^{18}O species into the liquid was observed for a number of products (e.g. RSO_2H and RSO_3H). These observations were in agreement with data published by Benedikt *et al.* for a phenol model investigating a micro atmospheric plasma jet (APPJ).⁶² Additionally, a strong role of the plasma treated target (cysteine solution in water) as an additional source of reactive species was identified. The compound cysteine-S-sulfonate (RSSO_3H) almost exclusively contained liquid phase-derived oxygen. Most other products did not show such a clear-cut oxygen incorporation, indicating a mixed attack of gas and liquid phase derived species.

Using principal component analysis (Fig. 3), general differences in product formation and oxygen incorporation due to the various treatment conditions were easily observable in the two principal components explaining the largest differences between samples (39.6% and 34.9%, respectively). Ar/O_2 (kINPen) and He/O_2 (COST-jet) treatment were found in close proximity to each other, indicating similar products and isotope distributions after treatment, which was in good agreement with previous works. The loadings of the principal components (Fig. 3b) indicated a significant impact due to the presence or absence of incorporated ^{18}O .

The products cysteine sulfinic and sulfonic acid. Both molecules are created by CAP treatment due to the stepwise oxidation of the thiol moiety,^{40,50} and were observed for all direct

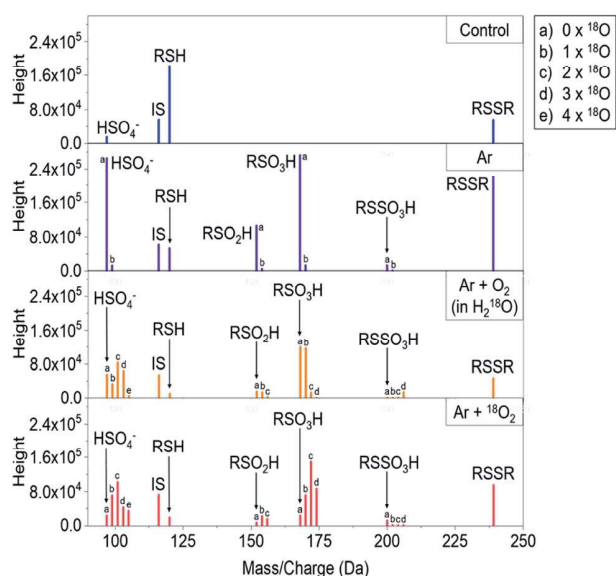
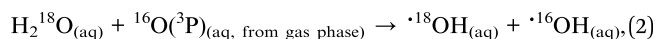
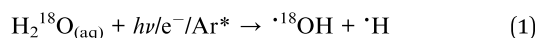


Fig. 2 Raw mass spectra showing the inclusion of ^{16}O or ^{18}O oxygen atoms under different labeling strategies into cysteine after kINPen treatment. RSH = cysteine, RSSR = cystine, RSO_2H = cysteine sulfinic acid, RSO_3H = cysteine sulfonic acid, RSSO_3H = cysteine-S-sulfonate, IS = internal standard (valine), SO_4^{2-} = sulfate ion. "b"-labeled signals in Ar-only samples are stemming from ^{13}C isotopes and their normalized intensities were subtracted from corresponding signals in oxygen-containing conditions to handle isotope shadowing effects, see Experimental section for details.

plasma treatment conditions. Without molecular oxygen, admixture (kINPen Ar-only) small yields of sulfonic acid indicate the strong role of gas phase-derived oxygen species for its formation (Fig. 4). Additionally, a limited incorporation of liquid phase species was observed that might stem from the initiation of the oxidative chain:



(^{18}O water used as solvent, ^{16}O molecular oxygen in the gas phase).

Here, water is cleaved either by the impact of electrons, UV photons, or energy-rich (metastable) noble gas species (reaction (1)). Atomic oxygen ($\text{O}({}^3\text{P})$) has been suggested as another potential reactant for water cleavage (reaction (2)),^{62,67} however in conditions with the highest levels of $\text{O}({}^3\text{P})$ present (COST jet He/O_2),⁶⁸ the lowest overall inclusion of aqueous ^{18}O species into RSO_2H and RSO_3H was found (Fig. 4 and Table 1). With that, reaction (2) is not a major pathway in the existing conditions and $\text{O}({}^3\text{P})$ predominantly reacts directly with the present organic molecules without a detour *via* liquid phase derived OH radicals. A similar formation rate of cysteine sulfinic acid was observed for the kINPen Ar only in comparison to Ar/O_2 , while RSO_3H yields were only 25% of that of Ar/O_2 . Either this suggest a low conversion rate of RSO_2H into RSO_3H in Ar-only treatment, or that the formation of RSO_3H follows a different

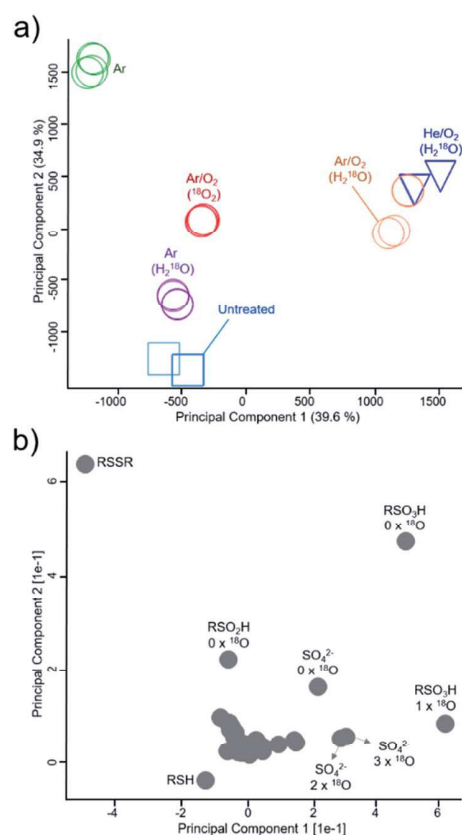


Fig. 3 Mapping of inclusion of gas phase and liquid phase-derived species in major cysteine derivatives. PCA analysis (a) and corresponding loadings ((b), loadings in relation to isotope incorporations are marked) indicate general differences in species distribution. Samples were treated with the kINPen (circles, colors indicate treatment conditions) or as control experiments with the COST-jet (triangles, He/O_2 mixture in H_2^{18}O) or left untreated (squares). $^{18}\text{O}_2$ enriched feed gas or H_2^{18}O as solvent was used to determine species origin. RSO_2H = cysteine sulfinic acid, RSO_3H = cysteine sulfonic acid, RSSO_3H = cysteine-S-sulfonate SO_4^{2-} = sulfate. All treatments (represented by different symbols/colors) were performed in triplicates and plotted individually to check for reproducibility.

reaction path than RSO_2H . The incorporation of $^{18}\text{O}_{(\text{water})}$ was increased in the argon-only case, indicating that a proportional larger number of ^{18}OH radicals from the solvent were created when limited amounts of gas phase ROS ($\text{O}({}^3\text{P})$, $\text{O}_2({}^1\Delta_g)$) were available. Hence, the lysis of water is achieved according to reaction (1) by electrons (in the case of the kINPen), Ar or He higher energy states (discussed in ref. 26), and (V)UV photons which are highest if no molecular gas admixture is made.⁶⁹

Taken together, a mixture of gas phase-derived and liquid phase secondary species attacks cysteine. Concordantly, reactive molecular dynamics simulations indicate that a proton abstraction from the thiol moiety by one hydroxyl radical followed by addition of another hydroxyl radical yielding cysteine sulfenic acid paved the way for all further modifications.⁴⁹ A liquid phase-localized hydroxyl radical seems to perform this initial attack predominantly:

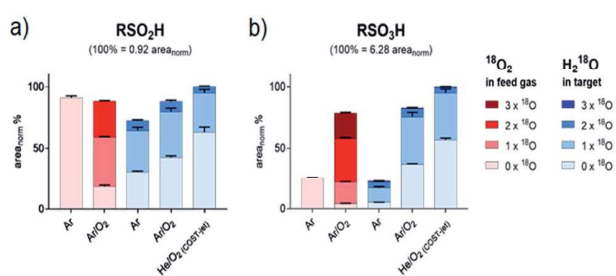
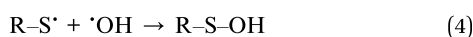
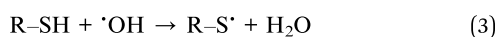


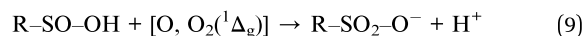
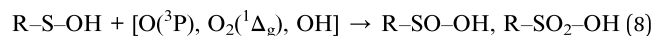
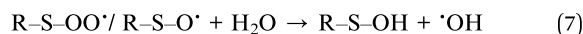
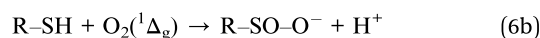
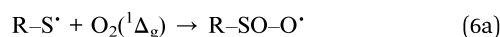
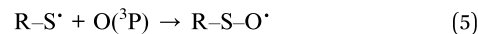
Fig. 4 Isotopic distribution of oxygen in sulfinic (a) and sulfonic (b) acid after CAP treatment areas for each signal were normalized on total intensities of each species (including all isotope variations). Isotope distributions were observed with labeled oxygen present in the feed gas (red) or in the target liquid (blue). Cysteine was treated by the kINPen using Ar-only (Ar) plasma or Ar with 1% O₂ admixture (Ar/O₂). Alternatively, treatment was performed using the COST-jet running with a He plasma with 1% O₂ admixture (He/O₂).



(R = C₃H₆NO₂).

Further reaction to sulfonic acid seem to be dominated by gas phase-derived oxygen species. For the kINPen, argon-only treatment of cysteine in H₂¹⁸O, the ¹⁶O/¹⁸O ratio of 2 : 1 indicated that precisely one oxygen atom out of the three included in the RSO₃H stems from the liquid as suggested by the reactions (3) and (4). In contrast, the ratios for kINPen Ar/O₂ and COST He/O₂ (¹⁶O/¹⁸O 4 : 1) showed that on average less than one atom derived from the water lysis, fostering the relevance of gas phase-derived species for the production of the products and provide evidence that O(³P) plays an important role in introducing observed modifications. O(³P) interacts with a rate constant of about $k = 1 \times 10^{12-13} \text{ cm}^3 \text{ mol}^{-1} \text{ s}^{-1}$ with free thiols,⁷⁰ indicating high modification efficacies. It is capable of oxidizing a thiol moiety directly to sulfenic acid.⁷¹ Especially the final oxidation step from sulfinic to sulfonic acid requires a gas phase-derived oxygen species, with O(³P) and O₂(¹Δ_g) as

potential candidates as shown from gas phase measurements and 0D/2D model simulation (reactions (5)–(9)).^{27,72–75}



(R = C₃H₆NO₂).

Treatment with the COST-jet, known for high fluxes of O(³P),⁶⁸ resulted in the largest proportion of gas phase-derived oxygen in RSO₂H/RSO₃H (¹⁶O_{gas}/¹⁸O_{liquid} 5 : 1 for RSO₃H). This further emphasized the transport of gas phase O(³P) into the interphase region, and presumably, the upper layers of the bulk liquid and its direct chemical reactivity with thiols and oxidized thiol moieties. Omlid *et al.* showed that O(³P) can migrate to a limited extent in an aqueous system.⁷⁶ Besides O(³P), O₂(¹Δ_g) is the other species of interest, since it is capable of producing many of the observed products on its own (reactions (6)–(9)).^{77,78} While it reacts with a rate constant of $k = 8.3 \times 10^6 \text{ M}^{-1} \text{ s}^{-1}$ with free thiols, it can penetrate significantly further into the liquid bulk due to its much longer half-life⁷⁹ as compared to O(³P), thereby offsetting its lower reaction rate. In the light of its biological impact in cell models and therapy, both O(³P)^{81,80} and O₂(¹Δ_g)⁸¹ must receive a significant attention when interpreting CAP affect in biomedical research or (re)design plasma sources for the application.

The products S-sulfonate and sulfate. RSSO₃H and SO₄²⁻ were produced in significant amounts, with the COST-jet being more effective than the kINPen (Fig. 5). Different pathways may generate RSSO₃H: the photolytic or radical driven cleavage of a C–S bond of the intermittently formed cystine (RSSR) and subsequent oxidation of the outer sulfur moiety, the oxidative

Table 1 Distribution of oxygen isotopes ¹⁶O and ¹⁸O in major products after plasma treatment of cysteine in labeled double-distilled water (H₂¹⁸O). Atom%, mean of 3 experiments

H ₂ ¹⁸ O label	RSO ₂ H (cysteine sulfinic acid)			RSO ₃ H (cysteine sulfonic acid)			RSSO ₃ H (cysteine-S-sulfonate)		
	Ar	Ar/O ₂	COST He/O ₂	Ar	Ar/O ₂	COST He/O ₂	Ar	Ar/O ₂	COST He/O ₂
¹⁶ O/%	65.6	69.4	79.0	65.0	78.5	83.8	11.9	9.7	8.9
¹⁸ O/%	34.4	30.6	21.0	34.9	21.7	16.2	87.9	90.3	91.1
H ₂ ¹⁸ O label	SO ₃ ²⁻ (sulfite) ^a			SO ₄ ²⁻ (sulfate) ^a					
	Ar	Ar/O ₂	COST He/O ₂	Ar	Ar/O ₂	COST He/O ₂			
¹⁶ O/%	15.0	50.2	49.2	45.9	54.9	60.7			
¹⁸ O/%	85.0	49.8	50.8	54.1	45.1	39.3			

^a Detected as singly charged bisulfite/bisulfate ion.

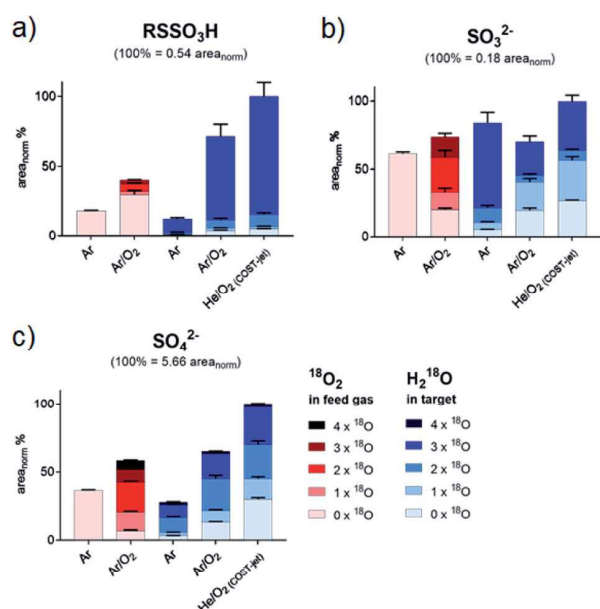
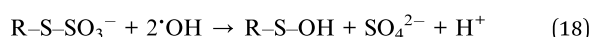
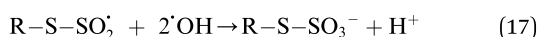
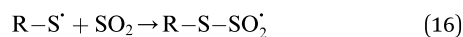
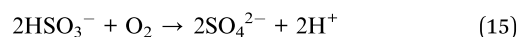
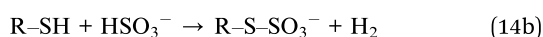
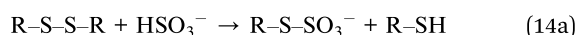
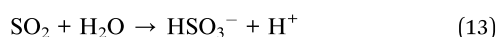
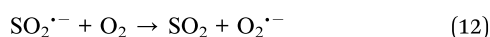
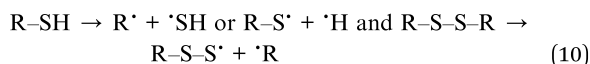


Fig. 5 Isotopic distribution of oxygen in cysteine *S*-sulfonate (a), sulfate (b) and sulfite (c) after CAP treatment. Areas for each signal were normalized on total intensities of each species (including all isotope variations). Isotope distributions were observed with labeled oxygen present in the feed gas (red) or in the target liquid (blue). Cysteine was treated by the kINPen using Ar-only (Ar) plasma or Ar with 1% O₂ admixture (Ar/O₂). Alternatively, treatment was performed using the COST-jet running with a He plasma with 1% O₂ admixture (He/O₂). Sulfite (b) and sulfate (c) were detected as bisulfite/bisulfate.

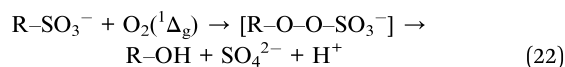
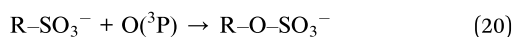
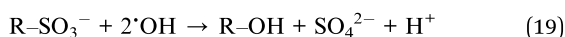
cleavage of oxidized cystine derivatives, or RSSO₃H is formed from the attack of a 'SH-derived species, *e.g.* sulfite (SO₃²⁻) on cysteine, cystine, or the thiyl radical R-S'.⁸²⁻⁸⁶ While a single reaction pathway cannot be determined with the current data, and several reactions ultimately yield the same product, the following proposed reactions will contribute to the formation of RSSO₃H. Further oxidation leads to the destruction of the S-S bond of RSSO₃H, yielding SO₄²⁻ again.⁸⁷⁻⁸⁹



(R = C₃H₆NO₂).

While the cleavage of disulfides by sulfite ions is well-described,^{89,90} its contribution must be debated. In contrast to RSO₂H and RSO₃H, between 80% and 90% of oxygen added to RSSO₃H stemmed from liquid phase species (Fig. 5 and Table 1). The gas phase-derived ROS are not directly involved in its formation, precluding the formation of sulfite ions from SH radicals *via* reactions (11) and (12), or from the cleavage of a C-S bond in cysteine sulfinic or sulfonic acid (R-SO-O⁻/R-SO₂-O⁻, reactions (5)-(9)). However, sulfite ions found after the plasma treatment contain a 50% mix of gas and liquid derived oxygen, indicating that also reactions precluding gas phase-derived oxygen lead to its formation. While no information is available on the reaction mechanisms of hydroxyl radicals with sulfhydryl radicals in liquids, their impact is the key to the observed isotope pattern of RSSO₃H. Following reaction (1), the photolysis of H₂¹⁸O yields ¹⁸OH. However, RSSO₃H yields are highest when oxygen is present in the gas phase (Ar/O₂, He/O₂ conditions). Due to the absorption of molecular O₂ below 180 nm this leads to an attenuation of the VUV, and such photolysis.⁹¹ Additionally, the COST jet emits negligible VUV radiation,⁶⁴ yet yielded the highest levels of RSSO₃H. In contrast, when water photolysis is strongest (kINPen Ar plasma) by far the lowest amounts of RSSO₃H were detected (Fig. 5a).⁸⁶ This suggests, that (a) the local production of OH radicals from photolysis in the interface zone does not favour the production of RSSO₃H or (b), that RSSO₃H generated in the interfacial zone is immediately decayed again. With that, it must be assumed that RSSO₃H is produced in the bulk by the action of OH radicals generated from the liquid. The question is; how do they get there – given their short live time they cannot penetrate that far. Interestingly, it is the O(³P) atom that may act as an intermediate carrier of chemical energy: according to recent experiments, the atom can penetrate a measurable distance in aqueous solutions,⁷⁶ and following reaction (2) can lead to the formation of OH radicals distant from the interface region.⁶⁷ Such, the number of accessible precursors increases while the local OH radical density is comparably low, reducing the decay of RSSO₃H once it formed *via* reaction (18) and other short lived gas phase species. However, the cleavage of water according to (2) yields a 1 : 1 mixture of ¹⁶OH and ¹⁸OH. That is clearly not reflected in the product (>90% ¹⁸O). Beside a potential isotope effect, the "migration" of O-H single bonds between a ¹⁶OH radical and a neighbouring H₂¹⁸O water molecule results in a switch from a ¹⁶OH to an ¹⁸OH.⁹² Given the magnitudes higher density of water compared with the plasma generated ¹⁶O(³P) atoms, most ¹⁶OH radicals are lost resulting in the observed dominance of ¹⁸OH. This is an interesting result indicating that the impact of highly reactive species is not confined to the interface layer but can extent into the liquid bulk, and corroborates computational work done by Yusupov *et al.*⁹³

Compared to the transient RSSO₃H, the stable sulfate ion SO₄²⁻ is the final product of thiol moiety oxidation:



(R = C₃H₆NO₂).

It can be formed from numerous precursors by breaking the C-S bond both before and after oxidation events (reactions (19)–(22)). Beside the chemical breakage, VUV radiation may contribute as the binding energy of C-S bonds (272 kJ mol⁻¹, 2.8 eV) lies well within the range of the emitted photons.⁹⁴ In addition, a chemical cleavage *via* three or four-atom transition states is possible, potentially with the contribution of radical species.⁹⁵ It was observed that all cysteine products decay with further treatment, with RSO₃H as a final product.⁴⁹ Ultimately, its accumulation also stops, indicating that consumption processes leading to the formation of SO₄²⁻ counteract further build-up. The sulfate ion SO₄²⁻ showed a very heterogeneous origin of its oxygen atoms, confirming the end product character (Table 1). In contrast to the kINPen, the SO₄²⁻ ion's oxygen isotopes for COST jet treatment showed a significant larger proportion of gas phase-derived species that can be attributed to the higher density of O(³P) generated. Besides SO₄²⁻, small amounts of SO₃²⁻ were observed. Interestingly, the ¹⁶O/¹⁸O composition indicated a higher contribution of the liquid phase species than seen for SO₄²⁻, implying bulk generated $\cdot\text{OH}$ radical oxidation of $\cdot\text{SH}$ as major chemical route to its formation. The ion plays a contributing role in the formation of RSSO₃H (see Tables 1 and 2).

Origin of oxygen in oxidized cysteine derivatives: gas phase versus liquid phase species. Using the measured abundances of each product and its respective isotope pattern, the distribution of ¹⁸O and ¹⁶O in all major cysteine oxidation products were determined. Adding the areas of all variants (*e.g.* RS¹⁶O₃H, RS¹⁶O₂¹⁸OH, RS¹⁶O¹⁸O₂H and RS¹⁸O₃H) the fraction of each single variant was then used to calculate the atomic fraction the two oxygen isotopes (see Tables 1 and 2). The overall pattern indicated that there is no 100% contribution of either gas-phase-derived species or liquid-phase derived species. However, there are clear indications for diametric origins of the incorporated oxygen atoms in some products. The extremes

were RSO₃H, that incorporated a majority of gas phase-derived oxygen (up to 83.8%), and RSSO₃H, that predominantly included liquid phase-derived oxygen (maximum 91.1%). The other products showed a more equally shared origin of the oxygen atoms from gas-phase and liquid-phase, especially the sulfite SO₃²⁻ ion with almost 50 : 50 distribution in all experiments. The assumed oxidation end product SO₄²⁻ also shows a commensurate isotope distribution, but with a significant tilt towards gas-phase derived oxygen.

kINPen versus COST-jet – atomic vs. singlet oxygen? kINPen (Ar/O₂) and COST-jet (He/O₂) yielded similar amounts of the major products that also share a similar oxygen isotope distribution. However, the COST-jet featured slightly higher oxygen incorporation from the gas phase compared to that of the kINPen. In addition to ubiquitous hydroxyl radicals produced by both sources under all conditions,^{30,57} other components of a discharge might affect radical formation in the liquid. Currently, electrons influencing the liquid surface are discussed as initiators for various liquid chemistry processes.⁹⁶ However, electrons play a minor role for the two sources used here. The COST-jet features an electric field perpendicular to the gas flux,⁶⁴ thereby preventing electrons from leaving the electrode area. While the kINPen is ignited using a linear electric field, the discharge is relatively remote from the treatment zone (12 mm in total taking into account liquid displacement due to the gas flux). A known difference between both plasma sources is generation of O(³P) and O₂(¹Δ_g) and the observed isotope pattern differences seem to be related to these species. The COST-jet produces high amounts of O(³P)⁶⁴ with about 8 × 10¹⁴ cm⁻³ atoms at the working distance of 4 mm.⁹⁷ In comparison, calculated O(³P) densities for the kINPen reach a similar level (5 × 10¹⁴ cm⁻³).⁵⁸ However, TALIF spectroscopy measurements indicate a highly dynamic density of O(³P) in the kINPen's effluent. Starting as high as 3.5 × 10¹⁵ cm⁻³, densities quickly decrease with a rate of 0.5 × 10¹⁵ cm⁻³ mm⁻¹ along the z-axis of the effluent resulting in lower O(³P) levels at the gas-liquid interphase in normal conditions (9 mm nozzle – liquid). In contrast to O(³P), O₂(¹Δ_g) densities in the effluent of both sources are comparable, with a tendency to higher production rates in the COST jet (1 × 10¹⁵ cm⁻³ in normal conditions, up to 6 × 10¹⁵ cm⁻³ at high power settings⁹⁸) than in the kINPen (8 × 10¹⁴ cm⁻³ at standard conditions²⁷). O₂(¹Δ_g) has a significantly longer half-life. For the kINPen, O₂(¹Δ_g) was still measured at 192 mm away from the nozzle. However, the loss starting from

Table 2 Distribution of oxygen isotopes ¹⁶O and ¹⁸O in major products after gas-phase labeled plasma treatment of cysteine in normal double-distilled water (H₂¹⁶O). Working gas Ar/0.5% ¹⁸O₂, atom%, mean of 3 experiments

Gaseous ¹⁸ O ₂ label	Ar/ ¹⁸ O ₂ (kINPen)		RSO ₂ H (cysteine sulfinic acid)	RSO ₃ H (cysteine sulfonic acid)	RSSO ₃ H (cysteine-S-sulfonate)
	SO ₃ ²⁻ ^a (sulfite)	SO ₄ ²⁻ ^a (sulfate)			
¹⁶ O/%	50.4	54.9	43.6	35.6	80.4
¹⁸ O/%	49.6	45.1	56.4	64.4	19.6

^a Detected as singly charged bisulfite/bisulfate ion.

100 mm was significant (2/3 of the initial value). Both jets produce ozone, especially at high oxygen admixtures and long distances from the nozzle. Due to limitations in solubility and negligible effects in control experiments using an ozonizer (data not shown), a limited role in respect to liquid chemistry can be assumed. Taken together, the higher inclusion of gas phase species in COST-jet treated cysteine might be due to higher levels of $O(^3P)$ interacting either directly with the cysteine molecule or with the liquid, yielding OH radicals.

Summary and conclusions

Heavy oxygen ($^{18}O_2$) was used to track the fate of plasma-generated ROS in a cysteine model using mass spectrometry. Furthermore, $H_2^{18}O$ was used in a reverse experiment to observe the role of liquid-derived reactive species under the same conditions. It became apparent that gas and liquid phase species play different roles: while some products are mostly driven by gas phase species, others require the presence of liquid phase species derived from the solvent system (Fig. 6). The observed isotope distribution pattern allows the assumptions that, (a) gas-phase derived short-lived reactive species are active in the gas-liquid interphase, (b) short-lived reactive species are generated in the liquid phase especially from gas-phase derived ROS (e.g. atomic oxygen), and (c) the formation of liquid phase species occurs in the interface and in deeper layers. The dominant gas phase-derived species was found to be $O(^3P)$ and OH radicals in the liquid phase.

Concerning the application of CAP in the clinics, these results suggest a significant role of the target onto the treatment efficacy: in a humid environment such as the mucosa or during surgery, target derived species as OH radicals intensify the

oxidative impact of the CAP. When treating dry tissue such as intact skin, gas phase derived species dominate and an overall milder impact of the CAP results. Recent data on the oxidation of complex lipids by CAP corroborate these conclusions.⁹⁹

Conflicts of interest

There are no conflicts to declare.

Acknowledgements

Funding from the German Federal Ministry of Education and Research (grant number 03Z22DN12 to K. W., grant number 03Z22DN11 to S. B.) supported this work. The authors would like to thank Volker Schulz von-der-Gathen and Patrick Preissing for their great support with the COST-jet.

References

- S. Bekeschus, A. Schmidt, A. Kramer, H. R. Metelmann, F. Adler, T. von Woedtke, F. Niessner, K. D. Weltmann and K. Wende, *Environ. Mol. Mutagen.*, 2018, **59**, 268–277.
- K. Wende, S. Bekeschus, A. Schmidt, L. Jatsch, S. Hasse, K. D. Weltmann, K. Masur and T. von Woedtke, *Mutat. Res., Genet. Toxicol. Environ. Mutagen.*, 2016, **798–799**, 48–54.
- S. Kluge, S. Bekeschus, C. Bender, H. Benkhail, A. Sckell, H. Below, M. B. Stope and A. Kramer, *PLoS One*, 2016, **11**, e0160667.
- H.-R. Metelmann, C. Seebauer, V. Miller, A. Fridman, G. Bauer, D. B. Graves, J.-M. Pouvesle, R. Rutkowski, M. Schuster, S. Bekeschus, K. Wende, K. Masur, S. Hasse, T. Gerling, M. Hori, H. Tanaka, E. H. Choi, K.-D. Weltmann, P. Metelmann, D. von Hoff and T. von Woedtke, *Clin. Plasma Med.*, 2018, **9**, 6–13.
- M. Keidar, D. Yan, I. I. Beilis, B. Trink and J. H. Sherman, *Trends Biotechnol.*, 2018, **36**, 586–593.
- G. Isbary, J. Heinlin, T. Shimizu, J. Zimmermann, G. Morfill, H. U. Schmidt, R. Monetti, B. Steffes, W. Bunk and Y. Li, *Br. J. Dermatol.*, 2012, **167**, 404–410.
- G. Isbary, G. Morfill, H. U. Schmidt, M. Georgi, K. Ramrath, J. Heinlin, S. Karrer, M. Landthaler, T. Shimizu, B. Steffes, W. Bunk, R. Monetti, J. L. Zimmermann, R. Pompl and W. Stolz, *Br. J. Dermatol.*, 2010, **163**, 78–82.
- T. Shimizu and Y. Ikehara, *J. Phys. D: Appl. Phys.*, 2017, **50**, 503001.
- H. Tanaka, K. Ishikawa, M. Mizuno, S. Toyokuni, H. Kajiyama, F. Kikkawa, H.-R. Metelmann and M. Hori, *Rev. Mod. Plasma Phys.*, 2017, **1**, 3.
- J. Gay-Mimbrera, M. C. Garcia, B. Isla-Tejera, A. Roder-Serrano, A. V. Garcia-Nieto and J. Ruano, *Adv. Ther.*, 2016, **33**, 894–909.
- F. Brehmer, H. Haenssle, G. Daeschlein, R. Ahmed, S. Pfeiffer, A. Görlitz, D. Simon, M. Schön, D. Wandke and S. Emmert, *J. Eur. Acad. Dermatol. Venereol.*, 2015, **29**, 148–155.
- C. Ulrich, F. Kluschke, A. Patzelt, S. Vandersee, V. A. Czaika, H. Richter, A. Bob, J. Hutten, C. Painsi, R. Huge, A. Kramer,

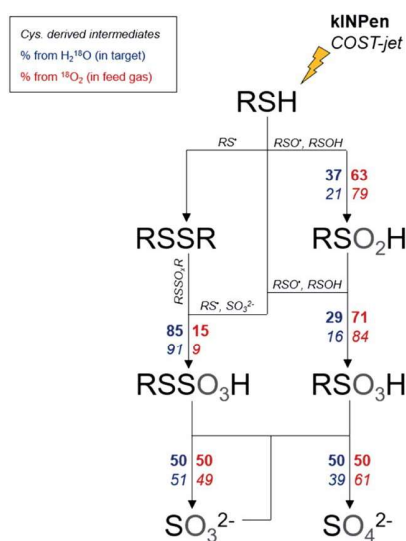


Fig. 6 Labeled oxygen branching ratios for monitored species. Branching ratios are indicated for the kINPen (bold) and COST-jet (italic). Oxygen can either stem from the water in the treated target (blue, left side of arrows) or from the plasma (red, right side of arrows). For clarity, the actual protonation/deprotonation is not reflected.

- O. Assadian, J. Lademann and B. Lange-Asschenfeldt, *J. Wound Care*, 2015, **24**, 196, 198–200, 202–193.
- 13 T. Maisch, T. Shimizu, Y. F. Li, J. Heinlin, S. Karrer, G. Morfill and J. L. Zimmermann, *PLoS One*, 2012, **7**, e34610.
- 14 A. Schmidt, S. Bekeschus, K. Wende, B. Vollmar and T. von Woedtke, *Exp. Dermatol.*, 2017, **26**, 156–162.
- 15 S. Arndt, A. Schmidt, S. Karrer and T. von Woedtke, *Clin. Plasma Med.*, 2018, **9**, 24–33.
- 16 S. Arndt, P. Unger, M. Berneburg, A. K. Bosserhoff and S. Karrer, *J. Dermatol. Sci.*, 2018, **89**, 181–190.
- 17 J. R. Liu, G. M. Xu, X. M. Shi and G. J. Zhang, *Sci. Rep.*, 2017, **7**, 11698.
- 18 A. Schmidt and S. Bekeschus, *Antioxidants*, 2018, **7**, 146.
- 19 N. Kaushik, N. Uddin, G. B. Sim, Y. J. Hong, K. Y. Baik, C. H. Kim, S. J. Lee, N. K. Kaushik and E. H. Choi, *Sci. Rep.*, 2015, **5**, 8587.
- 20 J. Xia, W. Zeng, Y. Xia, B. Wang, D. Xu, D. Liu, M. G. Kong and Y. Dong, *J. Biophotonics*, 2019, **12**, e201800046.
- 21 F. Virard, S. Cousty, J. P. Cambus, A. Valentin, P. Kemoun and F. Clement, *PLoS One*, 2015, **10**, e0133120.
- 22 K. Rödder, J. Moritz, V. Miller, K.-D. Weltmann, H.-R. Metelmann, R. Gandhirajan and S. Bekeschus, *Appl. Sci.*, 2019, **9**, 660.
- 23 G. Pasqual-Melo, R. K. Gandhirajan, I. Stoffels and S. Bekeschus, *Clin. Plasma Med.*, 2018, **10**, 1–8.
- 24 S. Bekeschus, C. Seebauer, K. Wende and A. Schmidt, *Biol. Chem.*, 2018, **400**, 63–75.
- 25 A. Lin, Y. Gorbanev, P. Cos, E. Smits and A. Bogaerts, *Clin. Plasma Med.*, 2018, **9**, 9.
- 26 P. J. Bruggeman, M. J. Kushner, B. R. Locke, J. G. E. Gardeniers, W. G. Graham, D. B. Graves, R. C. H. M. Hofman-Caris, D. Maric, J. P. Reid, E. Ceriani, D. F. Rivas, J. E. Foster, S. C. Garrick, Y. Gorbanev, S. Hamaguchi, F. Iza, H. Jablonowski, E. Klimova, J. Kolb, F. Krema, P. Lukes, Z. Machala, I. Marinov, D. Mariotti, S. M. Thagard, D. Minakata, E. C. Neyts, J. Pawlat, Z. L. Petrovic, R. Pflieger, S. Reuter, D. C. Schram, S. Schroter, M. Shiraiwa, B. Tarabova, P. A. Tsai, J. R. R. Verlet, T. von Woedtke, K. R. Wilson, K. Yasui and G. Zvereva, *Plasma Sources Sci. Technol.*, 2016, **25**, 053002.
- 27 H. Jablonowski, J. S. Sousa, K.-D. Weltmann, K. Wende and S. Reuter, *Sci. Rep.*, 2018, **8**, 12195.
- 28 H. Jablonowski, A. Schmidt-Bleker, K. D. Weltmann, T. von Woedtke and K. Wende, *Phys. Chem. Chem. Phys.*, 2018, **20**, 25387–25398.
- 29 A. Lin, Y. Gorbanev, J. De Backer, J. Van Loenhout, W. Van Boxem, F. Lemièrre, P. Cos, S. Dewilde, E. Smits and A. Bogaerts, *Adv. Sci.*, 2019, 1802062.
- 30 Y. Gorbanev, C. C. W. Verlaack, S. Tinck, E. Tuentner, K. Foubert, P. Cos and A. Bogaerts, *Phys. Chem. Chem. Phys.*, 2018, **20**, 2797–2808.
- 31 S. Mitra, L. N. Nguyen, M. Akter, G. Park, E. H. Choi and N. K. Kaushik, *Cancers*, 2019, **11**, 1030.
- 32 N. Jha, J. J. Ryu, E. H. Choi and N. K. Kaushik, *Oxid. Med. Cell. Longev.*, 2017, **2017**, 7542540.
- 33 G. Bauer and D. B. Graves, *Plasma Processes Polym.*, 2016, **13**, 1157–1178.
- 34 D. Yan, H. Xiao, W. Zhu, N. Nourmohammadi, L. G. Zhang, K. Bian and M. Keidar, *J. Phys. D: Appl. Phys.*, 2017, **50**, 055401.
- 35 A. Schmidt, S. Dietrich, A. Steuer, K.-D. Weltmann, T. von Woedtke, K. Masur and K. Wende, *J. Biol. Chem.*, 2015, **290**, 6731–6750.
- 36 R. K. Gandhirajan, K. Rodder, Y. Bodnar, G. Pasqual-Melo, S. Emmert, C. E. Griguer, K. D. Weltmann and S. Bekeschus, *Sci. Rep.*, 2018, **8**, 12734.
- 37 C. C. Winterbourn, *Nat. Chem. Biol.*, 2008, **4**, 278–286.
- 38 N. K. Kaushik, B. Ghimire, Y. Li, M. Adhikari, M. Veerana, N. Kaushik, N. Jha, B. Adhikari, S. J. Lee, K. Masur, T. von Woedtke, K. D. Weltmann and E. H. Choi, *Biol. Chem.*, 2018, **400**, 39–62.
- 39 A. Mesbah and D. B. Graves, *J. Phys. D: Appl. Phys.*, 2019, **52**, 30LT02.
- 40 E. Takai, T. Kitamura, J. Kuwabara, S. Ikawa, S. Yoshizawa, K. Shiraki, H. Kawasaki, R. Arakawa and K. Kitano, *J. Phys. D: Appl. Phys.*, 2014, **47**, 285403.
- 41 J.-W. Lackmann, S. Schneider, E. Edengeiser, F. Jarzina, S. Brinckmann, E. Steinborn, M. Havenith, J. Benedikt and J. E. Bandow, *J. R. Soc., Interface*, 2013, **10**, 20130591.
- 42 M. Yusupov, J.-W. Lackmann, J. Razzokov, S. Kumar, K. Stapelmann and A. Bogaerts, *Plasma Processes Polym.*, 2018, **15**, 1800022.
- 43 E. Takai, K. Kitano, J. Kuwabara and K. Shiraki, *Plasma Processes Polym.*, 2012, **9**, 77–82.
- 44 J. W. Lackmann, S. Baldus, E. Steinborn, E. Edengeiser, F. Kogelheide, S. Langklotz, S. Schneider, L. I. O. Leichert, J. Benedikt, P. Awakowicz and J. E. Bandow, *J. Phys. D: Appl. Phys.*, 2015, **48**, 494003.
- 45 J.-W. Lackmann, E. Edengeiser, S. Schneider, J. Benedikt, M. Havenith and J. E. Bandow, *Plasma Med.*, 2013, **3**, 115–124.
- 46 M. Yusupov, K. Wende, S. Kupsch, E. C. Neyts, S. Reuter and A. Bogaerts, *Sci. Rep.*, 2017, **7**, 5761.
- 47 S. Maheux, G. Frache, J. S. Thomann, F. Clement, C. Penny, T. Belmonte and D. Duday, *J. Phys. D: Appl. Phys.*, 2016, **49**, 344001.
- 48 G. Bruno, T. Heusler, J.-W. Lackmann, T. von Woedtke, K.-D. Weltmann and K. Wende, *Clin. Plasma Med.*, 2019, **14**, 100083.
- 49 J. W. Lackmann, K. Wende, C. Verlaack, J. Golda, J. Volzke, F. Kogelheide, J. Held, S. Bekeschus, A. Bogaerts, V. Schulz-von der Gathen and K. Stapelmann, *Sci. Rep.*, 2018, **8**, 7736.
- 50 C. Klinkhammer, C. Verlaack, D. Smilowicz, F. Kogelheide, A. Bogaerts, N. Metzler-Nolte, K. Stapelmann, M. Havenith and J. W. Lackmann, *Sci. Rep.*, 2017, **7**, 13828.
- 51 K. Wende, P. Williams, J. Dalluge, W. V. Gaens, H. Aboubakr, J. Bischof, T. von Woedtke, S. M. Goyal, K. D. Weltmann, A. Bogaerts, K. Masur and P. J. Bruggeman, *Biointerphases*, 2015, **10**, 029518.
- 52 S. Bekeschus, J. Kolata, C. Winterbourn, A. Kramer, R. Turner, K. D. Weltmann, B. Broker and K. Masur, *Free Radic. Res.*, 2014, **48**, 542–549.

- 53 J.-W. Lackmann, G. Bruno, H. Jablonowski, F. Kogelheide, B. Offerhaus, J. Held, V. Schulz-von der Gathen, K. Stapelmann, T. von Woedtke and K. Wende, *PLoS One*, 2019, **14**, e0216606.
- 54 C. T. Stomberski, H. L. Zhou, L. Wang, F. van den Akker and J. S. Stamler, *J. Biol. Chem.*, 2019, **294**, 1568–1578.
- 55 G. Merényi, J. Lind and L. Engman, *J. Chem. Soc., Perkin Trans. 2*, 1994, 2551–2553.
- 56 D. T. Sawyer, *Oxygen chemistry*, Oxford University Press, 1991.
- 57 H. Tresp, M. U. Hammer, J. Winter, K. D. Weltmann and S. Reuter, *J. Phys. D: Appl. Phys.*, 2013, **46**, 435401.
- 58 A. Schmidt-Bleker, J. Winter, A. Bösel, S. Reuter and K.-D. Weltmann, *Plasma Sources Sci. Technol.*, 2015, **25**, 015005.
- 59 S. Schroter, A. Wijaikhum, A. R. Gibson, A. West, H. L. Davies, N. Minesi, J. Dedrick, E. Wagenaars, N. de Oliveira, L. Nahon, M. J. Kushner, J. P. Booth, K. Niemi, T. Gans and D. O'Connell, *Phys. Chem. Chem. Phys.*, 2018, **20**, 24263–24286.
- 60 P. Lukes, E. Dolezalova, I. Sisrova and M. Clupek, *Plasma Sources Sci. Technol.*, 2014, **23**, 015019.
- 61 Y. Gorbanev, D. O'Connell and V. Chechik, *Chemistry*, 2016, **22**, 3496–3505.
- 62 J. Benedikt, M. Mokhtar Hefny, A. Shaw, B. R. Buckley, F. Iza, S. Schakermann and J. E. Bandow, *Phys. Chem. Chem. Phys.*, 2018, **20**, 12037–12042.
- 63 S. Reuter, T. von Woedtke and K.-D. Weltmann, *J. Phys. D: Appl. Phys.*, 2018, **51**, 233001.
- 64 J. Golda, J. Held, B. Redeker, M. Konkowski, P. Beijer, A. Sobota, G. Kroesen, N. S. J. Braithwaite, S. Reuter, M. M. Turner, T. Gans, D. O'Connell and V. Schulz-von der Gathen, *J. Phys. D: Appl. Phys.*, 2016, **49**, 084003.
- 65 A. Schmidt-Bleker, J. Winter, S. Iseni, M. Dunnbier, K. D. Weltmann and S. Reuter, *J. Phys. D: Appl. Phys.*, 2014, **47**, 145201.
- 66 S. Tyanova, T. Temu, P. Sinitcyn, A. Carlson, M. Y. Hein, T. Geiger, M. Mann and J. Cox, *Nat. Methods*, 2016, **13**, 731–740.
- 67 R. G. Quiller, T. A. Baker, X. Deng, M. E. Colling, B. K. Min and C. M. Friend, *J. Chem. Phys.*, 2008, **129**, 064702.
- 68 D. Ellerweg, A. Von Keudell and J. Benedikt, *Plasma Sources Sci. Technol.*, 2012, **21**, 034019.
- 69 S. Schneider, J.-W. Lackmann, F. Narberhaus, J. E. Bandow, B. Denis and J. Benedikt, *J. Phys. D: Appl. Phys.*, 2011, **44**, 295201.
- 70 S. M. Omlid, M. Zhang, A. Isor and R. D. McCulla, *J. Org. Chem.*, 2017, **82**, 13333–13341.
- 71 M. Zhang, G. E. Ravilious, L. M. Hicks, J. M. Jez and R. D. McCulla, *J. Am. Chem. Soc.*, 2012, **134**, 16979–16982.
- 72 S. Reuter, J. Winter, A. Schmidt-Bleker, D. Schroeder, H. Lange, N. Knake, V. Schulz-von der Gathen and K. D. Weltmann, *Plasma Sources Sci. Technol.*, 2012, **21**, 024005.
- 73 J. Waskoenig, K. Niemi, N. Knake, L. M. Graham, S. Reuter, V. Schulz-von der Gathen and T. Gans, *Plasma Sources Sci. Technol.*, 2010, **19**, 045018.
- 74 C. C. W. Verlackt, W. Van Boxem and A. Bogaerts, *Phys. Chem. Chem. Phys.*, 2018, **20**, 6845–6859.
- 75 G. R. Buettner and R. D. Hall, *Biochim. Biophys. Acta, Gen. Subj.*, 1987, **923**, 501–507.
- 76 S. M. Omlid, S. A. Dergunov, A. Isor, K. L. Sulkowski, J. T. Petroff, E. Pinkhassik and R. D. McCulla, *Chem. Commun.*, 2019, **55**, 1706–1709.
- 77 T. P. A. Devasagayam, A. R. Sundquist, P. Di Mascio, S. Kaiser and H. Sies, *J. Photochem. Photobiol., B*, 1991, **9**, 105–116.
- 78 M. Rougee, R. V. Bensasson, E. J. Land and R. Pariente, *Photochem. Photobiol.*, 1988, **47**, 485–489.
- 79 A. U. Khan and T. Wilson, *Chem. Biol.*, 1995, **2**, 437–445.
- 80 S. Bekeschus, K. Wende, M. M. Hefny, K. Rödder, H. Jablonowski, A. Schmidt, T. v. Woedtke, K.-D. Weltmann and J. Benedikt, *Sci. Rep.*, 2017, **7**, 2791.
- 81 M. T. Jarvi, M. S. Patterson and B. C. Wilson, *Biophys. J.*, 2012, **102**, 661–671.
- 82 J. B. Kohl, A. T. Mellis and G. Schwarz, *Br. J. Pharmacol.*, 2019, **176**, 554–570.
- 83 L. Pecci, M. Costa, A. Antonucci, G. Montefoschi and D. Cavallini, *Biochem. Biophys. Res. Commun.*, 2000, **270**, 782–786.
- 84 A. Kotronarou, G. Mills and M. R. Hoffmann, *Environ. Sci. Technol.*, 1992, **26**, 2420–2428.
- 85 G. H. Morine and R. R. Kuntz, *Photochem. Photobiol.*, 1981, **33**, 1–5.
- 86 H. Jablonowski, R. Bussiahn, M. U. Hammer, K.-D. Weltmann, T. von Woedtke and S. Reuter, *Phys. Plasmas*, 2015, **22**, 122008.
- 87 T. N. Das, R. E. Huie, P. Neta and S. Padmaja, *J. Phys. Chem. A*, 1999, **103**, 5221–5226.
- 88 G. Mills, K. H. Schmidt, M. S. Matheson and D. Meisel, *J. Phys. Chem.*, 1987, **91**, 1590–1596.
- 89 J. L. Bailey and R. D. Cole, *J. Biol. Chem.*, 1959, **234**, 1733–1739.
- 90 T. W. Thannhauser, Y. Konishi and H. A. Scheraga, *Anal. Biochem.*, 1984, **138**, 181–188.
- 91 P. H. Krupenie, *J. Phys. Chem. Ref. Data*, 1972, **1**, 423–534.
- 92 P. Jiang, X. Chi, Q. Zhu, M. Cheng and H. Gao, *Nat. Commun.*, 2019, **10**, 3175.
- 93 M. Yusupov, E. C. Neyts, P. Simon, G. Berdiyrov, R. Snoeckx, A. C. T. van Duin and A. Bogaerts, *J. Phys. D: Appl. Phys.*, 2014, **47**, 025205.
- 94 S. Soorkia, C. Dehon, S. S. Kumar, M. Pedrazzani, E. Frantzen, B. Lucas, M. Barat, J. A. Fayeton and C. Jouvett, *J. Phys. Chem. Lett.*, 2014, **5**, 1110–1116.
- 95 E. L. Clennan, *Acc. Chem. Res.*, 2001, **34**, 875–884.
- 96 P. Rumbach, D. M. Bartels, R. M. Sankaran and D. B. Go, *Nat. Commun.*, 2015, **6**, 7248.
- 97 D. Ellerweg, J. Benedikt, A. von Keudell, N. Knake and V. Schulz-von der Gathen, *New J. Phys.*, 2010, **12**, 013021.
- 98 J. S. Sousa, K. Niemi, L. J. Cox, Q. T. Algwari, T. Gans and D. O'Connell, *J. Appl. Phys.*, 2011, **109**, 123302.
- 99 J. Striesow, J.-W. Lackmann, Z. Ni, S. Wenske, K. D. Weltmann, M. Fedorova, T. von Woedtke and K. Wende, *Chem. Phys. Lipids*, 2019, 104786.

Article A2

Nitrosylation vs. oxidation - How to modulate cold physical plasmas for biological applications

J.-W. Lackmann & [G. Bruno](#), H. Jablonowski, F. Kogelheide, B. Offerhaus, J. Held, V. S.-von der Gathen, K. Stapelmann, T. von Woedtke, K. Wende. *PLoS One*, vol. 14, no. 5, p. e0216606, 2019.

© 2019 Lackmann et al.

RESEARCH ARTICLE

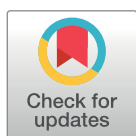
Nitrosylation vs. oxidation – How to modulate cold physical plasmas for biological applications

Jan-Wilm Lackmann¹*, Giuliana Bruno¹, Helena Jablonowski¹, Friederike Kogelheide², Björn Offerhaus², Julian Held³, Volker Schulz-von der Gathen³, Katharina Stapelmann^{2,4}, Thomas von Woedtke¹, Kristian Wende¹*

1 ZIK *plasmatis* at Leibniz Institute for Plasma Science and Technology (INP Greifswald e.V.), Greifswald, Germany, **2** Institute for Electrical Engineering and Plasma Technology, Ruhr University Bochum, Bochum, Germany, **3** Experimental Physics II, Ruhr University Bochum, Bochum, Germany, **4** Plasma for Life Sciences, Department of Nuclear Engineering, North Carolina State University, Raleigh, North Carolina, United States of America

* These authors contributed equally to this work.

* jan-wilm.lackmann@inp-greifswald.de (JWL); kristian.wende@inp-greifswald.de (KW)



OPEN ACCESS

Citation: Lackmann J-W, Bruno G, Jablonowski H, Kogelheide F, Offerhaus B, Held J, et al. (2019) Nitrosylation vs. oxidation – How to modulate cold physical plasmas for biological applications. PLoS ONE 14(5): e0216606. <https://doi.org/10.1371/journal.pone.0216606>

Editor: Mohammed Yousfi, Universite Toulouse III Paul Sabatier, FRANCE

Received: November 30, 2018

Accepted: April 24, 2019

Published: May 8, 2019

Copyright: © 2019 Lackmann et al. This is an open access article distributed under the terms of the [Creative Commons Attribution License](https://creativecommons.org/licenses/by/4.0/), which permits unrestricted use, distribution, and reproduction in any medium, provided the original author and source are credited.

Data Availability Statement: The data underlying this study have been deposited to OSF and are freely accessible via https://osf.io/w6tdg/?view_only=576dfc8057ae42039f0011ca1224a054.

Funding: K. W. acknowledges funding by the German Federal Ministry of Education and Research (BMBF) - Grant No. 03Z22DN12. J.H. and V. SvdG acknowledge funding by the German Research Foundation by the PlaCID project (DFG, PAK816) and the SFB1316. The funders had no role in study design, data collection and analysis,

Abstract

Thiol moieties are major targets for cold plasma-derived nitrogen and oxygen species, making CAPs convenient tools to modulate redox-signaling pathways in cells and tissues. The underlying biochemical pathways are currently under investigation but especially the role of CAP derived RNS is barely understood. Their potential role in protein thiol nitrosylation would be relevant in inflammatory processes such as wound healing and improving their specific production by CAP would allow for enhanced treatment options beyond the current application. The impact of a modified kINPen 09 argon plasma jet with nitrogen shielding on cysteine as a thiol-carrying model substance was investigated by FTIR spectroscopy and high-resolution mass spectrometry. The deposition of short-lived radical species was measured by electron paramagnetic resonance spectroscopy, long-lived species were quantified by ion chromatography (NO_2^- , NO_3^-) and xylenol orange assay (H_2O_2). Product profiles were compared to samples treated with the so-called COST jet, being introduced by a European COST initiative as a reference device, using both reference conditions as well as conditions adjusted to kINPen gas mixtures. While thiol oxidation was dominant under all tested conditions, an Ar + N_2/O_2 gas compositions combined with a nitrogen curtain fostered nitric oxide deposition and the desired generation of S-nitrosocysteine. Interestingly, the COST-jet revealed significant differences in its chemical properties in comparison to the kINPen by showing a more stable production of RNS with different gas admixtures, indicating a different *NO production pathway. Taken together, results indicate various chemical properties of kINPen and COST-jet as well as highlight the potential of plasma tuning not only by gas admixtures alone but by adjusting the surrounding atmosphere as well.

decision to publish, or preparation of the manuscript.

Competing interests: The authors have declared that no competing interests exist.

Introduction

Cold atmospheric plasmas (CAP) are used in a wide variety of fields. In particular, the interest in medical applications has increased in recent years. Multiple scientific studies and case studies confirm CAPs effectiveness for therapeutic purposes, such as wound healing and skin regeneration but also cancer treatment [1–3]. Plasma sources have different designs and discharge concepts, and consequently vary in gas composition and chemical properties of the produced plasma [4–6]. In particular, various reactive oxygen and nitrogen species (RONS) are deposited in treated liquids or in the cellular environment. Production of these species in the gas phase and interaction at the gas-liquid interface vary according to the chosen plasma source and related parameters, leading to a distinct deposition of RONS in the liquid bulk [7–9]. In biological systems, these plasma-generated species modulate redox-signaling processes, ultimately leading to functional consequences [10]. Among these, an increased expression of anti-oxidant proteins such as members of the glutathione metabolism, changes in cell migration rate and cell viability have been observed in cell [11] and animal models [12]. Given the fact, that most of the plasma-derived species are short lived, the question arises which biochemical mechanisms are relevant to relay the chemical information from the plasma to the cell. Several studies focus on the deposition and production of RONS in liquid media for biomedical applications. Chauvin *et al.* investigated several media after treatment with a plasma jet and demonstrated efficient deposition of both long (hydrogen peroxide, nitrite, and nitrate) and short-living (superoxide, hydroxyl radicals) species [13]. Furthermore, a possible pathway is the (covalent) modification of biomolecules, *e.g.* at the amino acid cysteine. Its thiol group can bear oxidation states from -2 to +6, forming a number of chemotypes with biological importance [14]. An initial oxidation product is cysteine sulfenic acid (RSOH). RSOH rapidly reacts with other thiols to form disulfides (RSSR), such as cystine. Strong oxidizing agents can lead to a progressive oxidation of cysteine to its sulfinic (RSO₂H) and/or sulfonic acids (RSO₃H) [14, 15]. In mammalian cells, this reactivity is harnessed in redox signaling processes where an initial step in signal transduction is the controlled oxidation of cysteines, *e.g.* in peroxiredoxins, that subsequently lead to changes in protein conformation, trafficking, or downstream chemical processes (“thiol switches”) [16–18]. Other biologically active modifications are S-glutathionylation and S-nitrosylation, modulating the cysteine residue activity and protein function [19, 20]. Comparable covalent modifications, especially oxidations, have been reported for the reaction of cold plasma with thiol groups, leading to the formation of disulfides, partially oxidized disulfides, and cysteine-thiooxo acids. Besides thiols, other protein compounds were also shown to be modified by CAP treatment, such as phenylalanine and proline [21] as well as histidine, methionine, and tryptophan [22]. Predominantly reactive oxygen species have been attributed as plasma-derived precursors fostering these reactions [3, 17, 23–28]. Despite the considerable abundance of nitric oxides (NO^{*}, N₂O₃, *NO₂) and other RNS in the gas phase of many plasma sources, little is known about the role in plasma liquid chemistry. Plasma derived RNS contribute to oxidative processes but presumably lead to the formation of nitrosylated products, such as S-nitrosocysteine. Physiologically, thiols play a key role in the nitric oxide pathway as sink and activity modulator.

S-nitrosocysteine occurs during inflammation processes and defense responses, *e.g.* against pathogens or cancerous cells [29–31]. Thiol nitrosylation protects proteins during oxidative stress by scavenging *NO₂ and N₂O₃, and by avoiding the formation of irreversible sulfur oxidation procured by oxygen derivatives such as O₂^{*}, *O and O₃ [19, 32]. However, the erroneous production of S-nitrosothiol has been associated with cancer development as well as with pulmonary, cardiac, and neurological pathologies [33, 34]. S-nitrosothiols are considered as efficient *NO-donors acting as substrates for various *NO-producing enzymes, and their action

as anticancer agents has been proven both *in vivo* and *in vitro* applications [35–38]. Therefore, the deposition of $\cdot\text{NO}$ by cold plasmas and the potential formation of nitrosylated thiols is of great interest for their (bio-)medical application.

In this study, we investigate the impact of two different plasma sources, the kINPen [39] and the COST-jet [40], on cysteine model solutions, in order to investigate the production of S-nitrosocysteine. The structure, origin, and kinetic profiles of the resulting cysteine derivatives were determined using FTIR spectroscopy and time-of-flight high-resolution mass spectrometry. At the same time, the production of reactive oxygen and nitrogen species in the treated solutions has been studied using spin trap enhanced electron paramagnetic resonance spectroscopy (EPR, for liquid phase $\cdot\text{NO}$), a colorimetric assay (for H_2O_2) and ion chromatography (for NO_2^- and NO_3^-).

Materials and methods

Plasma sources

The kINPen 09 (kINPen; neoplas GmbH) and the COST Reference Microplasma Jet (COST-jet) were investigated in parallel. The kINPen consists of a high-voltage needle electrode located in the center of a ceramic capillary having a 1.6 mm diameter. A radio frequency of around 1 MHz drives the needle electrode, with an averaged power of about 1.1 W. For the experiments, a gas flow rate of 3 standard liters per minute (slm) [41, 42] was kept constant and either pure argon was used or 1% of the feed gas was replaced with N_2 or O_2 . Alternatively, a mixture of 0.3% N_2 and 0.7% O_2 (all gases at 5.0 purity or 4.8 for O_2 , all gases purchased from Air Liquide) was used. The distance of the jet nozzle to the liquid surface was set to 9 mm for all experiments. The atmosphere has an impact on the plasma-induced chemistry for jets where the plasma propagates out of the nozzle. While the COST-jet is less affected as the discharge is confined between the electrodes, the kINPen can be influenced as the discharge propagates out of the nozzle. To allow for more stable ambient conditions in case of the kINPen, an external curtain gas consisting of N_2 with a flow rate of 5 slm was applied. The curtain gas device is formed by a concentric channel, which outlet was located exactly 1.9 mm from the jet's nozzle. It was shown that the presence of a curtain gas during the treatments influences the production of reactive species resulting in a different interaction with the treated fluids in which they are deposited [43–47].

The COST-jet is the outcome of the European COST action MP 1101 “Biomedical Applications of Atmospheric Pressure Plasma Technology” (2011–2015). It is intended as a general “baseline” onto which the efficacy of other plasma sources can be compared. It consists of two 1 mm thick metal plate electrodes spaced 1 mm apart in between the plasma is ignited. Two quartz glass windows make up the other sides of the rectangular gas channel, resulting in a plasma volume of 30 mm^3 . The plasma is ignited capacitively and is driven by an AC voltage at a frequency of 13.56 MHz. For further details see Golda *et al.* [40]. COST-Jet treatments were facilitated at a sample distance of 4 mm with the discharge power held constant at about 300 mW and a total gas flow of 1 slm. For gas mixtures, pure helium was used as well as the COST-jet “baseline” condition using an admixture of 0.5% O_2 . Additionally, to allow a closer comparison to the kINPen, admixtures of 1% O_2 , 1% N_2 or a mixture of both gases (0.3% N_2 + 0.7% O_2) were used. For all experiments with the exception of the EPR measurements, the COST-jet setup featured an additional cold trap using dry ice to purge the feed gases from any additional water residues and all gases were of 5.0 purity (Linde). Due to the short-lived nature of radicals, even spin-trapped ones, the COST-jet was transported to the INP for EPR measurements. Therefore, no cold trap was used for these experiments and O_2 admixture was of 4.8 purity (Air Liquide).

Sample preparation & plasma treatments

The cysteine model solutions were prepared daily by dissolving crystalline cysteine (Sigma-Aldrich) in double-distilled water (ddH₂O, Millipore) for a final concentration of 300 μM before each analysis, in order to minimize cysteine spontaneous oxidation. A 750 μL volume of each solution was treated in 24-well plates, with a 9 mm distance from the kINPen and 4 mm from the COST-jet, respectively. Prior to treatments, the well plates were cleaned with methanol in order to remove all kinds of compound that might interfere with downstream analytics. Treated samples were divided into aliquots and subjected to subsequent analysis.

Based on previous experiments, certain general treatment conditions were chosen for all of the following experiments. For both sources, conditions were chosen, which are already well investigated for their physio-chemical properties, e.g. production of certain RONS. Such groundwork is essential when trying to understand the impact of plasma-generated species onto biological targets. The COST-jet was employed using the reference conditions described in [40], as here, most information about RONS fluxes are known. The same is true for the chosen gas compositions. Using the COST-jet in this way allows other research groups to compare and adjust their own experiments to the data presented here using the COST-jet as a reference in the same way by performing experiments once with their own source and once with a COST-jet source. Further gas variations were chosen for the COST-jet to mimic molecular gas admixtures used with the kINPen. For the kINPen, standard conditions were chosen as well as these offer the most information to allow for data interpretation. In previous experiments, 1% of molecular gas admixtures were shown to yield a good balance between species production and discharge stability. Besides pure molecular gas admixtures, one condition was chosen where previous studies could demonstrate a high production of *NO radicals [48]. Furthermore, using 3 slm total gas flux at a distance of 9 mm was investigated in detail as well. These conditions allow treatments of liquids in 24 well plates without pushing the liquid to the well walls, which would result in the treatment of the well bottom instead of the liquid. Furthermore, the curtain gas setup was chosen for the kinpen as its discharge propagates out of the nozzle into the air and previous experiments have shown the strong impact of ambient conditions [49]. The COST-jet is less affected by ambient air due to its discharge being completely encased in its housing. Treatment times of 30 s were chosen after previous experiments showed a strong degradation of labile cysteine compounds at longer treatments [50]. For example, one product of high interest, S-nitrosocysteine, is known to be relatively unstable. Therefore, treatment times were further reduced compared to previous publications to increase yield of such unstable but potentially highly valuable products. However, to indicate general behavior of product formation over time, mass spectrometry experiments were performed for several time points (5 s, 15 s, 30 s, 45 s, 60 s) and resulting products assessed.

FTIR spectroscopy

For FTIR spectroscopy of cysteine silicon wafers (Siltronic AG) were chosen as substrate material, because of their transmission in the desired wavelength range. Wafers were cut into pieces (approx. 10 mm × 10 mm) and rinsed with ethanol prior to sample preparation. Droplets of 10 μl (COST-jet) or 15 μl (kINPen), respectively, of the plasma-treated cysteine model solutions were pipetted on the silicon wafers and dried by desiccation. A Bruker VERTEX FTIR-micro spectrometer was used for analysis of the L-cysteine samples according to Kogelheide *et al.* [26] The FTIR spectra were recorded from 750 cm⁻¹ to 4000 cm⁻¹ with a spectral resolution of 4 cm⁻¹ and a special focus on the free thiol signal (ν(S-H)) at 2545 cm⁻¹. For each droplet of cysteine, 10 spectra at different positions of the sample were recorded with each spectrum representing the mean of 64 measurements at each given position. Background

spectra were taken for each measurement to correct the influence of carbon dioxide and water in certain regions of the spectra. All transmission spectra (T) are converted into absorption spectra (A) using the relation

$$A = \log\left(\frac{1}{T}\right)$$

and baseline correction is carried out. Normalizing of the corrected data are carried out as follows:

$$x_{i,\text{norm}} = \frac{x_i}{\|x\|},$$

where $\|x\|$ denotes the Euclidean norm, x_i is the data point of wavenumber i and x denotes the vector of all sample points. The standard deviation was calculated assuming a Student's t -distribution. The relative peak intensities were calculated by integrating the peaks and subtracting the corresponding peak intensity, which is taken from the control sample.

Mass spectrometry

To elucidate the cysteine modifications caused by plasma treatment, high-resolution mass spectrometry (MS) was performed using a TripleTOF 5600 system (Sciex). Isotopically labelled cysteine (L-Cysteine- $^{13}\text{C}_3$ ^{15}N ; Sigma-Aldrich, #658057) served as internal standard (IS) at a fixed concentration of 100 μM . It was mixed with the sample directly before the emitter tip of the mass spectrometer through a capillary mixing tee using an electronically controlled syringe pump to prevent long-lived reactive species-derived modifications to the IS before analysis. Each sample was diluted 1:1 with 0.3% ammonium hydroxide in methanol (both Sigma, MS grade), to improve negative electrospray ionization. A flow of 10 $\mu\text{L}\cdot\text{min}^{-1}$ of each solution was injected into the Turbo V electrospray source (Sciex), using the following experimental parameters: capillary temperature 150°C, curtain gas: 35 slm N_2 , ion source gas 1: 20 slm N_2 , ion source gas 2: 25 slm N_2 , ion spray voltage: -4000 V.

Survey spectra acquisition (MS) was performed in a 50–400 m/z range and with negative polarity (accumulation time 250 ms). Fragmentation spectra (MS/MS) of each identified peak were acquired in product ion mode (collision energy -24 eV, declustering potential -10 kV) in order to obtain structural information and to identify the cysteine derivatives following each kind of treatment. The formula of each compound and the accurate mass have been identified through the support of the "Formula Finder" and "Mass Calculator" tools included in Peak-View 1.2.0.3 (Sciex). For data analysis, a threshold value of 300 counts of the peak height (15 times background) was set for the integration of the total ion current (TIC) signals to ensure proper signal-to-noise ratio. Calibration of the mass spectrometer was performed daily against the mass-to-charge ratios of cysteine and its most representative derivative products. Cysteine-free double-distilled water solutions and cysteine solutions with H_2O_2 were used as control solutions for subsequent analyses and data evaluation. For data analysis, the area of each identified peak in a spectrum was first normalized on the total area of each spectrum (area percent) to adjust peak areas for variances in injection. Afterwards, the area percent of each identified molecule was normalized to that of the IS to adjust for variation in ionization efficacy and spray stability.

Electron paramagnetic resonance spectroscopy

For the detection of $\cdot\text{NO}$ in solution, electron paramagnetic resonance (EPR) spectroscopy measurements were performed. An X-band (9.87 GHz) spectrometer (EMXmicro, Bruker)

was used with a modulation frequency of 100 kHz, modulation amplitude of 0.1 mT, microwave power of 5.024 mW, receiver gain of 30 dB, and time constant of 0.01 ms. To detect $\cdot\text{NO}$, a nitronyl nitroxyl radical (NNR) spin trap (Carboxy-PTIO (2-(4-Carboxyphenyl)-4,4,5,5-tetramethylimidazoline-1-oxyl-3-oxide, Dojindo Laboratoire), was used at 60 μM , which forms an imino nitroxyl radical (INR) with $\cdot\text{NO}$. BMPO (5-tert-Butoxycarbonyl-5-methyl-1-pyrroline-N-oxide, also Dojindo) was used as a spin trap for sulfur, hydroxyl, and superoxide anion radicals. For some experiment, 60 μM Carboxy-PTIO were mixed with 2 mM BMPO immediately before use. The spin trap solutions were freshly prepared prior each experiment and untreated samples were measured as respective controls. The maximum handling delay between treatment and measurement was three minutes. The spectra were recorded and evaluated by Bruker's Xenon software. More details about the measurement procedure and evaluation of the spectra can be found in a previous publication [47].

Ion chromatography

The quantification of nitrite (NO_2^-) and nitrate (NO_3^-) was performed via ion chromatography (ICS-5000, Thermo Fisher Scientific). After treatment, samples were diluted three fold using ultrapure water (MilliQ) before injecting 10 μL onto an IonPac AS23 anion exchange column (2 x 250 mm, Thermo Fisher Scientific). An isocratic mobile phase (4.5 mM $\text{Na}_2\text{CO}_3/0.8$ mM NaHCO_3) with 250 $\mu\text{L}/\text{min}$ flow rate was used. Chromatographic data was collected using a combined UV (210 nm) and conductivity detector. The system was calibrated using the Dionex 7-anions standard (Thermo Fisher Scientific) on a weekly basis.

Colorimetric hydrogen peroxide assay

Hydrogen peroxide (H_2O_2) was quantified via the colorimetric reaction with xylenol orange using a commercially available assay (Pierce Quantitative Peroxide Assay Kit, Thermo Scientific) according to the manufacturer's protocol. The assay is based on the oxidation of ferrous to ferric ion by hydrogen peroxide in presence of the dye which can be detected photometrically (Tecan Infinite M200 Pro, Tecan) at 595 nm. Each 96-well plate contained a standard curve (0 to 150 μM , in triplicates) and the samples ($n = 4$, each sample in triplicates).

Results

First screening of appropriate gas variations

In a first step, the general impact of plasma treatment on the cysteine probe was examined. From previous publications, it could be expected that the thiol moiety would be the most susceptible target of plasma-generated species [50]. As a quick first screening, the $\nu(\text{S-H})$ band (2545 cm^{-1}) was observed for all treatment conditions (Fig 1). A decrease of this band indicates a loss of free thiol moieties in the sample, suggesting weak or strong interaction of plasma-generated species with the thiol group, respectively. Several conditions were screened and the most promising variations are presented here and used for further study. kINPen treatment showed a notable influence on the thiol group regardless of gas composition. Ar + O_2 or the combined $\text{O}_2 + \text{N}_2$ mixture show a slightly stronger reduction of the thiol band as the other conditions. For the COST-jet, oxygen admixtures, especially 1% O_2 showed a very strong effect on $\nu(\text{S-H})$ intensity, whereas treatments using either N_2 or pure He were least effective in thiol conversion.

Determination of cysteine derivatives after plasma treatment

Mass spectrometry was used to determine the observed cysteine modifications at different treatment times with a special focus on nitrosylated cysteine derivatives. Table 1 shows details

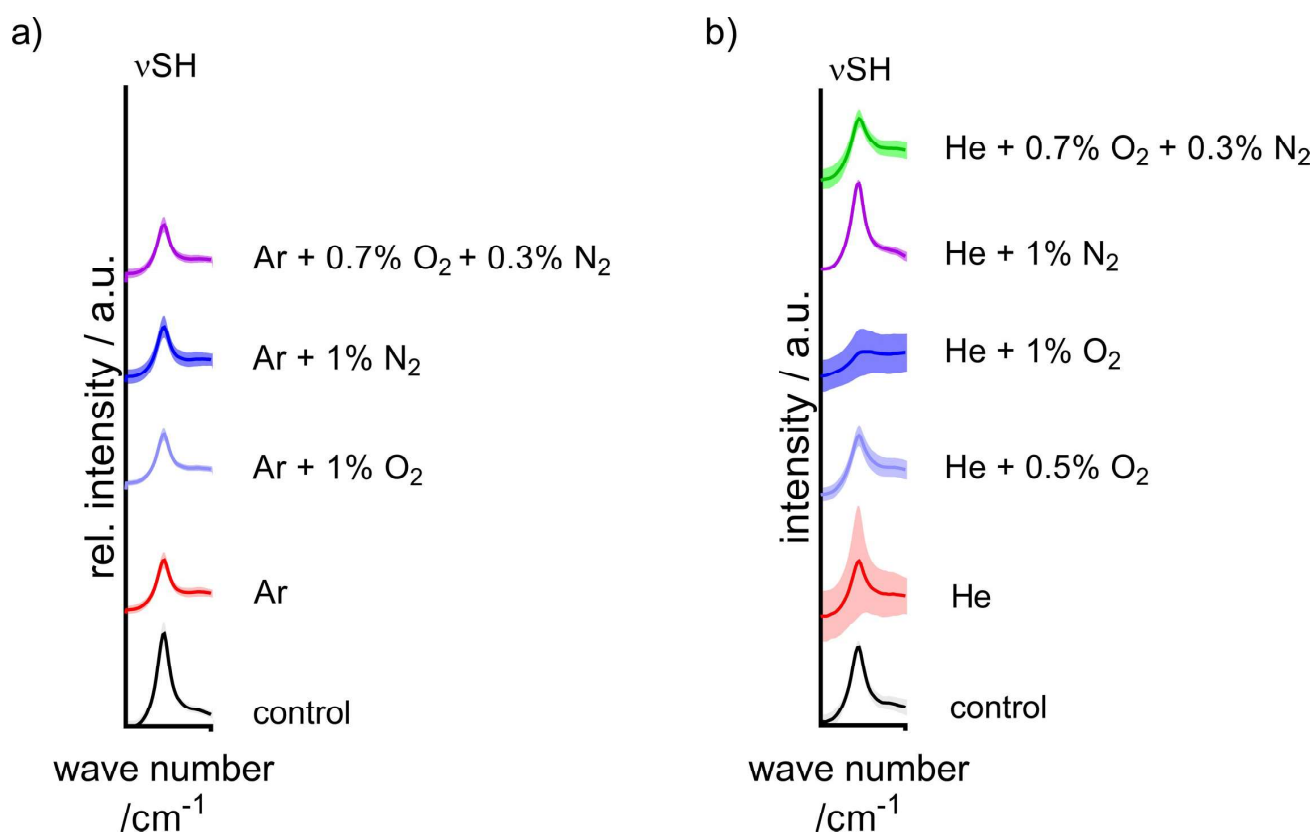


Fig 1. Thiol band signal of cysteine after plasma treatment. The FTIR signal at 2545 cm^{-1} was observed as an indicator of free thiols in the plasma-treated samples. The ν (S-H) band after 30 s of kINPen (a) and COST-jet (b) treatment used for rapid screening to identify plasma conditions with the highest impact on cysteine. Means are shown (lines) with shadowed area denoting standard errors calculated from all respective measurements ($n = 3 \times 64$ spectra). Peak annotation following Pawlukojc *et al.* [51].

<https://doi.org/10.1371/journal.pone.0216606.g001>

of the identified major compounds for easier reference. In Fig 2, a representative spectrum recorded for untreated and treated cysteine solution is shown. The structures of the different cysteine derivatives were identified by MS/MS analysis of signals of interest and respective fine masses.

As shown in Fig 2, the dominant changes observed after kINPen treatment were of oxidative nature and predominantly concerned the thiol structure. Cystine ($\text{C}_6\text{H}_{12}\text{N}_2\text{O}_4\text{S}_2$, 239.0160

Table 1. Major compounds, formula, and mass to charge value of identified compounds before and after cysteine treatments with CAP.

Compound	Formula	m/z
Cysteine	$\text{C}_3\text{H}_7\text{NO}_2\text{S}$	120.0119
Cysteine- $^{13}\text{C}_3$, ^{15}N (IS)	$\text{C}_3\text{H}_7\text{NO}_2\text{S}$	124.0191
Cystine	$\text{C}_6\text{H}_{12}\text{N}_2\text{O}_4\text{S}_2$	239.016
Cysteine sulfinic acid	$\text{C}_3\text{H}_7\text{NO}_4\text{S}$	152.0017
Cysteine sulfonic acid	$\text{C}_3\text{H}_7\text{NO}_5\text{S}$	167.9967
S-nitrosocysteine	$\text{C}_3\text{H}_6\text{N}_2\text{O}_3\text{S}$	149.0021

<https://doi.org/10.1371/journal.pone.0216606.t001>

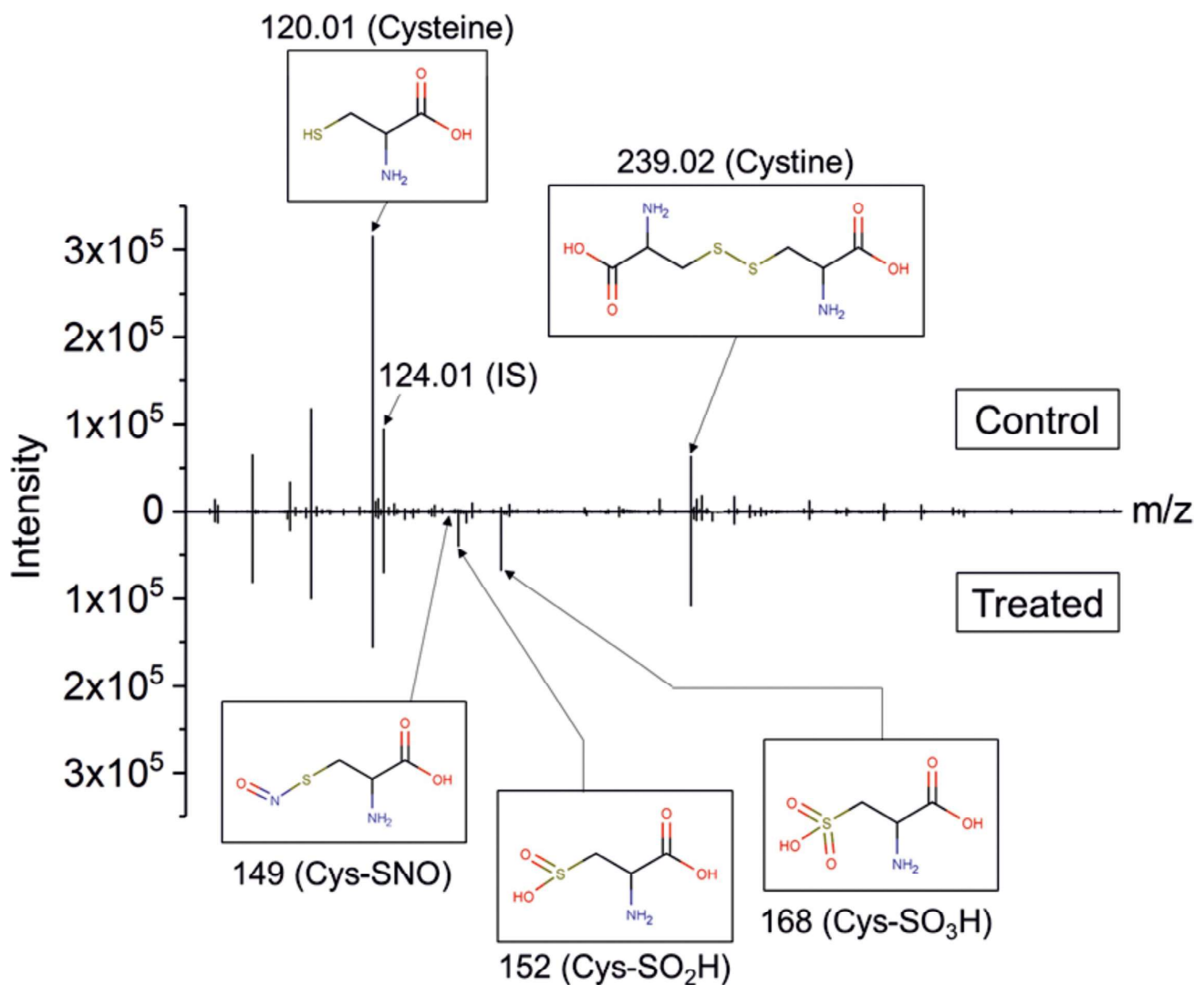


Fig 2. Representative MS spectra of untreated control and kINPen-treated cysteine solutions. Cysteine was treated with kINPen for 30 s using Ar with 0.3% O₂ + 0.7% N₂ as working gas and 5 slm N₂ as curtain gas. The peak at 124.02 m/z represents the internal standard (IS). Selection of identified peaks: cysteine (120.01 m/z), cystine (239.02 m/z), S-nitrosocysteine (Cys-SNO, 149 m/z) (not visible in the spectra), cysteine sulfinic acid (Cys-SO₂H, 152 m/z), cysteine sulfonic acid or Cys-SO₃H (168 m/z).

<https://doi.org/10.1371/journal.pone.0216606.g002>

m/z) and cysteine sulfonic acid (Cys-SO₃H, C₃H₆NO₃S, 167.9967 m/z) were the most abundant compounds, followed by cysteine sulfinic acid (Cys-SO₂H, C₃H₆NO₄S, 152.0018 m/z), which is in good agreement with previous experiments [17]. The initial product of these derivatives, cysteine sulfenic acid (Cys-SOH, C₃H₆NO₃S, 136.0068 m/z), was not observed, most likely due to its instability during ionization. To allow a more comprehensive overview of the production efficacies of the various sources and conditions, spectral intensities were normalized on the spiked-in IS (heavy cysteine, ¹³C₃H₇¹⁵N₂S, 124.02 m/z) and the normalized peak areas plotted for the different identified products (Fig 3 and Fig 4). Treatments with the kINPen (Fig 3A, 3C, 3E and 3G) showed the highest consumption of cysteine (Fig 3A) and subsequent production of oxidized stable derivatives, such as cysteine sulfonic acid (Fig 3G), were

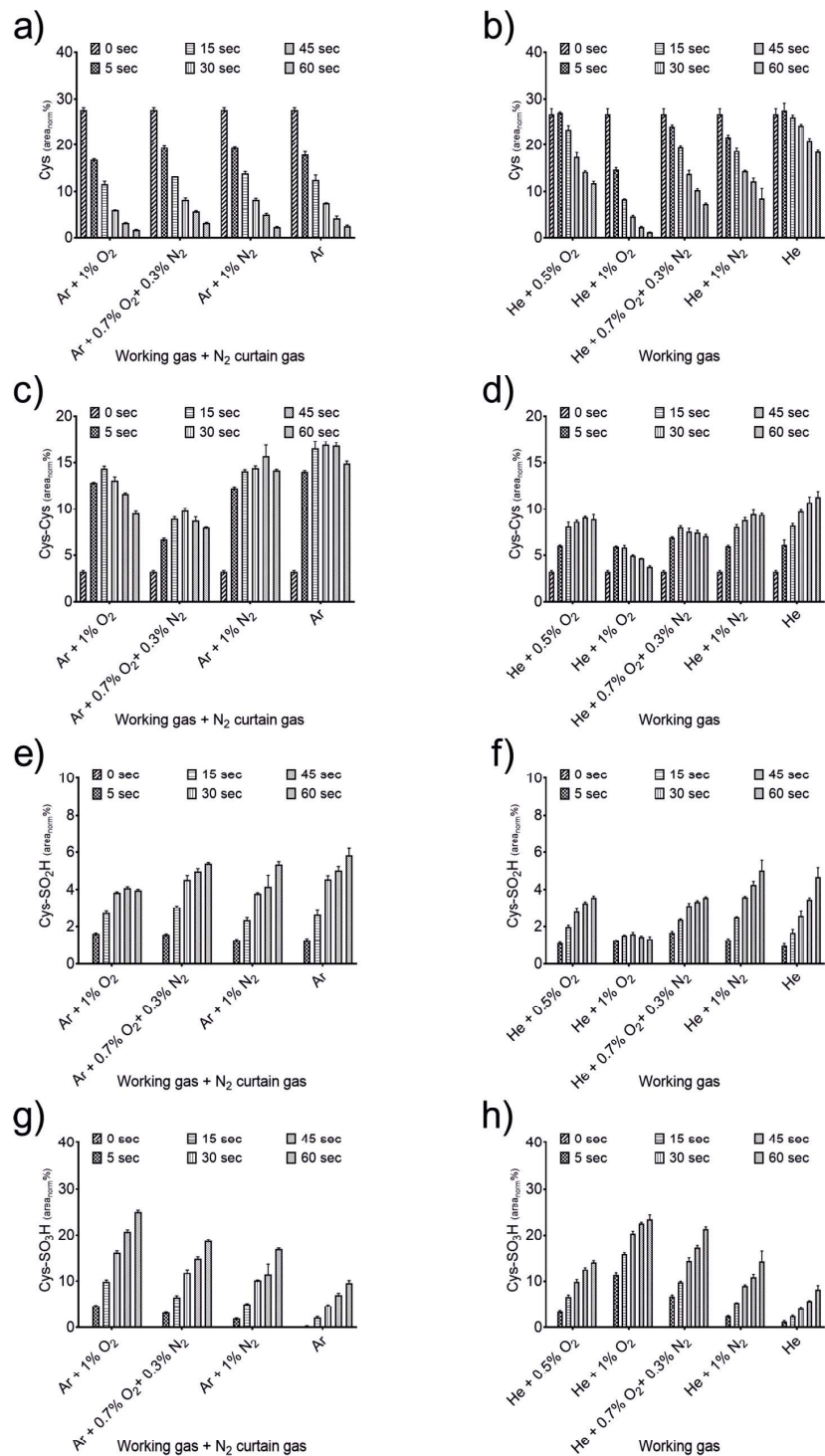


Fig 3. Relative abundances of cysteine and produced oxidative derivatives after plasma treatment. Either the kINPen with N₂ curtain gas (a, c, e, g) or COST-jet (b, d, f, h) were used for treatments of different durations (5, 15, 30,

45, 60 s) with the denoted gas variations. Spectra were normalized on the IS and peak areas were calculated. Triplicates ($n = 3$) with standard deviation are shown.

<https://doi.org/10.1371/journal.pone.0216606.g003>

observed for 1% O₂ admixture and prolonged treatment times. Under the same conditions, labile derivatives, such as cystine (Fig 3C) and cysteine sulfinic acid (Fig 3E), decreased over time. In contrast, admixture of either 1% N₂ or the O₂-N₂ mixture led to fewer stable oxidized products, combined with an increase of labile compounds, showing a lower oxidative impact.

Treating the cysteine solution with the COST-jet led to the formation of a largely similar product range and yields (Fig 3B, 3D, 3F and 3H). Indeed, by using 1% O₂ in He working gas, an even higher cysteine oxidation was achieved (Fig 3B). A strong production of sulfonic acid was observed (Fig 3H), while cystine (Fig 3D) and sulfinic acid (Fig 3F) decreased. As observed for the kINPen treatment, working gas with lower amounts of oxygen resulted in a lower oxidative impact on cysteine and its chemical relatives. The observed product range clearly indicate a major role of reactive oxygen species in CAP-derived liquid phase chemistry of both plasma sources investigated. It is not manifest, which species play the most dominant role, though atomic oxygen and singlet oxygen must be considered because oxygen-enriched CAPs produce these species in high amounts [8, 52, 53]. Conditions where predominantly hydrogen peroxide is deposited (pure Ar or Ar + 1% N₂), were found less effective in the production of higher oxidized cysteine derivatives. Similarly, a limited oxidation of cysteine is evident in conditions of low or non-oxygen admixtures in the feed gas, such as pure helium, by the predominant production of cystine (Fig 3E and 3F).

Although oxidative modifications of the cysteine's thiol moiety were dominant S-nitroso-cysteine (Cys-SNO, C₃H₆N₂O₃S, 149.0021 m/z) was found in small quantities, indicating the presence and direct reaction of plasma-derived nitrogen reactive species (Fig 4). For the

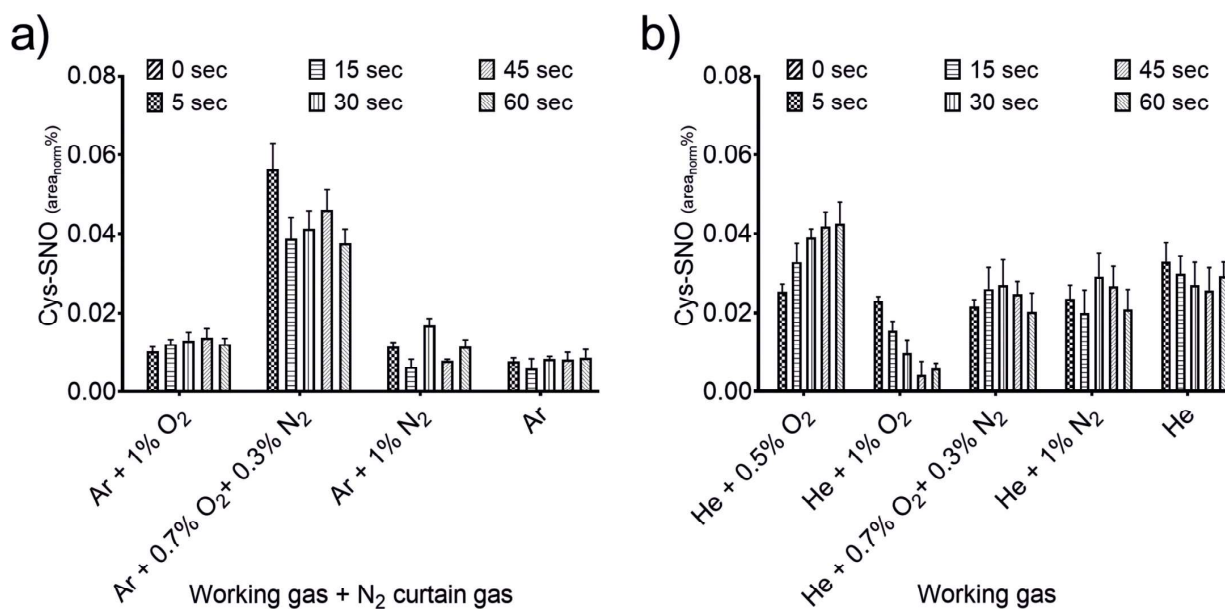


Fig 4. Production of Cys-SNO due to plasma treatment. Either kINPen with N₂ curtain gas (a) or COST-jet (b) were used for treatments of different durations (5, 15, 30, 45, 60 s) with the indicated feed gas variations. Spectra were normalized on the IS and peak areas were calculated. Triplicates ($n = 3$) with standard deviation are shown.

<https://doi.org/10.1371/journal.pone.0216606.g004>

kINPen (Fig 4A), modulation of the working gas had a strong impact on Cys-SNO production. While admixture of oxygen quenched its production, treatment of the cysteine solutions with pure Ar as well as N₂ or N₂ + O₂ admixtures resulted in a significantly higher production. In contrast, relatively stable concentrations were observed for all COST-jet conditions in ambient air environment (Fig 4B). Interestingly, it became obvious that the implementation of the curtain gas setup yielded a higher Cys-SNO production than using the kINPen in ambient air [50]. As production of oxidative modifications were in good agreement between both sources, the variations in Cys-SNO production were further investigated to reveal the related liquid chemistry occurring during plasma treatment.

Elucidation of free radicals in cysteine-containing solutions

Deposition of free radicals was analyzed for both sources using EPR spectroscopy. In Fig 5, the resulting concentrations of the [•]NO-adduct (INR, imino nitroxide) are given for the different feed gas compositions after kINPen (a) or COST-jet (b) treatment of ddH₂O. No clear difference could be determined for feed gas admixture containing either 1% O₂ or 0.7% O₂ + 0.3% N₂ (Fig 5A). In cases where no O₂ was present in the feed gas (Ar or Ar + 1% N₂) as well as for the gas control (Ar + 0.3% N₂ + 0.7% O₂ without plasma ignition) no [•]NO-adduct was measured. This is in agreement with a previous study, where the origin of the liquid phase [•]NO was investigated [54]. There, the optimum of [•]NO production in phosphate buffered solution has been found to be at O₂ amounts of 0.7% O₂ + 0.3% N₂ in the argon feed gas using N₂ as curtain gas. A lower amount of O₂ in the feed gas resulted in a lower [•]NO-adduct concentration in the liquid. Moreover, a small amount of N₂ in the feed gas increased production. Details about possible formation pathways of [•]NO in the liquid can be found in Jablonowski *et al.* [54].

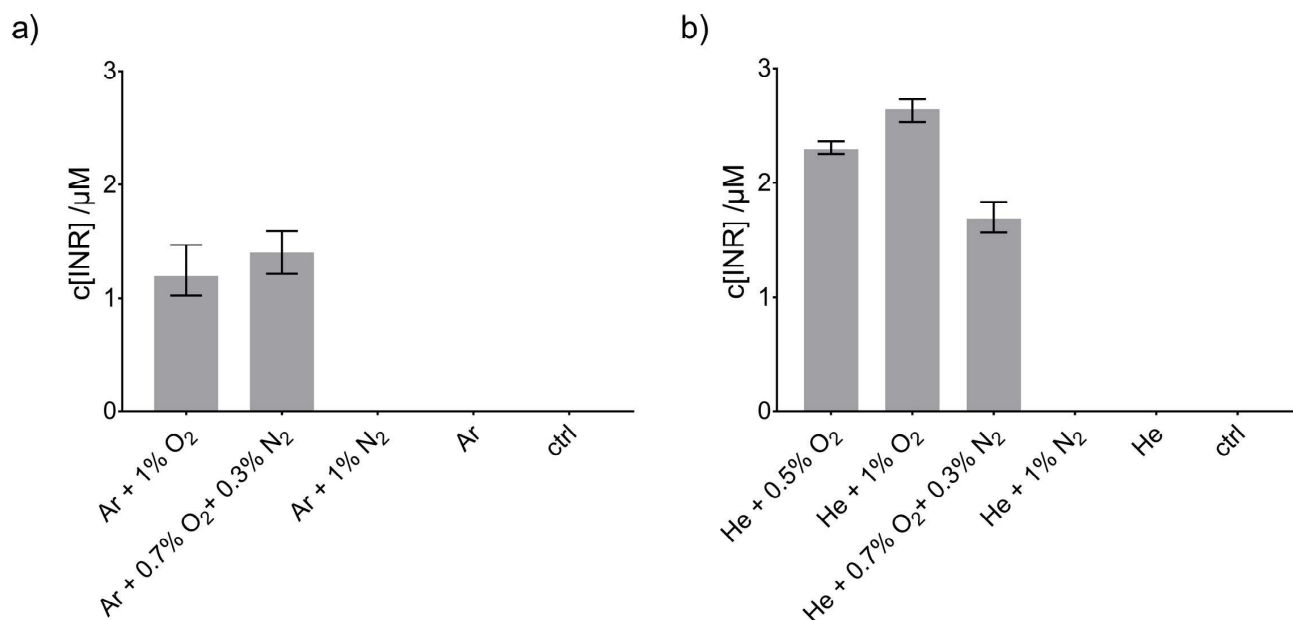


Fig 5. Concentration of the [•]NO-spin trap adduct (INR) after treatment of ddH₂O. Treatment was performed with the kINPen in N₂ environment (a) using the curtain gas device for 9 mm distance between the nozzle and the liquid surface or the COST-jet (b) at 4 mm nozzle-liquid distance in atmospheric air environment. For both plasma sources, different feed gas compositions were studied. Triplicates (n = 3) with standard deviation are shown.

<https://doi.org/10.1371/journal.pone.0216606.g005>

The deposition of NO by the COST-jet was in the same concentration range with highest amounts determined for He with 0.5% and 1% O₂ admixture. When the feed gas contained both O₂ and N₂, yields decreased.

To meet reference conditions, the COST-jet was operated at 4 mm electrode-liquid distance, compared to 9 mm for the kINPen, which might result in higher [•]O densities near the gas-liquid interface for the COST-jet. However, [•]O densities can also be affected by the mean gas velocity, which is higher for kINPen, as well as the gas flux dynamics (turbulent in kINPen, laminar in COST-jet) [49, 55]. The COST-jet is well known to produce relevant amounts of [•]O in the gas and liquid phase [56, 57]. Without the O₂ in the feed gas, one of the precursors of liquid [•]NO would be missing, and in this condition no dissolved [•]NO was detectable for both plasma jets by EPR.

In the presence of cysteine, no [•]NO-adduct was detected. However, the absence of any [•]NO-adduct signal does not necessarily mean that no [•]NO is produced. Carboxy-PTIO reacts with [•]NO to the imino nitroxide and [•]NO₂ ($k_1 = 0.5\text{--}16 \times 10^4 \text{ M}^{-1} \text{ s}^{-1}$) [58]. A faster reaction partner, e.g. low molecular weight thiols, may scavenge [•]NO. The reaction rate of such a reaction was determined to be $1.5\text{--}3 \times 10^5 \text{ M}^{-1} \text{ s}^{-1}$, being slightly higher than the reaction of [•]NO with Carboxy-PTIO and such result in its underestimation by EPR in the presence of cysteine [59].

The role of cysteine in altering NO detection via scavenging or other secondary effects was investigated by combining Carboxy-PTIO and BMPO to trap interfering radicals and measure these alongside [•]NO. The measured EPR spectra together with the simulated sum spectra are shown in Fig 6A. Fig 6B shows the simulated spectra of the [•]NO-adduct (INR), whereas Fig 6C–6E shows the adducts formed by BMPO: BMPO-OH (c), BMPO-OOH (d), BMPO-S (thiyl radical, e). The calculated concentrations of the spin adducts is given in Fig 6F. It needs to be kept in mind that all radicals have distinct reaction rates with the spin traps and different efficacies of being trapped.

Interestingly, by combination of the two spin traps, the [•]NO-adduct became detectable again (Fig 6C). Moreover, also adducts of [•]OH- and O₂^{•-} adducts of BMPO as well as a thiyl radical adduct of BMPO (BMPO-S) were detected. This demonstrates that the radicals interacting with cysteine hinder the detection of [•]NO by Carboxy-PTIO. As soon as they were scavenged by BMPO, they were not able to interact with cysteine, and therefore, did not hinder the measurement any further. A potential underlying reaction pathway runs via hydroxyl radicals. Highly reactive [•]OH is a likely candidate to attack the thiol group of cysteine [60], as the S-H bond energy is only 3.6 eV [61], yielding water and the detected thiyl radical. The latter can react with [•]NO forming Cys-SNO, which is not EPR sensitive. Alternative reaction mechanism leading to S-H bond cleavage would have a similar effect [50]. Hence, it can be postulated that in the presence of thiyl radicals [•]NO is scavenged to form Cys-SNO, evading detection by Carboxy-PTIO. For the COST-jet, the spin trap/cysteine mixture was performed as well. In contrast to the kINPen, this measurement only yielded the initial NNR signal and no BMPO-adducts or INR were detected after COST-jet treatment showing a complete absence of (detectable) [•]NO (data not shown). This indicates that the [•]NO-formation pathway is different for both plasma sources. Furthermore, the absence of [•]OH and O₂^{•-} indicates a different oxygen chemistry in the liquid as well. With that, the BMPO-S adduct was also missing as expected according to its formation by [•]OH.

Profile of the RNS reservoir (NO₂⁻) and dump (NO₃⁻)

To complement the analysis of short-lived species, the deposition of the reservoir RNS, nitrite (NO₂⁻) and nitrate (NO₃⁻) in presence or absence of cysteine was determined. Figs 8 (kINPen) and 7 (COST-jet) show the respective nitrite and nitrate profiles. For the kINPen, a large

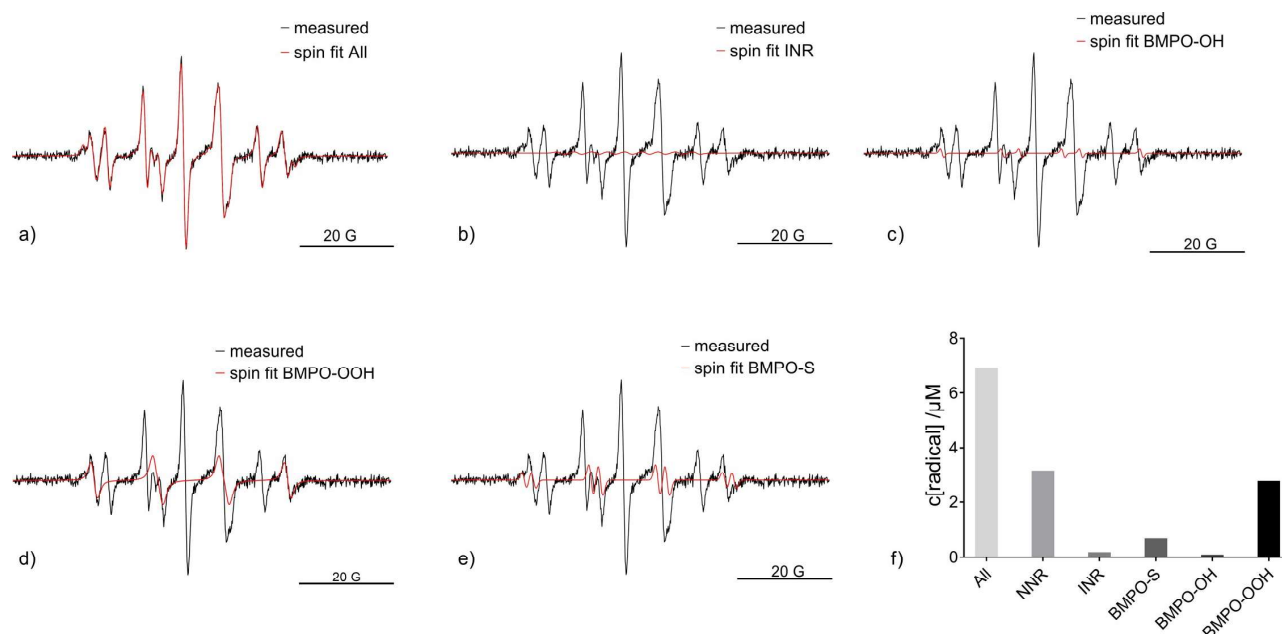


Fig 6. Measured and simulated EPR spectra after kINPen treatment. Measurements and fitted spectra are presented for (a) after treatment of ddH₂O + cysteine with the kINPen with Ar + 0.7% O₂ + 0.3% N₂ and N₂ curtain gas using both BMPO and Carboxy-PTIO as spin traps. In b), the measured spectra together with the [•]NO-adduct (INR) are given. The measured spectra and simulated spectra of BMPO spin adducts of the hydroxyl (c), the superoxide anion (d), and the sulfur (e) radicals are shown (n = 1). In f), the resulting concentrations of the spin trap adducts after 30 seconds treatment of ddH₂O+cysteine with the kINPen using N₂ as curtain gas are given. The bars represent the overall radical concentration in the solution (all), NNR represents the concentration of the unreacted Carboxy-PTIO, INR of the [•]NO-adduct, BMPO-S of the BMPO-trapped sulfur radicals, BMPO-OH of the BMPO-adduct of the hydroxyl radical, and BMPO-OOH of the BMPO-adducts of superoxide anion radicals.

<https://doi.org/10.1371/journal.pone.0216606.g006>

impact on deposition rate was found for the feed gas variation with the highest seen for O₂ + N₂ combination. The presence of cysteine modulated NO₂⁻/NO₃⁻ deposition ratio, with higher amounts of NO₂⁻ detected in its absence.

In contrast, COST-jet treatment (Fig 7) resulted in lower and relatively equal levels of NO₂⁻ with little impact of chosen feed gas composition. In the presence of cysteine, a slight trend following kINPen results could be observed. However, NO₃⁻ production using the COST-jet was independent of cysteine presence in the treated solution. Most likely, the presence of ambient air around the effluent instead of nitrogen as for the kINPen, its different geometry and relative low gas flux contribute to the disparities. As already discussed above, the reaction pathways of RNS seem to be different from the kINPen. The stable production of low amounts of NO₂⁻ and NO₃⁻ under certain conditions (e.g. pure He or He + 1% N₂) indicate that the observed species are not produced by secondary liquid reactions but predominantly by gas phase reactions. These species dissolve into the treated liquid and, given identical treatment times and gas flow pattern at the liquid surface, explain the rather invariable deposition. However, this notion also assumes a RNS gas phase chemistry that only slightly depends on feed gas composition and pointing towards the active He states.

After generation, further liquid chemistry affects (final) levels of NO₂⁻ and NO₃⁻. In ddH₂O, deposited NO₂⁻ can react further to ultimately yield NO₃⁻ via two major pathways: either oxidation by H₂O₂ leading to the (transient) formation of peroxyntirite (ONOO⁻) [62, 63] or disproportionation forming NO₂ and [•]NO [64], with subsequent disproportion of nitrogen dioxide and oxidation of [•]NO by air or CAP derived oxygen species. A number of

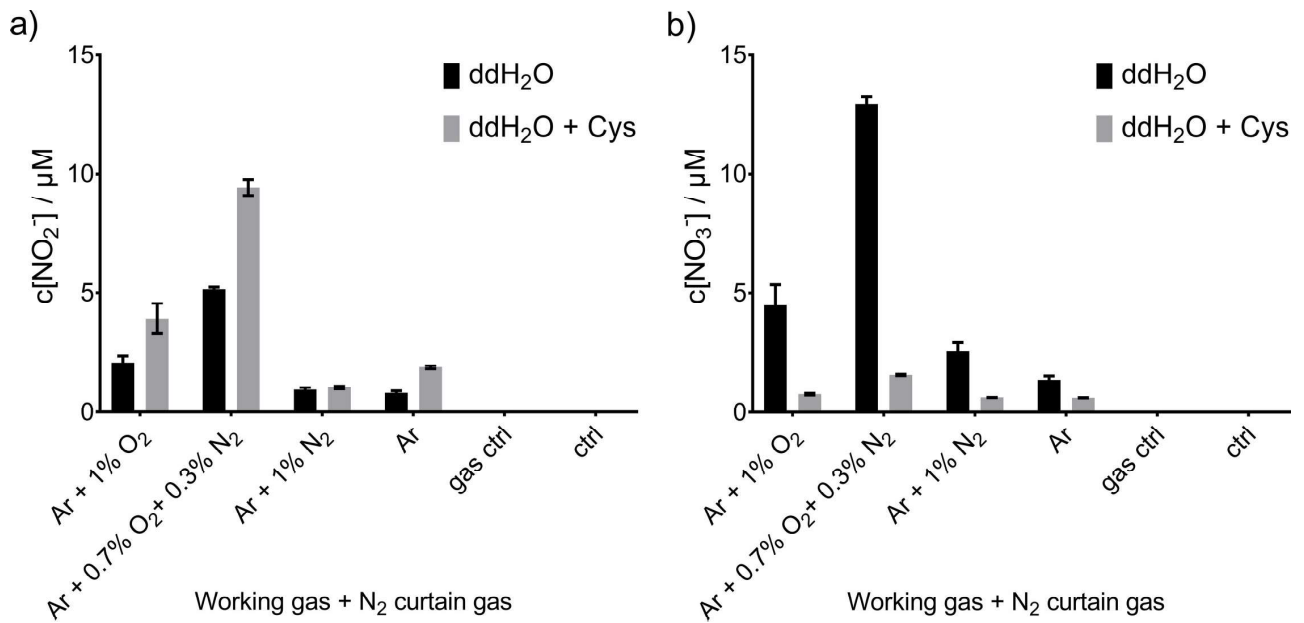


Fig 7. NO_2^- (a) and NO_3^- (b) concentration after kINPen treatment. kINPen was used with N₂ curtain gas and with different feed gas compositions in a N₂ environment provided by the curtain gas. Triplicates (n = 3) with standard deviation are shown.

<https://doi.org/10.1371/journal.pone.0216606.g007>

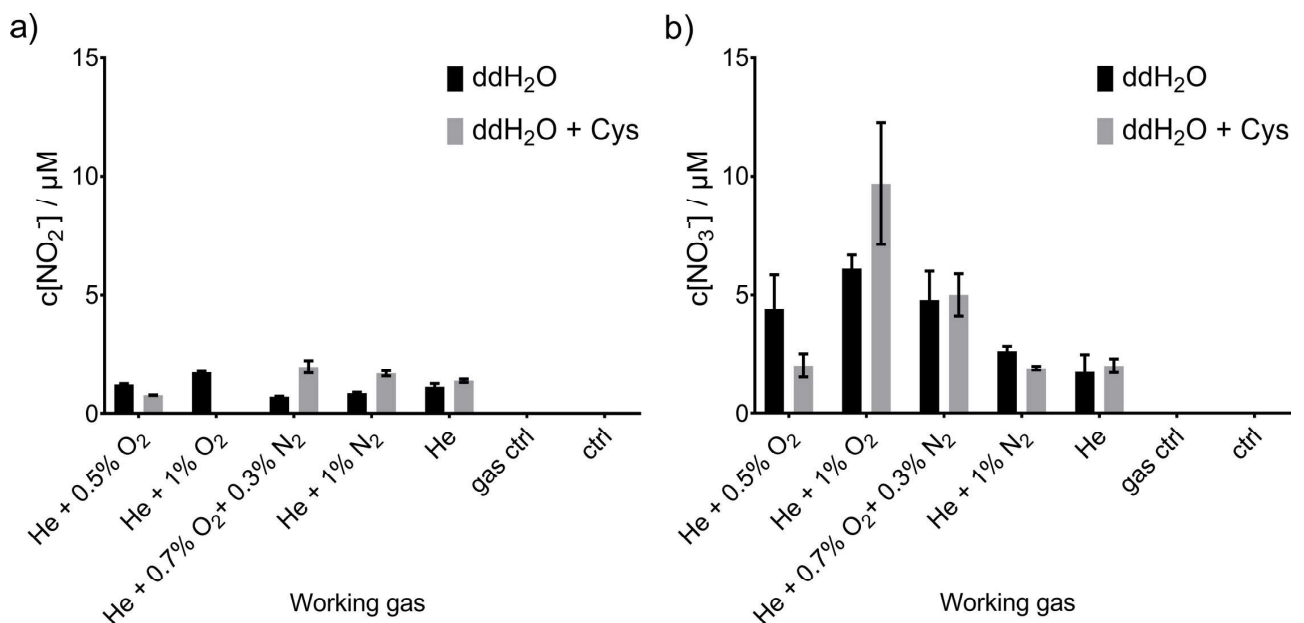
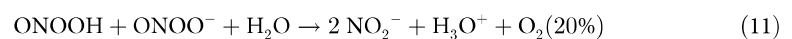
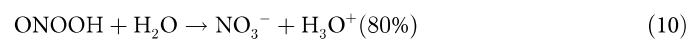
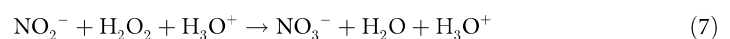
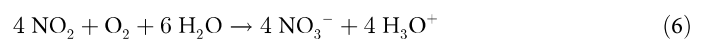
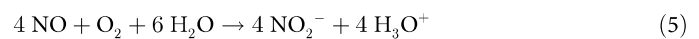
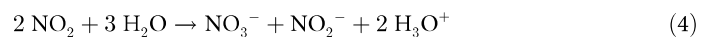
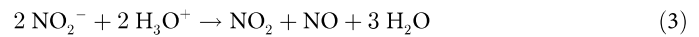
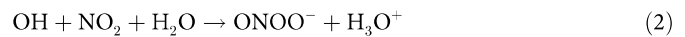
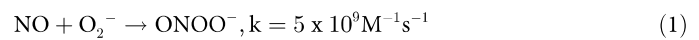


Fig 8. Nitrite, NO_2^- (a) and NO_3^- (b) concentration after COST-jet treatment. Treatment was performed in ambient air with the different feed gas compositions. Triplicates (n = 3) with standard deviations are shown.

<https://doi.org/10.1371/journal.pone.0216606.g008>

concurrent reactions allow a rapid rearrangement of the RNS in the liquid phase, with peroxy-nitrite as an important intermediate and nitrite and nitrate as the final, stable product [65]:



Both reaction pathways benefit from lower pH, and can be reduced via buffering at neutral to alkaline pH. Higher concentrations of NO_3^- than NO_2^- were expected in case of oxidizing conditions and cysteine, acting as a scavenger for oxidative species, subsequently increases the detected nitrite levels. Additionally, the NO_2^- generated as a by-product by the direct reaction of the intermediates N_2O_3 or ONOO^- with cysteine to form S-nitrosocysteine may contribute to the observation [66].

Deposition of hydrogen peroxide

Hydrogen peroxide (H_2O_2) is a long-lived reactive species known to affect various liquid chemistry reactions triggered by cold plasma treatment. The kINPen (Fig 9A) showed clear dependency of H_2O_2 -production on the presence of cysteine and on the feed gas composition. The maximal H_2O_2 concentration was determined for pure argon feed gas (38 μM), with higher concentrations in dd H_2O than for cysteine containing solutions. This was expected, as cysteine reacts with H_2O_2 forming predominantly cystine, with some other derivatives [50]. According to the observed product spectrum, it seems likely that H_2O_2 precursor compounds oxidize cysteine, which ultimately results in lower detectable H_2O_2 concentrations. Under dedicated conditions, one thiol moiety can react with up to five $\cdot\text{OH}$ (one electron oxidants) to form a single cysteine sulfonic acid molecule [67]. Using the kINPen with oxygen admixture, no H_2O_2 was detectable in treated cysteine-containing solutions. Interestingly, these were the conditions where most $\cdot\text{NO}$ was generated in the liquid and the highest production of Cys-SNO was observed. One reason could be that $\cdot\text{OH}$, a dominant precursor of H_2O_2 , reacted directly with the cysteine, abstracting hydrogen and enabled $\cdot\text{NO}$ and NO_2^- to react directly with the cysteine and thereby being itself consumed.

For the COST-jet without cysteine present in the liquid, the highest concentration ($5 \mu\text{M}$) was reached for He + 1% N_2 , the other investigated conditions yielded similar concentration range with He + 1% O_2 as lowest concentration reached (Fig 9B). Interestingly, the COST-jet seemed to be not so sensitively responding to molecular admixtures regarding the stable reactive oxygen and nitrogen species formation. A possible explanation might be the usage of the cold trap reducing the amount of water impurities, which most likely are the main source of H_2O_2 , from the feed gas.

Discussion

It is evident that the products derived from the plasma-assisted oxidation of cysteine mainly concern its thiol group, with the cysteine sulfonic acid and cysteine sulfinic acid as the main products even after short treatments. Cysteine sulfinic acid, which is a dominant precursor for downstream oxidation products, was not observed. According to the presence of cystine as a major product, it plays a role as intermediate. Assumingly its fast decay in the oxidative environment and further its instability during MS ionization contribute to this observation. These results are in good agreement with previous works conducted with a DBD, the COST-jet with other parameters, or the kINPen without curtain gas [26, 68]. Oxidation processes are the driving force under all tested conditions, suggesting that the plasma derived liquid chemistry in water is less variable than expected from gas phase measurements but seem to be strongly influenced by the chemical attributes of the presented target.

Besides the strongly oxidized products (sulfur oxidation state $> +2$), cystine (oxidation state $= -1$) was highly abundant but further targeted by the plasma derived species with increasing treatment time to yield partially or fully oxidized disulfides (oxidation state $= +1$ and higher) [68]. As the targeted formation of disulfide bonds would allow the modulation of numerous cellular redox processes, shorter treatment times and/or less oxidizing conditions

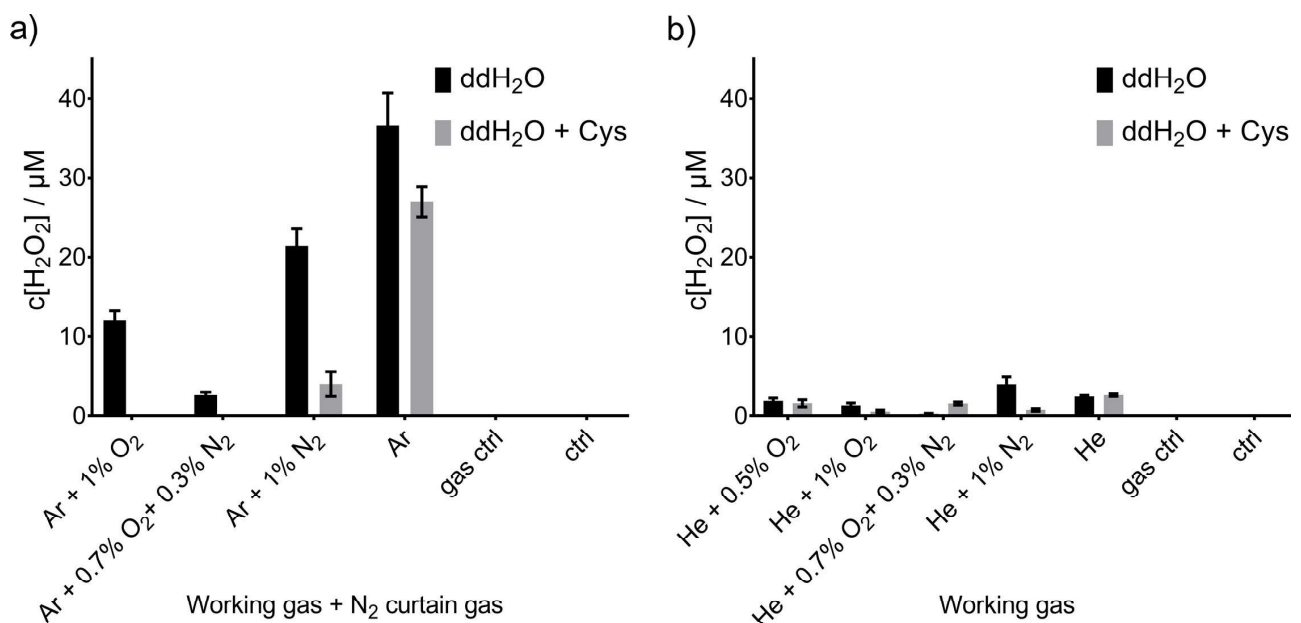


Fig 9. Hydrogen peroxide concentration after plasma treatment using the kINPen (a) or COST-jet (b). Treatment with the kINPen were performed in N_2 environment due to curtain gas, COST-jet was operated in open air. Triplicates ($n = 3$) with standard deviation are shown.

<https://doi.org/10.1371/journal.pone.0216606.g009>

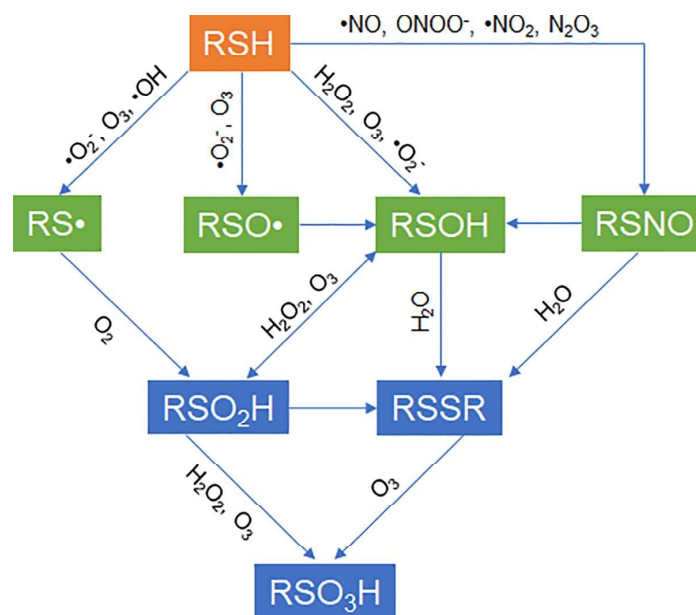


Fig 10. Possible pathway of formation of the main cysteine derivatives in oxidative cellular conditions. Cysteine (RSH, upper row) can react to the intermediary derivatives (middle row) cysteine sulfenic acid (RSOH), S-nitrosocysteine (RSNO), cysteinyl radicals (RS \cdot) and cysteine sulfenyl radicals (RSO \cdot). In turn, these react to the stable derivatives (lower two rows) cysteine sulfenic acid (RS $_2$ OH), cystine (RSSR), and cysteine sulfonic acid (RSO $_3$ H). Pathways taken from [80–83].

<https://doi.org/10.1371/journal.pone.0216606.g010>

would allow control over the target instead of over-oxidation. However, experiments in more complex model systems as well as with other plasma sources are necessary to prove these points.

Besides a moderate target oxidation, an increased production of biologically active and clinically relevant S-nitrosocysteine directly at the location of interest and in combination with the other advantages of a plasma treatment would be highly beneficial in several pathologies including, *e.g.* chronic wounds [69–71]. Therefore, optimizing CAPs for the production of S-nitrosocysteine would open up additional medical treatment options as well as increase efficacies of current treatment regimes. However, with oxidative cysteine modifications making up the majority of products, formation of S-nitrosocysteine was observed to a limited extent only, even when discharge conditions were optimized for NO deposition (Fig 10). Compared to previous results [50], the usage of an N $_2$ curtain combined with an admixture of 0.7% N $_2$ + 0.3% O $_2$ led to a threefold increase in Cys-SNO production compared to all other tested conditions. It seems likely that further tuning of the discharge parameters and ambient conditions could favor an increase in thiol nitrosylation. The low amounts detected may be attributed to a faster formation of the oxidative modifications and/or a fast decay of the nitrosylated thiols under the prevailing conditions. This is in line with formerly published data on nitrosothiol decay indicating an immediate decomposition in aqueous liquids, especially when the β -carbon atom carries an amino group yielding the corresponding disulfide (cystine) and nitric oxide [72]. Interestingly, the COST-jet was efficient at creating comparable amounts of Cys-SNO under all tested conditions, which is in good agreement with the observed working gas independent deposition of NO $_2^-$ and NO $_3^-$ and the likewise unaffected NO deposition as detected by EPR. It can be speculated that in the bulk liquid less oxidizing conditions than in kINPen prevail. Table 2 shows the qualitative performance of kINPen and COST jet sources as the

Table 2. Qualitative overview of CAP performance using different working gases and for 30 seconds of treatment with kINPen (Ar-driven jet) and COST jet (He-driven jet).

	no treat.	Ar only	Ar/N ₂ 1%	Ar/N ₂ /O ₂ 0.3/0.7%	Ar/O ₂ 1%	He only	He/N ₂ 1%	He/N ₂ /O ₂ 0.3/0.7%	He/O ₂ 0.5%	He/O ₂ 1%
RSH ^{°a}	o ¹	--	--	--	---	-	--	--	-	---
RSSR ^{°a}	o	+	+	+	++	o	o	+	+	o
RSO ₃ H ^{°a}	o	+	++	++	+++	+	++	++	+	+++
RSO ₂ H ^{°a}	o	++	++	++	++	++	++	++	++	+
RSNO ^{*a}	n.d.	+	+	+++	+	++	++	++	++	+
*NO ^d	n.d.	n.d.	n.d.	n.d.	n.d.	n.d.	n.d.	n.d.	n.d.	n.d.
NO ₂ ^{-b}	o	+	o	+++	++	o	o	o	n.d.	o
NO ₃ ^{-b}	o	o	o	+	o	+	+	++	+	+++
H ₂ O ₂ ^{-c}	o	o	+	o	++	+	o	o	o	o
*NO ^d	n.d.	n.d.	n.d.	++	+	n.d.	n.d.	++	+++	+++
NO ₂ ^{-b}	o	o	o	++	+	o	o	o	o	o
NO ₃ ^{-b}	o	+	+	+++	++	+	+	++	++	++
H ₂ O ₂ ^{-c}	o	++	++	+	+++	+	+	o	o	o

^a = MS quantification

^b = IC quantification

^c = FOX quantification

^d = EPR quantification

* = quantification with cysteine in solution

° = quantification without cysteine in solution

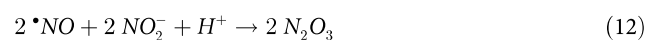
¹ = relative abundance similar to control

n.d. = not determined

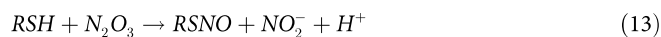
<https://doi.org/10.1371/journal.pone.0216606.t002>

working gas varies. Consequently, the production of reactive species (long and short-lived) and cysteine derivatives has been summarized here in order to compare the data and have an overall overview. In particular, it was possible to compare the two jets considering the fact that their qualitative performance fluctuates in the same qualitative production range.

Several reaction pathways to yield nitrosylated thiols are described. In principle, a radical-driven formation is possible for direct plasma treatment. After an [•]OH-induced H-abstraction at the thiol the resulting thiyl radical allows recombination with NO yielding the S-nitrosothiol. Although the formation of the thiyl radicals has been observed, this pathway may not contribute substantially as the number of species is low and the highly reactive OH radicals can attack all positions of the cysteine (radical). Further, at low pH (< 3) a direct addition of nitric oxide to the thiol can occur. However, this relatively inefficient reaction requires a 3rd reaction partner to accept an excess electron [73]. In addition, while both COST-jet and kIN-Pen are capable of pH reduction, the relatively large treated volume (750 μl) as well as the short treatment time (30 s) did not cause pH to drop to 3, thereby leaving direct Cys-SNO formation as a minor side reaction. Further pathways rely on nitric oxide oxidations products, such as [•]NO₂ and/or N₂O₃ [74]. At physiological pH, [•]NO reacts with molecular oxygen forming principally ONOONO, a precursor of [•]NO₂ and/or N₂O₃, and the stable products NO₂⁻, NO₃⁻ [74]. It was shown that [•]NO₂ reacts with thiols to form the S-nitroso derivatives [74, 75]. A potentially major player of thiol nitrosylation is N₂O₃, which is formed by the following reaction [34]:



N_2O_3 in turn reacts with free thiol groups and can interact both with low molecular weight thiols, such as cysteine ($2.6 \times 10^{-5} M^{-1}s^{-1}$) or glutathione ($2.9 \times 10^{-5} M^{-1}s^{-1}$), and thiols in proteins ($0.3 \times 10^{-5} M^{-1}s^{-1}$ for human serum albumin, all taken from [59]) by



The higher observed NO_2^- concentrations in the presence of cysteine might partly be related to this reaction. Furthermore, future experiments will have to reveal if the chosen O_2 - N_2 mixture in correlation with the N_2 shielding might promote the direct formation of N_2O_3 , thereby also circumventing the relatively slow formation of N_2O_3 in solution ($\sim 6.6 \times 10^6 M^{-2}s^{-1}$, see [76]).

This would explain the higher amount of observed Cys-SNO after kINPen compared to COST-jet treatment, which seems to contradict EPR results showing larger amounts of the NO product INR after COST-jet exposure. However, it has to be kept in mind that the competing oxidative reactions, e.g. interaction with superoxide (around $10^{2-3} M^{-1}s^{-1}$ as discussed in [77]) are significantly faster, thereby a total switch from oxidative to nitrosative conditions will not be possible. Under physiological conditions, nitroglutathione (GSNO) and S-nitrosothioredoxin levels regulate the formation of S-nitrosothiols, as they are responsible of the nitroso-group transfer, and indirectly, by the action of GSNO reductase [19]. This occurs as negative feedback for *NO synthase and other downstream products of the pathway, e.g. the modified proteins [78, 79].

Cold physical plasma jets promise to be a valuable tool for optimizing the production and studying the action of bioactive compounds such as Cys-SNO. The obtained knowledge highlights a profound impact of cold plasma on protein thiol groups, with subsequent consequences in the cellular redox-signaling pathway including *NO storage via nitrosylation. The question remaining is if optimized discharge conditions allow the production of sufficient amounts of Cys-SNO in complex environments to result in cellular responses, which have to be challenged in future work.

Conclusions and outlook

The impact of an optimized treatment on the model target cysteine was compared to the COST reference jet using both standard conditions and adjusted molecular gas admixtures. Compared to a previous study using the kINPen without curtain gas, the usage of a curtain gas setup for the kINPen and modulation of the feed gas conditions increased the presence of nitrosative modifications on the thiol moiety of cysteine. While oxidative modifications still dominate the modification patterns, the first steps towards more nitrosative conditions are promising. Results are in good agreement with the observation of the *NO-adduct, determined by EPR spectroscopy, and long-lived reactive species, namely H_2O_2 , NO_2^- , and NO_3^- . It can be concluded that the general liquid chemistry induced by plasma treatment seems to be strongly influenced by the offered target even when changing atmospheric conditions to N_2 . Pending further investigations, it seems like the implementation of the curtain gas for certain clinical applications of CAPs might be a useful step to enhance the clinical potential of cold plasma treatment. Feed gas admixtures more readily modulated Cys-SNO production with active curtain gas compared to Cys-SNO production with comparable gas admixtures in ambient air.

Further studies will focus on using the COST-jet in a N_2 atmosphere as well, as the ambient atmosphere seems to play a major role in RNS-driven liquid chemistry. Due to the much lower gas flux, a curtain gas system would cause much stronger distortion in case of the COST-jet, thereby the transfer of the whole setup into a controlled atmosphere seem more readily to facilitate. The impact can be expected to be less pronounced than with the kINPen as its discharge

is not in direct contact with the ambient atmosphere. In addition, usage of the COST-jet with its standard conditions allows a straightforward comparison to other sources using it as a reference to gain insight into similarities and differences between various plasma sources located in other labs. A critical step will be the implementation of stable isotope labels to elucidate the role of both gas and liquid phase chemistry. This would foster understanding if plasmas should be tuned specifically towards a desired gas chemistry or more towards initiating required liquid chemistry. Furthermore, translation of the results from the chemical model system into biological models is necessary to evaluate the predicted functional response.

Acknowledgments

The authors want to thank D. Hüther for assistance in FTIR sample preparation and measurement, D. Sponholz for assistance in EPR measurements, and P. Preissing for his great support in setting up the COST-jet at the INP.

Author Contributions

Conceptualization: Jan-Wilm Lackmann, Helena Jablonowski, Kristian Wende.

Data curation: Björn Offerhaus.

Formal analysis: Giuliana Bruno, Helena Jablonowski, Friederike Kogelheide, Björn Offerhaus, Kristian Wende.

Funding acquisition: Kristian Wende.

Investigation: Jan-Wilm Lackmann, Giuliana Bruno, Helena Jablonowski.

Methodology: Jan-Wilm Lackmann, Giuliana Bruno, Julian Held, Kristian Wende.

Project administration: Jan-Wilm Lackmann.

Resources: Julian Held, Volker Schulz-von der Gathen.

Supervision: Jan-Wilm Lackmann, Volker Schulz-von der Gathen, Katharina Stapelmann, Thomas von Woedtke, Kristian Wende.

Validation: Jan-Wilm Lackmann.

Visualization: Jan-Wilm Lackmann, Katharina Stapelmann.

Writing – original draft: Jan-Wilm Lackmann, Giuliana Bruno, Helena Jablonowski, Friederike Kogelheide, Julian Held, Volker Schulz-von der Gathen, Katharina Stapelmann, Thomas von Woedtke, Kristian Wende.

Writing – review & editing: Jan-Wilm Lackmann, Julian Held, Volker Schulz-von der Gathen, Katharina Stapelmann, Thomas von Woedtke, Kristian Wende.

References

1. Weltmann KD, von Woedtke T. Plasma medicine—current state of research and medical application. *Plasma Physics and Controlled Fusion*. 2017; 59(1):014031. <https://doi.org/10.1088/0741-3335/59/1/014031> WOS:000387795200006.
2. Ulrich C, Kluschke F, Patzelt A, Vandersee S, Czaika VA, Richter H, et al. Clinical use of cold atmospheric pressure argon plasma in chronic leg ulcers: A pilot study. *Journal of Wound Care*. 2015; 24(5):196–203. <https://doi.org/10.12968/jowc.2015.24.5.196> WOS:000355762400002. PMID: 25970756
3. Emmert S, Brehmer F, Hänßle H, Helmke A, Mertens N, Ahmed R, et al. Atmospheric pressure plasma in dermatology: Ulcus treatment and much more. *Clinical Plasma Medicine*. 2013; 1(1):24–9. <https://doi.org/10.1016/j.cpme.2012.11.002>

4. Laroussi M, Lu X, Keidar M. Perspective: The physics, diagnostics, and applications of atmospheric pressure low temperature plasma sources used in plasma medicine. *J Appl Phys*. 2017; 122(2):020901. <https://doi.org/10.1063/1.4993710> WOS:000405663800001.
5. Park GY, Park SJ, Choi MY, Koo IG, Byun JH, Hong JW, et al. Atmospheric-pressure plasma sources for biomedical applications. *Plasma Sources Science and Technology*. 2012; 21(4).
6. Bruggeman PJ, Iza F, Brandenburg R. Foundations of atmospheric pressure non-equilibrium plasmas. *Plasma Sources Sci T*. 2017; 26(12):123002. <https://doi.org/10.1088/1361-6595/aa97af> WOS:000425761500001.
7. van Gils CAJ, Hofmann S, Boekema BKHL, Brandenburg R, Bruggeman PJ. Mechanisms of bacterial inactivation in the liquid phase induced by a remote RF cold atmospheric pressure plasma jet. *Journal of Physics D: Applied Physics*. 2013; 46(17):175203. <https://doi.org/10.1088/0022-3727/46/17/175203>
8. Wende K, Williams P, Dalluge J, Gaens WV, Aboubakr H, Bischof J, et al. Identification of the biologically active liquid chemistry induced by a nonthermal atmospheric pressure plasma jet. *Biointerphases*. 2015; 10(2):029518. Epub 2015/05/08. <https://doi.org/10.1116/1.4919710> PMID: 25947392.
9. Jablonowski H, von Woedtke T. Research on plasma medicine-relevant plasma-liquid interaction: What happened in the past five years? *Clinical Plasma Medicine*. 2015; 3(2):42–52. Epub 23.11.2015. <https://doi.org/10.1016/j.cpme.2015.11.003>
10. Schmidt A, Dietrich S, Steuer A, Weltmann K-D, von Woedtke T, Masur K, et al. Non-thermal plasma activates human keratinocytes by stimulation of antioxidant and phase II pathways. *Journal of Biological Chemistry*. 2015; 290(11):6731–50. <https://doi.org/10.1074/jbc.M114.603555> PMID: 25589789
11. Dezest M, Chavatte L, Bourdens M, Quinton D, Camus M, Garrigues L, et al. Mechanistic insights into the impact of Cold Atmospheric Pressure Plasma on human epithelial cell lines. *Scientific Reports*. 2017; 7:41163. ARTN 41163 <https://doi.org/10.1038/srep41163> WOS:000392666400001. PMID: 28120925
12. Mirpour S, Piroozmand S, Soleimani N, Jalali Faharani N, Ghomi H, Fotovat Eskandari H, et al. Utilizing the micron sized non-thermal atmospheric pressure plasma inside the animal body for the tumor treatment application. *Sci Rep*. 2016; 6:29048. <https://doi.org/10.1038/srep29048> PMID: 27383714; PubMed Central PMCID: PMC4935881.
13. Chauvin J, Judee F, Yousfi M, Vicendo P, Merbahi N. Analysis of reactive oxygen and nitrogen species generated in three liquid media by low temperature helium plasma jet. *Sci Rep*. 2017; 7(1):4562. Epub 2017/07/06. <https://doi.org/10.1038/s41598-017-04650-4> PMID: 28676723; PubMed Central PMCID: PMC5496897.
14. Paulsen CE, Carroll KS. Cysteine-mediated redox signaling: chemistry, biology, and tools for discovery. *Chemical Reviews*. 2013; 113(7):4633–79. Epub 2013/03/22. <https://doi.org/10.1021/cr300163e> PMID: 23514336; PubMed Central PMCID: PMC4303468.
15. Go YM, Chandler JD, Jones DP. The cysteine proteome. *Free radical biology & medicine*. 2015; 84:227–45. Epub 2015/04/07. <https://doi.org/10.1016/j.freeradbiomed.2015.03.022> PMID: 25843657; PubMed Central PMCID: PMC4457640.
16. Baez NO, Reisz JA, Furdul CM. Mass spectrometry in studies of protein thiol chemistry and signaling: opportunities and caveats. *Free radical biology & medicine*. 2015; 80:191–211. Epub 2014/09/28. <https://doi.org/10.1016/j.freeradbiomed.2014.09.016> PMID: 25261734; PubMed Central PMCID: PMC4355329.
17. Takai E, Kitamura T, Kuwabara J, Ikawa S, Yoshizawa S, Shiraki K, et al. Chemical modification of amino acids by atmospheric-pressure cold plasma in aqueous solution. *Journal of Physics D: Applied Physics*. 2014; 47(28):285403.
18. Trivedi MV, Laurence JS, Siahaan TJ. The role of thiols and disulfides on protein stability. *Current Protein & Peptide Science*. 2009; 10(6):614–25. Epub 2009/06/23. <https://doi.org/10.2174/138920309789630534> PMID: 19538140; PubMed Central PMCID: PMC3319691.
19. Gould N, Doulias PT, Tenopoulou M, Raju K, Ischiropoulos H. Regulation of protein function and signaling by reversible cysteine S-nitrosylation. *Journal of Biological Chemistry*. 2013; 288(37):26473–9. Epub 2013/07/19. <https://doi.org/10.1074/jbc.R113.460261> PMID: 23861393; PubMed Central PMCID: PMC3772194.
20. Randall LO. Reaction of thiol compounds with peroxidase and hydrogen peroxide. *Journal of Biological Chemistry*. 1946; 164(2):521–7. PMID: 21001149
21. Verlaack C, Van Boxem W, Dewaele D, Lemiere F, Sobott F, Benedikt J, et al. Mechanisms of Peptide Oxidation by Hydroxyl Radicals: Insight at the Molecular Scale. *J Phys Chem C*. 2017; 121(10):5787–99. <https://doi.org/10.1021/acs.jpcc.6b12278>
22. Aboubakr HA, Mor SK, Higgins L, Armien A, Youssef MM, Bruggeman PJ, et al. Cold argon-oxygen plasma species oxidize and disintegrate capsid protein of feline calicivirus. *PLoS one*. 2018; 13(3):

- e0194618. Epub 2018/03/23. <https://doi.org/10.1371/journal.pone.0194618> PMID: 29566061; PubMed Central PMCID: PMC5864060.
23. Baldus S, Schroder D, Bibinov N, Schulz-von der Gathen V, Awakowicz P. Atomic oxygen dynamics in an air dielectric barrier discharge: a combined diagnostic and modeling approach. *J Phys D Appl Phys*. 2015; 48(27):275203. <https://doi.org/10.1088/0022-3727/48/27/275203> WOS:000356625900011.
 24. Brandenburg R. Dielectric barrier discharges: progress on plasma sources and on the understanding of regimes and single filaments. *Plasma Sources Sci T*. 2017; 26(5):053001. <https://doi.org/10.1088/1361-6595/aa6426> WOS:000398259600001.
 25. Kartaschew K, Mischo M, Baldus S, Brundermann E, Awakowicz P, Havenith M. Unraveling the interactions between cold atmospheric plasma and skin-components with vibrational microspectroscopy. *Biointerphases*. 2015; 10(2):029516. <https://doi.org/10.1116/1.4919610> WOS:000357195600034. PMID: 25947390
 26. Kogelheide F, Kartaschew K, Strack M, Baldus S, Metzler-Nolte N, Havenith M, et al. FTIR spectroscopy of cysteine as a ready-to-use method for the investigation of plasma-induced chemical modifications of macromolecules. *J Phys D Appl Phys*. 2016; 49(8):084004. Artn 084004 <https://doi.org/10.1088/0022-3727/49/8/084004> WOS:000369480800007.
 27. Lackmann JW, Baldus S, Steinborn E, Edengeiser E, Kogelheide F, Langklotz S, et al. A dielectric barrier discharge terminally inactivates RNase A by oxidizing sulfur-containing amino acids and breaking structural disulfide bonds. *J Phys D Appl Phys*. 2015; 48(49):494003. <https://doi.org/10.1088/0022-3727/48/49/494003> WOS:000368442600003.
 28. Winter J, Brandenburg R, Weltmann KD. Atmospheric pressure plasma jets: an overview of devices and new directions. *Plasma Sources Science and Technology*. 2015; 24(6):064001. <https://doi.org/10.1088/0963-0252/24/6/064001>
 29. Ali AA, Coulter JA, Ogle CH, Migaud MM, Hirst DG, Robson T, et al. The contribution of N2O3 to the cytotoxicity of the nitric oxide donor DETA/NO: an emerging role for S-nitrosylation. *Bioscience Reports*. 2013; 33(2):333–U449. <https://doi.org/10.1042/BSR20120120> WOS:000321244100014. PMID: 23402389
 30. Belge C, Massion PB, Pelat M, Balligand JL. Nitric oxide and the heart: update on new paradigms. *Annals of the New York Academy of Sciences*. 2005; 1047(1):173–82. Epub 2005/08/12. <https://doi.org/10.1196/annals.1341.016> PMID: 16093495.
 31. Danson EJ, Choate JK, Paterson DJ. Cardiac nitric oxide: emerging role for nNOS in regulating physiological function. *Pharmacology & Therapeutics*. 2005; 106(1):57–74. Epub 2005/03/23. <https://doi.org/10.1016/j.pharmthera.2004.11.003> PMID: 15781122.
 32. Sun J, Steenbergen C, Murphy E. S-nitrosylation: NO-related redox signaling to protect against oxidative stress. *Antioxid Redox Signal*. 2006; 8(9–10):1693–705. Epub 2006/09/22. <https://doi.org/10.1089/ars.2006.8.1693> PMID: 16987022; PubMed Central PMCID: PMC162443861.
 33. Stamler JS, Lamas S, Fang FC. Nitrosylation: The Prototypic Redox-Based Signaling Mechanism. *Cell*. 2001; 106(6):675–83. [https://doi.org/10.1016/s0092-8674\(01\)00495-0](https://doi.org/10.1016/s0092-8674(01)00495-0) PMID: 11572774
 34. Jourd'heuil D, Jourd'heuil FL, Feelisch M. Oxidation and nitrosation of thiols at low micromolar exposure to nitric oxide—Evidence for a free radical mechanism. *Journal of Biological Chemistry*. 2003; 278(18):15720–6. <https://doi.org/10.1074/jbc.M300203200> WOS:000182680000034. PMID: 12595536
 35. Chattopadhyay M, Goswami S, Rodes DB, Kodala R, Velazquez CA, Boring D, et al. NO-releasing NSAIDs suppress NF-kappaB signaling in vitro and in vivo through S-nitrosylation. *Cancer Letters*. 2010; 298(2):204–11. Epub 2010/08/03. <https://doi.org/10.1016/j.canlet.2010.07.006> PMID: 20674154.
 36. Floyd RA, Kotake Y, Towner RA, Guo W-X, Nakae D, Konishi Y. Nitric oxide and cancer development. *Journal of toxicologic pathology*. 2007; 20(2):77–92.
 37. Katayama N, Nakajou K, Ishima Y, Ikuta S, Yokoe J, Yoshida F, et al. Nitrosylated human serum albumin (SNO-HSA) induces apoptosis in tumor cells. *Nitric Oxide*. 2010; 22(4):259–65. Epub 2009/10/13. <https://doi.org/10.1016/j.niox.2009.09.003> PMID: 19818866.
 38. McCarthy HO, Coulter JA, Worthington J, Robson T, Hirst DG. Human osteocalcin: a strong promoter for nitric oxide synthase gene therapy, with specificity for hormone refractory prostate cancer. *Journal of Gene Medicine*. 2007; 9(6):511–20. Epub 2007/05/02. <https://doi.org/10.1002/jgm.1045> PMID: 17471586.
 39. Reuter S, von Woedtke T, Weltmann K-D. The kINPen—a review on physics and chemistry of the atmospheric pressure plasma jet and its applications. *Journal of Physics D: Applied Physics*. 2018; 51(23):233001. <https://doi.org/10.1088/1361-6463/aab3ad>
 40. Golda J, Held J, Redeker B, Konkowski M, Beijer P, Sobota A, et al. Concepts and characteristics of the 'COST Reference Microplasma Jet'. *Journal of Physics D: Applied Physics*. 2016; 49(8). <https://doi.org/10.1088/0022-3727/49/8/084003>

41. Iseni S, Zhang S, van Gessel AFH, Hofmann S, van Ham BJT, Reuter S, et al. Nitric oxide density distributions in the effluent of an RF argon APPJ: effect of gas flow rate and substrate. *New J Phys*. 2014; 16(12):123011. <https://doi.org/10.1088/1367-2630/16/12/123011>
42. Schmidt-Bleker A, Reuter S, Weltmann KD. Quantitative schlieren diagnostics for the determination of ambient species density, gas temperature and calorimetric power of cold atmospheric plasma jets. *J Phys D Appl Phys*. 2015; 48(17):175202. <https://doi.org/10.1088/0022-3727/48/17/175202> WOS:000353329800008.
43. Jablonowski H, Hansch MA, Dunnbier M, Wende K, Hammer MU, Weltmann KD, et al. Plasma jet's shielding gas impact on bacterial inactivation. *Biointerphases*. 2015; 10(2):029506. <https://doi.org/10.1116/1.4916533> PMID: 25832438.
44. Reuter S, Tresp H, Wende K, Hammer MU, Winter J, Masur K, et al. From RONS to ROS: Tailoring Plasma Jet Treatment of Skin Cells. *Ieee T Plasma Sci*. 2012; 40(11):2986–93. <https://doi.org/10.1109/Tps.2012.2207130> WOS:000311355100005.
45. Reuter S, Winter J, Schmidt-Bleker A, Tresp H, Hammer MU, Weltmann KD. Controlling the Ambient Air Affected Reactive Species Composition in the Effluent of an Argon Plasma Jet. *Ieee T Plasma Sci*. 2012; 40(11):2788–94. <https://doi.org/10.1109/Tps.2012.2204280> WOS:000311353200002.
46. Tresp H, Hammer MU, Weltmann K-D, Reuter S. Effects of Atmosphere Composition and Liquid Type on Plasma-Generated Reactive Species in Biologically Relevant Solutions. *Plasma Medicine*. 2013; 3(1–2):45–55. <https://doi.org/10.1615/PlasmaMed.2014009711>
47. Tresp H, Hammer MU, Winter J, Weltmann KD, Reuter S. Quantitative detection of plasma-generated radicals in liquids by electron paramagnetic resonance spectroscopy. *J Phys D Appl Phys*. 2013; 46(43):435401. <https://doi.org/10.1088/0022-3727/46/43/435401> WOS:000325679400013.
48. Schmidt-Bleker A, Bansemer R, Reuter S, Weltmann K-D. How to produce an NOx- instead of Ox-based chemistry with a cold atmospheric plasma jet. *Plasma Process Polym*. 2016; 13(11):1120–7. <https://doi.org/10.1002/ppap.201600062>
49. Schmidt-Bleker A, Winter J, Bösel A, Reuter S, Weltmann K-D. On the plasma chemistry of a cold atmospheric argon plasma jet with shielding gas device. *Plasma Sources Science and Technology*. 2015; 25(1):015005. <https://doi.org/10.1088/0963-0252/25/1/015005>
50. Lackmann JW, Wende K, Verlackt C, Golda J, Volzke J, Kogelheide F, et al. Chemical fingerprints of cold physical plasmas—an experimental and computational study using cysteine as tracer compound. *Scientific Reports*. 2018.
51. Pawlukoic A, Leciejewicz J, Ramirez-Cuesta AJ, Nowicka-Scheibe J. L-Cysteine: Neutron spectroscopy, Raman, IR and ab initio study. *Spectrochimica Acta Part A: Molecular and Biomolecular Spectroscopy*. 2005; 61(11–12):2474–81. Epub 2005/07/05. <https://doi.org/10.1016/j.saa.2004.09.012> PMID: 15994116.
52. Sousa J, Niemi K, Cox L, Algwari QT, Gans T, O'connell D. Cold atmospheric pressure plasma jets as sources of singlet delta oxygen for biomedical applications. *J Appl Phys*. 2011; 109(12):123302.
53. Niemi K, O'Connell D, de Oliveira N, Joyeux D, Nahon L, Booth JP, et al. Absolute atomic oxygen and nitrogen densities in radio-frequency driven atmospheric pressure cold plasmas: Synchrotron vacuum ultra-violet high-resolution Fourier-transform absorption measurements. *Appl Phys Lett*. 2013; 103(3). <https://doi.org/10.1063/1.4813817> WOS:000322146300135.
54. Jablonowski H, Schmidt-Bleker A, Weltmann KD, von Woedtke T, Wende K. Non-touching plasma-liquid interaction—where is aqueous nitric oxide generated? *Phys Chem Chem Phys*. 2018; 20(39):25387–98. Epub 2018/09/29. <https://doi.org/10.1039/c8cp02412j> PMID: 30264836.
55. Kelly S, Golda J, Turner MM, Schulz-von der Gathen V. Gas and heat dynamics of a micro-scaled atmospheric pressure plasma reference jet. *J Phys D Appl Phys*. 2015; 48(44). Artn 444002 <https://doi.org/10.1088/0022-3727/48/44/444002> WOS:000365925800004.
56. Benedikt J, Mokhtar Hefny M, Shaw A, Buckley BR, Iza F, Schakermann S, et al. The fate of plasma-generated oxygen atoms in aqueous solutions: non-equilibrium atmospheric pressure plasmas as an efficient source of atomic O(aq). *Phys Chem Chem Phys*. 2018. Epub 2018/04/20. <https://doi.org/10.1039/c8cp00197a> PMID: 29671846.
57. Hefny MM, Pattyn C, Lukes P, Benedikt J. Atmospheric plasma generates oxygen atoms as oxidizing species in aqueous solutions. *J Phys D Appl Phys*. 2016; 49(40):404002. <https://doi.org/10.1088/0022-3727/49/40/404002> WOS:000384103200002.
58. Goldstein S, Russo A, Samuni A. Reactions of PTIO and carboxy-PTIO with *NO, *NO2, and O2-*. *J Biol Chem*. 2003; 278(51):50949–55. Epub 2003/09/05. <https://doi.org/10.1074/jbc.M308317200> PMID: 12954619.
59. Kharitonov VG, Sundquist AR, Sharma VS. Kinetics of nitrosation of thiols by nitric oxide in the presence of oxygen. *J Biol Chem*. 1995; 270(47):28158–64. Epub 1995/11/24. <https://doi.org/10.1074/jbc.270.47.28158> PMID: 7499306.

60. Stadtman ER. Protein oxidation and aging. *Free radical research*. 2006; 40(12):1250–8. Epub 2006/11/09. <https://doi.org/10.1080/10715760600918142> PMID: 17090414.
61. Zumdahl SS, Kelter PB. Study Guide: Chemistry, Seventh Edition, Zumdahl: Houghton Mifflin; 2007.
62. Wang J, Song M, Chen B, Wang L, Zhu R. Effects of pH and H₂O₂ on ammonia, nitrite, and nitrate transformations during UV254nm irradiation: Implications to nitrogen removal and analysis. *Chemosphere*. 2017; 184:1003–11. Epub 2017/07/01. <https://doi.org/10.1016/j.chemosphere.2017.06.078> PMID: 28658735.
63. Lukes P, Dolezalova E, Sisrova I, Clupek M. Aqueous-phase chemistry and bactericidal effects from an air discharge plasma in contact with water: evidence for the formation of peroxynitrite through a pseudo-second-order post-discharge reaction of H₂O₂ and HNO₂. *Plasma Sources Science and Technology*. 2014; 23(1):015019. <https://doi.org/10.1088/0963-0252/23/1/015019>
64. Goldstein S, Rabani J. Mechanism of Nitrite Formation by Nitrate Photolysis in Aqueous Solutions: The Role of Peroxynitrite, Nitrogen Dioxide, and Hydroxyl Radical. *Journal of the American Chemical Society*. 2007; 129(34):10597–601. <https://doi.org/10.1021/ja073609z> PMID: 17676847
65. Olson LP, Bartberger MD, Houk KN. Peroxynitrate and peroxynitrite: a complete basis set investigation of similarities and differences between these NO_x species. *J Am Chem Soc*. 2003; 125(13):3999–4006. <https://doi.org/10.1021/ja029619m> PMID: 12656637.
66. Conte ML, Carroll KS. The chemistry of thiol oxidation and detection. *Oxidative stress and redox regulation*: Springer; 2013. p. 1–42.
67. Chauvin JR, Pratt DA. On the Reactions of Thiols, Sulfenic Acids, and Sulfinic Acids with Hydrogen Peroxide. *Angewandte Chemie International Edition*. 2017; 56(22):6255–9. Epub 2016/12/10. <https://doi.org/10.1002/anie.201610402> PMID: 27933690.
68. Klinkhammer C, Verlact C, Smilowicz D, Kogelheide F, Bogaerts A, Metzler-Nolte N, et al. Elucidation of Plasma-induced Chemical Modifications on Glutathione and Glutathione Disulphide. *Scientific Reports*. 2017; 7(1):13828. Epub 2017/10/25. <https://doi.org/10.1038/s41598-017-13041-8> PMID: 29062059; PubMed Central PMCID: PMC5653798.
69. Ganzarolli de Oliveira M. S-Nitrosothiols as Platforms for Topical Nitric Oxide Delivery. *Basic Clin Pharmacol Toxicol*. 2016; 119 Suppl 3:49–56. Epub 2016/10/30. <https://doi.org/10.1111/bcpt.12588> PMID: 27030007.
70. Stamler JS, Jaraki O, Osborne J, Simon DI, Keaney J, Vita J, et al. Nitric oxide circulates in mammalian plasma primarily as an S-nitroso adduct of serum albumin. *Proceedings of the National Academy of Sciences*. 1992; 89(16):7674–7. <https://doi.org/10.1073/pnas.89.16.7674>
71. Singh RJ, Hogg N, Joseph J, Kalyanaraman B. Mechanism of nitric oxide release from S-nitrosothiols. *Journal of Biological Chemistry*. 1996; 271(31):18596–603. PMID: 8702510
72. Roy B, Dhardemare AD, Fontecave M. New Thionitrites—Synthesis, Stability, and Nitric-Oxide Generation. *Journal of Organic Chemistry*. 1994; 59(23):7019–26. <https://doi.org/10.1021/jo00102a028> WOS: A1994PT81200028.
73. Carver J, Doctor A, Zaman K, Gaston B. S-Nitrosothiol formation. *Methods in enzymology*. 2005; 396:95–105. [https://doi.org/10.1016/S0076-6879\(05\)96010-2](https://doi.org/10.1016/S0076-6879(05)96010-2) PMID: 16291225
74. Goldstein S, Czapski G. Mechanism of the nitrosation of thiols and amines by oxygenated•NO solutions: the nature of the nitrosating intermediates. *Journal of the American Chemical Society*. 1996; 118(14):3419–25.
75. Hess DT, Matsumoto A, Kim SO, Marshall HE, Stamler JS. Protein S-nitrosylation: purview and parameters. *Nature Reviews Molecular Cell Biology*. 2005; 6(2):150–66. Epub 2005/02/03. <https://doi.org/10.1038/nrm1569> PMID: 15688001.
76. Gaston B. Nitric oxide and thiol groups. *Biochimica et Biophysica Acta (BBA)—Bioenergetics*. 1999; 1411(2–3):323–33. [https://doi.org/10.1016/S0005-2728\(99\)00023-7](https://doi.org/10.1016/S0005-2728(99)00023-7)
77. Winterbourn CC, Metodiewa D. Reactivity of biologically important thiol compounds with superoxide and hydrogen peroxide. *Free radical biology & medicine*. 1999; 27(3–4):322–8. Epub 1999/09/01. [https://doi.org/10.1016/S0891-5849\(99\)00051-9](https://doi.org/10.1016/S0891-5849(99)00051-9) PMID: 10468205; PubMed Central PMCID: PMC10468205.
78. Marino SM, Gladyshev VN. Analysis and functional prediction of reactive cysteine residues. *Journal of Biological Chemistry*. 2012; 287(7):4419–25. Epub 2011/12/14. <https://doi.org/10.1074/jbc.R111.275578> PMID: 22157013; PubMed Central PMCID: PMC3281665.
79. Zhang Y, Hogg N. S-Nitrosothiols: cellular formation and transport. *Free radical biology & medicine*. 2005; 38(7):831–8. Epub 2005/03/08. <https://doi.org/10.1016/j.freeradbiomed.2004.12.016> PMID: 15749378.

80. Winterbourn CC. Revisiting the reactions of superoxide with glutathione and other thiols. *Arch Biochem Biophys.* 2016; 595:68–71. Epub 2016/04/21. <https://doi.org/10.1016/j.abb.2015.11.028> PMID: [27095219](https://pubmed.ncbi.nlm.nih.gov/27095219/).
81. Wink DA, Nims RW, Darbyshire JF, Christodoulou D, Hanbauer I, Cox GW, et al. Reaction Kinetics for Nitrosation of Cysteine and Glutathione in Aerobic Nitric Oxide Solutions at Neutral pH. Insights into the Fate and Physiological Effects of Intermediates Generated in the NO/O₂ Reaction. *Chemical Research in Toxicology.* 1994; 7(4):519–25. <https://doi.org/10.1021/tx00040a007> PMID: [7981416](https://pubmed.ncbi.nlm.nih.gov/7981416/)
82. Zeida A, Gonzalez Lebrero MC, Radi R, Trujillo M, Estrin DA. Mechanism of cysteine oxidation by peroxynitrite: An integrated experimental and theoretical study. *Arch Biochem Biophys.* 2013; 539(1):81–6. Epub 2013/09/10. <https://doi.org/10.1016/j.abb.2013.08.016> PMID: [24012807](https://pubmed.ncbi.nlm.nih.gov/24012807/).
83. Enami S, Hoffmann MR, Colussi AJ. Simultaneous detection of cysteine sulfenate, sulfinate, and sulfonate during cysteine interfacial ozonolysis. *J Phys Chem B.* 2009; 113(28):9356–8. Epub 2009/06/23. <https://doi.org/10.1021/jp904316n> PMID: [19537744](https://pubmed.ncbi.nlm.nih.gov/19537744/).

Article A3

On the liquid chemistry of the reactive nitrogen species peroxynitrite and nitrogen dioxide generated by physical plasmas

G. Bruno, S. Wenske, J.-L. Lackmann, M. Lalk, T. von Woedtke, K. Wende. *Biomolecules*, **under revision**, 2020.



[Biomolecules] Manuscript ID: biomolecules-1014036 - Minor Revisions

Biomolecules Editorial Office to: Kristian Wende

11/24/2020 03:20 AM

Sent by: **mars.tan@mdpi.com**

Cc: "Giuliana Bruno", "Sebastian Wenske", "Jan-Wilm Lackmann", "Michael Lalk", "Thomas von Woedtke", "Biomolecules Editorial Office"

Please respond to mars.tan

Dear Dr. Wende,

Thank you for submitting your manuscript:

Manuscript ID: biomolecules-1014036

Type of manuscript: Article

Title: On the liquid chemistry of the reactive nitrogen species peroxyxynitrite

and nitrogen dioxide generated by physical plasmas

Authors: Giuliana Bruno, Sebastian Wenske, Jan-Wilm Lackmann, Michael Lalk, Thomas von Woedtke, Kristian Wende *

Received: 9 November 2020

E-mails: giuliana.bruno@inp-greifswald.de, sebastian.wenske@inp-greifswald.de, jan-wilm.lackmann@uni-koeln.de, lalk@uni-greifswald.de, woedtke@inp-greifswald.de, kristian.wende@inp-greifswald.de

Submitted to section: Chemical Biology,

https://www.mdpi.com/journal/biomolecules/sections/Chemical_Bio

It has been reviewed by experts in the field and we request that you make minor revisions before it is processed further. Please find your manuscript and the review reports at the following link:

<https://susy.mdpi.com/user/manuscripts/resubmit/3793c7d0f859059d451c932367eaf5ee>

Your co-authors can also view this link if they have an account in our submission system using the e-mail address in this message.

Please revise the manuscript according to the reviewers' comments and upload

the revised file within 5 days. Use the version of your manuscript found at the above link for your revisions, as the editorial office may have made formatting changes to your original submission. Any revisions should be clearly highlighted, for example using the "Track Changes" function in Microsoft Word, so that they are easily visible to the editors and reviewers.

Please provide a short cover letter detailing any changes, for the benefit of the editors and reviewers. Please detail the revisions that have been made, citing the line number and exact change, so that the editor can check the changes expeditiously. Simple statements like 'done' or 'revised as requested' will not be accepted unless the change is simply a typographical error.

If the reviewers have suggested that your manuscript should undergo extensive English editing, please have the English in the manuscript thoroughly checked and edited for language and form. Alternatively, MDPI provides an English editing service checking grammar, spelling, punctuation and some improvement

of style where necessary for an additional charge (extensive re-writing is not included), see details at <https://www.mdpi.com/authors/english>.

Do not hesitate to contact us if you have any questions regarding the

revision of your manuscript or if you need more time. We look forward to hearing from you soon.

Kind regards,
Mr. Mars Tan
E-Mail: mars.tan@mdpi.com

Welcome to submit to /Biomolecules/:
<http://susy.mdpi.com/user/manuscripts/upload?journal=biomolecules>

MDPI Wuhan Office No.6 Jingan Road, 5.5 Creative Industry Park, 25th Floor,
Hubei Province, China

MDPI Biomolecules Editorial Office
St. Alban-Anlage 66, 4052 Basel, Switzerland
E-Mail: biomolecules@mdpi.com
<http://www.mdpi.com/journal/biomolecules>

1 Article

2 On the liquid chemistry of the reactive nitrogen 3 species peroxyxynitrite and nitrogen dioxide generated 4 by physical plasmas

5 G. Bruno ¹, S. Wenske ¹, J.-W. Lackmann ², M. Lalk ³, T. von Woedtke ⁴ and K. Wende ^{1*}

6 ¹ ZIK plasmatis, Leibniz Institute for Plasma Science and Technology, Greifswald, Germany

7 ² Cluster of Excellence Cellular Stress Responses in Aging-Associated Diseases, University of Cologne,
8 Cologne, Germany

9 ³ Institute of Biochemistry, University of Greifswald, Greifswald, Germany

10 ⁴ Leibniz Institute for Plasma Science and Technology, Greifswald, Germany

11 * Corresponding: kristian.wende@inp-greifswald.de

12 Received: date; Accepted: date; Published: date

13 **Abstract:** Cold physical plasmas modulates cellular redox signaling processes, leading to the
14 evolution of a number of clinical applications in the recent years. They are a source of small reactive
15 species, including reactive nitrogen species (RNS). Wound healing is a major application and since
16 its physiology involves RNS signaling, a correlation between clinical effectiveness and the activity
17 of plasma-derived RNS seems evident. To investigate type and reactivity of plasma-derived RNS in
18 aqueous systems, a model with tyrosine as a tracer was utilized. By high-resolution mass
19 spectrometry, 26 different tyrosine derivatives including the physiologic nitrotyrosine were
20 identified. The product pattern was distinctive in terms of plasma parameters, especially gas phase
21 composition. By scavenger experiments and isotopic labelling, gaseous nitric dioxide radicals and
22 liquid phase peroxyxynitrite ions were determined as dominant RNS. The presence of water molecules
23 in the active plasma favored the generation of peroxyxynitrite. A pilot study, identifying RNS driven
24 post-translational modifications of proteins in healing human wounds after the treatment with cold
25 plasma (kINPen) demonstrated the presence of the in vitro determined chemical pathways. The
26 plasma-driven nitration and nitrosylation of tyrosine allows the conclusion that covalent
27 modification of biomolecules by RNS contribute to the clinically observed impact of cold plasmas.

28 **Keywords:** cold physical plasmas; kINPen; redox signaling; reactive nitrogen species; nitrosative
29 stress; oxidative post-translational modifications

30

31 1. Introduction

32 Reactive nitrogen and oxygen species (RNS/ROS) are unstable compounds prone to react rapidly
33 with cellular molecules. In biological systems, they may be involved in redox signaling pathways
34 (e.g. oxygen sensing, muscles and vascular physiology, immune defense, inflammatory processes)
35 (1), mostly by covalently changing the structure of biomolecules such as lipids and proteins (2-5).
36 When their homeostasis is impaired, they become markers or drivers of pathological conditions like
37 cancer progression, metabolic and neurodegenerative diseases. While some species are constantly
38 formed as by-products of cell metabolism, others are generated for dedicated purposes (second
39 messengers, oxidative burst) (4, 6-9). Well-known endogenous radicals are hydroxyl radicals ($\cdot\text{OH}$),
40 superoxide anion ($\cdot\text{O}_2^-$), nitric oxygen radicals ($\cdot\text{NO}$), nitric dioxide radicals ($\cdot\text{NO}_2$) and other reactive
41 species like singlet oxygen ($^1\text{O}_2$), hydrogen peroxide (H_2O_2), peroxyxynitrite (ONOO^-), dinitrogen
42 trioxide (N_2O_3), and the nitrite ion (NO_2^-). The dual role of ROS and RNS is exploited by various

43 strategies aiming to control or modulate redox-signaling pathways (10-13). Among these, cold
44 plasma discharges - ionized gases with complex physical and chemistry properties, are being
45 investigated (14, 15). Most prominent components are small reactive species, many of which are also
46 endogenously generated. A large number of gas plasma sources with different gas phase chemistry
47 has been developed (16, 17). One of the best-characterized plasma sources is the kINPen, approved
48 as certified medical tool in the MED variation (18), currently applied in research (cancer immunology)
49 and in the clinics (wound care, skin-related diseases)(19-24). To the current knowledge, by tuning
50 central parameters of the discharge including working gas composition, distance, or power, the
51 variation of the resulting plasma chemistry is responsible for the biological and biochemical effects
52 observed (25-29). Besides a direct signaling by long-lived reactive species e.g. via peroxiredoxins,
53 short-lived reactive species can covalently modify biomolecules of cellular structures so far with
54 unknown impact (26, 30-33).

55 Gas plasma tuned to create high levels of oxygen species, dominated by singlet oxygen $^1\text{O}_2$,
56 atomic oxygen $\cdot\text{O}$, ozone O_3 , and to a lesser extent hydrogen peroxide H_2O_2 and hydroxyl radicals
57 $\cdot\text{OH}$ focus on applications like disinfection or cancer regression (34-38). In contrast, other conditions
58 foster a N_2 -driven chemistry, yielding species like $\cdot\text{NO}$, $\cdot\text{NO}_2$, N_3O_5 , HNO_2 , and HNO_3 (39, 40). The
59 nitrogen species are assumed to play a role in bactericidal (41, 42) and virucidal effects (43), and cell
60 stimulation, e.g. in wound healing (11, 44-50). In contrast, data on their transport, deposition, or
61 production in liquids, as well as their impact on biological systems are limited. While the long-lived
62 species nitrite and nitrate can be easily accessed by the Griess assay or the ion chromatography and
63 are almost inevitably observed for plasma discharges, both ions are in physiologic conditions not
64 reactive enough to contribute significantly to the effects seen after plasma treatments. Nitration (28,
65 51, 52) and nitrosylation (53) of biomolecules have been observed, indicating the presence (and
66 activity) of more reactive species at least under certain conditions. Potential candidates are e.g. $\cdot\text{NO}_2$,
67 N_2O_3 , and ONOO . The presence of peroxyxynitrite (52) and peroxyxynitrate (54) has been reported for
68 liquid systems under strongly acidic conditions. The capability of reactive nitrogen species to modify
69 biological structures and to modulate signaling pathway, e.g. via acting as a second messenger like
70 nitric oxide, a significant contribution of RNS can be assumed (55). Natural sources of RNS are
71 enzymes of the nitric oxide synthase complex, and subsequent reactions with mitochondrial
72 superoxide anion radical spill-off, forming peroxyxynitrite.

73 Tyrosine is a key amino acid reactive towards RNS and protein tyrosines are significant targets
74 in biological environments (56-58). Principal roles of tyrosine are the formation of hydrophobic cores
75 in proteins, as well as the transduction of signals via phosphorylation events. In this, tyrosine has a
76 superior relevance compared with serine or threonine due to the high specificity of some protein
77 kinases (59). The presence of the aromatic hydroxyl group also allows the reaction with non-protein
78 structures, in contrast to phenylalanine. Therefore, modifications of the tyrosine substructure could
79 yield to a gain or loss of function of proteins and subsequently alter signaling pathways or
80 immunological responses (57, 60). Protein nitration may also act as a signal for negative feedback
81 regulation, leading to ubiquitination and protein degradation (61, 62). Some studies suggest the
82 involvement of tyrosine nitration in the pathogenesis or as marker of nitro-oxidative stress (61, 63-
83 65). Nitric oxide and its oxidation products are also involved in wound healing processes, although
84 the mechanisms are still under investigation (66, 67). For example, tyrosine nitration occurring on the
85 metalloproteinase-13 (MMP-13) promoted its release by endothelial cells, triggering a faster cell
86 migration, angiogenesis and wound healing (63). In the same way, it was shown that protein tyrosine
87 nitration by exogenous $\cdot\text{NO}$ donors inhibited the degranulation processes in mast cell lines (68). The
88 release of exogenous $\cdot\text{NO}$ is a possible strategy to stimulate skin healing (69), potentially beneficial
89 in diabetic patients, where the increased hyperglycemia leads to a decreased $\cdot\text{NO}$ bioavailability and
90 delaying the wound healing process (70).

91 The effectiveness of cold plasmas was shown in the treatment of wounds both in diabetic and
92 normal subjects, and in wound models (22, 23, 71, 72). The responsible species are not completely
93 known, but recent observations emphasized the role of the local cell stimulation over wound bed

94 disinfection – suggesting that reactive nitrogen species may be involved. Therefore, this work intends
95 to further investigate the N₂-driven biochemistry induced by the kINPen plasma source, aiming to
96 define the principal formed bioactive reactive species and their mechanisms of action. To reach this
97 aim, tyrosine was chosen as a tracer molecule and modifications occurring due to the impact of
98 plasma-derived reactive nitrogen species were identified and quantified via high-resolution mass
99 spectrometry. Finally, the ability of kINPen plasmas in modulating the RNS-mediated pathways in
100 complex models was tested. Overall, significant impact of nitrosating and nitrosylating agents,
101 assumingly peroxyxynitrite, was observed, leading to a covalent modification of sensitive targets. Given
102 the prescinded role of tyrosine in numerous proteins, functional consequences will arise in both pro-
103 and eukaryotic cells.

104 2. Materials & Methods

105 2.1. Sample Preparation

106 2.1.1. Model Solutions

107 L-tyrosine (Sigma Aldrich) solutions with a concentration of 0.3 and 30 mM were prepared in 5
108 mM ammonium formate buffer pH 7.4 (Sigma Aldrich) fresh and kept on ice until use. The singlet
109 oxygen and superoxide scavenger ergothioneine (Enzo Life Sciences) and the nitric oxide scavenger
110 cPTIO (Dojindo fine chemicals, Lot. PK822) were dissolved in double distilled water to create a 10x
111 stock solution with 3 mM concentration (73-75).

112 2.1.2. Wound Exudates

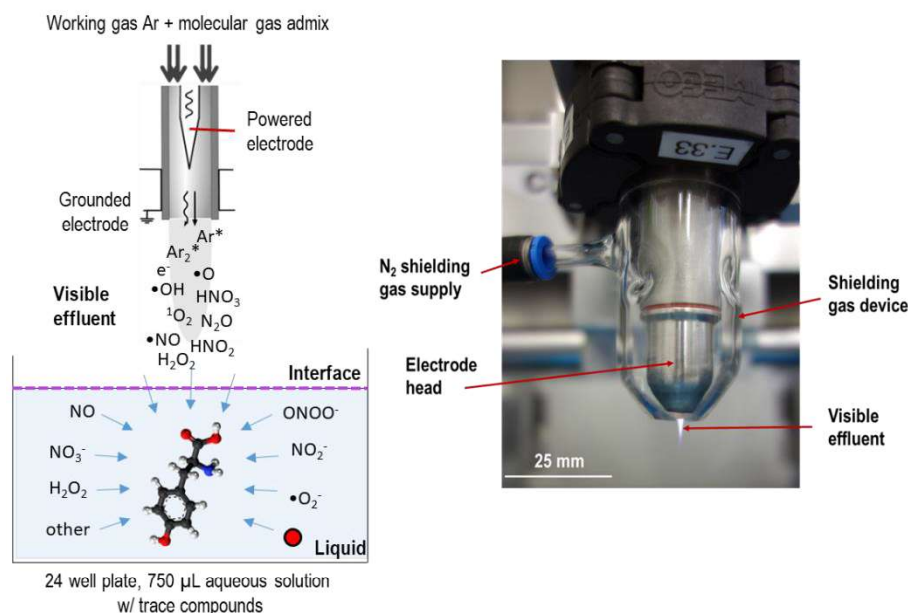
113 Wound exudates were obtained from seven diabetic patients with chronic wounds of the
114 Klinikum Kalsburg, Germany according to an existent ethics approval. After removal of the wound
115 bandage material, the patient wound was rinsed with sterile natural saline followed by blotting with
116 a dry gauze. Afterwards, eSwab samples (Copan) were taken in a circular, inside-out motion across
117 the treated wound surface, and rotated during sampling. Samples were placed in 1 ml of serum-free
118 RPMI 1640 medium (Invitrogen). Subsequently, wounds were plasma treated (see section 2.2), rinsed
119 again and sampled as before using eSwabs. The swabs were vortexed for the maximal elution of
120 wound exudates into the medium, and the supernatant was centrifuged at 4500 rpm for 5 minutes
121 and sterile-filtered (0.22 µm). All swabs and supernatants were kept at -80°C until further use.

122 2.2. Cold plasma and Control Treatments

123 For the model solutions, the kINPen09 with a shielding device was used as source of reactive
124 species, as shown in Figure 1. Briefly, 750 µL of tyrosine solutions was treated in 24 well plates at a
125 distance of 9 mm for 30 or 180 seconds. Argon (± 1 % of molecular gas admixture) served as working
126 gas using 3 standard liters per minute (slm). Admixtures were 1 % oxygen, 1 % nitrogen, or a mix of
127 both (0.7 % N₂ and 0.3 % O₂). For some treatments, isotopically labelled working gas admixtures (¹⁵N₂,
128 or ¹⁸O₂, Sigma Aldrich) or solvent (water, H₂¹⁸O, Sigma Aldrich) were used. The plasma effluent was
129 shielded against the ambient air by a gas shielding of 5 slm nitrogen. For some treatments, the
130 working gas was enriched with water (320 ppm) by guiding 1 % of the total flow through a gas wash
131 bottle containing double distilled water (39, 76, 77). Chronic wounds were treated in the Klinikum
132 Karlsburg using the kINPen MED under standard medical conditions (30 s per 1 cm² of wound area
133 and 5 slm of Argon (5.0, Air Liquide), without shielding device.

134 Buffered solutions (pH 7.4) of tyrosine 0.3 mM were incubated for 2 min at room temperature
135 under constant mixing with equimolar amounts of reactive species generators (300 µM). Those were
136 1) peroxyxynitrite at pH 14 (EMD Millipore); 2) peroxyxynitrite at pH 6.4, yielding to 30 % peroxyxynitrous
137 acid dissociation in nitric dioxide radicals and hydroxyl radicals (52, 78, 79); 3) the nitric oxide donor
138 DEA NONOate (Cayman Chemical); 4) nitrite and nitrate (Sigma Aldrich); 5) hydrogen peroxide
139 (Sigma Aldrich); 6) mixed solutions of nitrite, nitrate and hydrogen peroxide. For solutions 5) and 6),

140 300 μM of each standard species were included. After reaction, samples were put on ice and
 141 immediately subjected to mass spectrometry analysis.



142

143 **Figure 1.** Schematic layout of treatment of tyrosine model solutions (left), and KINPen device w/ gas
 144 shield installed (right).

145 2.3. Cold Plasma-Induced Modifications of Tyrosine

146 2.3.1. Qualitative Screening via Direct Infusion High-Resolution Mass Spectrometry

147 All samples were analyzed by high-resolution mass spectrometry using a TripleTOF 5600
 148 (Sciex). Samples were diluted 1:1 with acetonitrile/0.1 % formic acid to stimulate ionization and to
 149 facilitate evaporation and injected using a syringe pump (50 $\mu\text{L}/\text{min}$). Ionization was achieved by
 150 positive mode electro spray ionization with the following settings: +5.5 kV probe voltage, 300 $^\circ\text{C}$, +30
 151 V declustering potential, 40 psi curtain gas, 20 psi gas 1 and 25 psi gas 2 (Turbo Ion Source).
 152 Concentrated sample solutions (30 mM) were diluted 1:100 before injection. All spectra were acquired
 153 in the m/z range from 40 to 600 m/z . After a first qualitative scan of the produced compounds, their
 154 structure were elucidated by acquisition in tandem mass spectrometry (MS^2 spectra) and collisional
 155 energies for optimal fragmentation was tuned for each compound of interest.

156 2.3.2. HPLC- MS^2 Quantitation of Tyrosine and 3-Nitrotyrosine

157 Considering their relevance, L-tyrosine and 3-nitro-L-tyrosine (Sigma Aldrich) were absolutely
 158 quantified by coupling a chromatographic separation (Infinity II 1290, Agilent) to the mass
 159 spectrometry detection (qTRAP 5500, Sciex). A Hydrophilic Liquid Chromatography (HILIC)
 160 strategy was adopted, using a 2.1 mm \times 5 mm Acquity Amide VanGuard Pre-column followed by a
 161 2.1 mm \times 100 mm Acquity Amide Column (both 130 \AA pore size, 1.7 μm particle size, Waters). For
 162 the separation, the eluent A (85 % acetonitrile, 0.15 % of formic acid and 10 mM ammonium formate),
 163 and the eluent B (HPLC water, 0.15 % formic acid and 10 mM ammonium formate - pH 3), were used.
 164 A linear gradient at a flow rate of 0.8 mL/min was applied (time, B): 0 min, 99 %; 4 min – 92 %; 4.1
 165 min – 99 %; 5 min – 99 %. After a 1:5 dilution in buffer A, 20 μL of sample was injected. Ionization
 166 was achieved in positive mode, using the following parameters: +5.5 kV probe voltage at 150 $^\circ\text{C}$, +100
 167 V declustering potential, 35 psi curtain gas, 25 psi gas 1 and 30 psi gas 2. Compounds of interest were
 168 quantified by multiple reaction monitoring. The transitions and collisional energies (CE) were tuned
 169 differently for each compound: tyrosine 182 \rightarrow 136 m/z (quantitative), CE 18 V, and 165 m/z

170 (qualitative), CE 10 V. Nitro-tyrosine 227 → 181 m/z (quantitative) and 158 m/z (qualitative), both CE
171 10 V. For the quantification, external calibration curves were generated.

172 2.3.3. Data Analysis & Visualization

173 All experiments were performed three times with technical duplicates each. Statistical analysis
174 was performed using GraphPad Prism 7. The MarvinSketch software (version 18.8.0) was used to
175 identify the exact molecular weight and the formula of each compound, as well as to predict the
176 reactivity of tyrosine and standard reactive species in different pH. The spectra produced through
177 direct infusion high-resolution mass spectrometry were calibrated and analyzed with PeakView
178 (version 1.2.0.3, Sciex). The peak areas of each observed derivative was normalized on the peak area
179 of the control (untreated tyrosine), giving a relative estimate of the conversion. For treatments
180 involving isotopes, data were corrected according to (34), taking into account the natural distribution
181 of isotopes and the purity grade.

182 2.4. Characterization of Plasma-Induced Protein Modifications in Wound Exudates

183 Proteins were precipitated by incubating with 80 % ice-cold acetone (Carl Roth) overnight. The
184 pellets were washed twice and dissolved in 100 µl resuspension buffer (10 mM Tris/HCl with 1 mM
185 EDTA, pH 8, all Sigma Aldrich). Protein concentrations were determined by Bradford assay
186 following the vendor's high sensitivity protocol (Roti-Nanoquant, Roth). Single dimension
187 electrophoresis was achieved by loading 60 µg of each sample onto 10 % precast protein gels (Biorad),
188 followed by in-gel digestion (31). Briefly, gel slices were dried and incubated for 5 min with 50 µl of
189 10 mM tris(2-carboxyethyl)phosphine (Sigma Aldrich) at 60 °C followed by an incubation with 50 µl
190 of 50 mM iodoacetamide to alkylate reduced thiols at RT for 30 min (Merck). After brief drying, 2.5
191 µg trypsin (sequencing grade, Promega) was added and samples incubated at 37 °C for 16 h. Peptides
192 were eluted into ultra-pure water by ultra-sonication for 30 min. The peptides were further purified
193 by using Pierce C18 tips (Thermo Scientific) following the included protocol for peptide purification
194 and desalting.

195 Eluted peptides were subjected to nanoLC/HRMS. An UltiMate 3000 nanoLC (Dionex) was
196 coupled to a QExactive mass spectrometer using electrospray ionisation (both Thermo Scientific).
197 Sample aliquots of 1 µg were loaded onto an Acclaim PepMap 100 precolumn (2 cm x 100 µm, 5 µm
198 particle size, 100 Å pore size) for 6 min at 5 µl/min flow followed by separation on a PepMap RSLC
199 column (25 cm x 75 µm, 2 µm particle size, 100 Å pore size). The following gradient was used at 200
200 nl/min: 2 % to 35 % in 6 min, to 50 % B in 15 min, to 90 % B in 15 min, keeping at 90 % for 15 min,
201 equilibration at 2 % B for 20 min (A: H₂O + 0.1 % acetic acid, B: acetonitrile + 0.1 % acetic acid both
202 Merck). Each sample was injected twice. The QExactive was run in Top10 DDA mode with a dynamic
203 exclusion of 30 s. MS1 spectra were acquired with a resolution of 70,000, whereas MS2 spectra were
204 acquired in 17,500 resolution. Raw data files were analyzed with the Proteome Discoverer 2.2
205 (Thermo Scientific) software. At least two unique peptides had to be identified with a maximal mass
206 divergence of 5 ppm (MS1) and 0.02 Da (MS2) for the corresponding protein to be accepted. A
207 maximum FDR of 5 % was accepted for the datasets. Afterwards, abundances were normalized on
208 individual trypsin intensities and resulting relative intensities taken for label free quantification using
209 two-fold cut offs. In a second step, samples were analyzed by using the Byonic (Protein Metrics
210 Version 3.6) plug-in for Proteome Discoverer. Here, a list of oxidative chemical modifications were
211 identified using a machine-learning algorithm with a database, which was previously acquired using
212 model peptides (80). For normalization, the peptide spectrum matches with a modification where
213 counted and divided by the total number of peptide spectrum matches in each of the samples. The
214 modifications found with Byonic were filtered and scored to separate nonsense peptide spectrum
215 matches from correct identified.

216 3. Results & Discussion

217 3.1. Tyrosine Modification Induced by Plasma-Generated Reactive Oxygen and Nitrogen Species

218 Tyrosine solutions have been treated by cold plasma with varying parameters and incubated
 219 with standard solutions of reactive species. The generated products were identified via the accurate
 220 monoisotopic mass and on the Tandem-MS level identifying molecule substructures. All the
 221 identified structures are listed in Table 1, independently from the condition in which they were
 222 produced. The dominant modifications observed were all localized on the aromatic ring:
 223 hydroxylations, nitrosylations, nitrations, and a combination of different groups (up to four groups).
 224 Here, the addition of a functional group via electrophilic substitutions is stabilized by resonance
 225 effects (81, 82).

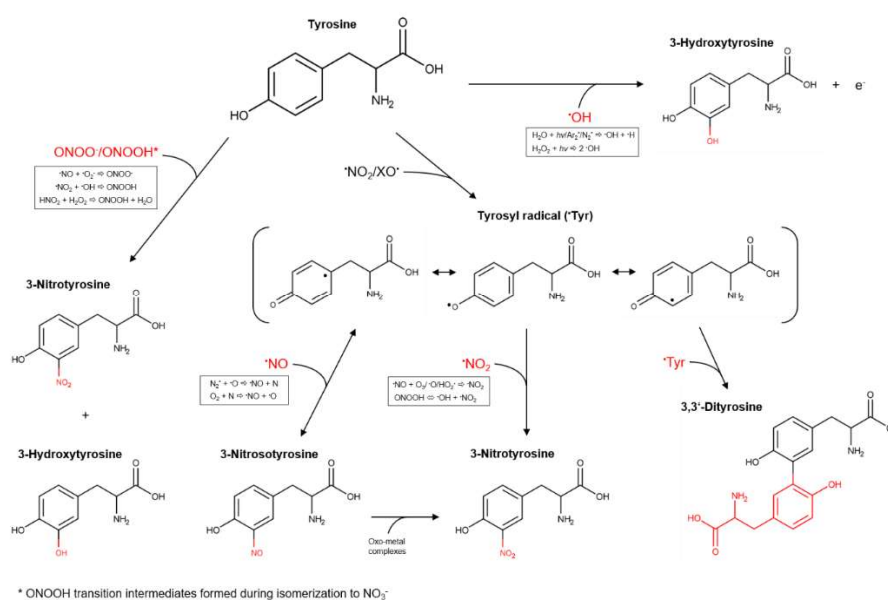
226 To a lesser extent, the dimerization of tyrosine to dityrosine and the functionalization of this
 227 structure with other groups were also detected. While hydroxylations were mostly driven by oxygen
 228 species, the presence of N-containing functional groups indicated an active RNS chemistry. This was
 229 partially shown previously by using cysteine as tracer, yielding S-nitroso-cysteine (30).

230 **Table 1.** Overview of modifications introduced in the tyrosine (Y) structure by tuning kINPen cold
 231 plasmas. *Assignment of a group letter in relation to the results obtained from the experiment
 232 performed in presence of scavengers (details in Paragraph 3.5, Figure S4). The areas of compounds
 233 scavenged in the same way were summed up to generate six groups (from a to f).

Functional group(s) on tyrosine	Formula	[M+H] ⁺	Compound code	Group letter*
None	C ₉ H ₁₁ NO ₃	182.081725	1	-
1 x OH	C ₉ H ₁₁ NO ₄	198.0766	2	-
2 x OH	C ₉ H ₁₁ NO ₅	214.071525	3	-
3 x OH	C ₉ H ₁₁ NO ₆	230.066425	4	-
4 x OH	C ₉ H ₁₁ NO ₇	246.061425	5	-
1 x NO	C ₉ H ₁₀ N ₂ O ₄	211.071925	6	e
2 x NO	C ₉ H ₉ N ₃ O ₅	240.062025	7	a, d
3 x NO	C ₉ H ₈ N ₄ O ₆	269.052225	8	b, d
4 x NO	C ₉ H ₇ N ₅ O ₇	298.042325	9	b, d
1 x NO ₂ + 1 x OH, 1 x NO	C ₉ H ₁₀ N ₂ O ₅	227.066825	10	c, e
2 x NO ₂ + 2 x OH, 2 x NO	C ₉ H ₉ N ₃ O ₇	272.051825	11	b, e
3 x NO ₂	C ₉ H ₈ N ₄ O ₉	317.036925	12	b, e
4 x NO ₂	C ₉ H ₇ N ₅ O ₁₁	362.022025	13	b, e
1 x Y	C ₁₈ H ₂₀ N ₂ O ₆	361.139925	14	-
1 x Y, 1 x OH	C ₁₈ H ₂₀ N ₂ O ₇	377.134925	15	-
1 x Y, 2 x OH	C ₁₈ H ₂₀ N ₂ O ₈	393.129825	16	-
1 x Y, 3 x OH	C ₁₈ H ₂₀ N ₂ O ₉	409.124725	17	-
1 x Y, 1 x NO	C ₁₈ H ₁₉ N ₃ O ₇	390.130125	18	c, d
1 x Y, 1 x NO ₂ + 1 x Y, 1 x OH, 1 x NO	C ₁₈ H ₁₉ N ₃ O ₈	406.125025	19	e
1 x OH, 2 x NO	C ₉ H ₉ N ₃ O ₆	256.056925	20	a, f
1 x OH, 3 x NO	C ₉ H ₈ N ₄ O ₇	285.047125	21	b, f
1 x OH, 1 x NO ₂ + 2 x OH, 1 x NO	C ₉ H ₁₀ N ₂ O ₆	243.061725	22	c, f
2 x OH, 1 x NO ₂ + 3 x OH, 1 x NO	C ₉ H ₁₀ N ₂ O ₇	259.056625	23	f
3 x OH, 1 x NO ₂	C ₉ H ₁₀ N ₂ O ₈	275.051525	24	f
1 x OH, 2 x NO ₂	C ₉ H ₉ N ₃ O ₈	288.046825	25	f
2 x OH, 2 x NO ₂	C ₉ H ₉ N ₃ O ₉	304.041725	26	a, f
1 x OH, 3 x NO ₂	C ₉ H ₈ N ₄ O ₁₀	333.031825	27	f

234 However, the detected amounts were low, suggesting that cysteine is not an optimal target for
 235 the intended downstream analysis technique. The number and amount of identified N-containing
 236 modifications of tyrosine shows a good suitability to study the RNS output of cold plasma discharges.
 237 An overview of oxidative modifications induced on tyrosine by different reactive species, possibly
 238 formed also by kINPen plasmas, is shown in Figure 2. When considering a radical-driven reaction
 239 mechanism, the first step for tyrosine derivatization is the formation of tyrosyl radicals by different
 240 one-electron oxidants ([•]NO₂, [•]OH). [•]NO₂ is a candidate species able to form tyrosyl radicals via a slow
 241 reaction ($k = 3.2 \times 10^5 \text{ M}^{-1} \text{ s}^{-1}$), while hydroxyl radicals react at rates $\geq 1 \times 10^9 \text{ M}^{-1} \text{ s}^{-1}$. Consequential

242 further direct reactions of tyrosyl radicals with tyrosine yield to dityrosine ($k = 2.3 \times 10^8 \text{ M}^{-1} \text{ s}^{-1}$); with
 243 $\cdot\text{NO}$, yield to nitrosotyrosine ($k = 1.0 \times 10^9 \text{ M}^{-1} \text{ s}^{-1}$); with $\cdot\text{NO}_2$, yield to nitrotyrosine ($k = 3.0 \times 10^9 \text{ M}^{-1}$
 244 s^{-1}); with $\cdot\text{O}_2$ yield to tyrosine hydroxyquinone ($k = 1.5 \times 10^9 \text{ M}^{-1} \text{ s}^{-1}$) (only on free tyrosines). This last
 245 product rapidly loose O_2 from the structure to reform tyrosine (55, 61, 83). After the formation of
 246 those derivatives, a further addition of groups led by reactive species was assumed. The conversion
 247 of NO-tyrosine to NO_2 -tyrosine can occur in oxidative conditions by first formation of an iminoxyl
 248 radical ($\cdot\text{NO}$ -tyrosine) and further oxygen addition. This two one-electron steps oxidation is a slow
 249 process, promoted by the presence of metals, which are not included in the used liquid model. In
 250 contrast, a direct reaction with $\cdot\text{OH}$ (and possibly $\cdot\text{O}$) leads to the formation of tyrosine hydroxyl
 251 radicals ($\cdot\text{OH}$ -tyrosine) ($k = 1.2 \times 10^{10} \text{ M}^{-1} \text{ s}^{-1}$), which rapidly lose an electron to became OH-tyrosine
 252 (61).



253

254 **Figure 2.** Formation pathways of tyrosine derivatives considering a neutral pH. The hypothesized
 255 possible responsible species generated by kINPen plasmas and the reactions leading to their origin
 256 are highlighted in the box (15, 61, 77, 84, 85).

257 A non-radical mechanism driven by peroxyxynitrous acid and peroxyxynitrite has also been
 258 proposed by (84), leading to tyrosine hydroxylation and nitration by formation of ONOOH
 259 intermediates during the H^+ driven isomerization of peroxyxynitrous acid to NO_3^- and H^+ . Indeed, the
 260 energy and the rate for the isomerization (18 kcal mol^{-1} and 1.3 s^{-1} , respectively) are equivalent to
 261 those necessary to achieve the nitration or hydroxylation of aromatic compounds, occurring
 262 independently from their concentrations. At very low pH (< 2.5), the formation of nityl anion (NO_2^+)
 263 by peroxyxynitrous acid or peroxyxynitrite heterolysis could occur and lead to tyrosine nitration (85).
 264 However, this mechanism can be excluded in our system, due to the controlled pH at 7.4.

265 3.2. Gas Composition: A Crucial Parameter to Regulate the NO_x Generation

266 Tyrosine solutions were treated using different working gas compositions and treatment times,
 267 yielding various products. While tyrosine and 3-nitrotyrosine were absolutely quantified by a
 268 multiple reaction monitoring approach (Figure 3), all other tyrosine derivatives were relatively
 269 quantified (Figure 4 – dry working gas, Figure 5 – humidified working gas).

270 The highest tyrosine consumption (68 %) was observed for a discharge regime rich in short-lived
 271 ROS (dry Ar/O_2) (25, 86). In contrast, hydrogen peroxide rich conditions (dry Ar) (77), yielded only
 272 in 14 % tyrosine conversion.

273 Using admixtures of molecular gases, more than 50 % of tyrosine was converted into
274 hydroxytyrosine. Target water ionization, homolysis or photolysis is promoted by excited states of
275 Ar₂ or N₂ (excimers), as well as from radical reactions (34, 87). The direct reaction with those species
276 (or for excimers, with their radiation) leads to the predominant formation in water of $\cdot\text{OH}$ and $\cdot\text{H}$
277 (88-90), which would react directly with tyrosine to form hydroxytyrosine. The higher OH-tyrosine
278 production in conditions with Ar/N₂ (up to 70 % converted tyrosine) confirmed the synergistic action
279 on the target of Ar₂ and N₂ excimers (15, 91). In contrast, in conditions including oxygen, gaseous
280 radicals (e.g. $\cdot\text{O}$) are predominantly formed, and could be responsible of tyrosine hydroxylation (up
281 to 4 -OH groups) via direct reaction with tyrosine or via water dissociation and $\cdot\text{OH}$ formation in
282 liquid (92, 93). In presence of both N₂ and O₂ in the working gas, a substantial consumption of tyrosine
283 was observed (\approx 55 %), alongside with the only detection of small amounts of 3-nitrotyrosine in dry
284 conditions (Figure 3).

285 Accordingly, the formation of primary or secondary nitrosative NO_x species can be assumed for
286 this condition, corroborating previous results determining S-nitrosocysteine formation. Here, a
287 deposition of $\cdot\text{NO}$ in the liquid did not yield in S-nitrosylation, and $\cdot\text{NO}$ oxidation products (e.g.
288 ONOO \cdot , N₂O₃) were assumed to be of relevance (30). Considering the strong accumulation of nitrate
289 in this discharge condition (30), an end product that can derive from the decomposition of
290 peroxyxynitrite, ONOO \cdot could be responsible for both the S-nitrosylation and the nitrotyrosine
291 formation (94).

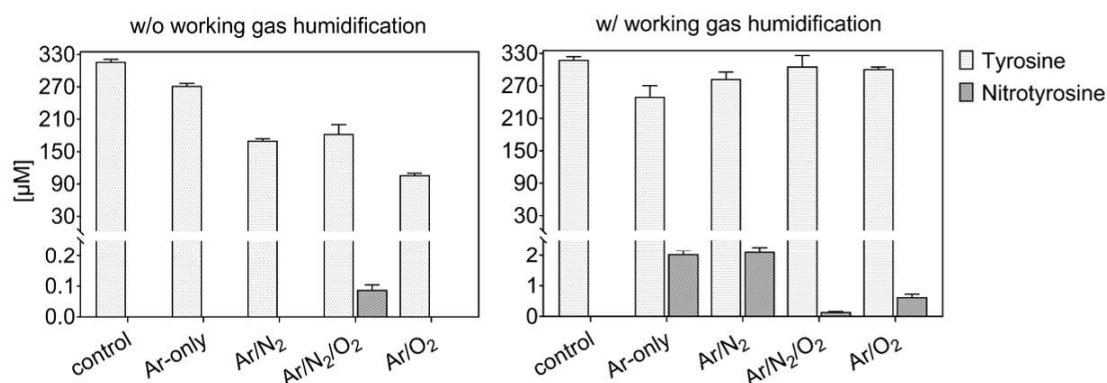
292 The incorporation of 2 -NO₂ (2 %) and 4 -NO (up to 5 %) groups was detected in major amounts
293 in admixtures including oxygen (Figure 4), confirming an active nitrogen chemistry in the liquid also
294 using shielding N₂ as source (40, 95). Considering quantitative data, an isobaric structure for
295 nitrotyrosine (e.g. hydroxy-nitrosotyrosine, see Table 1) was detected in conditions with oxygen only
296 as admix.

297 Previous simulation studies shown the highest gas phase formation of $\cdot\text{NO}_2$ ($\sim 8 \times 10^{13} \text{ cm}^{-3}$) and
298 N₂O ($\sim 5 \times 10^{12} \text{ cm}^{-3}$) using dry working gases (N₂ shielded) containing 1 % N₂/O₂ with O₂ in less than
299 50 %. Those species decreased by increasing the O₂ %, with the increase of highly oxidized species,
300 such as O₃ ($\sim 1.5 \times 10^{15} \text{ cm}^{-3}$) and N₂O₅ ($\sim 3 \times 10^{13} \text{ cm}^{-3}$) (77). Considering the higher production of
301 nitrotyrosine in conditions with 1:1 N₂/O₂ admixtures (Figure 3), $\cdot\text{NO}_2$ could be a direct nitrating
302 agent of tyrosyl radicals in the target. However, it must be considered that only a minimal amount of
303 $\cdot\text{NO}_2$ would be able to diffuse from the gas phase into the bulk of the liquid, due to its low solubility
304 in water ($H^{\text{CP}} = 3.4 \times 10^{-2} \text{ Pa}^{-1}$) (96). Most likely, a direct nitration due to gaseous $\cdot\text{NO}_2$ could occur at
305 the interface. These limitations could justify the overall low production of nitrotyrosine.

306 Alternatively, the production of other nitrating agents that have $\cdot\text{NO}_2$ as precursor can be
307 considered. The reaction between $\cdot\text{NO}_2$ and water molecules generates HNO₂, which is highly soluble
308 (53). However, at a pH of 7.4, the nitrous acid cannot be considered as nitrating agent. $\cdot\text{NO}_2$ could
309 form N₂O₃, a nitrating agent, by reaction with $\cdot\text{NO}$, that is present in gas and liquid phase (77).
310 However, due to the low solubility of N₂O₃ ($H^{\text{CP}} = 6.0 \times 10^{-1} \text{ Pa}^{-1}$) (96), its penetration to the target is
311 unlikely. With that, the well soluble peroxyxynitrite could be a prominent candidate for the effective
312 nitrating species, acting on tyrosine via dissociation in $\cdot\text{NO}_2$ (61), or transition intermediates of
313 peroxyxynitrous acid formed during its isomerization in nitrate (97). ONOOH/ONOO \cdot production is
314 promoted by reaction of gaseous $\cdot\text{NO}$ and $\cdot\text{O}_2$ (77), but considering $\cdot\text{NO}_2$ as major gaseous precursor,
315 interface/bulk reaction of $\cdot\text{NO}_2$ (gas) with $\cdot\text{OH}$ (in liquid), or HNO₂ with H₂O₂ (in liquid) are possible
316 formation pathways (97-99). The production in liquid of H₂O₂ and $\cdot\text{OH}$ by water
317 dissociation/ionization driven by radicals and vacuum UV radiation was previously shown (34, 87).
318 The formation of peroxyxynitrite by the reaction of HNO₂ with H₂O₂ is favored by low pH (< 4), which
319 may be achieved in the gas-liquid interface (97, 99) and not in the liquid bulk (Figure S1) (100).

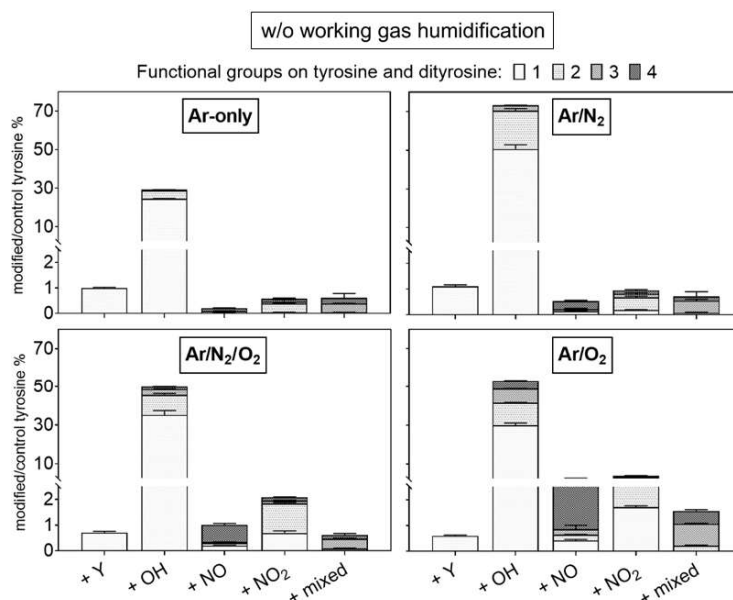
320 As shown in Figure 3 and 5, the addition of humidity in the working gas reduced the general
321 tyrosine oxidation in conditions containing oxygen, increasing drastically in Ar and Ar/N₂ the
322 production of nitrotyrosine (up to 2 μM), nitrosotyrosine (1 and 4 -NO groups, 2 %), mixed
323 modifications (2 %), and multiple nitration events (2 -NO₂ groups, 8 %). Conditions with Ar-only in

324 the working gas became slightly more oxidative (25 % oxidized tyrosine) than dry conditions. In
 325 contrast, tyrosine oxidation was lower than in dry conditions with molecular admixtures (7 % and 5
 326 %, for Ar/O₂ and Ar/N₂/O₂, respectively), as well as the production of tyrosine derivatives (Figure 5).
 327 This can be explained by interaction of water molecules in the effluent with gaseous species formed
 328 using Ar/O₂ and Ar/N₂/O₂ (e.g. [•]O, ¹O₂, [•]NO₂). In parallel, it was shown that this interaction, mostly
 329 with Ar₂⁺ and [•]O, generated [•]OH, [•]H and [•]O₂⁻ in the effluent area, which partially diffuse into the
 330 target, forming high amounts of H₂O₂ by recombination of [•]OH (38, 101). In the gas phase of
 331 humidified kINPen plasmas with low O₂ %, a boost of gaseous nitrogen chemistry was also detected,
 332 with higher production of HNO₃ (~4 × 10¹³ cm⁻³) and [•]NO (~6 × 10¹³ cm⁻³), rather than [•]NO₂, which
 333 densities increased only increasing O₂ % (39).



334

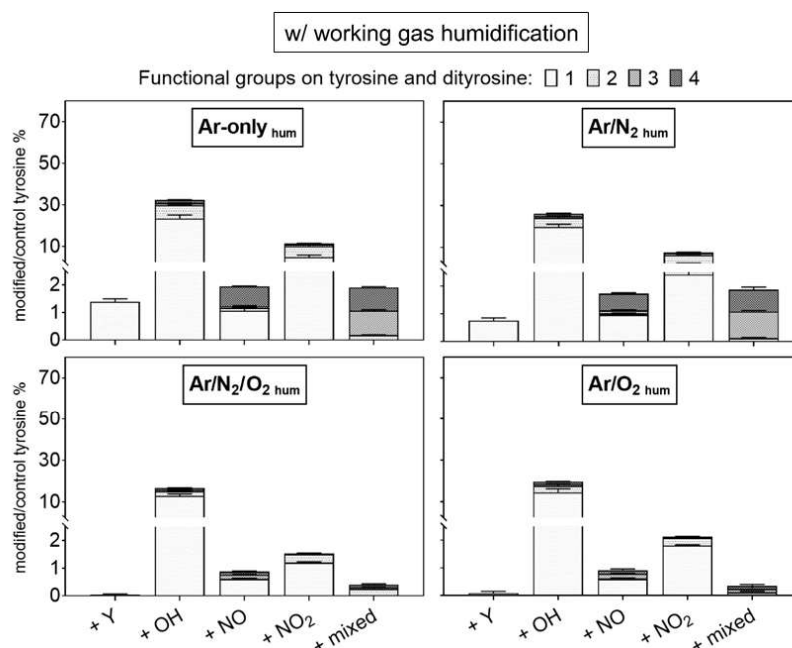
335 **Figure 3.** Tyrosine consumption and 3-nitrotyrosine formation by plasma-derived ROS. The presence
 336 of water in the working gas reduced gas phase oxidation of RNS and yielded in higher activity of RNS
 337 in the liquid (3min, 0.3 mM tyrosine in 5 mM ammonium formate, pH 7.4). Plasma is formed from
 338 dry (left) or humid (320 ppm H₂O, right) working gas.



339

340 **Figure 4.** Modifications of tyrosine observed after plasma treatment using dry working gas are
 341 dominated by hydroxylation. Multiple nitrations/nitrosylations were observed predominantly when
 342 O₂ was present in the working gas. Labels: + Y (tyrosyl, +180.066 Da), + OH (hydroxyl, +15.9949 Da),
 343 + NO (nitroso, +28.9902 Da), and + NO₂ (nitro, +44.9851 Da). Up to four groups were observed per
 344 molecule (indicated by light to dark grey). The introduction of diverse groups is represented as
 345 “mixed” (Compounds 20 to 27, Table 1). Treatment time 3 min, 0.3 mM tyrosine in 5 mM ammonium
 346 formate, pH 7.4. Relative compound intensities are given (tyrosine ~ 4445 counts in control).

347 Considering the 10-times higher production of nitrotyrosine in humid conditions with Ar-only
 348 or Ar/N₂, than in conditions with Ar/O₂ and Ar/N₂/O₂, a higher formation of nitrogen species in liquid
 349 is key. Rather than a direct impact of gaseous [•]NO₂, the formation of peroxyntirite via different
 350 pathways is facilitated. The reaction of gaseous [•]NO with [•]O₂ at the interface or in the
 351 bulk of the liquid is a substantial pathway. Additionally, the high amounts of HNO₃ in the gas phase
 352 favor an attacked of [•]OH, forming [•]NO₃, which is an unstable species generating H₂O₂ and [•]NO₂ in
 353 contact with water. Alternatively, [•]NO₂ could form HNO₂ by reacting with water molecules. The
 354 subsequent reaction with H₂O₂ yielding ONOOH is not favored at the pH of 7.4, precluding this as a
 355 major reaction route (100). At the interface, [•]NO₂ could form peroxyntirite by the reaction with [•]OH
 356 radicals.



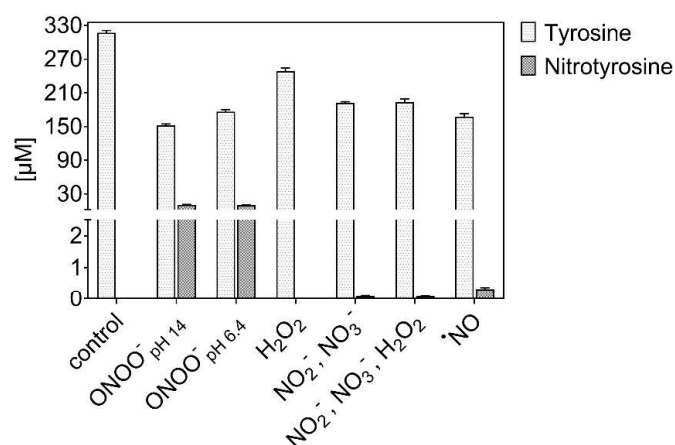
357

358 **Figure 5.** Modifications of tyrosine observed after plasma treatment using humidified working gas
 359 show a substantial introduction of one nitroso or nitro group. Labels: + Y (tyrosyl, +180.066 Da), + OH
 360 (hydroxyl, +15.9949 Da), + NO (nitroso, +28.9902 Da), and + NO₂ (nitro, +44.9851 Da). Up to four
 361 groups were observed per molecule (indicated by light to dark grey). The introduction of diverse
 362 groups is represented as “mixed” (Compounds 20 to 27, Table 1). Treatment time 3 min, 0.3 mM
 363 tyrosine in 5 mM ammonium formate, pH 7.4. Relative compound intensities are given (tyrosine ~
 364 4445 counts in control).

365 3.3. Tyrosine Modification Induced by Control Oxidants

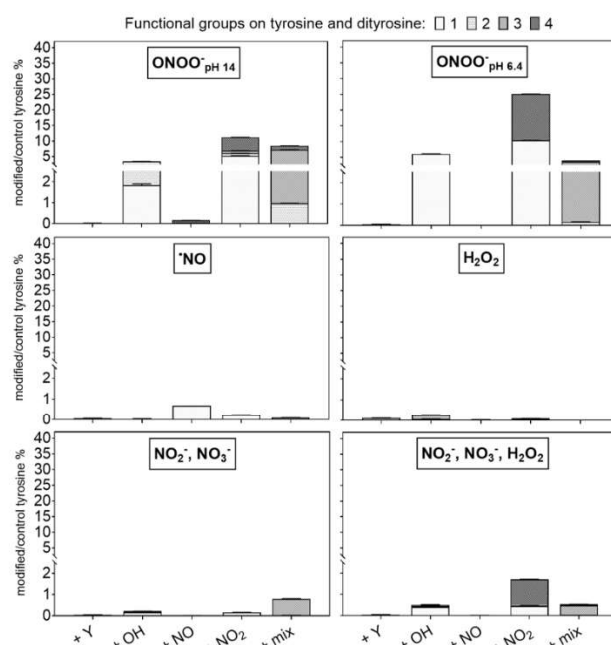
366 Incubations with standards (NO donor, NO₂/NO₃⁻, H₂O₂/NO₂⁻/NO₃⁻) were performed at neutral
 367 pH (7.4). Peroxynitrite was tested at two different pH (pH 14 and 6.4) (78, 79). The observed tyrosine
 368 derivatives are shown in Figure 6 (quantitative) and 7 (qualitative). Peroxynitrite was most efficient
 369 in modifying tyrosine (46% and 37%, respectively at pH 14 and 6.4). In particular, nitrotyrosine (~10
 370 μM) was formed (Figure 6). The substantial functionalization observed for ONOO⁻ at near neutral pH
 371 is due to the protonation of the ion, yielding instable peroxyntirous acid (ONOOH, 58.7 %
 372 considering the pK_a = 6.8). This rapidly isomerizes into NO₃⁻ and H⁺, and dissociates in [•]OH and [•]NO₂
 373 (30 % yield) (57, 61, 65). However, at pH 14 a similar nitration yield was observed, likely induced by
 374 the direct reaction of tyrosine with ONOO⁻ and ONOOH via the formation of a transition
 375 intermediate generated in the isomerization of ONOOH to NO₃⁻ (84). The functionalization of
 376 tyrosine via non-radical processes was confirmed, inducing also an higher incorporation of up to four
 377 different functional groups into the tyrosine moiety (+ 2 -OH groups, 2 and 4 mixed groups) (Figure
 378 7). In contrast, pH 6.4 yielded to an incorporation of up to 4 -NO₂ groups in the tyrosine structure,

379 emphasizing the favored formation of $\cdot\text{NO}_2$ by peroxyntirite dissociation. According to (84, 85), the
 380 hydroxylation was stronger at lower pH, due to the formation of a peroxyntirous acid intermediate
 381 that facilitates the cleavage of the ions O-O bond. Incubations with any other compound (mix) yielded
 382 very low amounts of nitrotyrosine ($< 0.5 \mu\text{M}$), and only the $\cdot\text{NO}$ donor could induce nitroso-groups
 383 on tyrosine, confirming a direct reaction with the aromatic ring (Figure 7) (61). The low formation of
 384 nitrosotyrosine indicate the low reactivity of $\cdot\text{NO}$ itself with the ring and a limited oxidation of $\cdot\text{NO}$
 385 to nitrite ions respectively nitrous acid. A partial oxidation to $\cdot\text{NO}_2$ in presence of O_2 could justify the
 386 formation of nitrotyrosine.



387

388 **Figure 6.** Tyrosine consumption and 3-nitrotyrosine formation by controls. Peroxyntirite efficiently
 389 introduced a nitro group, but independently from pH. (3 min incubation of 0.3 mM tyrosine in 5 mM
 390 ammonium formate, pH 7.4, 300 μM of each standard).



391

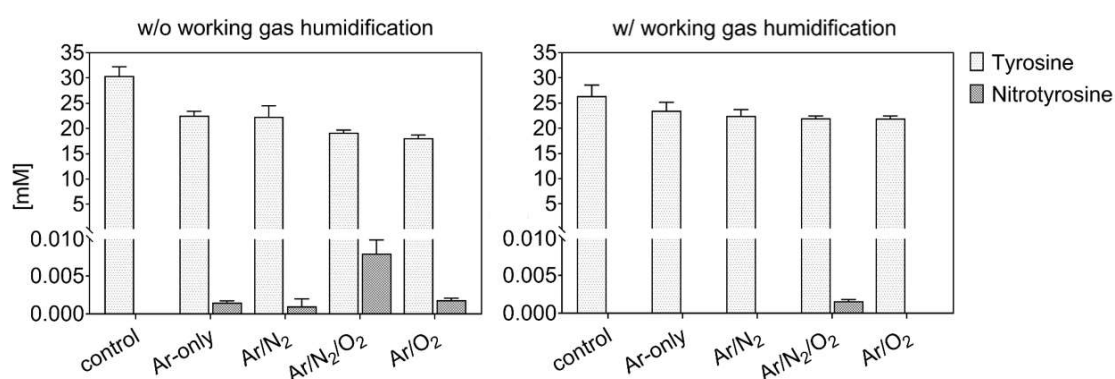
392 **Figure 7.** Modifications of tyrosine observed after treatment using 300 μM standards. Peroxyntirite
 393 was most efficient, with higher pH boosting the introduction of multiple groups. Labels: + Y (tyrosyl,
 394 +180.066 Da), + OH (hydroxyl, +15.9949 Da), + NO (nitroso, +28.9902 Da), and + NO₂ (nitro, +44.9851
 395 Da). Up to four groups were observed per molecule (indicated by light to dark grey). The introduction
 396 of diverse groups is represented as “mixed” (Compounds 20 to 27, Table 1). Treatment time 3 min,
 397 0.3 mM tyrosine in 5 mM ammonium formate, pH 7.4, direct infusion high-resolution MS. Relative
 398 compound intensities are given (tyrosine ~ 4948 counts in control).

399 By the incubation with H₂O₂, only 11 % of the tyrosine was consumed, and yielded in
 400 hydroxylated products. When nitrite and nitrate ions were available at the same, a few nitration were
 401 observed. Of note, no nitrosylation occurred, indicating that peroxyxynitrite, formed from H₂O₂ and
 402 NO₂, was responsible. However, due to the pH of 7.4 in the experiment this reaction was not favored.
 403 Likewise, the pH in the plasma treatment never reached below pH 7, even after 10 min of treatment
 404 (Figure S1 in SI), excluding a substantial formation of peroxyxynitrite in the bulk. When nitrite/nitrate
 405 were the sole available compounds, no modification of tyrosine occurs. The apparent consumption
 406 of tyrosine was in conditions with high sodium content overestimated due to the formation of
 407 tyrosine salts that evaded detection in the applied experimental conditions.

408 3.4. Both Gas Phase- and Liquid Phase-Derived Species Contribute to Tyrosine Modification

409 To investigate the role of solvent-derived reactive species, higher concentrated solutions of
 410 tyrosine (30 mM) were treated. The identified products were similar to the more diluted solutions
 411 (see Figure S2/dry working gas and Figure S3/humidified working gas for a complete overview).
 412 While the total number of oxidized molecules increased, the turnover rate was proportionally lower
 413 and indicated a limitation of the produced ROS/RNS in liquid. In condition with Ar-only, Ar/N₂ and
 414 Ar/O₂, a conversion of respectively 3.2×10^{18} , 3.0×10^{18} and 5.0×10^{18} molecules per second occurred
 415 (Figure 8). This corresponds to a total of 24 %, 22% and 36% tyrosine conversion in derivatives. In
 416 comparison, treatments of 0.3 mM tyrosine solutions yielded in a conversion rate of 1.8×10^{16} , $6.6 \times$
 417 10^{16} and 9.5×10^{16} molecules per second, corresponding to 12.8 % (Ar-only), 45 % (Ar/N₂) and 66 %
 418 (Ar/O₂) converted tyrosine. On average, the turnover rate in concentrated tyrosine solutions was a
 419 factor of ≈ 50 fold higher than in diluted solutions, while their concentration was 100 fold higher. This
 420 would suggest that, using these working gases and high tyrosine concentration, the amount of
 421 induced modifications was reduced due to a limited production/action of species in liquid. In parallel,
 422 gaseous species were still effective on the target.

423 In contrast, conditions with both N₂ and O₂ in the dry working gas led to an identical
 424 proportional formation of nitrotyrosine (0.026 % of converted tyrosine) for both concentrations. In
 425 this case, the high amounts of generated \cdot NO₂ in the gas phase could directly modify tyrosine
 426 molecules at the interface or in the underlying water layers of both high and low concentrated
 427 solutions. The apparent reaction probability remained constant, indicating that the interface
 428 occupation by the tyrosine molecules did not change with the concentration or that a corresponding
 429 decay reaction (e.g. formation of hydroxytyrosine from nitrotyrosine) increased proportionally.

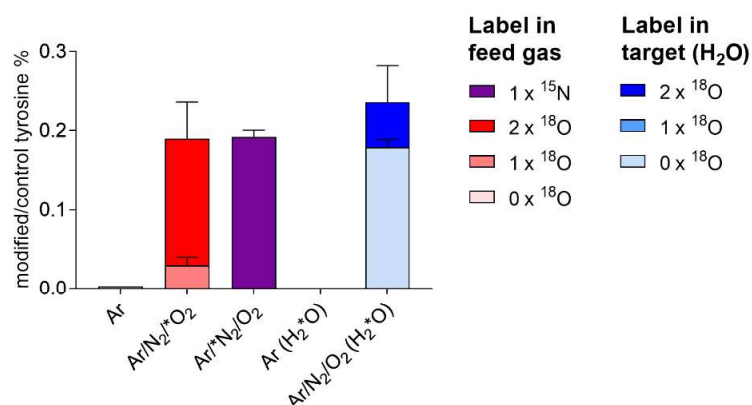


430

431 **Figure 8.** Tyrosine consumption and 3-nitrotyrosine formation by plasma-derived ROS in
 432 concentrated tyrosine solutions. The activity of peroxyxynitrite (humid conditions) is quenched in favor
 433 of nitrogen dioxide (dry conditions). 3min, 30 mM tyrosine in 5 mM ammonium formate, pH 7.4.
 434 Plasma is formed from dry (left) or humid (320 ppm H₂O, right) working gas.

435 The role of gaseous \cdot NO₂ in forming nitrotyrosine was determined using heavy isotopes (¹⁵N₂ or
 436 ¹⁸O₂, or H₂¹⁸O). Almost 80 % ¹⁸O and 100 % ¹⁵N originated from the gas phase (Figure 9), confirming

437 the direct nitration of tyrosine by $\cdot\text{NO}_2$, rather than other species (e.g. peroxyxynitrite) originating from
 438 liquid chemistry.



439
 440 **Figure 9.** Nitrotyrosine formed from plasma treatment of tyrosine incorporates predominantly gas
 441 phase derived atoms (100 % N, \approx 80 % O). 20 % of oxygen atoms are introduced from the solvent
 442 (water), indicating a role for water derived OH radicals (for details see text). Dry argon working gas
 443 contained ¹⁸O₂ and ¹⁵N₂. In independent experiments, tyrosine was dissolved in labelled water (H₂¹⁸O).
 444 Measurements performed via direct infusion mass spectrometry in triplicates.

445 By introducing humidity in the working gas, the oxidation of tyrosine, as well as the production
 446 of nitrotyrosine (Figure 8) and others tyrosine derivatives, such as dityrosine and nitrosotyrosine
 447 (Figure S3) was drastically reduced in relation to dry conditions (Figure S2). This suggests that in
 448 humidified conditions, relevant species act or/and are formed in the bulk of the liquid. It was
 449 observed that, for working gases with < 0.5 O₂ %, the presence of water molecules induced mostly the
 450 formation of species such as HNO₃ and $\cdot\text{NO}$, along with water-derived species H₂O₂, $\cdot\text{OH}$, $\cdot\text{H}$ and
 451 O₂ \cdot^- , rather than highly oxidized gaseous species, such as N₂O₅, O₃ and $\cdot\text{NO}_2$ (39). When treating 0.3
 452 mM tyrosine solutions with humid plasmas, nitrotyrosine was detected in a 10-fold higher amount
 453 then for the respective dry discharges. Considering that high concentrated solutions limited the
 454 formation/action of reactive species in liquid, gaseous species formed in humidified working gases
 455 (< 0.5 O₂ %) acted only in the bulk liquid or most likely as precursors of other nitrating species (e.g.
 456 peroxyxynitrite) formed in liquid.

457 3.5. Identification of Plasma-Derived Reactive Nitrogen Species

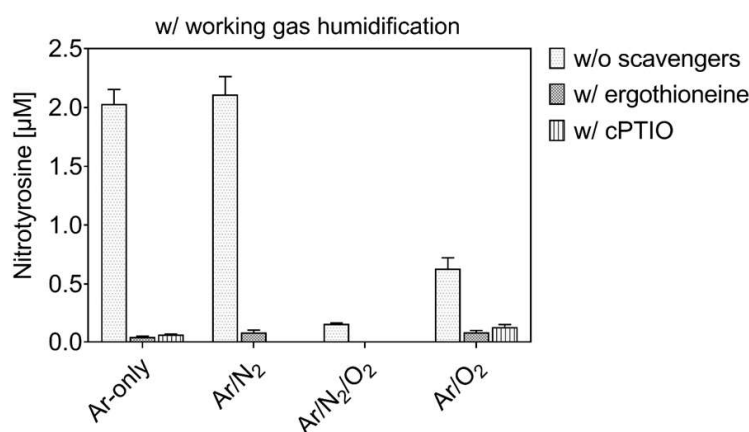
458 In presence of the $\cdot\text{NO}$ scavenger cPTIO or the peroxyxynitrite scavenger ergothioneine, the
 459 formation of N-containing tyrosine derivatives was differential.

460 A general overview of all identified compounds containing nitrogen is given in Figure S4, while
 461 Figure 10 shows quantitative data achieved by HILIC-MRM for nitrotyrosine. As shown in Figure 10,
 462 in conditions with humidified working gases, the production of nitrotyrosine was almost abolished
 463 in presence of cPTIO or ergothioneine. Further, almost all other N-containing tyrosine derivatives
 464 were shunned (Figure S4). These results are in good agreement with the hypothesis that the addition
 465 of humidity to the working gas favor the production of peroxyxynitrite, predominantly originating by
 466 reaction of $\cdot\text{NO}$ with O₂ \cdot^- derived by water dissociation. The conversion of HNO₃ in $\cdot\text{NO}_2$ in liquid,
 467 and its further reaction with $\cdot\text{OH}$ could still be an additional route for peroxyxynitrite formation.

468 The formation and activity of reactive nitrogen species in liquids could not be excluded for dry
 469 working gases (Figure S4). Indeed, the formation of some compounds that bear nitroso-groups was
 470 prevented only by cPTIO ($< 0.5\%$ in Ar/N₂/O₂, Figure S4a), indicating a role for a direct or indirect
 471 role of $\cdot\text{NO}$, reformed in the liquid phase from gaseous $\cdot\text{NO}_2$ (77). Furthermore, almost 2.5 % of
 472 tyrosine was converted in conditions with dry Ar/N₂/O₂ in derivatives scavenged by ergothioneine
 473 (Figure S4b and c). These data confirm the formation and chemical activity of peroxyxynitrite in dry

474 working gas conditions. Finally, conditions with dry working gases produced the maximal amount
 475 of nitrogen-containing derivatives in presence of gas admixtures (3 % oxidized tyrosine). Their
 476 formation was due paramount to the direct action of gaseous $\cdot\text{NO}_2$ and to a lesser extent to a
 477 reformation of nitrosative species in the liquid (e.g. H^+/NO_2^- , ONOO^-). For humidified working gas,
 478 an increase of nitrogen-containing derivatives was evident, provided when no oxygen was added (>
 479 14% oxidized tyrosine). Here, the nitrosative peroxyxynitrite formed in liquid (Figure S4).

480 However, it must be considered that non-specific reactions. It was reported that the NO
 481 scavenger cPTIO partially reacts with $\cdot\text{NO}_2$ (74), while ergothioneine is able to scavenge $^1\text{O}_2$ and $\cdot\text{OH}$
 482 (75, 102). No discriminative derivatives produced by the reaction of scavengers with standard
 483 reactive species could be identified in this work.



484

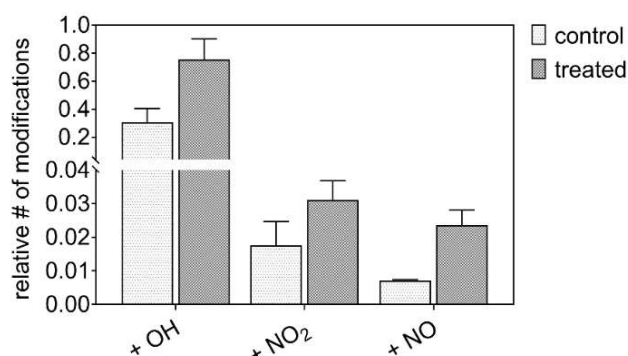
485 **Figure 10.** Nitrotyrosine formation by plasma treatment is prevented in the presence of scavengers. 3
 486 min treatment, 0.3 mM tyrosine in 5 mM ammonium formate, pH 7.4, with and without ergothioneine
 487 or cPTIO, using Ar \pm 1% N₂/O₂ as humidified working gas and N₂ as shielding gas.

488 3.6. Plasma Induces Oxidative and Nitrosative Protein Modifications in Wounds

489 In order to verify if nitrosative modifications can be introduced in biological molecules in
 490 complex environments, and consequentially potentially *in vivo*, wound exudates of patients before
 491 and after plasma treatment under certified conditions were collected and analyzed. The MS-based
 492 proteomic analysis revealed 62 up regulated proteins and 225 down regulated proteins in relation to
 493 the treatment. Specifically, (non-enzymatic) protein modifications were searched that may have been
 494 introduced via reactive species generated by or in connection to the plasma discharge. Compared to
 495 the control, an increase of 63, 44 and 69 % respectively for oxidation, nitration and nitrosylation events
 496 was determined in the wound proteome (Figure 11).

497 These modifications were attributed to the impact of plasma, suggesting a crosstalk of plasma-
 498 derived species with cellular redox signaling pathways regulating processes related to acute and
 499 chronic wound healing like blood coagulation, immune cell migration, and cell proliferation. The
 500 introduction of nitro groups into protein bound tyrosine by nitric oxide related pathways was
 501 reported to have a key role in the regulation of cell migration, angiogenesis, and mast cell
 502 degranulation (63, 68).

503 Consequentially, a regulation of wound healing processes via protein modifications is likely to
 504 be involved in the observed outcome of plasma treatment on chronic wounds and well in line with a
 505 recent study that emphasized the role of target cell stimulation over anti-microbial effects (22). The
 506 presented results suggest a switch from the current condition (argon only) to argon/N₂/O₂ as a
 507 working gas to increase the impact of the plasma derived RNS on biomolecules and subsequent
 508 signaling events.



509

510

511

512

513

Figure 11. Cold plasma induced post-translational modifications in the proteome of wound exudates of diabetic patients. Proteome analysis performed via nLC-MS, with detection of mass shifts correspondent to the introduced functional group (OH = 15.9949 Da; NO = 28.9902 Da, NO₂ = 44.9851 Da), according to (80).

514

4. Summary and Conclusions

515

516

517

518

519

520

This work studied the liquid chemistry of argon plasmas generated by the kINPen, with a special focus on reactive nitrogen species. Assuming that the liquid chemistry is the bridge between the gaseous plasma and biological systems, we looked for the impact of nitrogen species on the model biomolecule tyrosine. Using a mass spectrometry driven approach, 26 different compounds were identified. Their respective pattern was exploited to determine the dominant reactive species formed in the gas or in/at the liquid phase.

521

522

523

524

525

526

527

528

529

530

531

532

533

534

535

536

Nitration reactions were significant for dry Ar/O₂/N₂ plasma. Gaseous [•]NO₂ was found responsible for a direct nitration of tyrosine at the gas-liquid interface and to be involved in the formation of peroxyntirite and nitric oxide radicals at the same location. While the relevance of nitric oxide for the product formation was limited, peroxyntirite contributed to a substantial extent. When water molecules were present in the working gas, its role was further emphasized due to a higher peroxyntirite formation via additional pathways: the reaction of gaseous nitric oxide with superoxide anion radicals and the reaction of hydrogen peroxide and nitrous acid/nitrite at the gas-liquid interface. In conditions with a high prevalence of ROS (e.g. dry Ar/O₂), the impact of RNS was minimized. Here, stable species like N₂O₅ that do not penetrate the interface evolve from [•]NO₂ in the gas phase and the formation of peroxyntirite decreases. Due to the high activity of ROS at the interface and the liquid bulk, potentially formed nitrated/nitrosylated tyrosine products are eliminated in favor of hydroxylated compounds. Finally, the introduction of nitroso and nitro groups into proteins *in vivo* by cold plasma treatments was confirmed in human diabetes 2-related chronic wounds. The tyrosine moiety was particularly attacked, allowing for changes in the protein functionality. This suggests a contribution of plasma-derived RNS via covalent changes to the observed efficacy in wound healing.

537

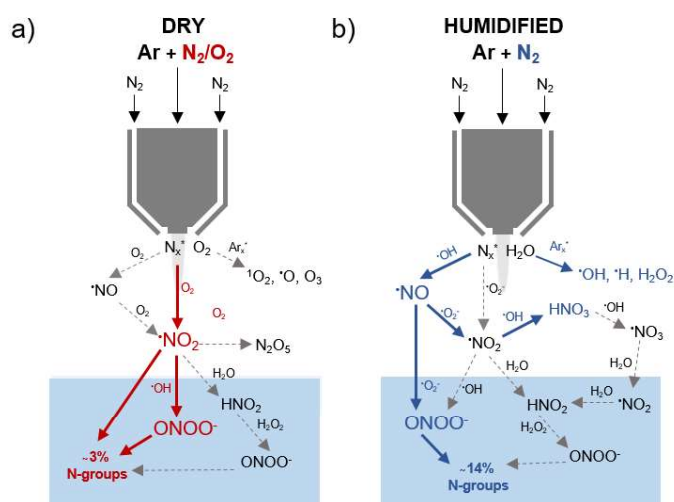
538

539

540

541

In conclusion, this work verified the controllability of kINPen plasmas to achieve a relevant production of reactive nitrogen species (Figure 12). The deposited or at the interface generated species, especially [•]NO₂ and ONOO[•] led to nitrosative reactions on biomolecules, both in complex and in model conditions. A relevant contribution to the observed biomedical effects of plasmas must be assumed.



542

543

544

545

546

Figure 12. Suggested chemical pathways for the production of bioactive RNS species in plasma treated tyrosine solutions in dry (a) and humidified (b) conditions. Represented species were previously detected for the kINPen (39, 77, 95), except for peroxynitrite. Pathway confirmed in liquids (compact lines) by use of scavengers or isotope labels.

547

548

Acknowledgements: Funding from the German Federal Ministry of Education and Research (grant number 03Z22DN12 to K.W.) supported this work.

549

550

551

552

553

Author Contributions: Conceptualization, G.B., K.W.; methodology, G.B., K.W., S.W./J.W.L (proteome and PTMs analysis); formal analysis, G.B., S.W./J.W.L (proteome and PTMs analysis); investigation, G.B.; data curation, G.B.; writing—original draft preparation, G.B., S.W. (proteome and PTMs analysis); writing—review and editing, G.B., K.W. & M.L.; visualization, G.B. All authors have read and agreed to the published version of the manuscript.

554

Conflicts of Interest: The authors declare no conflict of interest.

555

References

556

557

558

559

560

561

562

563

564

565

566

567

568

569

570

571

572

573

574

575

576

577

- Alfadda AA, Sallam RM. Reactive oxygen species in health and disease. *J Biomed Biotechnol.* 2012;2012:936486.
- Parvez S, Long MJC, Poganik JR, Aye Y. Redox Signaling by Reactive Electrophiles and Oxidants. *Chem Rev.* 2018;118(18):8798-888.
- Törnvall U. Pinpointing oxidative modifications in proteins—recent advances in analytical methods. *Analytical Methods.* 2010;2(11).
- Sies H. Hydrogen peroxide as a central redox signaling molecule in physiological oxidative stress: Oxidative eustress. *Redox Biology.* 2017;11:613-9.
- Cai Z, Yan LJ. Protein Oxidative Modifications: Beneficial Roles in Disease and Health. *J Biochem Pharmacol Res.* 2013;1(1):15-26.
- Halliwell B. Free Radicals and Other Reactive Species in Disease. *Encyclopedia of Life Sciences: John Wiley & Sons, Ltd;* 2005.
- Winterbourn CC. Reconciling the chemistry and biology of reactive oxygen species. *Nat Chem Biol.* 2008;4(5):278-86.
- Adams L, Franco MC, Estevez AG. Reactive nitrogen species in cellular signaling. *Exp Biol Med (Maywood).* 2015;240(6):711-7.
- Hancock JT, Desikan R, Neill SJ. Role of reactive oxygen species in cell signalling pathways. *Biochem Soc Trans.* 2001;29(Pt 2):345-50.
- von Woedtke T, Schmidt A, Bekeschus S, Wende K, Weltmann KD. Plasma Medicine: A Field of Applied Redox Biology. *In vivo (Athens, Greece).* 2019;33(4):1011-26.
- Privat-Maldonado A, Schmidt A, Lin A, Weltmann KD, Wende K, Bogaerts A, et al. ROS from Physical Plasmas: Redox Chemistry for Biomedical Therapy. *Oxid Med Cell Longev.* 2019;2019:9062098.

- 578 12. Agostinis P, Berg K, Cengel KA, Foster TH, Girotti AW, Gollnick SO, et al. Photodynamic therapy of cancer:
579 an update. *CA Cancer J Clin.* 2011;61(4):250-81.
- 580 13. Vozenin MC, Hendry JH, Limoli CL. Biological Benefits of Ultra-high Dose Rate FLASH Radiotherapy:
581 Sleeping Beauty Awoken. *Clin Oncol (R Coll Radiol).* 2019;31(7):407-15.
- 582 14. Adamovich I, Baalrud SD, Bogaerts A, Bruggeman PJ, Cappelli M, Colombo V, et al. The 2017 Plasma
583 Roadmap: Low temperature plasma science and technology. *J Phys D Appl Phys.* 2017;50(32):323001.
- 584 15. Bruggeman PJ, Kushner MJ, Locke BR, Gardeniers JGE, Graham WG, Graves DB, et al. Plasma-liquid
585 interactions: a review and roadmap. *Plasma Sources Science & Technology.* 2016;25(5):053002.
- 586 16. Laroussi M, Lu X, Keidar M. Perspective: The physics, diagnostics, and applications of atmospheric
587 pressure low temperature plasma sources used in plasma medicine. *J Appl Phys.* 2017;122(2):020901.
- 588 17. Park GY, Park SJ, Choi MY, Koo IG, Byun JH, Hong JW, et al. Atmospheric-pressure plasma sources for
589 biomedical applications. *Plasma Sources Science & Technology.* 2012;21(4).
- 590 18. Reuter S, von Woedtke T, Weltmann KD. The kINPen-a review on physics and chemistry of the
591 atmospheric pressure plasma jet and its applications. *J Phys D Appl Phys.* 2018;51(23).
- 592 19. Semmler ML, Bekeschus S, Schafer M, Bernhardt T, Fischer T, Witzke K, et al. Molecular Mechanisms of
593 the Efficacy of Cold Atmospheric Pressure Plasma (CAP) in Cancer Treatment. *Cancers (Basel).* 2020;12(2).
- 594 20. Pasqual-Melo G, Sagwal SK, Freund E, Gandhirajan RK, Frey B, von Woedtke T, et al. Combination of Gas
595 Plasma and Radiotherapy Has Immunostimulatory Potential and Additive Toxicity in Murine Melanoma
596 Cells in Vitro. *Int J Mol Sci.* 2020;21(4).
- 597 21. Lin A, Gorbanev Y, De Backer J, Van Loenhout J, Van Boxem W, Lemiere F, et al. Non-Thermal Plasma as
598 a Unique Delivery System of Short-Lived Reactive Oxygen and Nitrogen Species for Immunogenic Cell
599 Death in Melanoma Cells. *Adv Sci (Weinh).* 2019;6(6):1802062.
- 600 22. Stratmann B, Costea TC, Nolte C, Hiller J, Schmidt J, Reindel J, et al. Effect of Cold Atmospheric Plasma
601 Therapy vs Standard Therapy Placebo on Wound Healing in Patients With Diabetic Foot Ulcers: A
602 Randomized Clinical Trial. *JAMA Netw Open.* 2020;3(7):e2010411.
- 603 23. Schmidt A, Bekeschus S. Redox for Repair: Cold Physical Plasmas and Nrf2 Signaling Promoting Wound
604 Healing. *Antioxidants (Basel).* 2018;7(10).
- 605 24. Preissner S, Kastner I, Schutte E, Hartwig S, Schmidt-Westhausen AM, Paris S, et al. Adjuvant antifungal
606 therapy using tissue tolerable plasma on oral mucosa and removable dentures in oral candidiasis patients:
607 a randomised double-blinded split-mouth pilot study. *Mycoses.* 2016;59(7):467-75.
- 608 25. Jablonowski H, Santos Sousa J, Weltmann KD, Wende K, Reuter S. Quantification of the ozone and singlet
609 delta oxygen produced in gas and liquid phases by a non-thermal atmospheric plasma with relevance for
610 medical treatment. *Sci Rep.* 2018;8(1):12195.
- 611 26. Bruno G, Heusler T, Lackmann J-W, von Woedtke T, Weltmann K-D, Wende K. Cold physical plasma-
612 induced oxidation of cysteine yields reactive sulfur species (RSS). *Clinical Plasma Medicine.*
613 2019;14:100083.
- 614 27. Wende K, von Woedtke T, Weltmann KD, Bekeschus S. Chemistry and biochemistry of cold physical
615 plasma derived reactive species in liquids. *Biol Chem.* 2018;400(1):19-38.
- 616 28. Wende K, Williams P, Dalluge J, Gaens WV, Aboubakr H, Bischof J, et al. Identification of the biologically
617 active liquid chemistry induced by a nonthermal atmospheric pressure plasma jet. *Biointerphases.*
618 2015;10(2):029518.
- 619 29. Jablonowski H, von Woedtke T. Research on plasma medicine-relevant plasma-liquid interaction: What
620 happened in the past five years? *Clinical Plasma Medicine.* 2015;3(2):42-52.
- 621 30. Lackmann J-W, Bruno G, Jablonowski H, Kogelheide F, Offerhaus B, Held J, et al. Nitrosylation vs.
622 oxidation - How to modulate cold physical plasmas for biological applications. *PLoS One.*
623 2019;14(5):e0216606.
- 624 31. Lackmann JW, Baldus S, Steinborn E, Edengeiser E, Kogelheide F, Langklotz S, et al. A dielectric barrier
625 discharge terminally inactivates RNase A by oxidizing sulfur-containing amino acids and breaking
626 structural disulfide bonds. *J Phys D Appl Phys.* 2015;48(49).
- 627 32. Striesow J, Lackmann JW, Ni Z, Wenske S, Weltmann KD, Fedorova M, et al. Oxidative modification of
628 skin lipids by cold atmospheric plasma (CAP): A standardizable approach using RP-LC/MS(2) and DI-
629 ESI/MS(2). *Chem Phys Lipids.* 2020;226:104786.

- 630 33. Lackmann JW, Bandow JE. Inactivation of microbes and macromolecules by atmospheric-pressure plasma
631 jets. *Appl Microbiol Biotechnol.* 2014;98(14):6205-13.
- 632 34. Wende K, Bruno G, Lalk M, Weltmann K-D, von Woedtke T, Bekeschus S, et al. On a heavy path –
633 determining cold plasma-derived short-lived species chemistry using isotopic labelling. *Rsc Adv.*
634 2020;10(20):11598-607.
- 635 35. Benedikt J, Mokhtar Hefny M, Shaw A, Buckley BR, Iza F, Schakermann S, et al. The fate of plasma-
636 generated oxygen atoms in aqueous solutions: non-equilibrium atmospheric pressure plasmas as an
637 efficient source of atomic O(aq). *Phys Chem Chem Phys.* 2018;20(17):12037-42.
- 638 36. Bekeschus S, Wende K, Hefny MM, Rodder K, Jablonowski H, Schmidt A, et al. Oxygen atoms are critical
639 in rendering THP-1 leukaemia cells susceptible to cold physical plasma-induced apoptosis. *Sci Rep.*
640 2017;7(1):2791.
- 641 37. Winter J, Tresp H, Hammer MU, Iseni S, Kupsch S, Schmidt-Bleker A, et al. Tracking plasma generated
642 H₂O₂ from gas into liquid phase and revealing its dominant impact on human skin cells. *J Phys D Appl*
643 *Phys.* 2014;47(28).
- 644 38. Reuter S, Winter J, Iseni S, Schmidt-Bleker A, Dunnbier M, Masur K, et al. The Influence of Feed Gas
645 Humidity Versus Ambient Humidity on Atmospheric Pressure Plasma Jet-Effluent Chemistry and Skin
646 Cell Viability. *IEEE T Plasma Sci.* 2015;43(9):3185-92.
- 647 39. Schmidt-Bleker A, Bansemer R, Reuter S, Weltmann K-D. How to produce an NO_x- instead of Ox-based
648 chemistry with a cold atmospheric plasma jet. *Plasma Processes and Polymers.* 2016;13(11):1120-7.
- 649 40. Schmidt-Bleker A, Winter J, Bosel A, Reuter S, Weltmann KD. On the plasma chemistry of a cold
650 atmospheric argon plasma jet with shielding gas device. *Plasma Sources Science & Technology.*
651 2016;25(1):015005.
- 652 41. Zhou R, Zhou R, Prasad K, Fang Z, Speight R, Bazaka K, et al. Cold atmospheric plasma activated water as
653 a prospective disinfectant: the crucial role of peroxyxynitrite. *Green Chemistry.* 2018;20(23):5276-84.
- 654 42. Naïtali M, Herry J-M, Hnatiuc E, Kamgang G, Brisset J-L. Kinetics and Bacterial Inactivation Induced by
655 Peroxyxynitrite in Electric Discharges in Air. *Plasma Chemistry and Plasma Processing.* 2012;32(4):675-92.
- 656 43. Yamashiro R, Misawa T, Sakudo A. Key role of singlet oxygen and peroxyxynitrite in viral RNA damage
657 during virucidal effect of plasma torch on feline calicivirus. *Sci Rep.* 2018;8(1):17947.
- 658 44. Ulrich C, Kluschke F, Patzelt A, Vandersee S, Czaika VA, Richter H, et al. Clinical use of cold atmospheric
659 pressure argon plasma in chronic leg ulcers: A pilot study. *Journal of Wound Care.* 2015;24(5):196-203.
- 660 45. Emmert S, Brehmer F, Haenßle H, Helmke A, Mertens N, Ahmed R, et al. Atmospheric pressure plasma in
661 dermatology: Ulcus treatment and much more. *Clinical Plasma Medicine.* 2013;1(1):24-9.
- 662 46. van Gils CAJ, Hofmann S, Boekema BKHL, Brandenburg R, Bruggeman PJ. Mechanisms of bacterial
663 inactivation in the liquid phase induced by a remote RF cold atmospheric pressure plasma jet. *Journal of*
664 *Physics D: Applied Physics.* 2013;46(17):175203.
- 665 47. Bekeschus S, Freund E, Spadola C, Privat-Maldonado A, Hackbarth C, Bogaerts A, et al. Risk Assessment
666 of kINPen Plasma Treatment of Four Human Pancreatic Cancer Cell Lines with Respect to Metastasis.
667 *Cancers (Basel).* 2019;11(9).
- 668 48. Bekeschus S, von Woedtke T, Weltmann K-D, Metelmann H-R. Plasma, Cancer, Immunity. *Clinical Plasma*
669 *Medicine.* 2018;9:13-4.
- 670 49. Bekeschus S, Favia P, Robert E, von Woedtke T. White paper on plasma for medicine and hygiene: Future
671 in plasma health sciences. *Plasma Processes and Polymers.* 2019;16(1):1800033.
- 672 50. Shekhter AB, Pekshev AV, Vagapov AB, Butenko AV, Fayzullin AL, Rudenko TG, et al. Dose-dependent
673 effect of plasma-chemical NO-containing gas flow on wound healing. An experimental study. *Clinical*
674 *Plasma Medicine.* 2020;19-20.
- 675 51. Bekeschus S, Kolata J, Winterbourn C, Kramer A, Turner R, Weltmann KD, et al. Hydrogen peroxide: A
676 central player in physical plasma-induced oxidative stress in human blood cells. *Free Radic Res.*
677 2014;48(5):542-9.
- 678 52. Lukes P, Dolezalova E, Sisrova I, Clupek M. Aqueous-phase chemistry and bactericidal effects from an air
679 discharge plasma in contact with water: evidence for the formation of peroxyxynitrite through a pseudo-
680 second-order post-discharge reaction of H₂O₂ and HNO₂. *Plasma Sources Sci T.* 2014;23(1):015019.
- 681 53. Lackmann JW, Bruno G, Jablonowski H, Kogelheide F, Offerhaus B, Held J, et al. Nitrosylation vs. oxidation
682 - How to modulate cold physical plasmas for biological applications. *PLoS One.* 2019;14(5):e0216606.

- 683 54. Ikawa S, Tani A, Nakashima Y, Kitano K. Physicochemical properties of bactericidal plasma-treated water.
684 J Phys D Appl Phys. 2016;49(42):425401.
- 685 55. Mikkelsen RB, Wardman P. Biological chemistry of reactive oxygen and nitrogen and radiation-induced
686 signal transduction mechanisms. *Oncogene*. 2003;22(37):5734-54.
- 687 56. Paulsen CE, Carroll KS. Cysteine-mediated redox signaling: chemistry, biology, and tools for discovery.
688 *Chem Rev*. 2013;113(7):4633-79.
- 689 57. Bartesaghi S, Radi R. Fundamentals on the biochemistry of peroxynitrite and protein tyrosine nitration.
690 *Redox Biol*. 2018;14:618-25.
- 691 58. Ischiropoulos H. Biological selectivity and functional aspects of protein tyrosine nitration. *Biochem*
692 *Biophys Res Commun*. 2003;305(3):776-83.
- 693 59. Betts MJ, Russell RB. Amino-Acid Properties and Consequences of Substitutions. *Bioinformatics for*
694 *Geneticists*2007. p. 311-42.
- 695 60. Bartesaghi S, Peluffo G, Zhang H, Joseph J, Kalyanaraman B, Radi R. Tyrosine nitration, dimerization, and
696 hydroxylation by peroxynitrite in membranes as studied by the hydrophobic probe N-t-BOC-L-tyrosine
697 tert-butyl ester. *Methods Enzymol*. 2008;441:217-36.
- 698 61. Ferrer-Sueta G, Campolo N, Trujillo M, Bartesaghi S, Carballal S, Romero N, et al. Biochemistry of
699 Peroxynitrite and Protein Tyrosine Nitration. *Chem Rev*. 2018;118(3):1338-408.
- 700 62. Rubbo H, Radi R. Protein and lipid nitration: role in redox signaling and injury. *Biochim Biophys Acta*.
701 2008;1780(11):1318-24.
- 702 63. Lizarbe TR, Garcia-Rama C, Tarin C, Saura M, Calvo E, Lopez JA, et al. Nitric oxide elicits functional MMP-
703 13 protein-tyrosine nitration during wound repair. *Faseb J*. 2008;22(9):3207-15.
- 704 64. Yakovlev VA, Bayden AS, Graves PR, Kellogg GE, Mikkelsen RB. Nitration of the tumor suppressor protein
705 p53 at tyrosine 327 promotes p53 oligomerization and activation. *Biochemistry*. 2010;49(25):5331-9.
- 706 65. Carballal S, Bartesaghi S, Radi R. Kinetic and mechanistic considerations to assess the biological fate of
707 peroxynitrite. *Biochim Biophys Acta*. 2014;1840(2):768-80.
- 708 66. Abaffy P, Tomankova S, Naraine R, Kubista M, Sindelka R. The role of nitric oxide during embryonic
709 wound healing. *BMC Genomics*. 2019;20(1):815.
- 710 67. Kitano T, Yamada H, Kida M, Okada Y, Saika S, Yoshida M. Impaired Healing of a Cutaneous Wound in
711 an Inducible Nitric Oxide Synthase-Knockout Mouse. *Dermatol Res Pract*. 2017;2017:2184040.
- 712 68. Sekar Y, Moon TC, Slupsky CM, Befus AD. Protein tyrosine nitration of aldolase in mast cells: a plausible
713 pathway in nitric oxide-mediated regulation of mast cell function. *J Immunol*. 2010;185(1):578-87.
- 714 69. Masters KS, Leibovich SJ, Belem P, West JL, Poole-Warren LA. Effects of nitric oxide releasing poly(vinyl
715 alcohol) hydrogel dressings on dermal wound healing in diabetic mice. *Wound Repair Regen*.
716 2002;10(5):286-94.
- 717 70. Luo JD, Chen AF. Nitric oxide: a newly discovered function on wound healing. *Acta Pharmacol Sin*.
718 2005;26(3):259-64.
- 719 71. Hartwig S, Doll C, Voss JO, Hertel M, Preissner S, Raguse JD. Treatment of Wound Healing Disorders of
720 Radial Forearm Free Flap Donor Sites Using Cold Atmospheric Plasma: A Proof of Concept. *J Oral*
721 *Maxillofac Surg*. 2017;75(2):429-35.
- 722 72. Shome D, von Woedtke T, Riedel K, Masur K. The HIPPO Transducer YAP and Its Targets CTGF and Cyr61
723 Drive a Paracrine Signalling in Cold Atmospheric Plasma-Mediated Wound Healing. *Oxid Med Cell*
724 *Longev*. 2020;2020:4910280.
- 725 73. Aruoma OI, Whiteman M, England TG, Halliwell B. Antioxidant action of ergothioneine: assessment of its
726 ability to scavenge peroxynitrite. *Biochem Biophys Res Commun*. 1997;231(2):389-91.
- 727 74. Goldstein S, Russo A, Samuni A. Reactions of PTIO and carboxy-PTIO with *NO, *NO₂, and O₂-. *J Biol*
728 *Chem*. 2003;278(51):50949-55.
- 729 75. Franzoni F, Colognato R, Galetta F, Laurenza I, Barsotti M, Di Stefano R, et al. An in vitro study on the free
730 radical scavenging capacity of ergothioneine: comparison with reduced glutathione, uric acid and trolox.
731 *Biomed Pharmacother*. 2006;60(8):453-7.
- 732 76. Winter J, Wende K, Masur K, Iseni S, Dunnbier M, Hammer MU, et al. Feed gas humidity: a vital parameter
733 affecting a cold atmospheric-pressure plasma jet and plasma-treated human skin cells. *J Phys D Appl Phys*.
734 2013;46(29).

- 735 77. Jablonowski H, Schmidt-Bleker A, Weltmann KD, von Woedtke T, Wende K. Non-touching plasma-liquid
736 interaction - where is aqueous nitric oxide generated? *Phys Chem Chem Phys*. 2018;20(39):25387-98.
- 737 78. Beckman JS, Beckman TW, Chen J, Marshall PA, Freeman BA. Apparent hydroxyl radical production by
738 peroxyxynitrite: implications for endothelial injury from nitric oxide and superoxide. *Proc Natl Acad Sci U S*
739 *A*. 1990;87(4):1620-4.
- 740 79. Squadrito GL, Pryor WA. Oxidative chemistry of nitric oxide: the roles of superoxide, peroxyxynitrite, and
741 carbon dioxide. *Free Radic Biol Med*. 1998;25(4-5):392-403.
- 742 80. Wenske S, Lackmann J-W, Bekeschus S, Weltmann K-D, Von Woedtke T, Wende K. Non-enzymatic post-
743 translational modifications in peptides by cold plasma-derived reactive oxygen and nitrogen species.
744 *Biointerphases*. 2020.
- 745 81. Radi R. Protein tyrosine nitration: biochemical mechanisms and structural basis of functional effects. *Acc*
746 *Chem Res*. 2013;46(2):550-9.
- 747 82. Bent DV, Hayon E. Excited state chemistry of aromatic amino acids and related peptides. I. Tyrosine. *J Am*
748 *Chem Soc*. 1975;97(10):2599-606.
- 749 83. Winterbourn CC, Parsons-Mair HN, Gebicki S, Gebicki JM, Davies MJ. Requirements for superoxide-
750 dependent tyrosine hydroperoxide formation in peptides. *Biochem J*. 2004;381(Pt 1):241-8.
- 751 84. Koppenol WH, Moreno JJ, Pryor WA, Ischiropoulos H, Beckman JS. Peroxyxynitrite, a cloaked oxidant
752 formed by nitric oxide and superoxide. *Chem Res Toxicol*. 1992;5(6):834-42.
- 753 85. Ramezani MS, Padmaja S, Koppenol WH. Nitration and hydroxylation of phenolic compounds by
754 peroxyxynitrite. *Chem Res Toxicol*. 1996;9(1):232-40.
- 755 86. Reuter S, Winter J, Schmidt-Bleker A, Schroeder D, Lange H, Knake N, et al. Atomic oxygen in a cold argon
756 plasma jet: TALIF spectroscopy in ambient air with modelling and measurements of ambient species
757 diffusion. *Plasma Sources Science & Technology*. 2012;21(2):024005 %&.
- 758 87. Jablonowski H, Bussiahn R, Hammer MU, Weltmann KD, von Woedtke T, Reuter S. Impact of plasma jet
759 vacuum ultraviolet radiation on reactive oxygen species generation in bio-relevant liquids. *Physics of*
760 *Plasmas*. 2015;22(12):122008.
- 761 88. Snyder HL, Smtih BT, Parr TP, Martin RM. Dissociative Excitation of Water by Metastable Argon. *Chemical*
762 *Physics*. 1982;65(3):397-406.
- 763 89. Zvereva GN. Using vacuum ultraviolet radiation to obtain highly reactive radicals. *J Opt Technol*.
764 2012;79(8):477-83.
- 765 90. Attri P, Kim YH, Park DH, Park JH, Hong YJ, Uhm HS, et al. Generation mechanism of hydroxyl radical
766 species and its lifetime prediction during the plasma-initiated ultraviolet (UV) photolysis. *Sci Rep*.
767 2015;5:9332.
- 768 91. Iseni S, Bruggeman PJ, Weltmann K-D, Reuter S. Nitrogen metastable ($N_2(A^3 \Sigma_u^+)$) in a cold argon
769 atmospheric pressure plasma jet: Shielding and gas composition. *Appl Phys Lett*. 2016;108(18):184101.
- 770 92. Plowman JE, Deb-Choudhury S, Grosvenor AJ, Dyer JM. Protein oxidation: identification and utilisation
771 of molecular markers to differentiate singlet oxygen and hydroxyl radical-mediated oxidative pathways.
772 *Photochem Photobiol Sci*. 2013;12(11):1960-7.
- 773 93. Wang ZC, Li YK, He SG, Bierbaum VM. Reactivity of amino acid anions with nitrogen and oxygen atoms.
774 *Phys Chem Chem Phys*. 2018;20(7):4990-6.
- 775 94. Conte ML, Carroll KS. The chemistry of thiol oxidation and detection. *Oxidative stress and redox*
776 *regulation*: Springer; 2013. p. 1-42.
- 777 95. Schmidt-Bleker A, Winter J, Iseni S, Dunnbier M, Weltmann KD, Reuter S. Reactive species output of a
778 plasma jet with a shielding gas device-combination of FTIR absorption spectroscopy and gas phase
779 modelling. *J Phys D Appl Phys*. 2014;47(14):145201.
- 780 96. Sander R. *Compilation of Henry's Law Constants for Inorganic and Organic Species of Potential*
781 *Importance in Environmental Chemistry*. Max-Planck Institute of Chemistry, Air Chemistry Department
782 Mainz, Germany; 1999.
- 783 97. Koppenol WH, Bounds PL, Nauser T, Kissner R, Ruegger H. Peroxyxynitrous acid: controversy and
784 consensus surrounding an enigmatic oxidant. *Dalton Trans*. 2012;41(45):13779-87.
- 785 98. Shilov VP, Fedoseev AM. Role of peroxyxynitrite in oxidation of f-element ions in HNO₃ solutions.
786 *Radiochemistry*. 2013;55(4):366-8.

- 787 99. Lobachev VL, Rudakov ES. The chemistry of peroxyxynitrite. Reaction mechanisms and kinetics. Usp Khim+.
788 2006;75(5):422-44.
- 789 100. Robinson KM, Beckman JS. Synthesis of peroxyxynitrite from nitrite and hydrogen peroxide. Methods
790 Enzymol. 2005;396:207-14.
- 791 101. Gorbanev Y, O'Connell D, Chechik V. Non-Thermal Plasma in Contact with Water: The Origin of Species.
792 Chemistry. 2016;22(10):3496-505.
- 793 102. Stoffels C, Oumari M, Perrou A, Termath A, Schlundt W, Schmalz HG, et al. Ergothioneine stands out from
794 hercynine in the reaction with singlet oxygen: Resistance to glutathione and TRIS in the generation of
795 specific products indicates high reactivity. Free Radic Biol Med. 2017;113:385-94.



© 2020 by the authors. Submitted for possible open access publication under the terms and conditions of the Creative Commons Attribution (CC BY) license (<http://creativecommons.org/licenses/by/4.0/>).

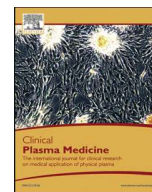
796

Article A4

Cold physical plasma-induced oxidation of cysteine yields reactive sulfur species (RSS)

G. Bruno, T. Heusler, J.-W. Lackmann, T. von Woedtke, K.-D. Weltmann, and K. Wende.
Clinical Plasma Medicine, vol. 14, p. 100083, 2019.

© 2019 Published by Elsevier GmbH



Original research article

Cold physical plasma-induced oxidation of cysteine yields reactive sulfur species (RSS)



Giuliana Bruno^a, Thea Heusler^a, Jan-Wilm Lackmann^a, Thomas von Woedtke^{b,c},
Klaus-Dieter Weltmann^b, Kristian Wende^{a,*}

^a ZIK plasmatis, Leibniz Institute for Plasma Science and Technology (INP Greifswald), Felix-Hausdorff-Straße 2, 17489 Greifswald, Germany

^b Leibniz Institute for Plasma Science and Technology (INP Greifswald), Felix-Hausdorff-Straße 2, 17489 Greifswald, Germany

^c Greifswald University Medicine, Fleischmannstraße 8, 17475 Greifswald, Germany

ARTICLE INFO

Keywords:

Redox signaling
Plasma liquid chemistry
Reactive sulfur species
Cold physical plasma
CAP

ABSTRACT

Purpose: Studying plasma liquid chemistry can reveal insights into their biomedical effects, i.e. to understand the direct and indirect processes triggered by the treatment in a model or clinical application. Due to the reactivity of the sulfur atom, thiols are potential targets for plasma-derived reactive species. Being crucial for protein function and redox signaling pathways, their controllable modification would allow expanding the application range. Additionally, models to control and standardize CAP sources are desired tools for plasma source design. **Methods:** Cysteine, a ubiquitous amino acid, was used as a tracer compound to scavenge the reactive species produced by an argon plasma jet (kINPen). The resulting product pattern was identified via high-resolution mass spectrometry. The Ellman's assay was used to screen CAP derived thiol consumption, and long-lived species deposition (hydrogen peroxide, nitrite, nitrate) was monitored in relation to the presence of cysteine. **Results:** The intensity of cysteine oxidation increased with treatment time and availability of oxygen in the feed gas. A range of products from cysteine was identified, in part indicative for certain treatment conditions. Several non-stable products occur transiently during the plasma treatment. Bioactive reactive sulfur species (RSS) have been found for mild treatment conditions, such as cysteine sulfoxides and cysteine-S-sulfonate. Considering the number of cysteine molecules in the boundary layer and the achieved oxidation state, short-lived species dominate in cysteine conversion. In addition, a boundary layer depletion of the tracer was observed. **Conclusion:** Translating these data into the in-vivo application, strong direct oxidation of protein thiol groups with subsequent changes in protein biochemistry must be considered. Plasma-derived RSS may in part contribute to the observed biomedical effects of CAP. Care must be taken to control the discharge parameter tightly as chemical dynamics at or in the liquid are subject to change easily.

1. Introduction

Plasma medicine has emerged as a therapeutic alternative in the area of cancer treatment and skin related acute and chronic diseases, such as acute or infected chronic wounds [1–4]. The enabling technology is cold atmospheric plasma (CAP) that can be generated by various sources, with plasma jets (APPJs) and dielectric barrier discharges (DBDs) being the most prevalent options for biomedical applications [3,5,6]. All CAPs are characterized by the action of a complex mixture of chemical entities, like electrons, ions, neutrals, and radical species as well as radiation and electric fields. This highly dynamic system so far successfully prevented the full discovery of all relevant entities in clinical application and in vitro research, especially when

focusing the liquid compartment like a tissue or cell [7]. In contrast, the gas phase composition of some CAPs is considerably well characterized, e.g. for kINPen [8–10], RF plasma jet [11–13], and the COST jet [14–16]. The reactive species considered most interesting in the biomedical field are those deposited in the liquid phase of a treated tissue or model cell system. Their origin and biochemical potential are under study, considering the large variety of species composition due to the different plasma sources and applied parameters (e.g. flow rate, energy input, working gas composition) and treatment conditions (e.g. distance to the target, duration). Even less understood is the role of the gas-liquid interphase and the subsequent transport of species into the liquid bulk. The chemical composition of the treated system further modulates the formation, propagation, and stability of primary and secondary/

* Corresponding author.

E-mail address: kristian.wende@inp-greifswald.de (K. Wende).

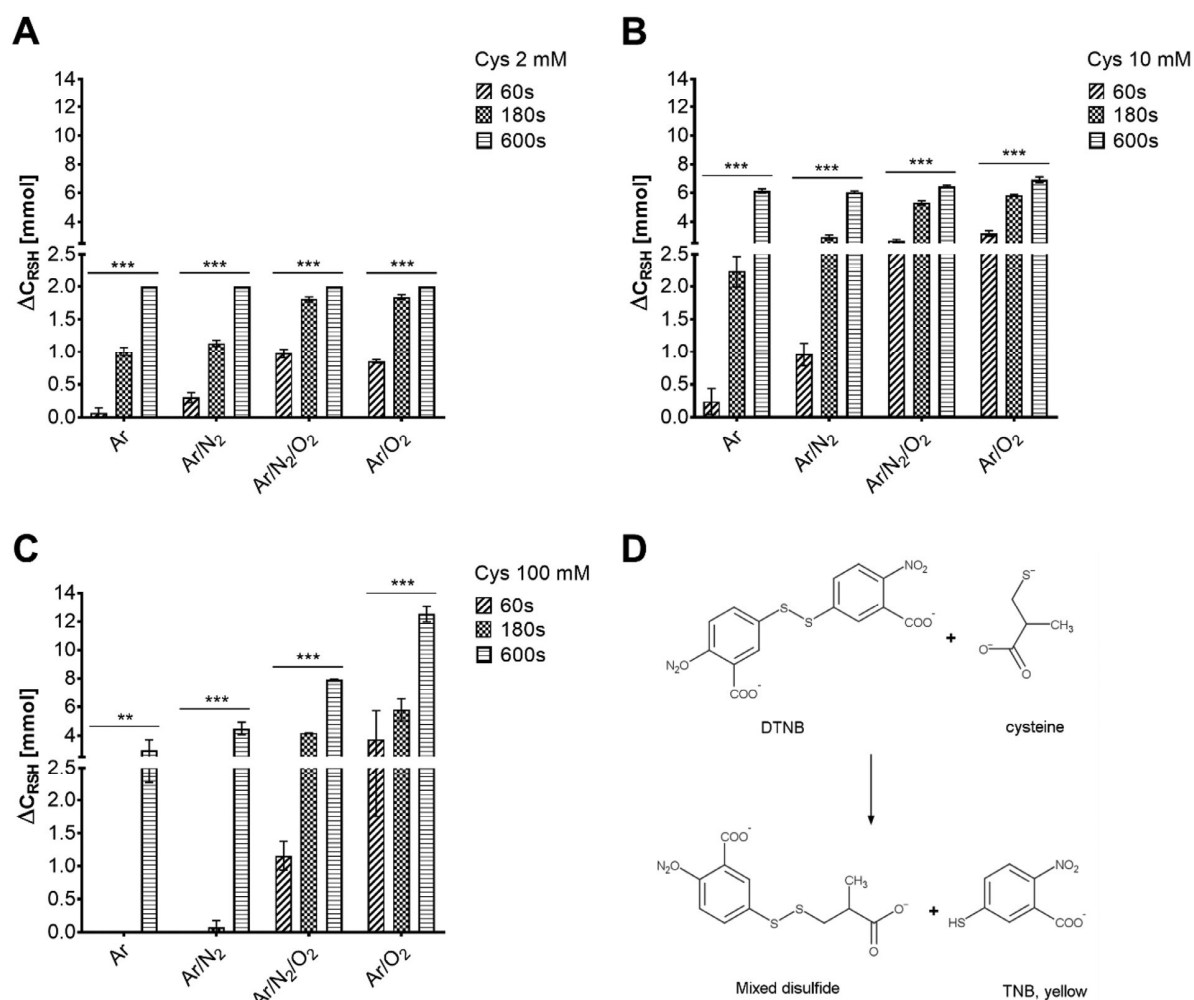


Fig. 1. Cysteine oxidation by varying the used feed gas, the duration of the treatment and cysteine concentration in 2 mM (A), 10 mM (B) and 100 mM (C), reaction scheme Ellman's assay (D) kINPen09, 3 slm Ar + 1% molecular gas admix.

tertiary species, and finally the efficacy of the plasma treatment.

In case of the argon-based kINPen, central primary species in the gas phase are metastable argon (Ar^*) and argon excimers (Ar_2^*). Secondary gas phase species are formed by interaction of primary species and feed gas admixtures (e.g. O_2 , N_2) or ambient species, creating species as hydroxyl radicals ($\cdot\text{OH}$), atomic oxygen ($\cdot\text{O}$), singlet oxygen ($^1\text{O}_2$), ozone (O_3), atomic nitrogen ($\cdot\text{N}$), and nitric oxides (N_xO_y) [17]. Secondary species can also be produced in the liquid by the impact of plasma-generated species, radiation, electrons; in this case, species as hydroxyl radicals ($\cdot\text{OH}$), superoxide radicals ($\cdot\text{O}_2^-$), nitrous (HNO_2), nitric acid (HNO_3), or peroxyxynitrite (ONOO^-) can be formed [18,19]. By interaction with ions or molecules present in the treated target, additional species like hypochlorite (OCl^-) can evolve [20]. Most of these species are hard to quantify with reasonable specificity, e.g. ozone, singlet oxygen, or hydroxyl radicals. Using electron paramagnetic resonance (EPR) radical species can be detected in CAP treated liquids, but quantitative statements are debatable [18,21,22]. In contrast, for the "stable" species H_2O_2 , nitrite, and nitrate various quantitative chemical assays exist, which subsequently led to the impression that these are of predominant biomedical relevance [9,23], e.g. H_2O_2 [24], or nitric oxide [25].

Taking the recent publications on short-lived species into account it must be assumed that also they can reach the biological target and in part control or at least modulate the functional outcome of CAP treatment. Given the poor selectivity of existing assay methods, chemically

modifiable tracer molecules pose an alternative way to study plasma liquid chemistry. Under controlled conditions, cysteine is a suitable sensitive and reactive molecule. Zhou et al. identified cysteine sulfonic acid beside cystine as major products after CAP treatment [26]. Especially its thiol moiety can be distinctively oxidized by CAP derived species, making cysteine a potential model for standardization efforts using the product pattern evolving by the CAP treatment as a fingerprint [27,28]. Furthermore, the amino acid is a ubiquitous and essential component of proteins and important partner in many redox-signaling processes, able to act both as an electron acceptor and donor [29]. Therefore, cysteine is present in body fluids and cell culture media, e.g. Dulbecco's Modified Eagle Medium (DMEM). With that, detailed knowledge of CAP derived species interaction with cysteine and related compounds is desirable as this may both prohibit and retard their impact in biological systems [30,31]. Subsequently, CAP derived cysteine derivatives, especially reactive sulfur species (RSS), could in turn influence the cellular redox balance [29, 32–34].

Here, an in-depth study of the CAP treatment derived cysteine product pattern beyond cystine and cysteine sulfonic acid is presented with the aim to foster plasma treatment standardization, to understand reactive species trajectories, and to estimate effects on thiols in bio-molecules in vitro and in vivo.

Table 1
Number of cysteine molecules present and oxidized during treatment (calculated, measured or assumed on models) and number of one electron equivalent species hitting the target during kINPen treatment of 24-well plate, 750 μ l volume of 2/10/100 mM cysteine solution.

Cysteine solution	No of cysteine molecules		Number of one-electron acceptor equivalents				Hitting target ($O_2^{\cdot-}$, O_3 , OH^{\cdot}) / s^{-1}
	Per cm^3	In vessel (0.75 cm^3)	In boundary surface model [38] / s^{-1}	In boundary surface (0.36 mm^2) measure [39] / s^{-1}	Oxidized cysteine molecules Ar/ O_2 , 60s (Ellman's) / s^{-1}	Cysteine > > cysteine / s^{-1}	
2 mM	1.20×10^{18}	9.00×10^{17}	3.60×10^{16}	6.32×10^{14}	5.62×10^{15}	2.81×10^{16}	6.09×10^{16}
10 mM	6.00×10^{18}	4.50×10^{18}	1.80×10^{17}	2.16×10^{15}	2.55×10^{16}	1.27×10^{17}	6.09×10^{16}
100 mM	6.00×10^{19}	4.50×10^{19}	1.80×10^{18}	2.16×10^{16}	3.00×10^{16}	1.50×10^{17}	6.09×10^{16}

* Calculated.

Assumed.

+ Measured.

^a One-electron acceptor equivalents used for calculation: hydroxyl radical = 1, atomic O = 2, singlet oxygen = 4, ozone = 6; species densities according to [17].

2. Materials and methods

2.1. Plasma source

The kINPen09 (neoplas GmbH, Germany), an atmospheric pressure plasma jet using argon as main feed gas was used in this study. It is driven by an alternating current at ≈ 1 MHz / 2–6 kV, with 1.1 W power deposition in the discharge. The central high-voltage electrode has a diameter of 1.6 mm and is surrounded by a ceramic capillary. If desired, the plasma effluent was shielded from ambient air by a controllable gas curtain [8].

2.2. Sample preparation and plasma treatments

Cysteine solutions with various concentrations (300 μ M, 2 mM, 10 mM, and 100 mM) were freshly prepared from cysteine (L-Cysteine, Sigma-Aldrich Co. LLC., St. Louis, USA) using double-distilled water (ddH_2O) (MilliQ, Milli-Q[®] Merck KGaA, Darmstadt, Germany), or 5 mM phosphate buffered saline pH 7.4. 750 μ l of each solution was treated directly in 24 well-plate for 45, 60, 180, 300 or 600 s, with a fixed distance jet's nozzle-liquid surface of 9 mm. A flow rate of 3 standard liters per minute (slm) of dry argon (argon N50, Air Liquide, Paris, France) was used as feed gas and for some experiments, 1% of nitrogen (nitrogen N50, Air Liquide, Paris, France), oxygen (oxygen N48, Air Liquide, Paris, France), or a 1:1 mixture of both was added. Treatments were made either with or without curtain gas (5 slm nitrogen or oxygen) around the effluent to reduce the impact of the ambient atmosphere.

2.3. Colorimetric assays

Ellman's reagent, or 5,5'-dithiobis-(2-nitrobenzoic) acid (DTNB, Sigma-Aldrich Co. LLC., St. Louis, USA), was used for the quantification of residual non-oxidized thiol groups in the treated cysteine solutions. The reaction solution consisted of 1 mM DTNB, 1 mM EDTA, 10 mM PO_4^{3-} and 144 mM NaCl. The DTNB is a disulfide consisting of two TNB molecules (2-nitro-5-thiobenzoate). It is reacting with the free thiols of cysteine by releasing a TNB molecule and forming a mixed disulfide between cysteine and the other TNB molecule. The absorbance of these is then detected at 412 nm (Tecan Infinite M200 Pro, Tecan Group Ltd., Männedorf, Switzerland). Hydrogen peroxide (H_2O_2) was quantified in treated buffer with and without cysteine using a xylenol orange based assay (Pierce[™] Quantitative Peroxide Assay Kit, Thermo Scientific, Rockford, USA). This dye was detected photometrically at 595 nm.

2.4. Ion chromatography

Nitrite (NO_2^-) and nitrate (NO_3^-) ions were detected through ion chromatography (ICS-5000, Dionex Corp., Sunnyvale, USA) in treated phosphate buffer or 2 mM cysteine in phosphate buffer. Before injection (10 μ l), all the treated solution were independently diluted threefold by adding ultrapure water (MilliQ, Milli-Q[®] Merck KGaA, Darmstadt, Germany). An IonPac[®] AS23 pre-column (2 \times 50 mm, Thermo Fisher Scientific Inc., Waltham, USA) coupled to an IonPac[®] AS23 anion exchange column (2 \times 250 mm, Thermo Fisher Scientific Inc., Waltham, USA) was used for separation in an isocratic mobile phase (4.5 mM Na_2CO_3 /0.8 mM $NaHCO_3$) regime and 250 μ l min^{-1} flow rate. The analytes were detected by conductivity and UV detection (210 nm). The instrument was daily calibrated with the Dionex 7-anions standard.

2.5. Cysteine derivatives characterization using high-resolution mass spectrometry

Cysteine derivatives were analyzed by direct injection into a high-resolution mass spectrometer (TripleTOF5600, Sciex Ltd., Darmstadt,

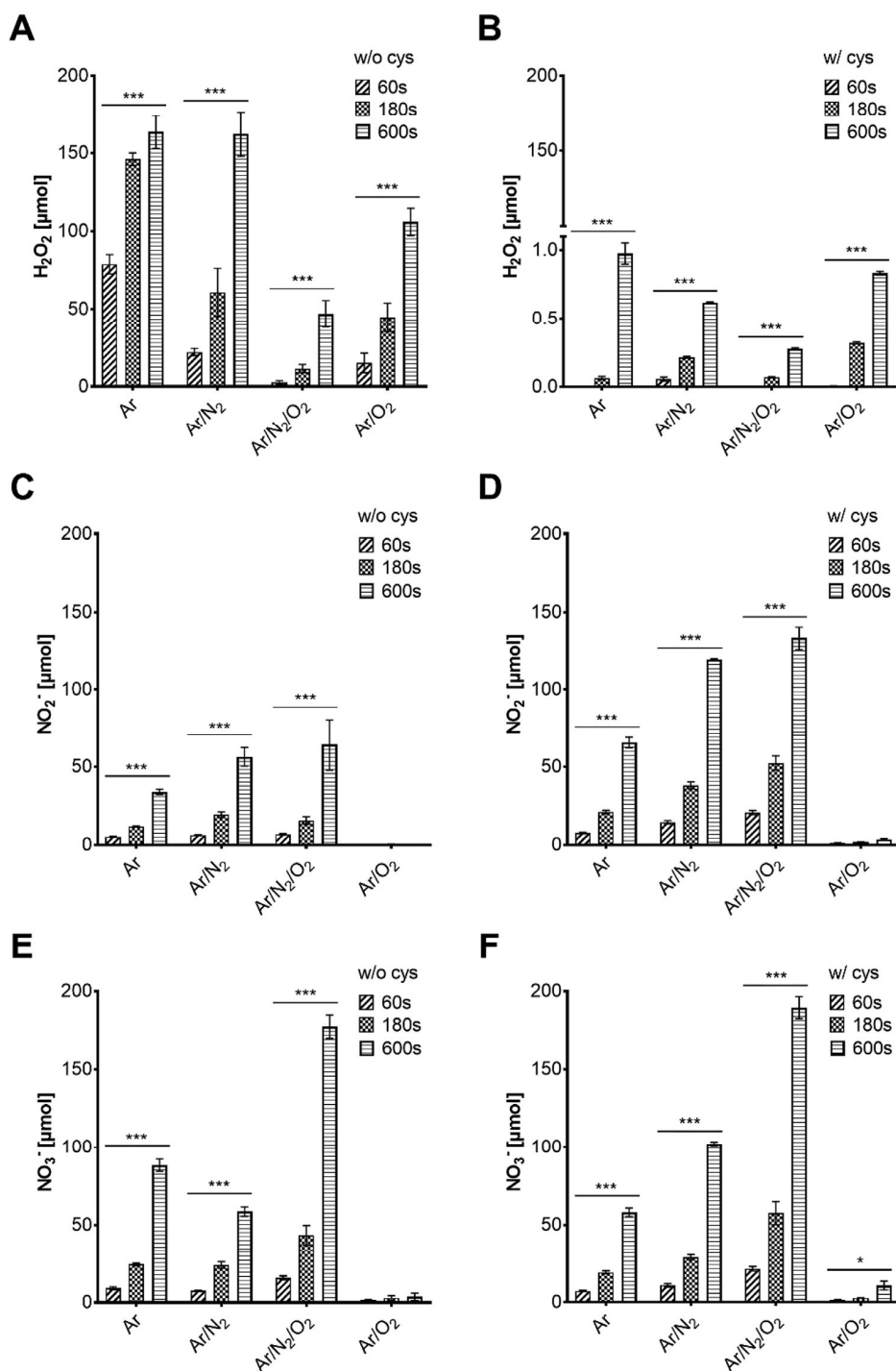


Fig. 2. Deposition of H₂O₂ (A), NO₂⁻ (C) and NO₃⁻ (E) in water or water with 2 mM cysteine (corresponding subfigures B, D, F) (kINPen09, 3 slm Ar + 1% molecular gas admix).

Germany). Each sample was diluted 1:1 with 0.3% ammonium hydroxide in methanol (negative mode) or 0.1% formic acid in methanol (positive mode) before injection. 10 μL·min⁻¹ were infused by a syringe pump into an electrospray ion source running on ± 4 kV (Turbo Spray V, Sciex Ltd., Darmstadt, Germany). The following parameters were used: capillary temperature 150 °C, curtain gas: 35 slm, ion source gas 1: 20 slm, and ion source gas 2: 25 slm. MS spectra were acquired in a mass range from 50 to 400 m/z (cycle time 275 ms, accumulation time 250 ms). MS/MS spectra for each peak were acquired in order to

identify the compounds (collision energy ± 24 eV, declustering potential ± 10 kV). Mass calibration was made before acquisition by using the exact mass of the most abundant compounds (e.g. cysteine, cystine). For peak identification, a minimum threshold of 300 counts s⁻¹ was set, and normalized areas% were extracted for further analysis.

Table 2

Common cysteine derivatives identified after the different plasma treatments (structures in Fig. 5).

	IUPAC name (systematic name)	Traditional name	Formula	Mass [M-H] ⁻
1	2-amino-3-sulfanylpropanoic acid	Cysteine	C ₃ H ₇ NO ₂ S	120.0119
2	2,3-didehydrocysteinulic acid		C ₃ H ₄ NO ₄ S	149.986
3	cysteine 3-sulfoprop-2,3-enoic acid		C ₃ H ₄ O ₅ S	150.9701
4	2-amino-3-sulfinothiopropanoic acid	Cysteine sulfinic acid	C ₃ H ₇ NO ₄ S	152.0017
5	(2E)-3-sulfoprop-2-enoic acid		C ₃ H ₅ NO ₃ S	165.981
6	2-amino-3-sulfopropanoic acid	Cysteine sulfonic acid	C ₃ H ₇ NO ₅ S	167.9967
7	2-amino-3-hydroxy-3-sulfopropanoic acid		C ₃ H ₇ NO ₆ S	183.9916
8	2-amino-3-(sulfosulfonyl)propanoic acid	Cysteine-S-sulfonate	C ₃ H ₇ NO ₅ S ₂	199.9687
9	2-amino-3-[(2-amino-2-carboxyethyl)disulfanyl]propanoic acid	Cystine	C ₆ H ₁₂ N ₂ O ₄ S ₂	239.016
10	sulfonilideneoxidane 2-amino-2-carboxyethane-1-sulfonate		C ₃ H ₉ NO ₉ S ₂	265.9635
11	(2Z)-2-amino-3-[(2-amino-2-carboxyethanesulfonyl)sulfonyl]prop-2-enoic acid		C ₆ H ₁₀ N ₂ O ₆ S ₂	268.9902
12	2-amino-3-[(2-amino-2-carboxyethanesulfonyl)sulfonyl]propanoic acid		C ₆ H ₁₂ N ₂ O ₆ S ₂	271.0056
13	2-amino-3-[(2-amino-2-carboxyethanesulfonyl)sulfonyl]propanoic acid		C ₆ H ₁₅ N ₂ O ₆ S ₂	302.9905
14	2,3-diamino-3-[(2-amino-2-carboxyethanesulfonyl)sulfonyl]propanoic acid		C ₆ H ₁₃ N ₃ O ₆ S ₂	318.0063
15	2-amino-3-[(2-amino-2-carboxyethanesulfonyl)sulfonyl]-3-hydroxypropanoic acid		C ₆ H ₁₂ N ₂ O ₉ S ₂	318.9899
16	2-amino-3-[(2-amino-1-[(2-amino-2-carboxyethanesulfonyl)sulfonyl]-2-carboxyethyl)sulfonyl]propanoic acid		C ₉ H ₁₆ N ₃ O ₈ S ₃	390.0100

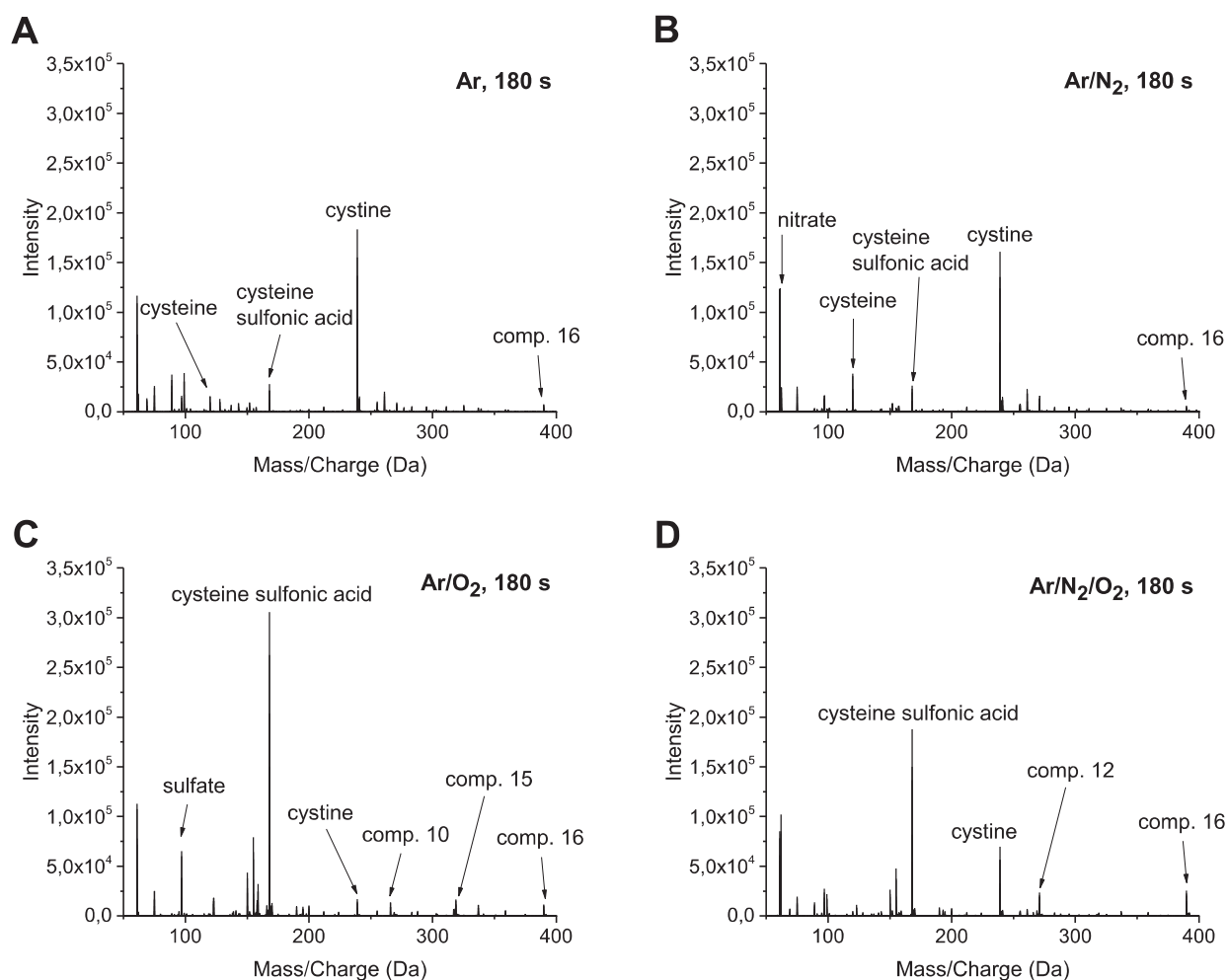


Fig. 3. High-resolution mass spectrometry traces between 50 and 400 m/z of 300 μM CAP treated cysteine (negative mode) after treatment of cysteine 300 μM by using feed gases without oxygen (Ar, Ar/N₂) (A, B), and with oxygen (Ar/O₂, Ar/N₂/O₂) (C, D) (kINPen09, 3 slm Ar + 1% molecular gas admix).

2.6. Calculation of species numbers and liquid volume in contact to gas phase

To calculate absolute numbers of cysteine molecules at the given concentration (2, 10, 100 mM) and volume (750 μl) the Avogadro constant ($6.02 \times 10^{23} \text{ mol}^{-1}$) was used, yielding 9×10^{17} , 4.5×10^{18} , and

4.5×10^{19} molecules to be treated. The number of species impinging on the treated surface was calculated using the data published by Schmidt-Bleker: a gas phase velocity of 25 m s^{-1} and a comoving volume element of 1 mm diameter describe the effluent [17]. Gas phase densities at treatment distance of 9 mm were calculated to be in the range of 10^{15} cm^{-3} for atomic O, 10^{14} cm^{-3} for ¹O₂ and ozone (O₃),

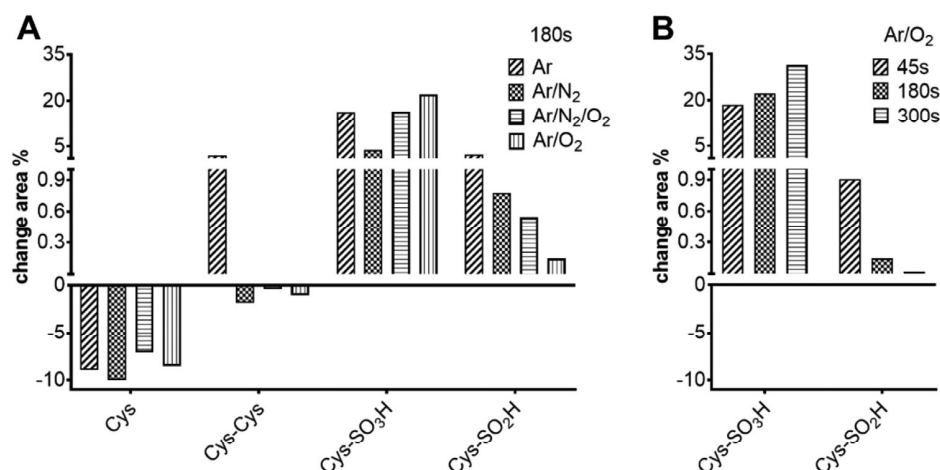


Fig. 4. Relative quantities of prominent cysteine (Cys) derivatives produced by using different feed gases (A) and treatment times (B), with focus on cystine (Cys-Cys), cysteine sulfonic acid (Cys-SO₃H) and cysteine sulfinic acid (Cys-SO₂H) (kINPen09, 3 slm Ar + 1% molecular gas admix).

and $4.5 \times 10^{13} \text{ cm}^{-3}$ for OH radicals [17]. To calculate the overall oxidation capacity of the mixture, the following one-electron acceptor equivalents were used: hydroxyl radical = 1, atomic O = 2, singlet oxygen = 4, ozone = 6. Superoxide anion radical was not taken into account for its reported low reactivity with cysteine. The number of cysteine molecules in the gas – liquid interface (boundary layer) was calculated using a liquid velocity of 1 m s^{-1} according to a 2-D fluid model [35] and presuming an inverted half globe shape of the liquid due to gas flow pressure (15 mm diameter). The resulting exchange of the superficial layer was estimated to take place 85 times per second. Assuming a thickness of the boundary layer of $1 \mu\text{m}$, the volume of the surface layer in contact with the gas phase species during one second of treatment is roughly 30 mm^3 in case of the 2-D fluid model. In contrast, van Rens et al. measured a flow of 12 mm s^{-1} , also using the kINPen [36], which would correspond to a volume of 0.36 mm^3 in contact with gas phase species.

2.7. Statistical analysis and software

Three independent experiments were carried out at least in duplicates. Statistical analysis was done with two-way-ANOVA using GraphPad Prism 7. *P* values under 0.05 were considered significant. The MarvinSketch[®] software (version 18.8.0) was used to identify the name, the exact molecular weight, the formula and the pKa of each compound, as well as to predict the percentual amount of thiolate forms of cysteine in different pH conditions.

3. Results and discussions

3.1. Bulk oxidation of thiol groups significantly varies with feed gas composition

The oxidation of cysteine at different concentrations with various feed gas compositions (Ar, Ar/N₂, Ar/O₂, Ar/N₂/O₂) and treatment duration was monitored by measuring the residual free thiols after plasma treatment via Ellman's assay (Fig. 1, Fig. 1D). Thiol group oxidation correlated with treatment time, and for 600 s all (most) free thiol groups were consumed for 2 mM (10 mM) cysteine. In contrast, only a minor increase of thiol oxidation was achieved when increasing the concentration to 100 mM (Fig. 1B/C). Further, a strong impact of feed gas composition was observed: O₂ admixture led to a significantly higher impact than argon only or nitrogen admix, which is specifically obvious with the 100 mM solution (Fig. 1C).

This indicates that reactive oxygen species generated in the gas phase from molecular oxygen, e.g. atomic O, singlet oxygen ¹O₂, ozone

or superoxide anion radicals are significant chemical partners in this model [9,17,37]. For lower concentrations (2 mM, 10 mM), cysteine conversion tends to meet a maximum which indicates saturation effects (Fig. 1A/B). From these observations, it can be concluded that long treatments and with oxygen admix in the feed gas can be considered “strongly” oxidative (Ar/O₂, Ar/N₂/O₂ – 300 s to 600 s), while shorter treatments, especially without oxygen in the feed gas, can be defined as “mildly” oxidative (Ar, Ar/N₂ – 60 s to 180 s). The cysteine thiol consumption efficacy is dependent on its initial concentration indicating saturation mechanisms: considering treatments of 60 s with Ar/O₂ feed gas, indeed, are oxidized around 0.75 mM of 2 mM solutions (Fig. 1A), around 3.4 mM in case of 10 mM solutions (Fig. 1B), and 4 mM in 100 mM cysteine solutions (Fig. 1C).

With that, thiol group consumption seems to be following a first-order kinetics at lower concentrations but decreases dramatically at higher concentrations (100 mM). Assumingly, the number of ROS seems to be too low in this situation. To achieve the observed oxidation, an effective flux of reactive species between $5.6 \times 10^{15} \text{ s}^{-1}$ and $3 \times 10^{16} \text{ s}^{-1}$ is necessary (table 1) and assuming a stoichiometry of 1:1 (one-electron equivalents, e.g. hydroxyl radicals) and cystine as final product (oxidation number of sulfur = –1). With cysteine sulfonic acid (oxidation number +4) as the final reaction product, a five times higher number of one-electron acceptor equivalents would be necessary (table 1). This range is in good agreement to simulations made by Schmidt-Bleker et al. [17]. At a gas phase velocity of 25 m s^{-1} and a comoving volume element of 1 mm diameter a number of $2 \times 10^{16} \text{ s}^{-1}$ oxygen atoms, each $2 \times 10^{15} \text{ s}^{-1}$ ¹O₂ and O₃ molecules, and $9 \times 10^{14} \text{ s}^{-1}$ OH radicals hit the liquid target. Taken together and weighed by their electron acceptor equivalents this corresponds to 6.1×10^{16} one-electron acceptor equivalents per second (table 1). While this amount is sufficient to oxidize the 2 mM cysteine solution in full, the number is too low in case of the 10 mM, and even more so the 100 mM solution. For both, the estimated number of electron acceptor equivalents matches about twice the number of equivalents necessary to transform cysteine into cystine. Subsequently, predominantly cysteine was observed for the 100 mM solution with very limited amounts of higher oxidized cysteine derivatives, showing the plausibility of these estimates.

For the 10 mM solution, a mixed behavior was observed: although the ratio of overall number of cysteine molecules being oxidized and number of electron acceptor equivalents deposited per second is 1:2. Hence, only limited further oxidation is possible and the theoretical final product would be cysteine sulfenic acid, which was not observed. Instead, a significant amount of higher oxidized derivatives was found, pointing at substrate limitation processes at the gas – liquid interface.

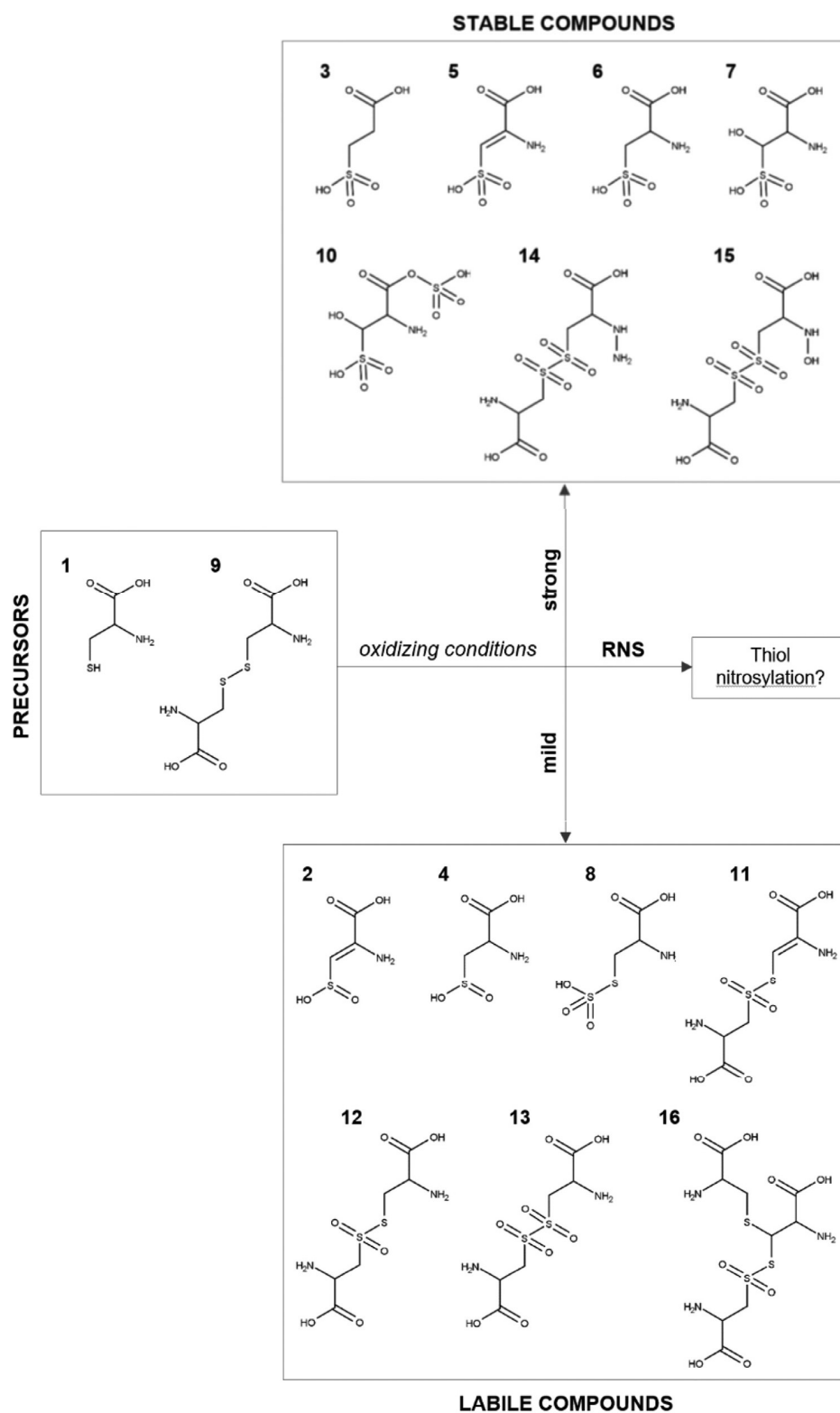


Fig. 5. Cysteine and cystine (compounds 1 and 9, shown as precursors here) derivatives categorization in labile and stable compounds in relation to their optimal conditions of production, which can be mild (Ar, Ar/N₂ – 60 s to 180 s) or strong (Ar/O₂, Ar/N₂/O₂ – 300 s to 600 s) conditions.

Atomic oxygen or hydroxyl radicals will react at the interfacial layer at very fast rates in the order of $10^{-9} \text{ M}^{-1} \text{ s}^{-1}$. Thus, the consumption of target molecules might be faster than bulk liquid transport (convection), resulting in the depletion of cysteine in the surface layer and

enrichment of reaction products which may be attacked further. When assuming a liquid phase velocity of 1 m s^{-1} or 12 mm s^{-1} , a half globe shape of the liquid due to gas flow, and a boundary (interface) layer of $1 \mu\text{m}$ thickness (see 2.6), the volume of the surface layer treated

during one second is roughly 30 mm^3 (2-D model) or 0.36 mm^3 (measurement). Consequently, an estimation of cysteine molecules exposed to the plasma-generated species at the boundary layer can be made, ranging between 6.3×10^{14} and 1.8×10^{18} (see table 1). Using the 2D-model assumption, the number of potentially exposed cysteine molecules in the boundary layer is 10 – 50 fold higher than oxidized in the experiment. In contrast, assuming the 12 mm s^{-1} velocity of the liquid, the observed number of oxidized cysteine molecules is 10 fold higher than the number of molecules present at the boundary in the 2 mM and 10 mM solutions, while model and observation correlate reasonably in the 100 mM case. Taken together, this seems to suggest that the 2D-model is wrong and the measured 80fold slower flow rate of the liquid correct. On the other hand, when considering a slow reaction rate of some species deposited in the liquid, e.g. the superoxide anion radical, a limited number of cysteine molecules can be attacked efficiently and the 2D-model correct. This disparity might further be augmented by various factors, like wrong assumptions regarding the boundary layer thickness and indicates that further research is necessary to explain these results in full.

In part, the aberration between assumption and measurement can be explained by pH effects, with high cysteine concentration leading to a slightly lower pH (10 mM, pH 6.02; 100 mM, pH 5.85) than lower concentrations (2 mM, pH 6.53). Due to the pKa of the thiol group (pKa \approx 10.2), the percentage of thiolates decrease with decreasing pH. Using the MarvinSketch[®] software, the equilibrium concentration of cysteine thiolate can be calculated to be $1.6 \mu\text{M}$ (2 mM solutions), $2 \mu\text{M}$ (10 mM solutions), and $10 \mu\text{M}$ (100 mM solutions). Considering the thiolate being more reactive than the thiol, the impact of long-lived hydrogen peroxide species would be emphasized. The data illustrate the necessity to observe or control pH during plasma treatment of biological materials as local conditions can vary drastically, e.g. between normal skin (pH 5.5), saliva (pH 7.4), or chronic wounds (pH 7.2 – 8.9) [40].

To obtain a general idea of the deposition of long lives species under the treatment conditions in the presence or absence of cysteine (2 mM), hydrogen peroxide (H_2O_2), nitrite (NO_2^-), and nitrate (NO_3^-) were quantified (Fig. 2). For all three species, it can be concluded that the deposition increases with treatment duration, regardless of working gas composition, marking them as “stable” species [18, 24]. As H_2O_2 is the final product of many ROS, nitrate ions are the end product accumulating from unstable reactive nitrogen species, such as peroxynitrite (ONOO^-) and nitric oxide radicals ($\cdot\text{NO}$).

High amounts of hydrogen peroxide are reached by treatments with Ar and Ar/ N_2 feed gas compositions (up to $170 \mu\text{M}$, Fig. 2A). When oxygen is in the feed gas admix, a maximum of $100 \mu\text{M}$ was detected. H_2O_2 derives from the recombination of OH radicals, that can be created in the gas phase from water vapor [41,42] or in the liquid phase, e.g. by photolysis of water [43] or electron impact. The contribution of the latter two might be significant, as a dry nitrogen gas curtain is used to reduce the lateral diffusion of ambient species into the effluent and limiting the formation of gas phase OH radicals. The second source of H_2O_2 is the disproportionation of OOH radicals, which is favored in slightly acidic conditions (see above). The contribution of this pathway seems to be minor, as O_2^- radicals are produced especially if molecular oxygen is present. However, under these conditions lowest H_2O_2 amounts were observed. The deposition of H_2O_2 is significantly reduced when cysteine is present ($\leq 1 \mu\text{M}$, Fig. 2B), indicating its consumption and/or reduced formation. RNS deposition (Fig. 2C/E), occurs predominantly in N_2/O_2 or N_2 admix when compared to Ar only treatment. For Ar/ O_2 , only negligible amounts of nitrite/nitrate were measured. In the presence of cysteine, nitrite deposition is generally higher than in its absence, with traces even with Ar/ O_2 detected while highest values were achieved for N_2/O_2 admix (Fig. 2D). Nitrate deposition (Fig. 2F) was unaffected by the presence of cysteine as a reaction partner, indicating its origin from gas phase derived precursors with little reaction probability (e.g. HNO_3 , N_2O_5). The nitrate ion itself is stable under the conditions present. In general, the presence of a potential reaction

partner modulates the observable deposition of long-lived species, a fact also observed by Privat-Maldonado [44]. While scavenging away the precursors of H_2O_2 formation (OH radicals, O_2^-/OOH radicals) or reacting with itself (thiolate ions, forming cystine) [28, 45], nitrite deposition is favored. As RNS chemistry is not well understood, several possibilities for explanation exist: reactive nitrogen species such as N_2O_3 or ONOO^- attack the cysteine and nitrite ions are byproducts, NO_2 radicals are not converted to NO but nitrite due to the lack of atomic oxygen [46], or – less likely – nitrite is oxidized to nitrate in a lesser extent. However, this latter option would require nitrate deposition to increase, which was not observed. Although closely related, this is a further indication that nitrite and nitrate are produced by different pathways and that nitrate does not originate from nitrite. Clearly, active RNS species and their trajectories need further attention.

3.2. CAP-derived reactive species generate a rich variety of cysteine derivatives

As has been suggested by Zhou and Takai that amino acids are targets for plasma-derived species [26,47]. In similar approaches, both looked into the oxidation of cysteine by CAP and found its dimer cystine and cysteine sulfonic acid. These major products have also been identified in the current approach along with around 20 further cysteine derivatives of different oxidation state and molecular structure, expanding the knowledge of the previous works. Cystine ($m/z = 239.016$) was identified as the dominant compound in Ar or Ar/ N_2 plasma treatments and cysteine sulfonic acid ($m/z = 167.9967$) dominant in O_2 admix plasma treatments (Ar/ O_2 , Ar/ N_2/O_2). Potentially bioactive cystine derivatives are generated predominantly with O_2 or N_2/O_2 admixtures with masses > 250 Da. Further prominent cysteine/cystine products detected and structurally resolved are shown in Table 2 and Fig. 5.

Clearly, an oxygen species driven oxidation of the thiol moiety is the most abundant modification, with some derivatives being biologically relevant (reactive sulfur species, RSS).

One of the key roles in the redox signaling is presumably assigned to cysteine sulfenic acid ($m/z = 136.0068$) that was not detected due to its instability. It is rapidly oxidized to cysteine sulfenic acid (Cys- SO_2H , compound 2) and to cysteine sulfonic acid (Cys- SO_3H , compound 3) [29,48], which may be a final product of plasma treatment. Cysteine sulfenic acid may react with itself, producing oxidized forms of cystine such as di-sulfoxides ($m/z = 268.9902$, compound 11; $m/z = 271.0056$, compound 12). Under the further impact of oxidative species, cysteine sulfonic acid appears as “apex” product.

Cystine (resp. its disulfide bridge as a structural element) is essential for protein structure, function, interactions, and subcellular localization [49]; indeed, the cysteine-cystine system is one of the most sensitive sensors of the redox state of a cell, both its physiological and pathological state [48,50]. Highly oxidized variants of cystine, such as di-sulfoxides or tetra-sulfoxides ($m/z = 302.9905$, compound 13; $m/z = 318.0063$, compound 14; $m/z = 318.9899$, compound 15), occur and have been shown to have an anti-proliferative effect on cancer cells [32,33,51]. Another bioactive derivative is the S-nitrosocysteine ($m/z = 149.0021$), which is one of the most important post-translational protein modifications. It is considered essential in cardiac functioning, cancer biology, and wound healing for its role in the nitric oxide pathway [52–55].

The production of S-nitrosocysteine was not observed albeit it was predicted by simulations [28]. Various reasons could lead to this discrepancy: (a) the reactive nitrogen species are not as effective as predicted; b) the products decay easily; c) RNS facilitate oxidation, but do not form covalent bonds between C or S and N. The first option seems least consistent, since in Ar/ N_2 conditions the oxidation of cysteine is considerably high (Fig. 1). However, significant deposition of the ROS H_2O_2 also occurs. Further studies focusing on the role of plasma-derived RNS on biomolecules are desirable.

3.3. Cysteine derivatives profiles reflect the treatment conditions and the ROS production

As indicated in Fig. 3, the generation of cysteine derivatives was dependent on the conditions used, with each parameter set producing a different product profile, either qualitatively or quantitatively (Fig. 3/4). In strongly oxidizing conditions (e.g. presence of oxygen in the feed gas) products showing a strong oxidation of the cysteine thiol group are observed (Fig. 4A); this is in accordance with the analysis of residual free thiols measured after the same treatment via colorimetric assay by using the Ellman's reagent (Fig. 1). In milder conditions, cystine (Cys-Cys) and cysteine sulfinic acid (Cys-SO₂H) can be detected after the treatment (e.g. Ar only), but in presence of molecular gases further oxidations of these occur, predominantly with O₂ admixtures, leading to their destruction (Fig. 4A). In contrast, cysteine sulfonic acid (Cys-SO₃H) accumulated, even with oxygen in the feed gas (Fig. 4B).

Besides the direct oxidation of cysteine, also the oxidation of cystine and its oxidized disulfides can lead to this product. It is the most abundant compound produced, even when the final products in the applied treatment regimen are inorganic sulfate and the amino acid alanine.

In general, cysteine sulfonic acid and cysteine sulfinic acid are compounds that are archetypical for the behavior of most other cysteine derivatives identified. Indeed, they could be divided into two groups: a) stable compounds, which increase in long and often oxygen-dominated treatments (Ar/O₂, Ar/N₂/O₂), b) labile compounds, which decrease in strong conditions but are present after short treatments predominantly without oxygen in the feed gas (Ar, Ar/N₂).

All identified cysteine derivatives as shown in Fig. 5 are classified on the base of these two groups. It can be stated that all compounds can be generated from cystine too, as the disulfide moiety can be easily attacked by plasma generated species except hydrogen peroxide which was ineffective (data not shown).

With that, the produced cysteine derivatives profiles represent the treatment conditions, reflecting the chemical footprint of cold plasma in liquids when discharge parameters are modulated. The reactive species predominantly deposited by the discharge in the aqueous system determined the product portfolio with the short-lived species, atomic oxygen (O), singlet oxygen (¹O₂), hydroxyl radicals (OH), and superoxide anion radicals (O₂⁻) being major players. The responsible short-lived species have so far not been pinpointed, but further investigations are underway. Hydrogen peroxide, which is deposited in large amounts under some conditions, reacts with the thiolate form of cysteine only and leads to the formation of cystine via cysteine sulfinic acid [28,56]. Indeed, the highest amount of deposited hydrogen peroxide was measured for argon feed gas (Fig. 4A), along with the highest amount of cystine (Fig. 2). This shows that H₂O₂ has a limited impact on the observed compound portfolio. The long-lived ROS ozone may be a candidate to be responsible for some of the products; however, its deposition in liquids remains debatable due to its solubility. Data suggest a potential for ozone to contribute to higher oxidized products, such as cysteine sulfonic acid (compound 3) or oxidized cystine derivatives, e. g. tetra-sulfoxides (compounds 14 and 15) [57].

Ultimately, the physiological impact of the plasma-derived species on biomolecule resident thiols needs to be shown. Already, the oxidation of the redox sensor protein NRF2-thiol groups was shown to be triggered by plasma treatment and led to changes in anti-oxidant protein transcription [58]. So far, it remains to be clarified if this oxidation was executed by plasma-derived species or secondary species deriving from oxidized lipid membranes or leaky mitochondria. In regard to the short free diffusion ranges of most plasma-derived species, it must be presumed that direct interaction with intracellular proteins is not likely. However, oxidation of membrane-bound proteins, such as structural proteins for cell-cell and cell-matrix contact, pore proteins, and receptors might be targeted directly. Further, bioactive derivatives of small molecules, like the here delineated CAP derived cysteine

products, may contribute. First experiments using oxidized cysteine solutions showed changes in mammalian cell migration and metabolism (Heusler et al., same special issue).

4. Summary and conclusion

The plasma liquid chemistry produced by an argon plasma jet (kINPen) has been investigated via cysteine as a model substance. The intensity of cysteine oxidation increased with treatment duration and presence of oxygen admixture in the feed gas, while it decreased with higher cysteine concentration in the liquid. The number of thiol groups consumed per second of discharge were two to ten-fold lower than the number of plasma-derived one-electron acceptor equivalents hitting the surface during this time. Taking into account the number of cysteine molecules in the boundary layer and the achieved oxidation state, it can be stated that short-lived species react at the interface with the target and only limited conversion takes place in the bulk. Especially the long-lived hydrogen peroxide was found ineffective in yielding oxidized cysteine derivatives. When comparing turnover rates for low and high concentration of tracer boundary layer depletion was observed, an indicator for short-lived ROS like atomic O or singlet oxygen. Still, as model and measurement do not correlate ideally, further research is needed to clarify the role of the interface in cysteine derivatization. A range of products from cysteine was identified, in part indicative for certain treatment conditions. Several non-stable products occur transiently during the plasma treatment. Bioactive reactive sulfur species (RSS) have been found for mild treatment conditions, such as cysteine sulfoxides and cysteine-S-sulfonate, allowing secondary effects being triggered via their cellular recognition. When translating these observations into the in-vivo application, strong direct oxidation of protein thiol groups with subsequent changes in protein biochemistry must be considered.

Acknowledgments

Funding from the German Federal Ministry of Education and Research (grant number 03Z22DN12 to K.W.) supported this work. The experimental contribution of Johann Volzke and Dana Sponholz is gratefully acknowledged.

Conflict of interest

The authors declare no conflict of interest.

Supplementary materials

Supplementary material associated with this article can be found, in the online version, at doi:10.1016/j.cpme.2019.100083.

References

- [1] K.D. Weltmann, T. von Woedtke, Plasma medicine-current state of research and medical application, *Plasma Phys. Control. Fusion* 59 (1) (2017) 014031.
- [2] C. Ulrich, F. Kluschke, A. Patzelt, S. Vandersee, V.A. Czaika, H. Richter, A. Bob, J. von Hutten, C. Painsi, R. Hugel, A. Kramer, O. Assadian, J. Lademann, B. Lange-Asschenfeldt, Clinical use of cold atmospheric pressure argon plasma in chronic leg ulcers: A pilot study, *J. Wound Care* 24 (5) (2015) 196–203.
- [3] S. Emmert, F. Brehmer, H. Hänßle, A. Helmke, N. Mertens, R. Ahmed, D. Simon, D. Wandke, W. Maus-Friedrichs, G. Däschlein, M.P. Schön, W. Viöl, Atmospheric pressure plasma in dermatology: Ulcus treatment and much more, *Clin. Plas. Med.* 1 (1) (2013) 24–29.
- [4] S. Bekeschus, A. Schmidt, K.-D. Weltmann, T. von Woedtke, The plasma jet kINPen—A powerful tool for wound healing, *Clin. Plas. Med.* 4 (1) (2016) 19–28.
- [5] P.J. Bruggeman, M.J. Kushner, B.R. Locke, J.G.E. Gardeniers, W.G. Graham, D.B. Graves, R.C.H.M. Hofman-Caris, D. Maric, J.P. Reid, E. Ceriani, D.F. Rivas, J.E. Foster, S.C. Garrick, Y. Gorbanev, S. Hamaguchi, F. Iza, H. Jablonowski, E. Klimova, J. Kolb, F. Krma, P. Lukes, Z. Machala, I. Marinov, D. Mariotti, S.M. Thagard, D. Minakata, E.C. Neyts, J. Pawlat, Z.L. Petrovic, R. Pflieger, S. Reuter, D.C. Schram, S. Schroter, M. Shiraiwa, B. Tarabova, P.A. Tsai, J.R.R. Verlet, T. von Woedtke, K.R. Wilson, K. Yasui, G. Zvereva, Plasma-liquid

- interactions: A review and roadmap, *Plasma Sources Sci. T* 25 (5) (2016) 053002.
- [6] T. von Woedtke, H.R. Metelmann, K.D. Weltmann, *Clinical Plasma Medicine, State and perspectives of in vivo application of cold atmospheric plasma*, *Contrib. Plasma Phys.* 54 (2) (2014) 104–117.
- [7] D.B. Graves, *Mechanisms of plasma medicine: Coupling plasma physics*, *Biochem. Biol.* 1 (4) (2017) 281–292.
- [8] A. Schmidt-Bleker, S. Reuter, K.D. Weltmann, *Quantitative schlieren diagnostics for the determination of ambient species density, gas temperature and calorimetric power of cold atmospheric plasma jets*, *J. Phys. D Appl. Phys.* 48 (17) (2015) 175202.
- [9] S. Reuter, H. Tresp, K. Wende, M.U. Hammer, J. Winter, K. Masur, A. Schmidt-Bleker, K.D. Weltmann, *From RONS to ROS: tailoring Plasma Jet Treatment of Skin Cells*, *IEEE Trans. Plasma Sci.* 40 (11) (2012) 2986–2993.
- [10] A. Schmidt-Bleker, S. Reuter, K.-D. Weltmann, *Non-dispersive path mapping approximation for the analysis of ambient species diffusion in laminar jets*, *Phys. Fluids (1994–present)* 26 (8) (2014) 083603.
- [11] B. Van Ham, S. Hofmann, R. Brandenburg, P. Bruggeman, *In situ absolute air, O₃ and NO densities in the effluent of a cold RF argon atmospheric pressure plasma jet obtained by molecular beam mass spectrometry*, *J. Phys. D Appl. Phys.* 47 (22) (2014) 224013.
- [12] S. Iseni, S. Zhang, A.F.H. van Gessel, S. Hofmann, B.J.T. van Ham, S. Reuter, K.D. Weltmann, P.J. Bruggeman, *Nitric oxide density distributions in the effluent of an RF argon APPJ: Effect of gas flow rate and substrate*, *New J. Phys.* 16 (12) (2014) 123011.
- [13] S. Zhang, W. van Gaens, B. van Gessel, S. Hofmann, E. van Veldhuizen, A. Bogaerts, P. Bruggeman, *Spatially resolved ozone densities and gas temperatures in a time modulated RF driven atmospheric pressure plasma jet: An analysis of the production and destruction mechanisms*, *J. Phys. D Appl. Phys.* 46 (20) (2013) 205202.
- [14] J. Golda, J. Held, B. Redeker, M. Konkowski, P. Beijer, A. Sobota, G. Kroesen, N.S.J. Braithwaite, S. Reuter, M.M. Turner, T. Gans, D. O'Connell, V. Schulz-von der Gathen, *Concepts and characteristics of the 'COST reference microplasma jet'*, *J. Phys. D Appl. Phys.* 49 (8) (2016) 084003.
- [15] S. Schneider, J.W. Lackmann, F. Narberhaus, J.E. Bandow, B. Denis, J. Benedikt, *Separation of VUV/UV photons and reactive particles in the effluent of a He/O₂ atmospheric pressure plasma jet*, *J. Phys. D Appl. Phys.* 44 (29) (2011) 295201.
- [16] Y. Gorbanev, C.C.W. Verlaack, S. Tinck, E. Tuenter, K. Foubert, P. Cos, A. Bogaerts, *Combining experimental and modelling approaches to study the sources of reactive species induced in water by the COST RF plasma jet*, *Phys. Chem. Chem. Phys.* 20 (4) (2018) 2797–2808.
- [17] A. Schmidt-Bleker, J. Winter, A. Bösel, S. Reuter, K.-D. Weltmann, *On the plasma chemistry of a cold atmospheric argon plasma jet with shielding gas device*, *Plasma Sources Sci. Technol.* 25 (1) (2015) 015005.
- [18] H. Tresp, M.U. Hammer, K.-D. Weltmann, S. Reuter, *Effects of atmosphere composition and liquid type on plasma-generated reactive species in biologically relevant solutions*, *Plasma Med.* 3 (1–2) (2013) 45–55.
- [19] H. Jablonowski, M.A.C. Häscher, M. Dünbier, K. Wende, M.U. Hammer, K.-D. Weltmann, S. Reuter, T. von Woedtke, *Plasma jet's shielding gas impact on bacterial inactivation*, *Biointerphases* 10 (2) (2015) 029506.
- [20] K. Wende, P. Williams, J. Dalluge, W. Van Gaens, H. Aboubakar, J. Bischof, T. von Woedtke, S.M. Goyal, K.-D. Weltmann, A. Bogaerts, P. Bruggeman, *Identification of the biologically active liquid chemistry induced by a nonthermal atmospheric pressure plasma jet*, *Biointerphases* 10 (2) (2015) 029518.
- [21] H. Jablonowski, J.S. Sousa, K.-D. Weltmann, K. Wende, S.J.S.R. Reuter, *Quantification of the ozone and singlet delta oxygen produced in gas and liquid phases by a non-thermal atmospheric plasma with relevance for medical treatment*, *8(1) (2018) 12195.*
- [22] Y. Gorbanev, N. Stehling, D. O'Connell, V. Chechik, *Reactions of nitroxide radicals in aqueous solutions exposed to non-thermal plasma: Limitations of spin trapping of the plasma induced species*, *Plasma Sources Sci. Technol.* 25 (5) (2016) 055017.
- [23] H. Jablonowski, T. von Woedtke, *Research on plasma medicine-relevant plasma-liquid interaction: What happened in the past five years?* *Clin. Plas. Med.* 3 (2) (2015) 42–52.
- [24] J. Winter, H. Tresp, M.U. Hammer, S. Iseni, S. Kupsch, A. Schmidt-Bleker, K. Wende, M. Dünbier, K. Masur, K.D. Weltmann, S. Reuter, *Tracking plasma generated H₂O₂ from gas into liquid phase and revealing its dominant impact on human skin cells*, *J. Phys. D Appl. Phys.* 47 (28) (2014) 285401.
- [25] A.R. Gibson, H.O. McCarthy, A.A. Ali, D. O'Connell, W.G. Graham, *Interactions of a non-thermal atmospheric pressure plasma effluent with PC-3 prostate cancer cells*, *Plasma Process. Polym.* 11 (12) (2014) 1142–1149.
- [26] R. Zhou, R. Zhou, J. Zhuang, Z. Zong, X. Zhang, D. Liu, K. Bazaka, K. Ostrikov, *Interaction of atmospheric-pressure air microplasmas with amino acids as fundamental processes in aqueous solution*, *PLoS One* 11 (5) (2016) e0155584.
- [27] C. Klinkhammer, C. Verlaack, D. Smilowicz, F. Kogelheide, A. Bogaerts, N. Metzler-Nolte, K. Stapelmann, M. Havenith, J.W. Lackmann, *Elucidation of plasma-induced chemical modifications on glutathione and glutathione disulphide*, *Sci. Rep.* 7 (1) (2017) 13828.
- [28] J.W. Lackmann, K. Wende, C. Verlaack, J. Golda, J. Volzke, F. Kogelheide, J. Held, S. Bekeschus, A. Bogaerts, V. Schulz-von der Gathen, K. Stapelmann, *Chemical fingerprints of cold physical plasmas—An experimental and computational study using cysteine as tracer compound*, *Sci. Rep.* 8 (1) (2018) 7736.
- [29] C.E. Paulsen, K.S. Carroll, *Cysteine-mediated redox signaling: chemistry, biology, and tools for discovery*, *Chem. Rev.* 113 (7) (2013) 4633–4679.
- [30] D. Yan, A. Talbot, N. Nourmohammadi, X. Cheng, J. Canady, J. Sherman, M. Keidar, *Principles of using cold atmospheric plasma stimulated media for cancer treatment*, *Sci. Rep.* 5 (2015) 18339.
- [31] E. Takai, T. Kitamura, J. Kuwabara, S. Ikawa, S. Yoshizawa, K. Shiraki, H. Kawasaki, R. Arakawa, K. Kitano, *Chemical modification of amino acids by atmospheric-pressure cold plasma in aqueous solution*, *J. Phys. D Appl. Phys.* 47 (28) (2014) 285403.
- [32] G.I. Giles, K.M. Tasker, C. Jacob, *Oxidation of biological thiols by highly reactive disulfide-S-oxides*, *Gen. Physiol. Biophys.* 21 (1) (2002) 65–72.
- [33] G.I. Giles, M.J. Nasim, W. Ali, C. Jacob, *The reactive sulfur species concept: 15 years on*, *Antioxidants (Basel)* 6 (2) (2017) 38.
- [34] C. Jacob, G.I. Giles, N.M. Giles, H. Sies, *Sulfur and selenium: the role of oxidation state in protein structure and function*, *Angew. Chem. Int. Ed. Engl.* 42 (39) (2003) 4742–4758.
- [35] C.C.W. Verlaack, W. Van Boxem, A. Bogaerts, *Transport and accumulation of plasma generated species in aqueous solution*, *Phys. Chem. Chem. Phys.* 20 (10) (2018) 6845–6859.
- [36] J.F.M. van Rens, J.T. Schoof, F.C. Ummelen, D.C. van Vugt, P.J. Bruggeman, E.M. van Veldhuizen, *Induced liquid phase flow by RF Ar cold atmospheric pressure plasma jet*, *IEEE T Plasma Sci.* 42 (10) (2014) 2622–2623.
- [37] A. Schmidt-Bleker, J. Winter, S. Iseni, M. Dünbier, K.D. Weltmann, S. Reuter, *Reactive species output of a plasma jet with a shielding gas device-combination of FTIR absorption spectroscopy and gas phase modelling*, *J. Phys. D: Appl. Phys.* 47 (14) (2014).
- [38] C.C.W. Verlaack, et al., *Transport and accumulation of plasma generated species in aqueous solution*, *Phys. Chem. Chem. Phys.* 20 (10) (2018) 6845–6859.
- [39] J.F. Van Rens, J.T. Schoof, F.C. Ummelen, D.C. Van Vugt, P.J. Bruggeman, E. Van Veldhuizen, *Induced liquid phase flow by RF Ar cold atmospheric pressure plasma jet*, *IEEE Trans. Plasma Sci.* 42 (10) (2014) 2622–2623.
- [40] L.M. Bannison, C.N. Miller, R.J. Summers, A.M. Minnis, G. Sussman, W. McGuiness, *The pH of wounds during healing and infection: A descriptive literature review*, *Wound Practice Res.* 25 (2) (2017) 7.
- [41] Y. Gorbanev, D. O'Connell, V. Chechik, *Non-thermal plasma in contact with water: The origin of species*, *Chemistry (Easton)* 22 (10) (2016) 3496–3505.
- [42] W. Van Boxem, J. Van der Paal, Y. Gorbanev, S. Vanuytsel, E. Smits, S. Dewilde, A. Bogaerts, *Anti-cancer capacity of plasma-treated PBS: Effect of chemical composition on cancer cell cytotoxicity*, *Sci. Rep.* 7 (1) (2017) 16478.
- [43] S. Robl, M. Worner, D. Maier, A.M. Braun, *Formation of hydrogen peroxide by VUV-photolysis of water and aqueous solutions with methanol*, *Photochem. Photobiol. Sci.* 11 (6) (2012) 1041–1050.
- [44] A. Privat-Maldonado, D. O'Connell, E. Welch, R. Vann, M.W. van der Woude, *Spatial dependence of DNA damage in bacteria due to low-temperature plasma application as assessed at the single cell level*, *Sci. Rep.* 6 (2016) 35646.
- [45] D. Luo, S.W. Smith, B.D. Anderson, *Kinetics and mechanism of the reaction of cysteine and hydrogen peroxide in aqueous solution*, *J. Pharm. Sci.* 94 (2) (2005) 304–316.
- [46] H. Jablonowski, A. Schmidt-Bleker, K.D. Weltmann, T. von Woedtke, K. Wende, *Non-touching plasma-liquid interaction—Where is aqueous nitric oxide generated?* *Phys. Chem. Chem. Phys.* 20 (39) (2018) 25387–25398.
- [47] E. Takai, T. Kitamura, J. Kuwabara, S. Ikawa, S. Yoshizawa, K. Shiraki, H. Kawasaki, R. Arakawa, K. Kitano, *Chemical modification of amino acids by atmospheric-pressure cold plasma in aqueous solution*, *J. Phys. D* 47 (28) (2014) 285403.
- [48] Y.-M. Go, J.D. Chandler, D.P. Jones, *The cysteine proteome*, *Free Radic. Biol. Med.* 84 (2015) 227–245.
- [49] N.O. Baez, J.A. Reisz, C.M. Furdul, *Mass spectrometry in studies of protein thiol chemistry and signaling: Opportunities and caveats*, *Free Radic. Biol. Med.* 80 (2015) 191–211.
- [50] L.B. Poole, *The basics of thiols and cysteines in redox biology and chemistry*, *Free Radic. Biol. Med.* 80 (2015) 148–157.
- [51] J. Borlinghaus, F. Albrecht, M.C. Gruhlke, I.D. Nwachukwu, A.J. Slusarenko, *Allucin: Chemistry and biological properties*, *Molecules* 19 (8) (2014) 12591–12618.
- [52] A.A. Ali, J.A. Coulter, C.H. Ogle, M.M. Migaud, D.G. Hirst, T. Robson, H.O. McCarthy, *The contribution of N(2)O(3) to the cytotoxicity of the nitric oxide donor DETA/NO: An emerging role for S-nitrosylation*, *Biosci. Rep.* 33 (2) (2013) e00031.
- [53] C. Belge, P.B. Massion, M. Pelat, J.L. Balligand, *Nitric oxide and the heart: Update on new paradigms*, *Ann. N. Y. Acad. Sci.* 1047 (2005) 173–182.
- [54] A.C. Kendall, J.L. Whatmore, P.G. Winyard, G.R. Smerdon, P. Eggleton, *Hyperbaric oxygen treatment reduces neutrophil-endothelial adhesion in chronic wound conditions through S-nitrosation*, *Wound Repair Regen.* 21 (6) (2013) 860–868.
- [55] B. Stallmeyer, H. Kampfer, N. Kolb, J. Pfeilschifter, S. Frank, *The function of nitric oxide in wound repair: inhibition of inducible nitric oxide-synthase severely impairs wound reepithelialization*, *J. Invest. Dermatol.* 113 (6) (1999) 1090–1098.
- [56] Z. Abedinzadeh, M. Gardesalbert, C. Ferradini, *Kinetic-study of the oxidation mechanism of glutathione by hydrogen-peroxide in neutral aqueous-medium*, *Can. J. Chem. Revue Canadienne De Chimie* 67 (7) (1989) 1247–1255.
- [57] G.N. Khairallah, A.T. Maccarone, H.T. Pham, T.M. Benton, T. Ly, G. da Silva, S.J. Blanksby, R.A. O'Hair, *Radical formation in the gas-phase ozonolysis of deprotonated cysteine*, *Angew. Chem. Int. Ed. Engl.* 54 (44) (2015) 12947–12951.
- [58] A. Schmidt, S. Dietrich, A. Steuer, K.-D. Weltmann, T. von Woedtke, K. Masur, K. Wende, *Non-thermal plasma activates human keratinocytes by stimulation of antioxidant and phase II pathways*, *J. Biol. Chem.* 290 (11) (2015) 6731–6750.

Article A5

Influence of aerosol injection on the liquid chemistry induced by an RF argon plasma jet

I. Sremački & G. Bruno, H. Jablonowski, C. Leys, A. Nikiforov, K. Wende. *Plasma Sources Science and Technology*, **under revision**, 2020.



Our initial decision on your article: PSST-104102

Plasma Sources Science and Technology

11/19/2020 03:51 PM

To: kristian.wende

Cc: ivana.sremacki, giuliana.bruno, helena.jablonowski,

christophe.leys, anton.nikiforov, kristian.wende

Please respond to psst

Dear Dr Wende,

Re: "Influence of aerosol injection on the liquid chemistry induced by an RF argon plasma jet" by Sremački, Ivana; Bruno, Giuliana; Jablonowski, Helena; Leys, Christophe; Nikiforov, Anton; Wende, Kristian
Article reference: PSST-104102

We have now received the referee report(s) on your Paper, which is being considered by Plasma Sources Science and Technology.

The referee(s) have recommended that you make some amendments to your article. The referee report(s) can be found below and/or attached to this message. You can also access the reports at your Author Centre, at <https://mc04.manuscriptcentral.com/psst-iop>

Please consider the referee and Editorial Board comments and amend your article according to the recommendations. You should then send us a clean final version of your manuscript. Please also send (as separate files) point-by-point replies to the referee comments including a list of changes you have made and an additional copy of your manuscript with the changes highlighted (for further information visit <https://publishingsupport.iopscience.iop.org/questions/how-to-prepare-your-revised-article/>). This will aid our referees in reviewing your revised article. Please upload the final version and electronic source files to your Author Centre by 03-Dec-2020.

If we do not receive your article by this date, it may be treated as a new submission, so please let us know if you will need more time.

We look forward to hearing from you soon.

Yours sincerely

Lucy Joy

On behalf of the IOP peer review team:
Editor - Natasha Leeper
Associate Editors - Sam Blomfield and Lucy Joy
Editorial Assistant - Cat McRoberts

IOP Publishing guidance on Covid19 (Coronavirus):
<https://iopublishing.org/news/coronavirus-covid-19-faqs/>

Want to find out what is happening to your submission right now? Track your article here:
https://publishingsupport.iopscience.iop.org/track-my-article/?utm_source=Track%20my%20article&utm_medium=Email

psst@iopublishing.org

Editor-in-Chief: Professor Igor Adamovich
Publisher: Iain Trotter

IOP Publishing
Temple Circus, Temple Way, Bristol, BS1 6HG, UK

www.iopscience.org/psst

2018 Impact Factor: 4.128

REFEREE REPORT(S):

Referee: 1

COMMENTS TO THE AUTHOR(S)

Commented PDF file attached - "Summary of Comments PSST 110920.pdf "

Referee: 2

COMMENTS TO THE AUTHOR(S)

In this paper, the plasma and bulk liquid chemistry of a RF plasma jet with aerosol injection were investigated. The paper is well written despite numerous grammatical and formatting errors and was easy to follow. All conclusions are supported by data and I in fact had no comments or questions that relate to the presented results. The biggest downside of his paper was the novelty effect; I was struggling to understand why the aerosol injection was investigated, especially since its introduction lowered the production rates of oxidative species. None of the results convinced me that this topic is of great interest, making me ponder about the impacts of the results. Is there anything new presented in Figure 15 that we hadn't known already? I do admit that one interesting result is the quenching of the VUV photons. All that being said, the community still may appreciate novel information that relates to the droplet-plasma chemistry.

Minor comments:

The introduction section should highlight the importance or novelty of using the jet with aerosol injection. What is expected for the aerosol addition to achieve?

Hydrogen peroxide assay...what is the sensitivity of the technique for H₂O₂ measurements? Fix superscripts for iron species.

Figure 3-be clear (include in the caption) what is the process gas used to drive the jet.

COMMENTS FROM EDITORIAL BOARD:

Associate Editor

Comments to the Author:

As the referees note, revisions are required. Although Referee 2 suggests that it be accepted, I ask that you specifically address their first comment about 'what is new' about this work. In essence, both referees note that you do not put your work within the context of the relatively large (and growing) literature about aerosols and plasmas. Please pay specific attention to addressing this weakness.



Letter reference: DSMo01 **Summary of Comments PSST 110920.pdf**

1
2
3 **Influence of aerosol injection on the liquid chemistry induced by an RF argon**
4 **plasma jet**
5

6
7 Ivana Sremački^{a,*}, Giuliana Bruno^{b,*}, Helena Jablonowski^b, Christophe Leys^a, Anton Nikiforov^a, Kristian Wende^b
8

9 ^a*Department of Applied Physics, Ghent University, Sint-Pietersnieuwstraat 41, Gent, 9000, Belgium*
10

11 ^b*ZIK plasmatis, Leibniz Institute for Plasma Science and Technology (INP Greifswald), Felix-Hausdorff-Straße 2, 17489*
12 *Greifswald, Germany*
13

14 ^{*}Both I. Sremački and G. Bruno contributed equivalently to the work
15

16 Correspondence to: kristian.wende@inp-greifswald.de and anton.nikiforov@ugent.be
17

18 Keywords: plasma aerosol, plasma jet, cysteine model, plasma liquid chemistry
19
20
21
22
23
24
25
26
27
28
29
30
31
32
33
34
35
36
37
38
39
40
41
42
43
44
45
46
47
48
49
50
51
52
53
54
55
56
57
58
59
60

Abstract:

In the last decade cold physical plasmas, particularly plasma jets have emerged as an alternative or adjuvant tool in biomedical research. Especially processes that involve reactive oxygen species (ROS) signaling, such as inflammation, were found susceptible to the manipulation by plasmas. Plasma-derived ROS are connected to stimulatory and inhibitory effects in cells/tissues, and to the introduction of covalent modifications in various biomolecules. Aiming for an adaptation for wound treatment and topical drug delivery, a radio-frequency (RF) plasma jet with annular geometry and additional aerosol injection into the effluent was developed. The role of the aerosol in modulating the reactive species production by the plasma source is investigated with a combination of physical and chemical analytics. Optical emission spectroscopy, EPR data, and a cysteine model reveal that aerosol injection shifts the production of ROS from atomic and singlet oxygen towards hydroxyl radicals that are generated in the droplets. Consequentially, chemical reactions occur mainly during the transport of the droplets through the effluent in the droplet's bulk and interface. This is accompanied by a strong distance dependence. In the absence of the aerosol, atomic and singlet oxygen dominate the gas and liquid chemistry as demonstrated by EPR and cysteine product patterns. Along with this, distance is less important due to the considerable gas-phase lifetime of singlet oxygen. The presence of reactive nitrogen species was negligible regardless of aerosol injection and only traces of the downstream products nitrate and nitrite were detected.

In summary, the aerosol injection into the effluent opens new avenues to control UV radiation and reactive species output for biomedical non-thermal plasma sources, reaching out towards application safety and drug release.

1. INTRODUCTION

The unique feature of cold physical plasmas (CPP) to produce a mixture of highly reactive species mimicking the multi-ROS reactive oxygen species inflammatory environment is central to the plasma medicine theme. Since the first reports in the mid-nineties, showing that CPP sources can successfully inactivate bacteria the field expanded significantly [1, 2]. Numerous plasma sources were developed for the decontamination of biotic/abiotic surfaces, deposition of bioactive coatings, and manipulation of eukaryotic cells and tissues [3-6]. CPPs show several direct and indirect effects in biological models, inducing cell signaling, proliferation, apoptosis, or senescence depending on the treatment intensity (“dose”) [7]. Currently, research focuses on applications such as chronic and acute wound healing, (pre-) cancerous lesions, and other conditions involving the immune system [8-13]. The design of cold plasma sources for biomedical applications evolves in two major directions: Dielectric Barrier Discharges (DBD) [14, 15] and Atmospheric Pressure Plasma Jets (APPJ) configuration [16].

Here, we present an RF sustained annular-shaped plasma jet in argon flow operating in ambient air [17]. The coaxial geometry allows the introduction of aerosol into the discharge effluent. By this unique design, the source allows the direct and controlled interaction of micro-droplets with plasma before reaching the (biological) target, modulating the generation of active species due to a large gas-liquid interface, and open the potential to introduce compounds or drugs for delivery to the target via the aerosol. To this end, a thorough understanding of the physics and the chemistry of this modular source is desired to determine future key points for an application both in the biomedical and in the technological scenario. So far, the biochemical potential of the plasma source has not been studied in detail, especially the impact of the RF argon discharge on the aerosol droplet carrying organic molecules remains to be determined.

Besides the primary species and radiation produced in the plasma core, species that can be generated in contact with air and water are of special interest for targeted applications. Among these are the reactive oxygen species (ROS): superoxide $O_2^{\cdot-}$, hydrogen peroxide H_2O_2 , hydroxyl radical $^{\cdot}OH$, singlet oxygen 1O_2 , atomic oxygen $^{\cdot}O$, ozone O_3 , and the reactive nitrogen species (RNS): atomic nitrogen $^{\cdot}N$, nitric oxides N_xO_y , peroxyxynitrite $ONOO^{\cdot}$, and nitrous resp. nitric acid with the corresponding ions (HNO_2/NO_2^- , HNO_3/NO_3^-). The species differ in their reactivity, affecting lifetime and specificity of detection. Most of them occur regularly in physiological processes of living tissues, often involved in signaling processes [18, 19]. Biological reactivity of species mirrors in oxidative changes of sensor molecules or – in case of excess – other biomolecules such as proteins or lipids [20]. The resulting outcome is still underexplored, but it has been observed that the oxidation of proteins changes their immunogenicity. In autoimmune type I diabetes patients, autoantibodies targeting experimentally oxidized insulin were detected [21]. It can be assumed that the introduction of covalent modifications in biomolecules is one mechanisms behind the observed biomedical effects of CPPs. Thus, the biochemical impact of a given plasma source is relevant. Biomolecules such as peptides or amino acids are a suitable model to investigate the reactive species produced or deposited in a target by a given plasma source and on the other hand reveal the chemical structures most sensitive to the attack of reactive oxygen and nitrogen species RONS [22-25].

In this work, an established model system employing the amino acid cysteine as the tracer molecule has been chosen to scavenge RONS generated by the RF plasma source. Cysteine is a key amino acid controlling structure, location, and functionality of proteins by its different oxidation states [26]. Applicability of the model has been validated using the argon plasma jet kINPen and the helium micro-plasma COST jet [22, 25]. By employing liquid chromatography and high-resolution mass spectrometry, the model can qualify and quantify the major cysteine derivatives produced by the interaction with the plasma-derived species. Beside the treatment of cysteine solutions

1
2
3 with various power and distance settings, especially the direct interaction between cysteine in the aerosol droplets
4 and the plasma effluent was investigated. Furthermore, electron paramagnetic resonance (EPR; $\cdot\text{OH}$, $\text{O}_2^{\cdot-}$, $\cdot\text{H}$, $\cdot\text{O}$,
5 O_3 , $^1\text{O}_2$), ion chromatography (IC, NO_2^- and NO_3^- ions) and a colorimetric H_2O_2 assay were used to detect the
6 deposition of short and long-lived reactive species into the liquid phase. Based on these data, the mechanisms of
7 species generation and the role of the aerosol injection on ROS and RNS production are discussed.
8
9
10
11
12
13
14
15
16
17
18
19
20
21
22
23
24
25
26
27
28
29
30
31
32
33
34
35
36
37
38
39
40
41
42
43
44
45
46
47
48
49
50
51
52
53
54
55
56
57
58
59
60

2. MATERIALS & METHODS

In this work, a special design of argon RF APPJ with aerosol droplets injection was used. Safe, stable and uniform operation of the source that is important for plasma medicine was shown in our recent work [17]. Hereby, in this work special attention is given to the effects of plasma-aerosol direct interaction on plasma efficiency of liquid media treatment. Correspondingly, varieties of diagnostic techniques were applied to support the study on chemical characterization of the source operation in ambient air with and without an aerosol. Optical emission spectroscopy (OES) and Fourier transform IR spectroscopy (FTIR) have been used to give insight into the composition of species in the plasma gas phase and plasma-aerosol medium. In next step, the treated liquid target was analyzed in terms of liquid-chemistry with colorimetric assays, ion chromatography (IC), and electron paramagnetic resonance (EPR) spectroscopy, with focusing on a model of cysteine oxidation in presence of plasma and plasma in contact with the aerosol.

2.1 Design of plasma reactor

The plasma reactor was constructed in a way to allow introduction of aerosol droplets in the effluent. Plasma jet in annular shape 1 mm thick with external diameter $d_{ex}=14\text{mm}$ was generated in coaxial hollow-electrode geometry. RF powered inner electrode was made of corrosion-resistant stainless steel, while an external grounded electrode was made of aluminum. All experiments were carried out for two applied powers further indicated as “low” $P=20\text{ W}$ and “high” $P=30\text{ W}$. The high power is a maximum discharge power when RF plasma exists in α mode of operation. On a top of the reactor, a NexTgen ultrasonic spraying nozzle was installed (**Fig. 1a**). Plasma forming gas argon was fixed at 3 standard liter per minute (slm) corresponding to maximal gas velocity in the effluent of 1.4 m/s. The flow rate was previously verified to generate uniform diffuse discharge in α -regime in a laminar gas flow regime (**Fig. 1b**). The flow rate of aerosol liquid to be sprayed was controlled with a syringe pump at a flow of 0.1 mL/min. The optimal value of flow rate was chosen, assuring a uniform and reproducible spray during a treatment time between 10 and 60 s. The mean size of the aerosol droplets was about 22 μm . Additionally, 1 slm flow of Ar gas was applied through the central electrode to push droplets downwards with a velocity of 0.05 m/s to prevent aerosol condensation.

2.2 Spatial resolved optical emission spectroscopy (OES)

Optical emission spectroscopy can be used as a qualitative method to give insight into the composition of excited species present in plasma. Emission from excited species in plasma effluent has been measured in the range of 250-900 nm. The Ocean Optics spectrometer with the resolution of 1.7 nm was used to record emission spectra from the plasma effluent. Spectral sensitivity of the spectrometer, transparency of the fiber and collection optics were calibrated with an Oriel model 63355 quartz tungsten-halogen lamp. The light emitted by the plasma effluent was collected with a fiber ($d=200\text{ }\mu\text{m}$) located 2 mm away from the region of interest resulting in an acceptance angle corresponding to the spatial resolution of 1 mm. Line-of-sight measurements were performed to record spectra for 3 positions perpendicular to the axis of the jet, 2 mm from the nozzle – in plasma effluent, 6-mm from the nozzle – the edge of visible effluent and 8 mm away from the nozzle – far effluent. The effluent was imaged using an Hamamatsu ICCD camera (5 μs exposition, 1000 integration), coupled to bandpass filters with a

transparency of 10 nm full width at half maxima FWHM centered at 751 and 298 nm corresponding to Ar I and OH(A-X) emission, respectively.

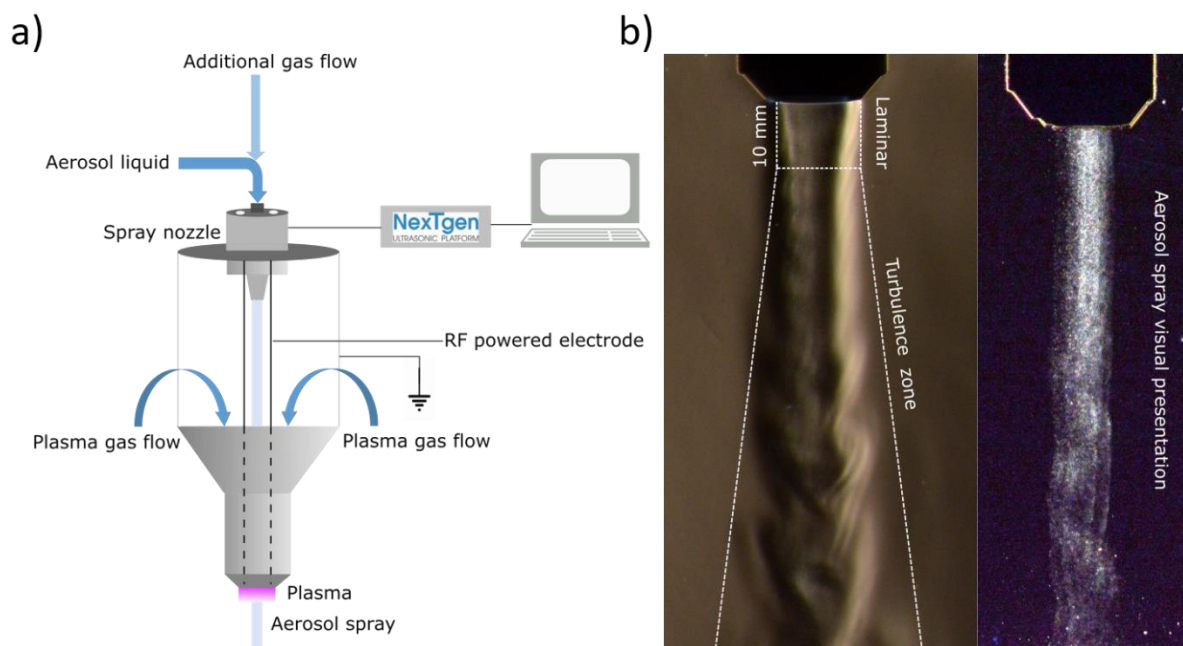


Figure 1. a) General view of the plasma jet reactor with aerosol injection, b) Visual view of the gas flow obtained by Schlieren imaging indicating two zones of different gas flow regime (on left) and visual view of the aerosol spray (on right).

2.3 Fourier-transform infrared spectroscopy (FTIR) analysis

FTIR high-resolution spectroscopy was performed with the use of Matrix-MG2 spectrometer of 0.5 cm^{-1} resolution in order to detect and estimate the absolute concentration of the most abundant long-living compounds generated in the gas phase with and without the aerosol. The spectrometer coupled with multi-pass cell of 5 m was calibrated for H_2O , N_2O , N_2O_5 , NO , NO_2 , O_3 compounds with a sensitivity of 0.1 ppm. Gas from the plasma was directed in a tube through which dry air was circulating in flow range 0.5-1 SLM, in order to simulate an open atmosphere operation. Once aerosol was introduced in the plasma, trapped gas was filtrated through a quartz wool to avoid any water droplets entering the FTIR system. The FTIR spectra were averaged 30 times in progression mode and recorded in the wavenumber range of $800\text{-}6200\text{ cm}^{-1}$.

2.4 Samples preparation and plasma treatments of liquids

For mass spectrometry analysis, 1 mM solutions of cysteine amino acid (L-Cysteine, Sigma Aldrich) were prepared fresh daily. The pH was stabilized at pH 7.4 by the use of 5 mM phosphate buffer (HPLC-MRM analysis) or 5 mM ammonium formate (direct infusion shotgun HRMS). For electron paramagnetic resonance (EPR) experiments, the spin trap / spin probe was solubilized in 5 mM phosphate buffer. In pilot experiments, a volume of 1.5 ml sample in a 6-well multiwell plate was determined to be optimal.

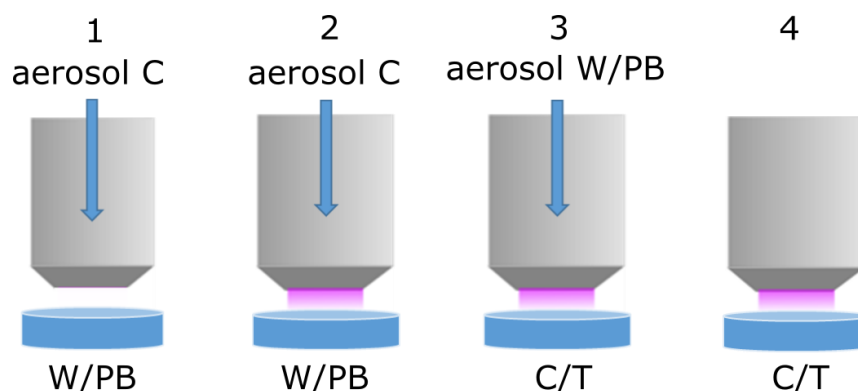


Figure 2. General experimental setups. Ultrasonic aerosol used in setups 1 to 3. Plasma off conditions (setup 1) used as background control. Abbreviations: C for cysteine, T for trapping trap/spin probe, W for water, and PB for phosphate buffer

Cysteine oxidation was investigated for plasma power of 20 and 30 W, treatment time variation (10, 35, 60 s), and distance variation (2, 6, 12 mm nozzle – target). Four different set-ups including or excluding aerosol injection were used (**Fig. 2/Tab. 1**). For some experiments, the aerosol was generated from a 1 mM cysteine solution and collected for analysis into either empty well plates or wells filled with 1.5 mL water. Plasma on and control experiments were performed.

Table 1. Overview of the plasma treatment protocol. PBS = phosphate buffered saline; spin trap/spin buffer = 2 mM BMPO or 100 mM TEMPD (see figure 2)

Set-up	Aerosol liquid	Target liquid	Power (watt)	Distance (mm)	Treatment time (s)
1	1 mM cysteine in water (C)	water (W) or phosphate buffer (PB)	0 (control)	2, 6, 12	10, 35, 60
2	1 mM cysteine in water (C)	water (W) or phosphate buffer (PB)	20, 30		
3	water (W) or phosphate buffer (PB)	1 mM cysteine in water (C) / spin trap in PBS (T)			
4	No aerosol	1 mM cysteine in water (C) / spin trap in PBS (T)			

The aerosol injection into the plasma effluent considerably changed the surface area of the effluent/liquid interaction. Assuming a droplet mean volume of $5.56 \times 10^{-6} \text{ mm}^3$, a droplet formation rate of 3.1×10^5 droplets/s at a flow rate of 0.1 mL/min, allows to estimate the surface area of the droplets as 4.7×10^3 , 1.65×10^4 , and $2.8 \times 10^4 \text{ mm}^2$ for the treatment of 10, 35, and 60 s, respectively. It has to be noted that aerosol droplets interact with plasma only during a short time when passing through the effluent (2 mm or 40 ms). This time was estimated based on the gas fluid model (not shown here). In comparison, an area of up to 500 mm^2 is treated in condition 4 (6-well plate, 2 mm distance).

2.5 High-Pressure Liquid Chromatography & Mass Spectrometry (HPLC-MS)

Qualitative high-resolution mass spectrometry analysis was achieved by direct infusion of the cysteine solutions into a TripleTOF 5600 (Sciex, Darmstadt, Germany). 10 $\mu\text{L}/\text{min}$ of solutions were infused using a Turbo V ion

1
2
3 source, using optimized parameters (negative polarity, curtain gas 35 psi, gas1 20 psi, gas2 25 psi, capillary
4 temperature 150 °C, spray voltage 4.5 kV). The spectra were acquired in a mass range of 30 to 400 mass to charge
5 ratio (m/z). Quantitative analysis was achieved by high-pressure liquid chromatography – mass spectrometry
6 coupling. An Infinity II 1290 system (Agilent Technologies, Waldbronn, Germany) was equipped with a HILIC
7 2.1 mm x 100 mm Acquity Amide Column (130 Å pore size, 1.7 µm particle size, Waters, Manchester, United
8 Kingdom) and a respective pre-column (2.1 mm x 5 mm). Using 400 µl flowrate and an 18 min gradient of A (10
9 mM ammonium formate plus 0.15% formic acid in water) and B (85% acetonitrile, 10 mM ammonium formate
10 buffer pH 3) the baseline separation of cysteine, cystine, cystine sulfonic acid, and cysteine-S-sulfonate was
11 achieved (Sigma, Deisenhofen, Germany). The details of the gradient are resumed in **Table S1**. A qTRAP 5500
12 triple quadrupole instrument (Sciex) was used in Multiple Reaction Monitoring (MRM) strategy for detection and
13 quantification. All compounds were analyzed in positive ion mode, and specific transitions were monitored in the
14 MRM experiments (**Table S2**). External calibration curves were prepared. All samples were injected or infused
15 twice (technical duplicates).
16
17
18
19
20
21
22
23

24 **2.6 Electron paramagnetic resonance spectroscopy (EPR)**

25
26 Spin trap enhanced electron paramagnetic resonance spectroscopy (EPR, EMXmicro, Bruker Biospin GmbH; X-
27 band 9.75 GHz; magnetic field up to 0.65 T) using the Xenon software in addition with the spin counting module
28 (Bruker Biospin GmbH) was applied to quantify radicals/reactive oxygen species. The following instrument
29 parameters were used: modulation frequency 100 kHz, modulation amplitude 0.1 mT, microwave power 5.024
30 mW, receiver gain 30 dB, and a time constant of 0.01 ms. 5-tert-Butoxycarbonyl-5-methyl-1-pyrroline-N-oxide
31 (BMPO, Dojindo Laboratoire, Japan) – a spin trap for $\cdot\text{OH}$, $\text{O}_2\cdot^-$, $\cdot\text{H}$, was dissolved in 5 mM phosphate buffer to
32 a final concentration of 2 mM, and 2,2,6,6-tetramethyl-4-piperidone (TEMPD, Sigma Aldrich) – spin probe for
33 $\cdot\text{O}$, O_3 , $\text{O}_2(\text{a}^1\Delta_g)$, was dissolved in the same system to a final concentration of 100 mM. For all experiments, an
34 untreated sample was measured prior to the plasma treatment. More details on the measurement procedure can be
35 found in [28-31].
36
37
38
39
40
41
42

43 **2.7 Hydrogen peroxide assay**

44
45 Hydrogen peroxide (H_2O_2) was detected via a colorimetric assay. 10 µL of sample were incubated for 15 minutes
46 with 100 µL of reagent, consisting in a solution of xylenol orange, sorbitol and ammonium ferrous (II) sulfate
47 (Pierce™ Quantitative Peroxide Assay Kit, Thermo Scientific). In aqueous solutions, sorbitol and hydrogen
48 peroxide react to form peroxy radicals, which oxidize Fe_2^+ to Fe_3^+ . This induces a color change of xylenol orange,
49 detectable at 595 nm through a spectrophotometer (Infinite M200 Pro plate reader, Tecan, Männedorf,
50 Switzerland). Each sample was analyzed in triplicate.
51
52
53
54
55

56 **2.8 Ion chromatography (IC)**

57
58 Nitrite (NO_2^-) and nitrate (NO_3^-), as well as sulfite (SO_3^-) and sulfate (SO_4^-), were quantified via ion
59 chromatography (ICS-5000, Thermo, Dreieich, Germany). For separation a weak ion exchange column (IonPac
60 AS23 2 x 250 mm) and respective precolumn (2 x 50 mm IonPac AG23) was used (Thermo Scientific). The ions

1
2
3 were separated in 25 min isocratic run, at a flow rate of 0.25 mL/min, using 80 mM HCO_3^- and 450 mM CO_3^{2-}
4 buffer as mobile phase. External calibration curves were measured for all ions using an Seven-anion standard
5 (Dionex/Thermo Scientific) or sodium sulfite analytical standard (Sigma Aldrich, Deisenhofen, Germany). Each
6 sample of three different experiments was injected in duplicate.
7
8
9
10
11
12
13
14
15
16
17
18
19
20
21
22
23
24
25
26
27
28
29
30
31
32
33
34
35
36
37
38
39
40
41
42
43
44
45
46
47
48
49
50
51
52
53
54
55
56
57
58
59
60

3. RESULTS & DISCUSSION

3.1 Active species generation in the effluent

Spatially resolved emission spectroscopy results for the plasma effluent in three different positions 2, 6 and 8 mm from the nozzle, in pure argon plasma and plasma in contact with aerosol, are shown in **Fig. 3**.

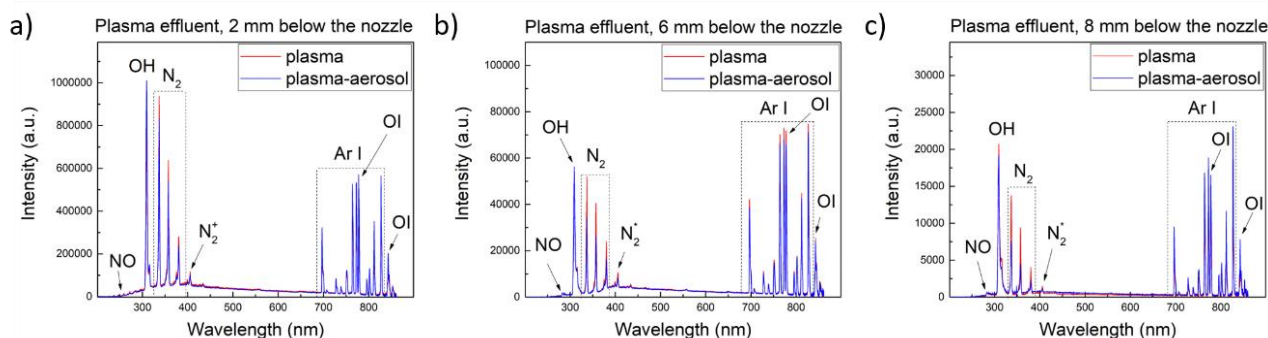


Figure 3. Overview of plasma emission without the use of aerosol (red) and plasma emission when in contact with aerosol (blue) in a range of 250-900 nm in the effluent positions corresponding to a) 2 mm, b) 6 mm and c) 8 mm below the nozzle, $P=30W$

The effluent emission in ambient air mainly consists of radiation of excited species Ar I, O I, OH(A-X) radicals, and N_2 (C-B) as marked in Figure 3a. However, weak emission from NO molecules has been also detected below 300 nm. Recorded continuum appearing in the region 300-600 nm is ascribed to the Bremsstrahlung radiation as explained in details in our work on similar RF discharge operating in a planar geometry [32]. Despite the Bremsstrahlung radiation appearance of very weak NO_2 chemiluminescence should not be neglected as a contribution to the observed continuum. Taking into account the spectral profile of the continuum radiation the contribution of the Bremsstrahlung radiation was dominant in all cases. Emission intensity was the highest in the active excitation zone (**Fig. 3a**) and exponentially decreased with the distance from the nozzle. In argon plasmas operating under ambient conditions, the energy transfer from Ar^* to N_2 is an important and effective process and it can be used as an indicator of plasma interaction with air. Energy transfer is expected to be high as soon as excited Ar atoms leave the active plasma volume and collide with surrounding air corresponding to a case presented in **Fig. 3b/c**. Presence of the aerosol in the effluent is effective in shielding the discharge from mixing with surrounding air especially in far effluent, **Fig. 3c**). Moreover, the presence of the aerosol in the effluent leads to an increase of OH radicals emission intensity more than 25% in position closest to the nozzle, indicating a probable increase in OH radicals production by water aerosol injection. The intensity of NO excited molecule emission is higher in Ar plasma without aerosol. Aerosol injection in effluent results in quenching of NO emission, in part due to a decrease of UV radiation below 300 nm [33] due to absorption by water droplets.

Despite some noticeable changes in OES revealed in case of aerosol injection, an overall impact of the aerosol on the discharge effluent is relatively weak and mostly attributed to drop in the emission of Ar I lines and increase of OH emission. The low impact of the aerosol was also confirmed by the effluent imaging presented in **Fig. 4** for both Ar I and OH (A-X) emission. In both conditions, with and without aerosol injection, the profile of the radiation is very similar that indicates a low impact of the aerosol on excited species production that well agrees with OES results. Visible emission of the effluent at 750 nm and 280 nm is detected only 1 mm below the nozzle (**Fig. 4**) what can be assigned to low signal to noise ratio of the camera $SNR=10$. It ensures that during the experiments

that no direct interaction of the plasma with treated media and effect of electrons or charged species on liquid chemistry in the absence of the aerosol can be neglected.

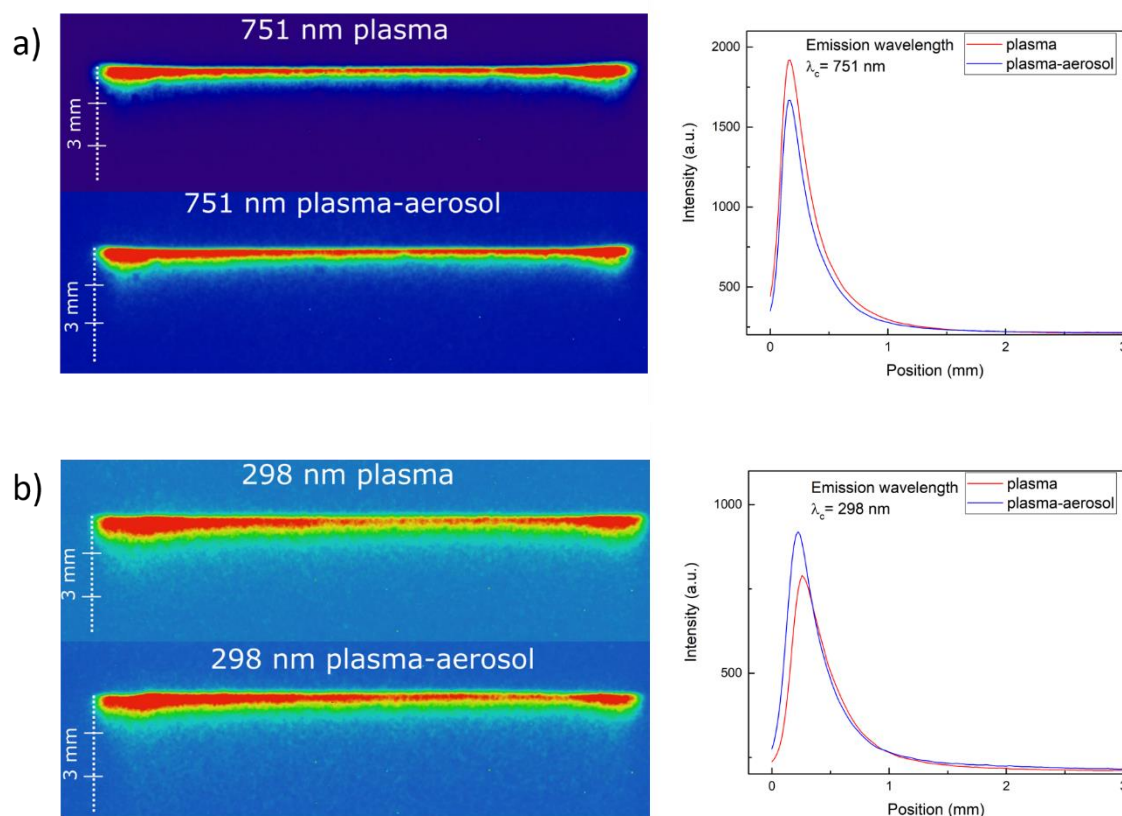


Figure 4. Plasma effluent imaging at two different wavelengths (left) and corresponding intensity profiles (right): a) 751 nm (Ar I emission); b) 298 nm (OH emission) at RF input power $P=30$ W

With the use of FTIR a low production of ozone, below 20 ppm in the gas phase, was confirmed for all plasma and plasma-aerosol conditions. FTIR spectra of Ar jet and jet in contact with water aerosol under operating power 20 W are presented in **Fig. 5**. Rotationally resolved spectra of water molecule bending vibrations $1400\text{--}2000\text{ cm}^{-1}$, and stretching vibration $3600\text{--}4300\text{ cm}^{-1}$, $5100\text{--}5600\text{ cm}^{-1}$ are dominant in all conditions, while ozone peak located at 1051 cm^{-1} , can be also seen in Ar plasma after 5 minutes of operation. In argon plasma without aerosol, a simultaneous decrease of water content and an increase of ozone has been noted from $c(\text{H}_2\text{O})=400$ ppm and $c(\text{O}_3)=1.04$ ppm to $c(\text{H}_2\text{O})=230$ ppm and $c(\text{O}_3)=9.5$ ppm at 20 W RF power after 5 minutes of operation. High amount of H_2O at the beginning of experiments was attributed to adsorption of water vapour on gas tubes and metal body of the jet that is decreasing during the operation. At higher RF power of 30 W higher $c(\text{O}_3)=12.7$ ppm was observed after 5 minutes of operation indicating positive effect of the discharge power on O_3 production. This trend was not observed when aerosol was introduced: the humidity of the trapped gas was significantly higher $c(\text{H}_2\text{O})=1175$ ppm increasing to $c_2(\text{H}_2\text{O})=1500$ ppm during the same time of 5 min, while ozone concentration was constant at $c(\text{O}_3)=3.5$ ppm. The observed lower concentration of ozone in the case of aerosol introduction is very probable due to quenching of O atoms (precursor of O_3 production) by H_2O with formation of OH radicals. No presence of any traces of N_xO_y products was revealed which is well agreed with OES results where both NO and NO_2 peaks were very weak, see Figure 3. This observation indicates that generation of nitrogen reactive species

in RF plasma operation in air with and without aerosol is very ineffective and can be neglected in the analysis of the plasma-initiated chemistry in liquid target.

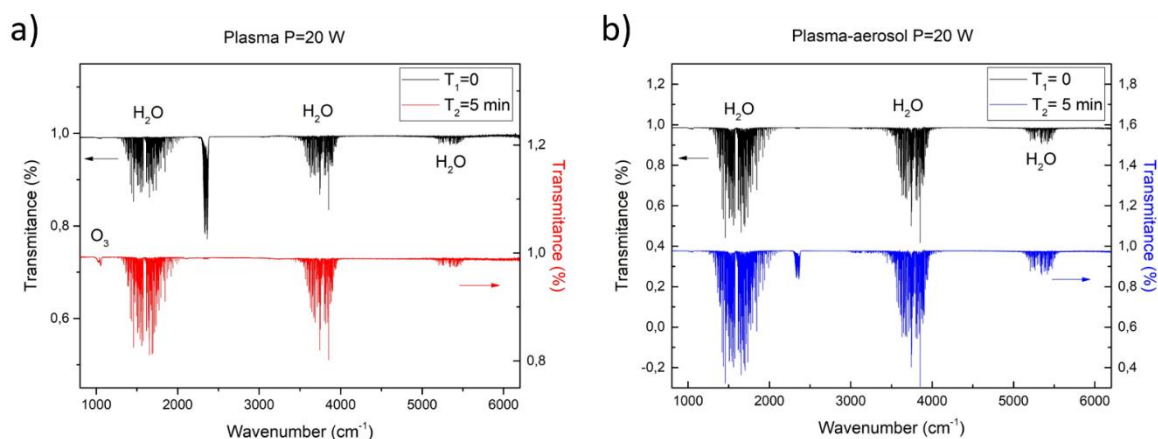


Figure 5. FTIR spectrum in range 800-6200 cm^{-1} of: a) argon plasma jet, b) plasma jet in contact with aerosol at power $P=20\text{W}$.

3.2 Deposition/production of RONS in treated liquids

Due to the importance of plasma-induced chemical process in liquid media for biomedical applications, a chemical analysis of RONS in liquid was performed. Short-lived reactive species, such as atomic oxygen ($\cdot\text{O}$), singlet oxygen ($^1\text{O}_2$), ozone (O_3), hydroxyl radicals ($\cdot\text{OH}$), superoxide anion radicals ($\cdot\text{O}_2^-$), and hydrogen radicals ($\cdot\text{H}$) were analyzed via EPR. The deposition of long-lived reactive species in the treated liquid target was investigated by ion chromatography (nitrite, NO_2^- and nitrate, NO_3^-), and a colorimetric assay (hydrogen peroxide, H_2O_2).

3.2.1 Short-lived reactive species

Using BMPO as a spin trap, hydroxyl radicals ($\cdot\text{OH}$), superoxide anion radicals ($\text{O}_2^{\cdot-}$), and atomic hydrogen ($\cdot\text{H}$) were detected in the liquid target, after treatments with plasma and plasma-aerosol (**Fig. 6**). According to the published trapping efficiencies, the measured concentrations of BMPO-OH represents $\sim 0.6\%$ of the hydroxyl radical [34], and 90% of the superoxide anion radical (BMPO-OOH) [35], while no trapping efficacy of BMPO is known for the hydrogen atoms (BMPO-H). Therefore, significant signal of hydroxyl radicals ($\cdot\text{OH}$) was detected, with considerably lower amounts of $\text{O}_2^{\cdot-}$ and $\cdot\text{H}$. In **Fig. S1**, the measured BMPO peaks and the different simulated BMPO-adducts for treatment with and without the presence of the aerosol after 60 s plasma treatment and for a distance of 12 mm are shown.

Interestingly, the observed species concentrations increased with treatment time and distance. The similar behavior suggested a common origin of the three species. Although keeping the same trends, the presence of aerosol led to their lower deposition. All the three radicals can be formed most likely by the interaction of water molecules with gas phase species, such as Ar metastables [36-39], radicals (e.g. $\cdot\text{O}$) or ozone decay products [40-42]. However, ozone formation is not favored in the discharge, as FTIR data showed trace amounts only.

Considering the reduced production of $\cdot\text{OH}$, $\text{O}_2^{\cdot-}$ and $\cdot\text{H}$ in liquid when water droplets were present in the effluent, the aerosol acted as scavenger partner for high reactive/energetic species. In this case, radiation could play a major role in plasma initiated chemistry in the target leading to water photolysis, due to the increased effective interaction-area between the jet and treated liquid. It has been estimated that effective area of gas-liquid interaction

in 2 mm effluent in case of injection of the aerosol increases from $4.7 \times 10^3 \text{ mm}^2$ to $16.4 \times 10^3 \text{ mm}^2$ and $28.2 \times 10^3 \text{ mm}^2$ at treatment time of 10, 35 and 60 s respectively.

The EPR data confirm the observed decrease in emission of Ar I in the presence of aerosols (**Fig. 4a**), in favor of OH radicals production (**Fig. 4b**). Therefore, the de-novo formation of species occurs mostly at the gas-liquid interface or in the bulk liquid, outcompeting the deposition of species formed in the gas phase. This assumption is supported by previous works, where $\cdot\text{OH}$ formed in the gas phase due to presence of humidity was not transported in the liquid [43, 44]. However, aerosol droplets increased the presence of $\cdot\text{H}$ and $\text{O}_2\cdot^-$ in the target at short distances, suggesting that water droplets transport species to the target liquid. For long distances (12 mm), this transport was not observed and the species decayed before reaching the spin traps/spin probes.

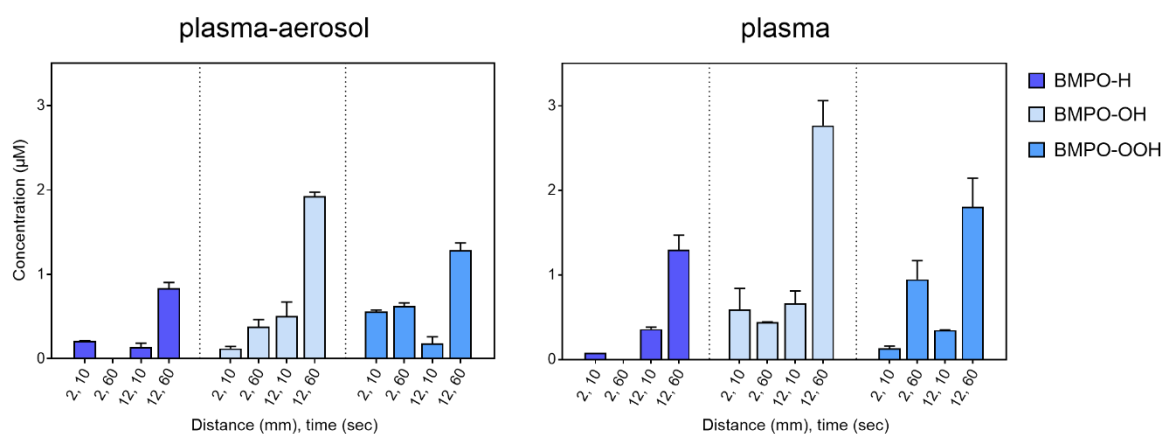


Figure 6. BMPO-adduct concentrations for the different detected radicals after different treatment times (10, 60 s) for 2 and 12 mm with and without the aerosol at RF power of 30 W, setups 3 and 4 respectively.

To obtain further insight, the deposition of O_3 , $^1\text{O}_2$, and $\cdot\text{O}$ were measured using TEMPD. In contrast to BMPO, TEMPD is a spin probe, which means it is reacting with reactive species without binding the species to itself, and therefore, it is not giving a characteristic spectrum for different species and identification is not possible [29, 45]. However, when considering the species different lifetimes, useful information could be obtained. In **Fig. S2**, the detected and simulated peaks of the TEMPD-adduct are given for 60 s and 2 mm treatment distance.

In contrast to the BMPO-adducts, the detected concentrations decreased with increasing treatment distance and increased with treatment time (**Fig. 7**). For 12 mm distance, no signal was detected indicating that long-lived ozone is not relevant for this plasma source. Since the formation of O_3 takes place via a three-body reaction of O_2 and $\cdot\text{O}$ with a third partner [29, 46], the concentrations usually increase with higher distances [29, 47]. However, as shown by FTIR spectroscopy data (Section 3.2), the ozone formation in the gas phase was low (12.7 ppm maximum with an applied plasma power of 30 W), probably due to low density of molecular oxygen in the effluent required for O_3 production [48]. In contrast, signals at 2 and 6 mm show the presence of short-lived atomic or singlet oxygen that are exclusively generated in the gas phase, via a reaction between argon metastables and O_2 [46, 49, 50].

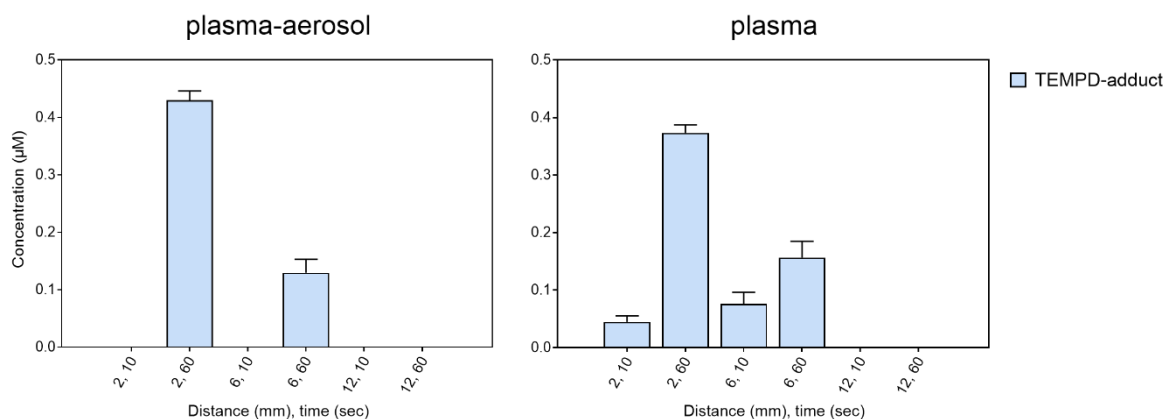


Figure 7. TEMPD-adduct concentrations for the detected species after different treatment times (10, 60 s) for 2, 6 and 12 mm with and without the aerosol presence, setups 3 and 4 respectively.

Summarizing, $\cdot\text{O}$ and/or $\text{O}_2(\text{a}^1\Delta_{\text{g}})$ were the potential candidates for the observed TEMPD adduct. Atomic oxygen is highly reactive and would react with $\cdot\text{OH}$, yielding $\text{HO}_2\cdot/\text{O}_2\cdot^-$ [44], which was not observed during the tests. Hence, the most likely candidate responsible for the EPR signal of TEMPD is $\text{O}_2(\text{a}^1\Delta_{\text{g}})$ in both plasma with and without aerosol. The slight increase of TEMPD-adduct in the presence of the aerosol, potentially reflects enhanced transport of $\text{O}_2(\text{a}^1\Delta_{\text{g}})$ in the aerosol droplets when distances and transfer times are short (2 mm of treatment distance aerosol droplet passes in 40 ms). Only in the case of 10 seconds plasma treatment without aerosol, a formation of an $\cdot\text{O}$ -adduct is possible as these were the conditions with the least interactions in the gas phase. Indeed, the presence of aerosol could scavenge the deposition of $\cdot\text{O}$ by interacting with the water droplets in the gas phase [51, 52].

3.2.2 Long-lived reactive species

The long-lived reactive species hydrogen peroxide (H_2O_2), nitrite (NO_2^-), and nitrate (NO_3^-) were quantified (**Fig. 8**). Nitrite and nitrate can be considered final stable products of the short-lived nitrogen species, such as peroxyxynitrite, NO , or NO_2 radicals [30, 31]. In the same way, hydrogen peroxide, an almost ubiquitous product of cold plasma discharges formed e.g. by the recombination of OH radicals or disproportionation of superoxide anion radicals [30, 31]. The deposited amount of H_2O_2 was significant, also in comparison with other plasma sources [22, 53], reflecting an intensive production of OH radicals in gas and/or liquid phase. In contrast, the deposition of nitrite and nitrate was below the average, indicating a strong dominance of oxygen species, which is in agreement with the FTIR results focused on detection of species in the gas phase. The presence of aerosol reduced the deposition of NO_x^- ions further, indicating that primary species, namely N_xO_y molecules, are generated in the plasma region and not in the plasma/aerosol droplets interface. Additionally, the low solubility of N_xO_y in aqueous media contributes to the observation.

The presence of the aerosol suppressed the deposition of H_2O_2 significantly. Interestingly, plasma only treatments led to a decreased deposition of H_2O_2 with increasing treatment time, while in presence of the aerosol an increased deposition with time was observed at overall low levels. This decay of H_2O_2 in plasma-only conditions could be due to UV radiation-driven photo-dissociation in liquid or the reaction of H_2O_2 with atomic oxygen at the

interphase. For longer distances, deposition decreased due to the lifetime of the precursor species OH and O₂⁻ and decay and competitive reactions occur.

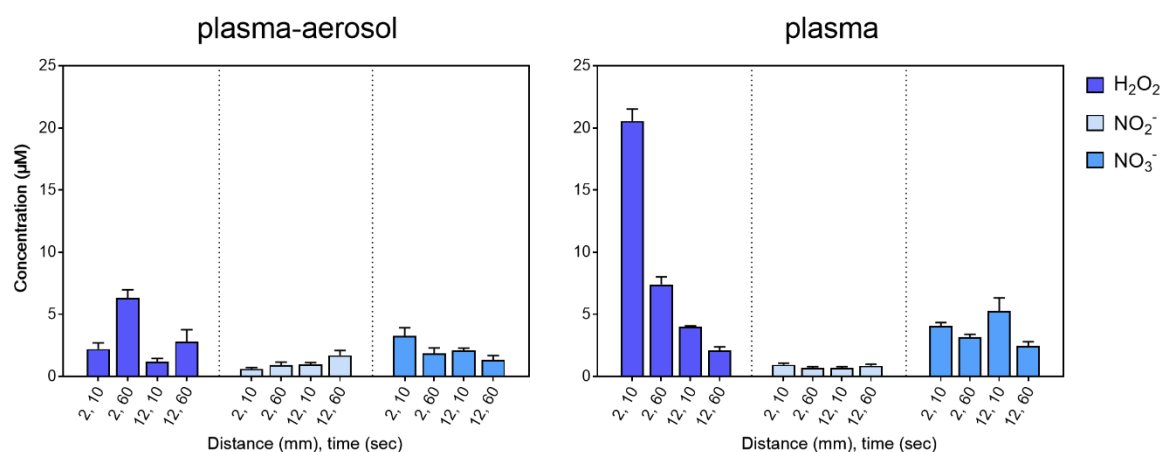


Figure 8. Hydrogen peroxide (H₂O₂), nitrite (NO₂⁻) and nitrate (NO₃⁻) concentrations for the detected species after different treatment times (10, 60 s) for 2 and 12 mm with and without the aerosol presence, setups 3 and 4 respectively.

Among these, the discussed interaction between OH radicals and atomic oxygen is most prominent. Furthermore, the photo-dissociation of long-lived species (or their precursors, e.g. [•]NO₂) occurring by increasing the treatment time could contribute to their decomposition in liquid both for N-containing species [54, 55], and for hydrogen peroxide [54, 56-59], mainly due to Ar excimers radiation (λ_{MAX} = 126 nm). To support this hypothesis, the high amount of species from water photolysis in long distances with plasma-only, shown in **Fig. 6**. As previously discussed, the impact of radiation, as well as other reactive species in the gas phase (e.g. [•]O and ¹O₂) is reduced by the presence of aerosol. This is a very important observation considering that VUV/UV radiation can have an impact on the density of long-living species in the liquid media. However, it has to be mentioned that (V)UV may also have a negative effect due to direct impact on biological samples, e.g. via lipid or protein photo-oxidation. Correspondingly, aerosol injection seems to be very effective method to control amount of (V)UV radiation reaching the target as well as plasma induced chemistry in the liquid phase.

3.3 Cysteine oxidation is modulated by the aerosol

A significant oxidation of cysteine was observed with the thiol group as a main target (**Tab. 2**). Depending on the treatment, oxidation levels of cysteine vary: for short treatments, compounds with a lower oxidation number of sulfur dominate, such as cysteine (2), cysteine sulfinic acid (3), cysteine *S*-sulfonate (6), and cysteine disulfoxides (7-9). These intermediates are not stable and are further oxidized by strong oxidizing conditions (e.g. long treatments, short distances) resulting in compounds with high oxidation states of sulfur, such as cysteine sulfonic acid (5) and sulfate (13), both end products of the cysteine oxidation pathway [22]. Some of the products indicate the presence of certain reactive species [60]: cysteine for the presence of H₂O₂, cysteine-*S*-sulfonate for [•]OH radicals, cysteine sulfonic acid for gas-phase ROS ([•]O, ¹O₂), and cysteine sulfinic acid for both short-lived ROS ([•]O, ¹O₂) and water-derived [•]OH. Control measurement excluded effects of argon flow on cysteine. For the

treatment of liquid targets without cysteine in the aerosol, a direct electron transfer was excluded since the effluent did not touch the liquid. The impact of heat was estimated by control tests performed by incubating cysteine for 1 min at 100 °C. A conversion of 17% cysteine to cystine was observed, and no other cysteine products were detected.

Table 2. Major cysteine derivatives induced by plasma treatment. Further details are described in previous publications [22, 53, 60].

No	Name	Formula	[M-H] ⁻ (m/z)	Reactive species*	Structure
1	Cysteine (RSH)	C ₃ H ₇ NO ₂ S	120.0119	none	
2	Cystine (RSSR)	C ₆ H ₁₂ N ₂ O ₄ S ₂	239.016	•OH, H ₂ O ₂	
3	Cysteine sulfinic acid (RSO ₂ H)	C ₃ H ₇ NO ₄ S	152.0017	•OH, •O, ¹ O ₂	
4	S-nitrosocysteine (RSNO)	C ₃ H ₅ N ₂ O ₃ S	149.0021	•NO, N ₂ O ₃ , •NO ₂ , ONOO•	
5	Cysteine sulfonic acid (RSO ₃ H)	C ₃ H ₇ NO ₅ S	167.9967	•O, ¹ O ₂ , O ₃	
6	Cysteine S-sulfonate (RSSO ₃ H)	C ₃ H ₇ NO ₅ S ₂	199.9687	•OH	
7	Cysteine disulfoxide I (RSO ₂ RS)	C ₆ H ₁₂ N ₂ O ₆ S ₂	271.0056	•OH, H ₂ O ₂	
8	Cysteine disulfoxide II (RSO ₂ RSSR)	C ₉ H ₁₆ N ₃ O ₈ S ₃	390.0100	•OH, H ₂ O ₂ , •O, ¹ O ₂ , O ₃	
9	Cysteine disulfoxone (RSO ₂ RSO ₂)	C ₆ H ₁₀ N ₂ O ₈ S ₂	301.9879	•OH, H ₂ O ₂	
10	Alanine (R)	C ₃ H ₇ NO ₂	88.03985	Radicals, photolysis	
11	Sulfite (SO ₃ ⁻)	SO ₃	79.95681	Radicals, photolysis, ROS	
12	Sulfate (SO ₄ ⁻)	SO ₄	95.95173	Radicals, photolysis, ROS	

*Oxygen and nitrogen reactive species potentially generated by plasma reacting with cysteine to form the correspondent derivative

Species as O₂⁻ could not be detected by using this model, due to their low reactivity towards the thiol moiety in a physiological pH. While the anion sulfite SO₃⁻ it is potentially involved in the formation pathway of the S-sulfonate [61-63], the sulfate ion SO₄⁻ is formed by over-oxidation of cysteine. Those two and the cysteine fragment alanine

could be formed by plasma-derived (V)UV radiation alone via cleavage of the C-S bond and subsequent oxidation of the SH radical [64-66].

3.4.1 The plasma parameters determine the chemistry in the liquid bulk/the interface

The observed cysteine derivatives varied significantly with applied plasma power, treatment time and distance. To obtain quantitative data, the multiple reaction monitoring (MRM) was applied and key molecules in the cysteine oxidation pathway (cysteine – RSH (1), cystine – RSSR (2), cysteine *S*-sulfonate – RSSO₃H (6), sulfinic acid – RSO₂H (3), and sulfonic acid - RSO₃H (5)) were absolutely quantified by HPLC-MS. The MRM technique is both sensitive and specific, relying on the detection of specific fragment ions.

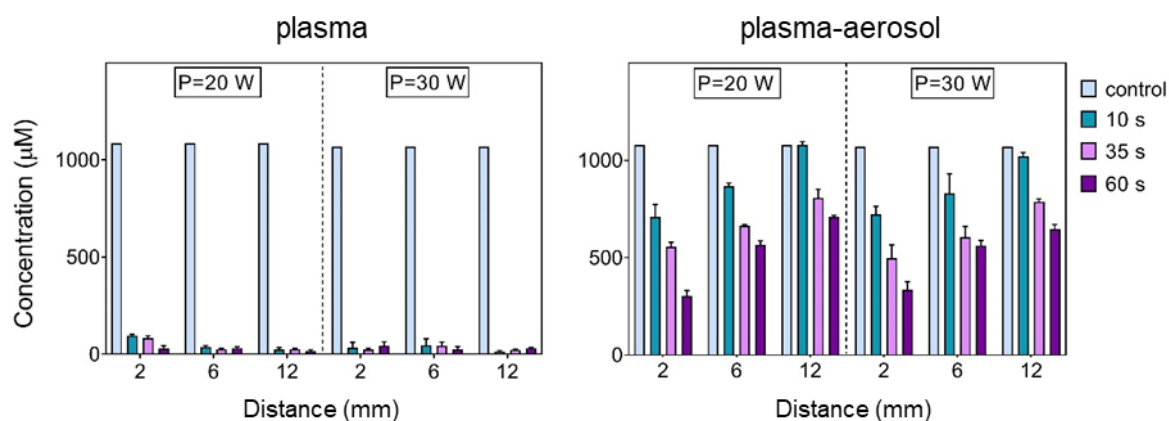


Figure 9. Absolute cysteine concentration after treatment of a cysteine solution by plasma with aerosol injection (setup 3, right) and without aerosol injection (setup 4, left). Power (20/30 W) and distance (2/6/12 mm) modulated. The injection of water into the plasma source massively changed reactive oxygen species output – the cysteine turnover is decreased markedly. See text. Mean of three independent experiments +SD.

Without aerosol injection, a strong, distance and treatment time independent cysteine oxidation was observed (**Fig. 9**). An almost complete oxidation of the available cysteine was observed and the residue was below 5%. In contrast, the presence of aerosol droplets reduced the oxidation efficacy markedly and the residual cysteine ranged between 100 % (20 W, 12 mm, 10 s) and 30 % (30 W, 2 mm, 60 s). Clearly, this indicates a “softer discharge” with a sharply decreased output of reactive oxygen species. The short-lived gas phase species O and ¹O₂ are quenched by the presence of the water, and at the droplets surface water is cleaved forming [•]OH radicals that do not survive the travel time (40 ms/2 mm). In contrast, when cysteine solutions are treated without aerosol injection, the local formation of [•]OH and [•]H by radiation and impact of argon metastables is promoted (see EPR data) and the additional impact of the short-lived gas phase species atomic O and ¹O₂ leads to the observed strong cysteine oxidation (**Fig. 10**). Their presence is distance-dependent, the significant drop of the cysteine-*S*-sulfonate (6) at 12 mm distance proves the limited availability of atomic oxygen at the gas-liquid interface and subsequently [•]OH radicals in accordance with previous results [60]. The formation of highly oxidized cysteine derivatives was still substantial at 12 mm distances. This highlights the potential of the RF jet to produce reactive species surviving 6 mm and more travel distance such as singlet oxygen and (V)UV radiation. With these elements replacing the atomic oxygen, changes related to the distance were less significant than in the plasma-aerosol mode (**Fig. 11**). Cystine could be generated by recombination of thiyl radicals (RS[•]) formed in reaction with [•]OH and [•]H, or by reaction with H₂O₂ [67, 68]. Possibly, the synergistic effect of singlet oxygen and radiation is reflected in the

sulfite and sulfate production. Indeed, radiation (vacuum UV) impact on cysteine molecules yielding to C-S breakage (bond energy 272 kJ mol⁻¹) [54]. The formed product could be further oxidized by oxygen species, e.g. singlet oxygen, to sulfate.

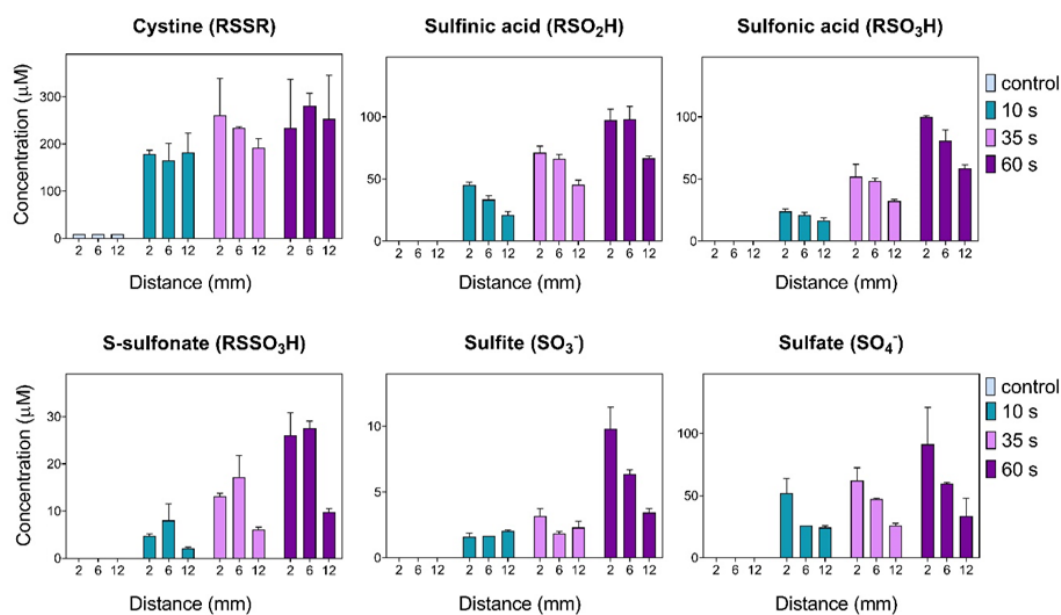


Figure 10. Absolute concentrations of cysteine derivatives after treatment by plasma without aerosol injection (setup 4, cysteine in target) at 30 W power. Time and distance were modulated. Mean of three independent experiments +SD. Cysteine oxidation products obtained with 20 W power are shown in **Fig. S3** and **S4**.

In presence of the aerosol the yield of the observed products changed, with some decreased (**Tab. 2**, compounds 2, 6, 12), others increased (**Tab. 2**, compound 11) or remained at similar level as under non-aerosol conditions (**Tab. 2**, compounds 3, 5). Obvious is a significant influence of the treatment distance, showing an inverted correlation with the product yield (e.g. cysteine sulfonic acid (5)). The pattern confirms the scavenging role of aerosol droplets in the effluent area for radiation and short-lived oxygen species. The resulting OH radicals are lost with distance leading to the observed loss in the yields of [•]OH-dependent derivatives (RSSR, RSSO₃H). Such, the formation of cysteine-S-sulfonate (**Tab. 2**, compound 6) occurred almost 10fold lower in the aerosol condition. In the presence of aerosol droplets, the formation of the stable derivative cysteine sulfonic acid (RSO₃H) increased with treatment time and decreased significantly with the distance. In contrast, distance was of minor impact in the plasma-only mode (**Fig. 10**). Backed up by the EPR data (**Fig. 7, 8**) and the H₂O₂ deposition (**Fig. 10**), atomic oxygen and singlet oxygen represent the most likely candidates to explain this formation pattern. Only small amounts of H₂O₂ and OH radicals are deposited in the aerosol-mode at short distances. In contrast, TEMPD-adducts show the occurrence of singlet oxygen for both conditions and the presence of atomic oxygen at short distances/plasma-only conditions, along with the formation of cysteine sulfonic acid. The transport of ¹O₂ in the liquid droplets might occur for short distances, yielding to the high concentrations of sulfonic acid in this case. This assumption is not fully backed by the EPR data (**Fig. 8**), however, due to fact that the reaction probability with the respective spin probe/label does not allow absolute quantification the transport might not be reflected to a full extent. The ¹O₂ deposition further leads to the decay of intermediate products (RSO₂H, RSSO₃H) yielding to sulfonic acid (RSO₃H) for long treatments.

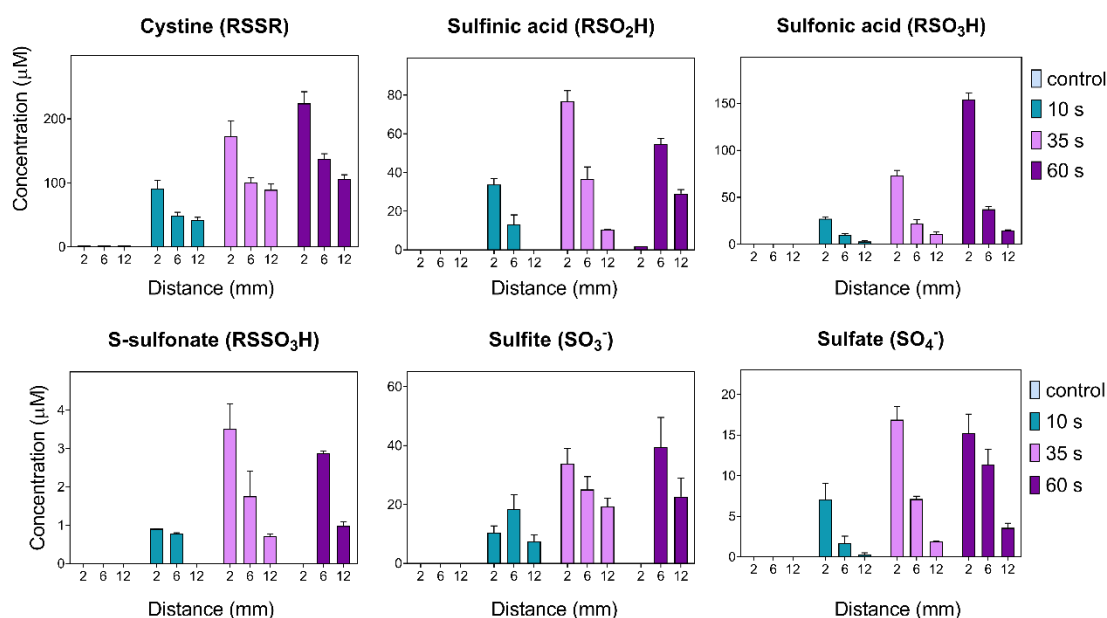


Figure 11. Absolute concentrations of cysteine derivatives after treatment by plasma with aerosol (setup 3, cysteine in target) at power 30 W. Time and distance were modulated. Mean of three independent experiments +SD. Cysteine oxidation products obtained with 20 W power are shown in **Fig. S3** and **S4**.

An interesting and not fully resolved pattern is present for the two ions sulfite and sulfate that both represent fragmentation products of cysteine. They can be formed by different pathways, including impact of (V)UV radiation. The decrease of sulfate deposition in the presence of aerosol confirms role of the droplets as scavengers for radiation and reactive species.

3.4.2 Liquid chemistry induced in the aerosol droplets

The plasma-induced chemistry in the aerosol droplets was investigated to determine the reactive species formed inside and what their fate is during transport (**Fig. 12**). When introducing cysteine into the aerosol droplets, a significant extent of oxidation was observed. The extent depended on the traveling time – with longer distance between nozzle and target (either dry collection into plate or water), yielding in stronger cysteine oxidation. For the 2 mm case when aerosol droplets remain 40 ms in the effluent zone, $37\% \pm 1.4$ and $39\% \pm 1.8$ of the available cysteine was oxidized. This impact was independent from collection time (10 s – 60 s), indicating that the majority of the reactions take place during the droplets transport to the target and not in the collection liquid/the droplet formed during collection. When quantifying the major cysteine derivatives for diverse distances and collection times (**Fig. 13**, **Fig. S5**), similar cysteine derivatives as for the treatment of a cysteine solution were observed. For longer distances, slightly higher amounts of the sulfinic acid (RSO_2H) and the S-sulfonate (RSSO_3H) were observed while the dominant product cysteine sulfonic acid remained unchanged. This sulfonic acid is a marker for short-lived gaseous ROS (e.g. O , $^1\text{O}_2$, [60]) showed a distance-insensitive behavior and accumulated during treatment time - its formation however only occurred during the passage through the active plasma zone emphasizing the interaction of the gas phase species with the surface of the droplets (Ar excimers and (V)UV photons, ^1O , $^1\text{O}_2$). The formation of OH radicals seems to extend beyond the visible effluent zone (2 mm) for some time, as the increased formation of RSO_2H and RSSO_3H with distance suggest..

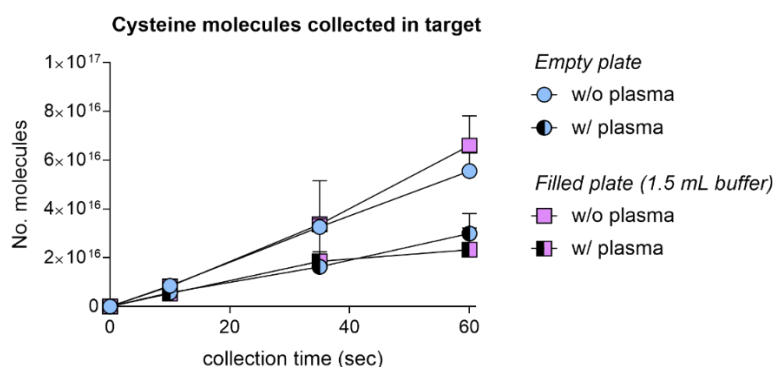


Figure 12. Cysteine turnover in aerosol droplets passing the plasma source with plasma off (full symbols) or plasma on (divided symbols) collected into empty wells (circles) and water filled wells (squares). Plasma power 30 W, 2 mm distance to target (setup 1 and 2). Cysteine oxidation occurs in the droplet during passage of the effluent only (40 ms).

These results confirmed the potential carrier role of droplets in short distances, as well as their scavenging role towards radiation and reactive species in longer distances in favor of the production of water homolysis species (Fig. 11).

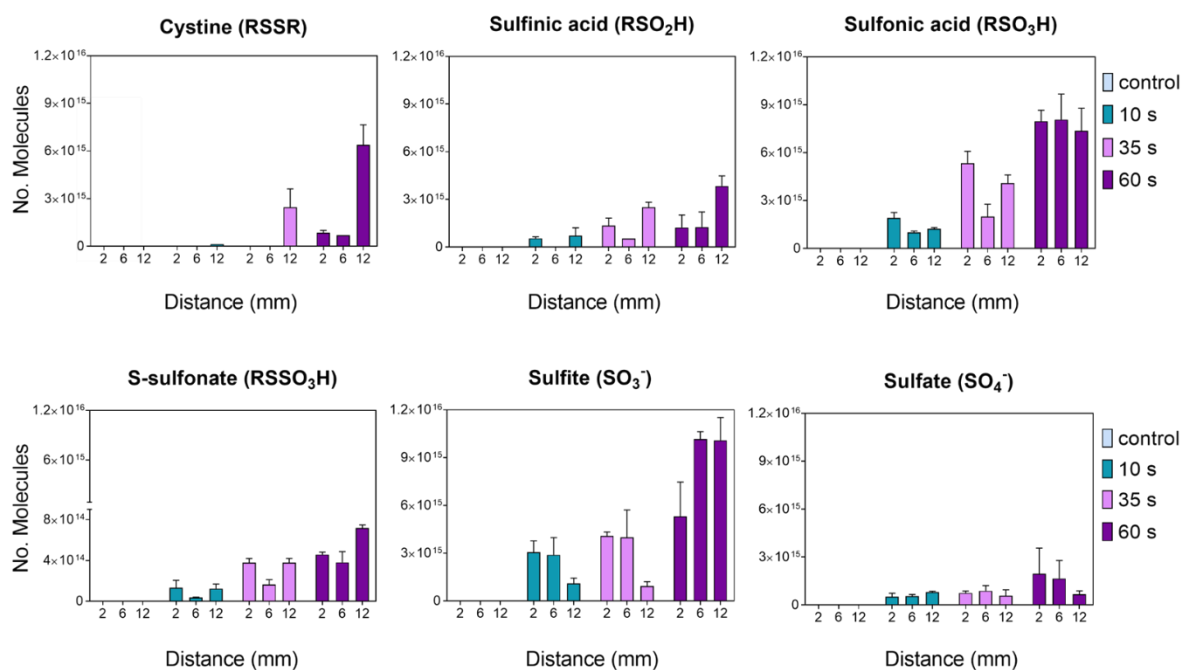


Figure 13. Major cysteine conversion products observed in cysteine-enriched aerosol droplets. Plasma power 30 W (setup 2, cysteine in aerosol), collected in water filled wells. The absolute number of molecules deposited are given. The limited impact of distance indicates that the majority of reactions occurs in the droplets. Further discussion see text.

3.4.3 Cysteine conversion pathways by RF jet derived species

In this work plasma interaction with liquid phase was investigated in 3 different model systems, namely, (i) plasma with cysteine in liquid target; (ii) plasma with aerosol and cysteine in liquid target; (iii) plasma interaction with cysteine-enriched aerosol injection into the effluent. To compare the effectiveness of different setups in terms of

cysteine oxidation and its conversion into derivatives, measured absolute concentration are hereby recalibrated in percentages % for each setup (**Fig. 14**). Additionally to the schematic of the cysteine oxidation, a complete overview for different treatment distances is summarized in **Tab. 3**.

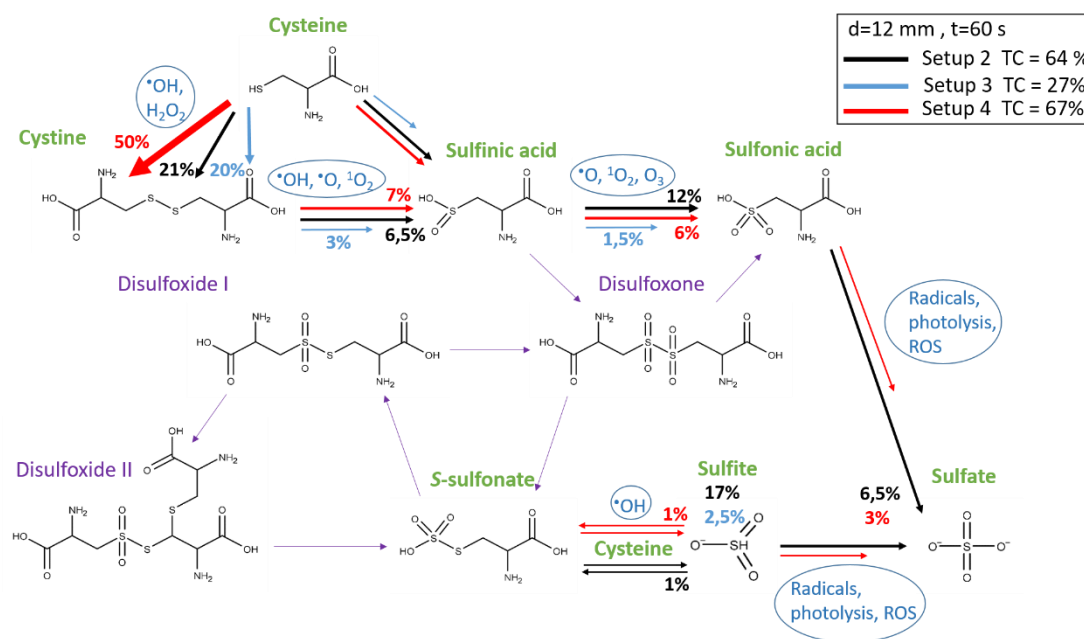


Figure 14. Cysteine oxidation pathway example and its total conversion for experimental parameters $P = 30$ W, $d = 12$ mm, $t = 60$ s. Generation of six major cysteine derivatives in Setup 2 (cysteine in aerosol, black), Setup 3 (plasma with aerosol-cysteine in target, blue) and Setup 4 (plasma-cysteine in target, red) is presented in percentage, for better comparison of processes. The quantified derivatives are labelled in green color.

As expected, the conversion of cysteine is highest for the direct plasma treatment of a cysteine-containing target liquid. In this case, the distance is of little importance and conversion is still massive at 12 mm. In contrast, when the discharge is injected with water droplets, the cysteine oxidation drops significantly even for 2 mm distance and further with increasing distance to the nozzle (**Tab. 3**). When the aerosol is enriched with cysteine, the observed product portfolio indicates that the majority of the reactions take place in the droplet during the passage of the visible effluent (40 ms/2 mm). The increase of the metastable cysteine products S-sulfonate and sulfinic acid with increasing distance show a residual formation of hydroxyl radicals beyond the effluent visible margins.

Table 3. Cysteine conversion into 6 quantified derivatives during the treatment time of 60 s for treatment distances 2, 6 and 12 mm from effluent in Setups 2,3 and 4.

Setup	Treatment distance (mm)	Cysteine conversion (%)
Setup 2 Plasma treatment of cysteine in aerosol liquid	2	45
	6	50
	12	64
Setup 3 Plasma-aerosol treatment of cysteine in liquid target	2	60
	6	43
	12	27
Setup 4 Plasma treatment of cysteine in liquid target	2	78
	6	83
	12	67

4. CONCLUSIONS

The chemistry at plasma/liquid interface and liquid chemistry induced in the effluent area and liquid target of a hybrid RF plasma jet was analyzed using cysteine as a bait molecule, particularly focusing on the role of aerosol droplets in the effluent. The deposition of OH, O₂⁻, and O, ¹O₂, and O₃ were measured via EPR; and the long-lived species H₂O₂, NO₂⁻, and NO₃⁻ were quantified by colorimetric assays and ion chromatography. Data analysis revealed that UV radiation (e.g. VUV of Ar excimers), followed by short-lived reactive oxygen species (e.g. [•]O, ¹O₂), are the dominant active elements in the studied RF plasma jet. Acting directly on the liquid target or on the aerosol droplets, cysteine oxidation products and water photolysis products ([•]OH, [•]H) were observed. A summary of the model and the observations made is presented in Figure 15.

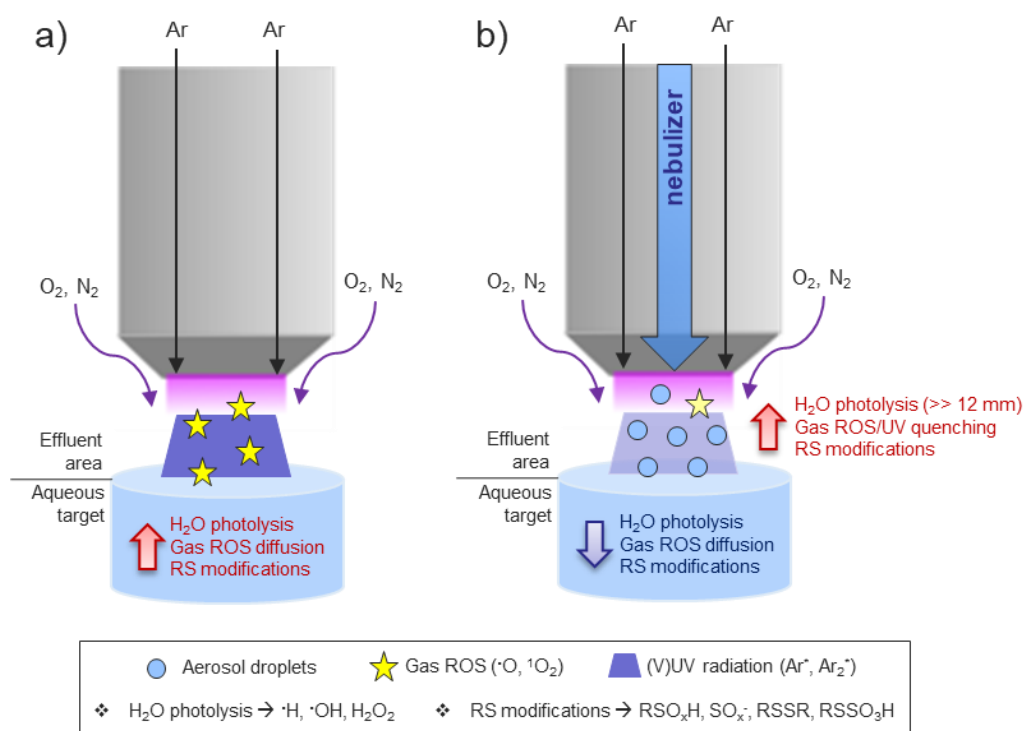


Figure 15. Overview of cold plasma effects without (a) and with (b) aerosol droplets in the effluent area.

By controlling distance, treatment time, and the presence of aerosol droplets the liquid phase chemistry can be adjusted. Short-lived gaseous species (e.g. [•]O, ¹O₂) were detected predominantly for short distances and in parallel, distinct cysteine oxidation products were observed, confirming ROS potential biological impact. In the presence of aerosol droplets, the impact of these species was diminished significantly yet cysteine sulfonic acid, a marker for gas phase ROS at the gas-liquid interface, was still detected. Taking the EPR data into account it was concluded that singlet oxygen ¹O₂ prevails for middle and long distances (6 - 12 mm) and in the presence of aerosol. The impact of (V)UV radiation on the liquid target was strong, leading to photo-dissociation of water molecules as well as cysteine and the formation of short-lived radicals (e.g. [•]OH, [•]H, SH), as confirmed by EPR and the detection of sulfite/sulfate by mass spectrometry. Again, the presence of aerosol droplets in the effluent quenched the (V)UV photons and related reactions in the target. Instead, water molecules in the droplets were attacked, forming e.g. OH radicals. The transport of species formed in or solvated by the droplets was found to be of minor importance. This hypothesis was confirmed by introducing cysteine solution directly in form of aerosol droplets and the

1
2
3 observation of cysteine derivatives produced predominantly by OH radicals (cystine, sulfinic acid, cysteine-S-
4 sulfonate). The impact of (V)UV radiation was observed by the formation of sulfite from cysteine-containing
5 droplets.
6

7 In conclusion, the chemical potential of the investigated hybrid RF plasma jet allows to be tuned in a wide range,
8 proposing its application for various biomedical purposes. The intense synergistic effects of radiation and short-
9 lived gaseous species achieved by using the plasma-only mode could be relevant for cancer treatment. In contrast,
10 softer conditions including aerosol droplets could limit the impact of radiation and other gaseous radical species,
11 and be of interest in wound care field.
12
13
14
15
16

17 **ACKNOWLEDGEMENTS**

18 The research work performed was supported by German Federal Ministry of Education and Research (grant
19 number 03Z22DN12 to K.W.) and FWO/ARRS agencies project “Plasma-skin interactions: from wound treatment
20 to topical introduction of molecules”, numbers G084917N and N3-0056, respectively.
21
22
23
24

25 **CONFLICT OF INTEREST**

26 The authors declare no conflict of interest.
27
28
29
30
31
32
33
34
35
36
37
38
39
40
41
42
43
44
45
46
47
48
49
50
51
52
53
54
55
56
57
58
59
60

REFERENCES

1. Laroussi, M., *Low temperature plasma-based sterilization: overview and state-of-the-art*. Plasma processes and polymers, 2005. **2**(5): p. 391-400.
2. Laroussi, M., *Sterilization of contaminated matter with an atmospheric pressure plasma*. Ieee Transactions on Plasma Science, 1996. **24**(3): p. 1188-1191.
3. Weltmann, K.D., et al., *Atmospheric-pressure plasma sources: Prospective tools for plasma medicine*. Pure and Applied Chemistry, 2010. **82**(6): p. 1223-1237.
4. Weltmann, K. and T. Von Woedtke, *Plasma medicine—current state of research and medical application*. Plasma Physics and Controlled Fusion, 2016. **59**(1): p. 014031.
5. Kong, M.G., et al., *Plasma medicine: an introductory review*. new Journal of Physics, 2009. **11**(11): p. 115012.
6. Bruggeman, P.J., F. Iza, and R. Brandenburg, *Foundations of atmospheric pressure non-equilibrium plasmas*. Plasma Sources Science & Technology, 2017. **26**(12): p. 123002.
7. Fridman, A.A., et al., *The Plasma Treatment Unit: An Attempt to Standardize Cold Plasma Treatment for Defined Biological Effects*. Plasma Medicine, 2018. **8**(2): p. 195-201.
8. Stratmann, B., et al., *Effect of Cold Atmospheric Plasma Therapy vs Standard Therapy Placebo on Wound Healing in Patients With Diabetic Foot Ulcers: A Randomized Clinical Trial*. JAMA Netw Open, 2020. **3**(7): p. e2010411.
9. Shome, D., et al., *The HIPPO Transducer YAP and Its Targets CTGF and Cyr61 Drive a Paracrine Signalling in Cold Atmospheric Plasma-Mediated Wound Healing*. Oxid Med Cell Longev, 2020. **2020**: p. 4910280.
10. Lin, A., et al., *Plasma Elicits Immunogenic Death In Melanoma Cells*. Clinical Plasma Medicine, 2018. **9**.
11. Bekeschus, S., et al., *Ex Vivo Exposure of Human Melanoma Tissue to Cold Physical Plasma Elicits Apoptosis and Modulates Inflammation*. Applied Sciences, 2020. **10**(6): p. 1971.
12. Schmidt, A., et al., *Nrf2 signaling and inflammation are key events in physical plasma-spurred wound healing*. Theranostics, 2019. **9**(4): p. 1066-1084.
13. Privat-Maldonado, A., et al., *ROS from Physical Plasmas: Redox Chemistry for Biomedical Therapy*. Oxid Med Cell Longev, 2019. **2019**: p. 9062098.
14. Xu, X., *Dielectric barrier discharge—properties and applications*. Thin solid films, 2001. **390**(1-2): p. 237-242.
15. Brandenburg, R., *Dielectric barrier discharges: progress on plasma sources and on the understanding of regimes and single filaments*. Plasma Sources Science & Technology, 2017. **26**(5): p. 053001.
16. Reuter, S., T. Von Woedtke, and K.-D. Weltmann, *The kINPen—a review on physics and chemistry of the atmospheric pressure plasma jet and its applications*. Journal of Physics D: Applied Physics, 2018. **51**(23): p. 233001.
17. Sremački, I., et al., *On diagnostics of an annular shape RF plasma jet operating in Ar at atmospheric conditions*. Plasma Sources Science and Technology, 2020.
18. von Woedtke, T., et al., *Plasma Medicine: A field of applied redox biology*. in vivo, 2019. **33**(4): p. 1011-1026.
19. Schieber, M. and N.S. Chandel, *ROS function in redox signaling and oxidative stress*. Current biology, 2014. **24**(10): p. R453-R462.
20. Weidinger, A. and A.V. Kozlov, *Biological activities of reactive oxygen and nitrogen species: oxidative stress versus signal transduction*. Biomolecules, 2015. **5**(2): p. 472-484.
21. Strollo, R., et al., *Antibodies to post-translationally modified insulin in type 1 diabetes*. Diabetologia, 2015. **58**(12): p. 2851-60.
22. Bruno, G., et al., *Cold physical plasma-induced oxidation of cysteine yields reactive sulfur species (RSS)*. Clinical Plasma Medicine, 2019. **14**: p. 100083.
23. Klinkhammer, C., et al., *Elucidation of Plasma-induced Chemical Modifications on Glutathione and Glutathione Disulphide*. Sci Rep, 2017. **7**(1): p. 13828.
24. Takai, E., et al., *Chemical modification of amino acids by atmospheric-pressure cold plasma in aqueous solution*. Journal of Physics D-Applied Physics, 2014. **47**(28): p. 285403.
25. Lackmann, J.W., et al., *Chemical fingerprints of cold physical plasmas - an experimental and computational study using cysteine as tracer compound*. Sci Rep, 2018. **8**(1): p. 7736.

- 1
2
3 26. Go, Y.M., J.D. Chandler, and D.P. Jones, *The cysteine proteome*. Free Radic Biol Med, 2015. **84**: p. 227-245.
- 4
5 27. Verlackt, C., W. Van Boxem, and A. Bogaerts, *Transport and accumulation of plasma*
6 *generated species in aqueous solution*. Physical Chemistry Chemical Physics, 2018. **20**(10): p.
7 6845-6859.
- 8
9 28. Tresp, H., et al., *Quantitative detection of plasma-generated radicals in liquids by electron*
10 *paramagnetic resonance spectroscopy*. Journal of Physics D: Applied Physics, 2013. **46**(43).
- 11
12 29. Jablonowski, H., et al., *Quantification of the ozone and singlet delta oxygen produced in gas*
13 *and liquid phases by a non-thermal atmospheric plasma with relevance for medical treatment*.
14 Sci Rep, 2018. **8**(1): p. 12195.
- 15
16 30. Jablonowski, H., et al., *Non-touching plasma-liquid interaction - where is aqueous nitric*
17 *oxide generated?* Phys Chem Chem Phys, 2018. **20**(39): p. 25387-25398.
- 18
19 31. Verlackt, C.C.W., W. Van Boxem, and A. Bogaerts, *Transport and accumulation of plasma*
20 *generated species in aqueous solution*. Phys Chem Chem Phys, 2018. **20**(10): p. 6845-6859.
- 21
22 32. Nikiforov, A.Y., et al., *Characterization of a planar 8 mm atmospheric pressure wide*
23 *radiofrequency plasma source by spectroscopy techniques*. Plasma Physics and Controlled
24 Fusion, 2015. **58**(1): p. 014013.
- 25
26 33. Jablonowski, H., et al., *Impact of plasma jet vacuum ultraviolet radiation on reactive oxygen*
27 *species generation in bio-relevant liquids*. Physics of plasmas, 2015. **22**(12): p. 122008.
- 28
29 34. Rosen, G.M., et al., *The role of tetrahydrobiopterin in the regulation of neuronal nitric-oxide*
30 *synthase-generated superoxide*. J Biol Chem, 2002. **277**(43): p. 40275-80.
- 31
32 35. Tong, H., et al., *Hydroxyl radicals from secondary organic aerosol decomposition in water*.
33 Atmospheric Chemistry and Physics, 2016. **16**(3): p. 1761-1771.
- 34
35 36. Lisovskaya, A.G., I.P. Edimecheva, and O.I. Shadyro, *A Novel Pathway of Photoinduced*
36 *Decomposition of Sphingolipids*. Photochemistry and Photobiology, 2012. **88**(4): p. 899-903.
- 37
38 37. Zvereva, G.N., *Using vacuum ultraviolet radiation to obtain highly reactive radicals*. Journal
39 of Optical Technology, 2012. **79**(8): p. 477-483.
- 40
41 38. Jablonowski, H., et al., *Plasma Jet (V) UV-Radiation Impact on Biologically Relevant Liquids*
42 *and Cell Suspension*. Bulletin of the American Physical Society, 2014. **59**.
- 43
44 39. Attri, P., et al., *Generation mechanism of hydroxyl radical species and its lifetime prediction*
45 *during the plasma-initiated ultraviolet (UV) photolysis*. Sci Rep, 2015. **5**: p. 9332.
- 46
47 40. Hoigne, J. and H. Bader, *Ozonation of Water - Kinetics of Oxidation of Ammonia by Ozone*
48 *and Hydroxyl Radicals*. Environmental Science & Technology, 1978. **12**,6(1): p. 79-84.
- 49
50 41. Hoigné, J., *The Chemistry of Ozone in Water*. 1988: p. 121-141.
- 51
52 42. Flyunt, R., et al., *Determination of $\cdot\text{OH}$, $\text{O}_2\cdot^-$, and Hydroperoxide Yields in Ozone Reactions*
53 *in Aqueous Solution*. The Journal of Physical Chemistry B, 2003. **107**(30): p. 7242-7253.
- 54
55 43. Gorbanev, Y., D. O'Connell, and V. Chechik, *Non-Thermal Plasma in Contact with Water:*
56 *The Origin of Species*. Chemistry, 2016. **22**(10): p. 3496-3505.
- 57
58 44. Winter, J., et al., *Feed gas humidity: a vital parameter affecting a cold atmospheric-pressure*
59 *plasma jet and plasma-treated human skin cells*. Journal of Physics D-Applied Physics, 2013.
60 **46**(29).
45. Hideg, E., et al., *Pure forms of the singlet oxygen sensors TEMP and TEMPD do not inhibit*
61 *Photosystem II*. Biochim Biophys Acta, 2011. **1807**(12): p. 1658-61.
46. Schmidt-Bleker, A., et al., *On the plasma chemistry of a cold atmospheric argon plasma jet*
62 *with shielding gas device*. Plasma Sources Science and Technology, 2016. **25**(1): p. 015005.
47. Zhang, S.Q., et al., *Spatially resolved ozone densities and gas temperatures in a time*
63 *modulated RF driven atmospheric pressure plasma jet: an analysis of the production and*
64 *destruction mechanisms*. Journal of Physics D-Applied Physics, 2013. **46**(20): p. 205202.
48. Pekárek, S., *Non-Thermal Plasma Ozone Generation*. Acta Polytechnica, 2003. **43**: p. 5.
49. Reuter, S., T. von Woedtke, and K.D. Weltmann, *The kINPen-a review on physics and*
65 *chemistry of the atmospheric pressure plasma jet and its applications*. Journal of Physics D-
66 Applied Physics, 2018. **51**(23).
50. Van Gaens, W. and A. Bogaerts, *Kinetic modelling for an atmospheric pressure argon plasma*
67 *jet in humid air*. Journal of Physics D: Applied Physics, 2013. **46**(27): p. 275201.
51. Quiller, R.G., et al., *Transient hydroxyl formation from water on oxygen-covered Au(111)*. J
68 Chem Phys, 2008. **129**(6): p. 064702.

- 1
2
3 52. Lifshitz, C., *Reaction mechanism of mononegative atomic oxygen + water .fwdarw. hydroxide*
4 *+ hydroxyl at low incident ion energies*. The Journal of Physical Chemistry, 1982. **86**(18): p.
5 3634-3637.
- 6 53. Lackmann, J.-W., et al., *Nitrosylation vs. oxidation - How to modulate cold physical plasmas*
7 *for biological applications*. PLoS One, 2019. **14**(5): p. e0216606.
- 8 54. Zoschke, K., H. Bornick, and E. Worch, *Vacuum-UV radiation at 185 nm in water treatment--*
9 *a review*. Water Res, 2014. **52**: p. 131-45.
- 10 55. Goldstein, S. and J. Rabani, *Mechanism of Nitrite Formation by Nitrate Photolysis in Aqueous*
11 *Solutions: The Role of Peroxynitrite, Nitrogen Dioxide, and Hydroxyl Radical*. Journal of the
12 American Chemical Society, 2007. **129**(34): p. 10597-10601.
- 13 56. Gölzenleuchter, H., et al., *Photodissociation of hydrogen peroxide at 157 nm: rotational*
14 *distribution of nascent OH(2Σ+, v', N')*. Chemical Physics, 1984. **89**(1): p. 93-102.
- 15 57. Nakamura, K., et al., *Hydroxyl radicals generated by hydrogen peroxide photolysis*
16 *recondition biofilm-contaminated titanium surfaces for subsequent osteoblastic cell*
17 *proliferation*. Sci Rep, 2019. **9**(1): p. 4688.
- 18 58. Ikai, H., et al., *Photolysis of hydrogen peroxide, an effective disinfection system via hydroxyl*
19 *radical formation*. Antimicrob Agents Chemother, 2010. **54**(12): p. 5086-91.
- 20 59. France, J.L., M.D. King, and J. Lee-Taylor, *Hydroxyl (OH) radical production rates in*
21 *snowpacks from photolysis of hydrogen peroxide (H2O2) and nitrate (NO3-)*. Atmospheric
22 Environment, 2007. **41**(26): p. 5502-5509.
- 23 60. Wende, K., et al., *On a heavy path – determining cold plasma-derived short-lived species*
24 *chemistry using isotopic labelling*. RSC Advances, 2020. **10**(20): p. 11598-11607.
- 25 61. Bailey, J.L. and R.D. Cole, *Studies on the Reaction of Sulfite with Proteins*. Journal of
26 Biological Chemistry, 1959. **234**(7): p. 1733-1739.
- 27 62. Gunnison, A.F. and E.D. Palmes, *Species variability in plasma S-sulfonate levels during and*
28 *following sulfite administration*. Chemico-Biological Interactions, 1978. **21**(2-3): p. 315-329.
- 29 63. Gunnison, A.F. and A.W. Benton, *Sulfur dioxide: Sulfite. Interaction with mammalian serum*
30 *and plasma*. Arch Environ Health, 1971. **22**(3): p. 381-8.
- 31 64. Darwent, B.d., *Bond dissociation energies in simple molecules*. NSRDS-NBS31. 1970,
32 [Washington]: U.S. National Bureau of Standards; for sale by the Supt. of Docs., U.S. Govt.
33 Print. Off. iv, 48 p.
- 34 65. Mackle, H., *The thermochemistry of sulphur-containing molecules and radicals—II*.
35 Tetrahedron, 1963. **19**(7): p. 1159-1170.
- 36 66. Jablonowski, H., et al., *Impact of plasma jet vacuum ultraviolet radiation on reactive oxygen*
37 *species generation in bio-relevant liquids*. Physics of Plasmas, 2015. **22**(12): p. 122008.
- 38 67. Kalyanaraman, B., *Thiyl radicals in biological systems: significant or trivial?* Biochem Soc
39 Symp, 1995. **61**: p. 55-63.
- 40 68. Sevilla, M.D., D. Becker, and M. Yan, *The formation and structure of the sulfoxyl radicals*
41 *RSO(·), RSOO(·), RSO2(·), and RSO2OO(·) from the reaction of cysteine, glutathione and*
42 *penicillamine thiyl radicals with molecular oxygen*. Int J Radiat Biol, 1990. **57**(1): p. 65-81.
43
44
45
46
47
48
49
50
51
52
53
54
55
56
57
58
59
60

7. **Eigenständigkeitserklärung**

Hiermit erkläre ich, dass diese Arbeit bisher von mir weder an der Mathematisch-Naturwissenschaftlichen Fakultät der Universität Greifswald noch einer anderen wissenschaftlichen Einrichtung zum Zwecke der Promotion eingereicht wurde.

Ferner erkläre ich, dass ich diese Arbeit selbstständig verfasst und keine anderen als die darin angegebenen Hilfsmittel und Hilfen benutzt und keine Textabschnitte eines Dritten ohne Kennzeichnung übernommen habe.

Date

Giuliana Bruno

8. Curriculum Vitae

Giuliana Bruno

Gützkower Landstraße 8H
17489 Greifswald, Germany
Phone: +39 345 32 55 711
Email: giuliana.bruno4@gmail.com

Born: May 4th, 1991 in Salerno, Italy
Nationality: Italian

Professional Experience

Since 06/2017	SCIENTIST, at Leibniz Institute for Plasma Science and Technology (INP), Greifswald, Germany
03/2016 – 04/2017	INTERNSHIP, at CEINGE – Advanced Biotechnologies, Naples, and at Laboratory Medicine Department of “Federico II” Hospital, Naples, Italy
09/2013 – 07/2014	INTERNSHIP, at LICA – Hydrology and Food Chemistry Lab, Pharmacy Department, University of Salerno, Fisciano, Italy

Education

Since 06/2017	PHD CANDIDATE, at Ernst Moritz Arndt University of Greifswald, Germany
10/2014 - 12/2016	MASTER of SCIENCE (in Pharmaceutical, Veterinary and Medical Biotechnologies), at University of Sannio, Benevento, Italy
09/2010 – 07/2014	BACHELOR of SCIENCE (in Pharmaceutical Sciences and Technologies), at University of Salerno, Fisciano, Italy
09/2005 – 07/2010	HIGH SCHOOL DIPLOMA (qualification in classical studies for university entrance), at Liceo Classico Torquato Tasso, Salerno, Italy

Honour & Awards

2014 | SCHOLARSHIP STUDENT (reserved for the 10 students admitted to the master course in Pharmaceutical, Veterinary and Medical Biotechnologies, offered by Biogem Campus, Ariano Irpino, Italy)

Date

Giuliana Bruno

9. List of Publications & Conference Contributions

Publications in Peer Reviewed Journals

- G. Bruno, S. Wenske, J.-L. Lackmann, M. Lalk, T. von Woedtke, K. Wende. "On the liquid chemistry of the reactive nitrogen species peroxyxynitrite and nitrogen dioxide generated by physical plasmas". *Biomolecules*, under revision, 2020.
- Sremački & G. Bruno, H. Jablonowski, C. Leys, A. Nikiforov, K. Wende. "Influence of aerosol injection on the liquid chemistry induced by an RF argon plasma jet". *Plasma Sources Science and Technology*, under revision, 2020.
- Z. Nasri, G. Bruno, S. Bekeschus, K.-D. Weltmann, T. von Woedtke, and K. Wende. "Development of an electrochemical sensor for in-situ monitoring of reactive species produced by cold physical plasma". *Sensors and Actuators B: Chemical*, vol. 326, accepted, 2021.
- K. Wende, G. Bruno, M. Lalk, K.-D. Weltmann, T. von Woedtke, S. Bekeschus, J.-W. Lackmann. "On a heavy path – determining cold plasma-derived short-lived species chemistry using isotopic labelling". *RSC Advances*, vol. 10, no. 20, pp. 11598-11607, 2020.
- J.-W. Lackmann & G. Bruno, H. Jablonowski, F. Kogelheide, B. Offerhaus, J. Held, V. S.-von der Gathen, K. Stapelmann, T. von Woedtke, K. Wende. "Nitrosylation vs. oxidation - How to modulate cold physical plasmas for biological applications". *PLoS One*, vol. 14, no. 5, p. e0216606, 2019.
- G. Bruno, T. Heusler, J.-W. Lackmann, T. von Woedtke, K.-D. Weltmann, and K. Wende, "Cold physical plasma-induced oxidation of cysteine yields reactive sulfur species (RSS)". *Clinical Plasma Medicine*, vol. 14, p. 100083, 2019.
- T. Heusler, G. Bruno, S. Bekeschus, J.-W. Lackmann, T. von Woedtke, and K. Wende. "Can the effect of cold physical plasma-derived oxidants be transported via thiol group oxidation?". *Clinical Plasma Medicine*, vol. 14, p. 100086, 2019.
- M. Caterino, M. Zacchia, M. Costanzo, G. Bruno, D. Arcaniolo, F. Trepiccione, R. A. Siciliano, M. F. Mazzeo, M. Ruoppolo, G. Capasso. "Urine Proteomics Revealed a Significant Correlation Between Urine-Fibronectin Abundance and Estimated-GFR Decline in Patients with Bardet-Biedl Syndrome". *Kidney and Blood Pressure Research* vol. 43(2), pp. 389-405, 2018.
- M. Costanzo, M. Zacchia, G. Bruno, D. Crisci, M. Caterino, M. Ruoppolo. "Integration of Proteomics and Metabolomics in Exploring Genetic and Rare Metabolic Diseases". *Kidney Diseases*, vol. 3(2), pp. 66-77, 2017.

Contributions to Workshops and Conferences

Oral presentations

- G. Bruno, H. Jablonowski, J.-L. Lackmann, M. Lalk, T. von Woedtke, K. Wende. "Gas plasmas as source of reactive species: cysteine as molecular beacon". *Oxidative Stress Reduction, Redox Homeostasis and Antioxidants (Paris Redox 2020)*. Virtual International Congress. October, 2020.
- G. Bruno, H. Jablonowski, J.-L. Lackmann, M. Lalk, T. von Woedtke, K. Wende. "Physical plasmas as source of reactive species: cysteine as molecular beacon". *Baltic Redox Workshop*. Virtual Conference. September, 2020.
- G. Bruno, J.-L. Lackmann, K.-D. Weltmann, T. von Woedtke, M. Lalk, K. Wende. "Potential of plasmas in inducing N₂-driven modifications on small bio-molecules". *Plasma-Biomed-Workshop*. Neumünster, Germany. October, 2019.
- G. Bruno, J.-L. Lackmann, K.-D. Weltmann, T. von Woedtke, K. Wende. "Plasma-induced species deposited in liquids: On the Sulphur oxidation path to elucidate predominant chemical dynamics". *24th International Symposium on Plasma Chemistry (ISPC24)*. Naples, Italy. June, 2019.
- G. Bruno, T. Heusler, J.-L. Lackmann, K.-D. Weltmann, T. von Woedtke, K. Wende. "Investigating the role of water derived species in cold plasma effectiveness". *7th Young Professionals Workshop on Plasma Medicine - Frontiers in Redox Biochemistry and Medicine (FiRBaM)*. Rostock, Germany. September, 2018.
- G. Bruno, T. Heusler, H. Jablonowski, J.-L. Lackmann, K. Wende. "Mass spectrometry based analysis of the oxidation compounds produced by cold atmospheric plasma (CAP) interaction with cysteine". *Frontiers in Redox Biology and Chemistry (FiRBaC)*. Rostock, Germany. October, 2017.

Poster presentations

- G. Bruno, J.-L. Lackmann, K.-D. Weltmann, T. von Woedtke, K. Wende. "MS-based strategies to study cold plasmas: a model based on thiol modifications". *52nd annual meeting of the German Society for Mass Spectrometry (DGMS)*. Rostock, Germany. March, 2019.
- G. Bruno, J.-L. Lackmann, T. Heusler, K.-D. Weltmann, T. von Woedtke, K. Wende. "MS-study of thiol modifications induced by cold plasma and their cellular effects". *Redox-omics Technologies and their Application in Health and Disease*. Spetses Island, Greece. September, 2018.
- G. Bruno, J.-L. Lackmann, S. Wenske, T. Heusler, K.-D. Weltmann, T. von Woedtke, K. Wende. "MS-based study of cold plasma-induced thiols redox chemistry in liquids". *22nd International Mass Spectrometry Conference (IMSC)*. Florence, Italy. August, 2018.

- G. Bruno, T. Heusler, H. Jablonowski, K. Stapelmann, J.-L. Lackmann, K. Wende. "Potential of thiols as biosensor of plasma generated reactive species in liquids". *7th International Conference on Plasma Medicine (ICPM)*. Philadelphia, USA. June, 2018.
- G. Bruno, H. Heusler, H. Jablonowski, J.-L. Lackmann, T. von Woedtke, K.-D. Weltmann, K. Wende. "Cysteine derivatives analysis as tool to monitor reactive species production by varying cold plasma conditions". *6th International Workshop on Plasma for Cancer Treatment (IWPCT 2019)*. Greifswald, Germany. March, 2018.
- G. Bruno, H. Heusler, H. Jablonowski, J.-L. Lackmann, T. von Woedtke, K.-D. Weltmann, K. Wende. "Cold physical plasma as source of bioactive ROS and RNS". *Gordon Research Conference "Oxygen Radicals"*. Ventura, USA. February, 2018.

Date

Giuliana Bruno

Acknowledgements

Four years ago, I moved from Italy to Germany for my PhD, and since this moment many things have changed. I went through a personal and professional evolution, culminating in this dissertation, which I would not have achieved without the support of various people.

Firstly, I would like to express my gratitude to my supervisor Dr. Kristian Wende, which allowed me to perform my PhD in his group. His true curiosity for science, creativity and input were a source of daily stimulation for me, keeping my motivation high until the last day. Thanks for mentoring my work, for the advices and for the fruitful discussions, which improved my scientific critical spirit. My acknowledgements also go to Prof. Woedtke and Prof. Lalk, for their outstanding availability, for supervising carefully my writings, for actively contributing in supporting my PhD through their key suggestions.

I wish to send my deepest gratitude also to Jan, Helena and Zahra, which have been for me true life mentors, helping me to find my way in both the professional and personal spheres. Your ideas, personality, and integrity inspired me to evolve and become a more confident scientist. Thanks also to all the members of my group: your daily presence and exchange of opinions contributed to boost my ideas and support the evolution of my PhD.

I would like to thank the entire staff of the ZIK Plasmatis, in particular Christine, Sander, Anke, Mehdi, Ramona, Julia, Juliane, Christina, for the stimulating work and discussions, which always fueled my curiosity, also helping me to improve my work and scientifically contextualize my achievements. I warmly thank all the new friendships I made, which accompanied me through this path, making it easier. In particular I thank Deba, Basti, Johanna, Marie, Gabriella, Talita and Laura for being always available to listen my stories and share theirs, and Ivana and Kerstin for the productive collaborations supported by the friendship we developed together.

A very special acknowledgement is for the closest persons I had during these four years, my friend-colleagues Basti and Johanna. We shared literally everything almost from day 0, creating a strong complicity, to the point that you have become (and will be) essential figures for me as a person and as a scientist. You made my path funnier and easier, never making me feel lonely in facing and handling any type of every-day event.

Vorrei ringraziare di cuore la mia famiglia, che ci e' sempre stata giorno dopo giorno, anche a distanza. Per sapere come supportarmi e come capirmi anche quando faccio silenzio. Per credere in me e nelle mie potenzialita', e per avere il coraggio e la forza di lasciarle esprimere anche quando la distanza fa soffrire. Vi dedico ogni mio raggiungimento, incluso questa tesi. Fortunatamente per me e per la mia vita, niente sarebbe e sara' senza di voi.

Finally, I thank the love of my life, which always knew how to comfort or challenge me in the right moment and with the right dose. I thank you for supporting me patiently and at any time, for always bringing your contagious smile and honesty with you. Thanks for building with me the feeling of home, even if my original home was far. It is because of you that my energies could be re-fueled day by day. Thank you for believing in my potential, even in features which I did not know to own, and to constantly support me in expressing myself fully and freely.